Lawrence Berkeley National Laboratory
Recent Work

Title
CURRENT DISTRIBUTION AND MASS TRANSFER IN ROTATING ELECTRODE SYSTEMS

Permalink
https://escholarship.org/uc/item/6m9348xg

Author
Nisancioglu, Kemal Mustafa.

Publication Date
1973-09-01

eScholarship.org Powered by the California Digital Library
University of California

LBL-1880

CURRENT DISTRIBUTION AND MASS TRANSFER IN ROTATING ELECTRODE SYSTEMS

Kemal Mustafa Nişancioğlu
(Ph. D. Thesis)

September 1973

Prepared for the U. S. Atomic Energy Commission
under Contract W-7405-ENG-48

For Reference

Not to be taken from this room

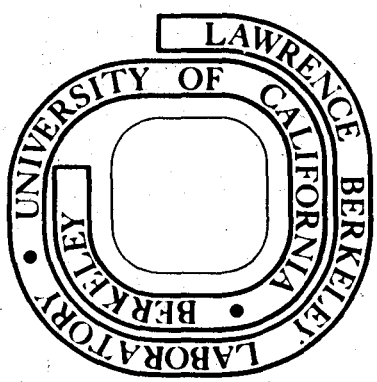

RECEIVED
LAWRENCE
RADIATION LABORATORY
NOV 16 1973
LIBRARY AND
DOCUMENTS SECTION

LBL-1880

DISCLAIMER

This document was prepared as an account of work sponsored by the United States Government. While this document is believed to contain correct information, neither the United States Government nor any agency thereof, nor the Regents of the University of California, nor any of their employees, makes any warranty, express or implied, or assumes any legal responsibility for the accuracy, completeness, or usefulness of any information, apparatus, product, or process disclosed, or represents that its use would not infringe privately owned rights. Reference herein to any specific commercial product, process, or service by its trade name, trademark, manufacturer, or otherwise, does not necessarily constitute or imply its endorsement, recommendation, or favoring by the United States Government or any agency thereof, or the Regents of the University of California. The views and opinions of authors expressed herein do not necessarily state or reflect those of the United States Government or any agency thereof or the Regents of the University of California.

0 0 0 0 3 5 9 0 7 1 2 9

CURRENT DISTRIBUTION AND MASS TRANSFER IN
ROTATING ELECTRODE SYSTEMS

Contents

0 0 0 0 3 9 0 7 3 1

CURRENT DISTRIBUTION AND MASS TRANSFER IN ROTATING ELECTRODE SYSTEMS

Kemal Mustafa Nişancioğlu

Inorganic Materials Research Division,
Lawrence Berkeley Laboratory, and
Department of Chemical Engineering;
University of California, Berkeley

ABSTRACT

Effective design and application of electrochemical systems require an adequate understanding of the principles of current distribution in the presence of mass transfer and complex electrode conditions. Recent advances in the theoretical methods are reviewed here and some specific applications presented for the disk- and spherical-electrode systems.

The steady-state current distribution on a disk and a sphere is compared below the limiting current. Numerical results are given for the secondary distribution and for Tafel kinetics. At high rotation speeds, the current distribution for the sphere depends only on the specified current level and becomes uniform when this level is set below 68 percent of the limiting current at high rotation speeds. The results disclose a number of complementary aspects of the spherical electrode alongside the disk electrode in electroanalytical applications.

Mass transfer to a rotating disk electrode is calculated at large times after a concentration step or a flux step at the surface. Radial dependence of concentration is ignored. Further application of results to treat more complex boundary conditions is discussed.

A mathematical model is given to treat the transient behavior of a disk in the absence of concentration gradients. The galvanostatic and potentiostatic cases are investigated separately. The analyses reduce to well-defined boundary value problems, which yield solutions in terms of newly defined eigenfunctions. The results allow the determination of time constants characteristic of decay due to an electrode reaction and due to a redistribution of charge within the double layer during the transient process. An experimental method is proposed to measure the double-layer capacity utilizing these results.

An asymptotic treatment is given for the short-time response of a disk electrode. Numerical results are obtained by expressing the potential in terms of an integral equation at the surface. A similar formulation is used also to calculate the steady-state current distribution for large exchange-current densities.

0 0 0 0 3 9 0 7 7 3 2

I. INTRODUCTION

The quality of design and efficiency of operation of industrial scale electrochemical systems depend on a knowledge of the principles of current distribution and electrode processes as well as the availability of accurate experimental data. The performance of an electrochemical cell is determined by the ohmic drop in the solution, the capacitive and faradaic impedances of the electrode-solution interface, and the rate at which reactants and products are replenished or depleted near the electrode. Information about the nature of these processes is usually obtained in the laboratory through studies of transport properties of electrolytic solutions, electrode kinetics, and double-layer effects. Meaningful interpretation of experimental data again requires an understanding of fundamental definitions and principles.

The necessity to collect fast, accurate, and reproducible experimental data has lead researchers to develop systems which are well defined from the standpoint of hydrodynamics, current distribution, and mass transfer and provide varying degrees of versatility in application. Some of these systems are reviewed by Newman[1] and Ibl.[2] Among the most commonly used are probably the so called rotating electrode systems, which include the rotating disk and cylinder systems in particular. The rotating spherical electrode has been introduced most recently[8] and promises a number of possible uses in electroanalytical applications alongside the disk and the cylinder.

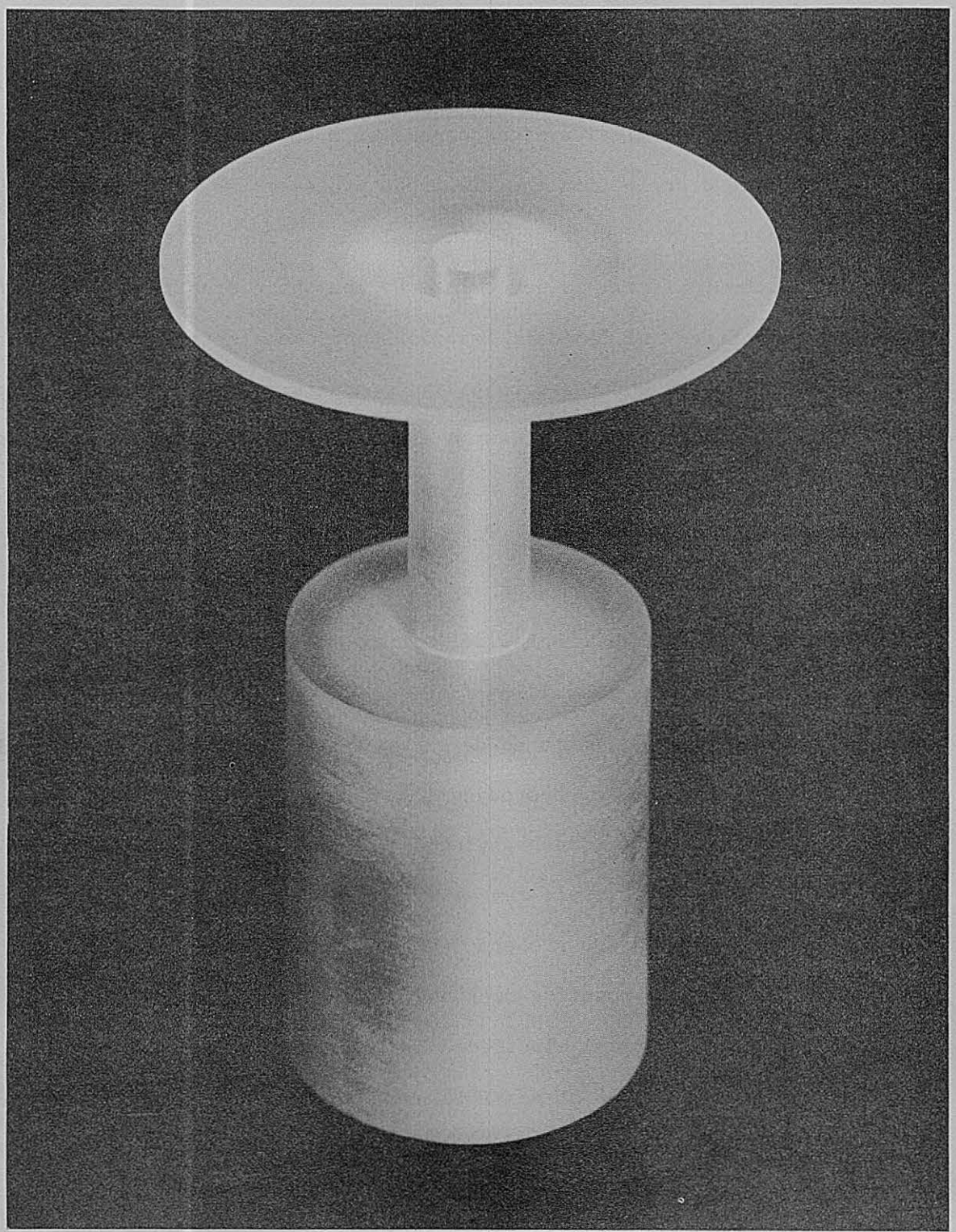

XBB 686-3955

Figure 1-1. Rotating disk electrode.

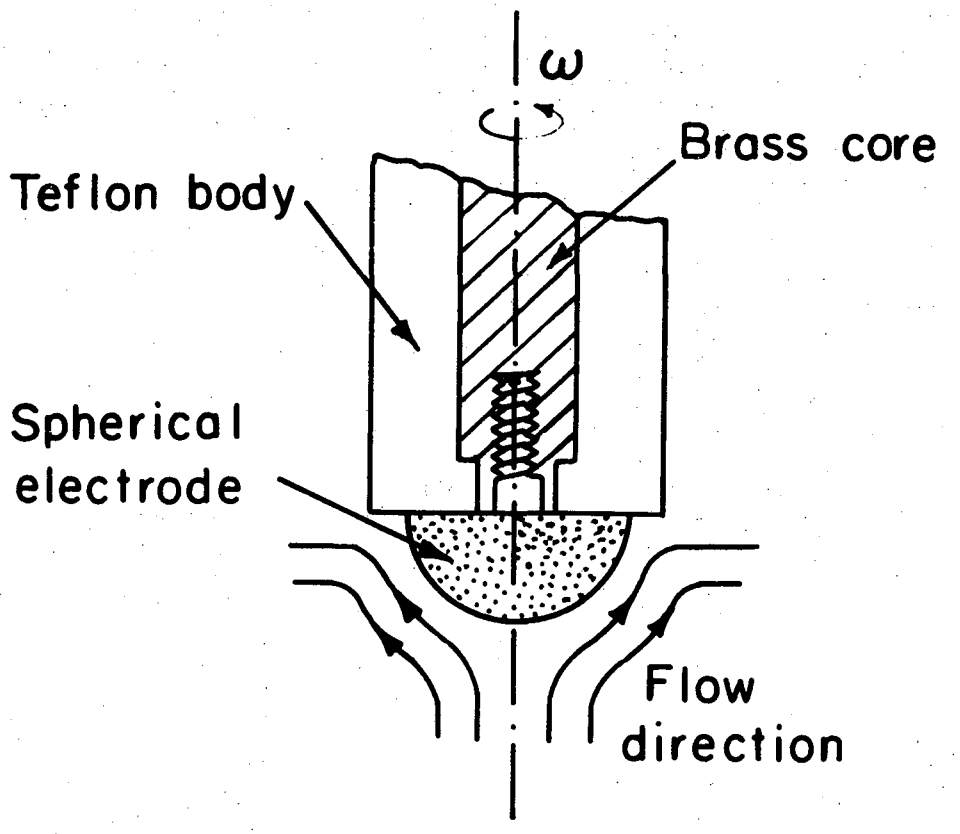

Figure 1-2. Rotating spherical electrode (from reference 8).

1.1. Historical Perspective

The disk, cylinder, and sphere geometries have been quite popular in the past in fundamental studies of heat conduction and fluid mechanics. The incentive to employ these geometries as electroanalytical tools gained momentum only a few decades ago after Levich[3] treated the convective diffusion problem at a rotating disk electrode. Levich showed that the disk surface is uniformly accessible to mass transfer under the limiting current conditions. Rotating cylinders have been employed shortly thereafter for mass-transfer research as reviewed by Eisenberg et al.[4] The disk electrode, however, has been more commonly employed in numerous applications evidently due to its simple design (see figure 1) and operation. Riddiford[5] gives a detailed account of the evolution of the disk electrode and its uses in electrochemistry. The rotating sphere (figure 2) has been proposed lately by Chin[8] as an alternative to the disk in high-rate deposition and dissolution studies.

After the verification and acceptance of Levich's results, uniform accessibility of the disk surface has been taken for granted also in applications below the limiting current. Newman[6] treated in the last decade mass transfer in thin diffusion layers, coupled with a non-uniform electric field in the solution and complex kinetics at the electrode. His results for the disk[7] showed that the current distribution at the surface can in fact be highly nonuniform even at current levels close to the limiting current.

As the methods of analysis of current distribution problems reached their present levels of sophistication, the need for equally complex models for faradaic and nonfaradaic electrode phenomena became

0 0 0 0 3 9 0 7 3 4

unavoidable in order to be able to simulate situations as close to the actual physical processes as possible. The electrochemical literature provides an abundance of models and data for the kinetics of electrode reactions,[99,100] which prove to be sufficient for study of steady-state processes. Additional complications due to double-layer charging have to be taken into account if transient processes are of interest. Faradaic and nonfaradaic phenomena have been treated in the past as two independent processes until Delahay[42] showed that this independence cannot be assumed a priori and has to be tested for each individual case. Improved methods to treat electrode conditions have subsequently been formulated.[43-46] A comprehensive review on this subject has been published by Parsons.[101]

1.2. Scope and Structure of Thesis

Due to the intricate coupling of faradaic reactions and double-layer charging at the surface and mass transfer in the presence of a nonuniform electric field in the solution, the design of many electrolytic systems and interpretation of data obtained by their use turn out to be more complicated than are usually anticipated. To cite a few examples, if the current distribution is nonuniform, the placement of the reference electrode becomes important; the measured values of ohmic drop and exchange-current density have to be corrected for the exact location of the reference probe in the solution. If, on the other hand, the current distribution is uniform, a uniform potential distribution near the surface is not necessarily guaranteed at the same time. This may have important consequences in the design and operation of electrochemical systems under controlled potential. Furthermore, the transient behavior

of an electrode is determined by the relaxation of a concentration gradient in the solution, capacitive discharge of the overpotential due to a faradaic reaction, or a redistribution of charge within the double layer. This thesis attempts to investigate the roles of some of these effects in determining the overall behavior of electrochemical systems.

Specific problems are worked out for the rotating disk and sphere electrodes under laminar flow considerations. The former system is already a basic set-up in many electrochemical laboratories, and the latter is a newly-proposed tool which has been subject to a relatively limited study so far. These geometries have been chosen for study also due to their nonuniform current distribution below the limiting current, a major complicating factor in the design and operation of electrochemical systems. The basic principles governing the application of rotating cylinders are adequately covered by Eisenberg et al.[4] Ring and sectioned electrodes are also not considered.

The emphasis is on mathematical techniques as well as the physical significance of results. The discussion carries the purpose of aiding the experimenter in the proper design and operation of electroanalytical tools in the laboratory and meaningful interpretation of data employing nonelementary numerical methods if necessary.

Chapter 2 gives a rigorous treatment of transport and current distribution in electrochemical systems. Equations are developed to express the hydrodynamics, potential and current distribution, and convective diffusion for the rotating disk and sphere geometries. Basic assumptions inherent in the analyses of these equations are listed.

0 3 8 0 3 9 8 7 3 5

The conditions which prevail at an electrode surface during steady-state or transient applications are discussed in chapter 3, so that the expressions of chapter 2 can be analyzed for certain specific cases to obtain numerical results. Thermodynamic arguments are used to express faradaic and nonfaradaic processes and relate reaction rates and double-layer charging effects to measurable quantities such as the over-potential, current density, and double-layer capacity.

Chapters 4 and 5 present steady-state applications of these equations to the rotating-disk and -spherical electrodes below the limiting current. The results are compared for the two geometries to determine some guidelines for various applications of each in electrochemistry.

The transient convective-diffusion equation is analyzed in chapter 6 for the disk electrode by ignoring radial convection. The effects of mass transfer and double-layer charging on the transient behavior are investigated.

Chapters 7 through 9 treat the transient response of a disk electrode in the absence of mass transfer. Galvanostatic, potentiostatic and alternating current situations are discussed. A singular-perturbation analysis is given to determine the short-time response. An experimental method is proposed to measure differential capacities of solid electrodes by utilizing these results.

II. FUNDAMENTAL PRINCIPLES OF TRANSPORT IN ELECTROCHEMICAL SYSTEMS

Even though electrochemistry is an old branch of the physical sciences, the fundamental treatment of mass transfer and current distribution in electrochemical cells has been a product of the last few decades. Levich's[3] work brought a new perspective to the treatment of convective diffusion problems in electrochemical systems. Since then, significant advances have been made in the improvement and application of the theory. These have been discussed extensively by Levich[9] and Newman[1,10-12] in a number of monographs and review articles. Some of the essentials immediately relevant to the thesis are developed here for application in the later chapters.

2.1. Basic Equations

A generalized treatment of transport in concentrated systems as well as dilute solutions has become possible lately.[10,13] The present discussion adheres to the simpler dilute solution theory,[9-11] which still finds frequent use since many applications employ dilute solutions or small amounts of reactants in excess supporting electrolyte. The flux $\underline{N}_i$ of a solute species is determined by migration in an electric field, diffusion due to a concentration gradient, and convection with the fluid flow,

$$\underline{N}_i = -z_i u_i F c_i \nabla\Phi - D_i \nabla c_i + \underline{v} c_i, \qquad (2\text{-}1)$$

where u_i and D_i are the mobility and the diffusion coefficient of species i, respectively. A differential material balance for the species i

0 0 0 0 3 9 0 / / 3 6

gives the conservation law,

$$\frac{\partial c_i}{\partial t} = - \nabla \cdot \underline{N}_i + R_i \quad , \tag{2-2}$$

where R_i represents production due to a reaction in the bulk and is normally zero in electrochemical systems. The electroneutrality assumption, which can be expressed as

$$\sum_i z_i c_i = 0 \quad , \tag{2-3}$$

is a good approximation for the bulk of the electrolyte. Furthermore, the motion of charged species creates a current density, given by

$$\underline{i} = F \sum_i z_i \underline{N}_i \quad . \tag{2-4}$$

The current density can be written in terms of the electric field and diffusion by combining equations 1, 3, and 4:

$$\underline{i} = -\kappa \nabla \Phi - F \sum_i z_i D_i \nabla c_i \quad . \tag{2-5}$$

In the presence of flow within the electrolyte, the hydrodynamics can be determined from the Navier-Stokes equation,

$$\rho(\partial \underline{v}/\partial t + \underline{v} \cdot \nabla \underline{v}) = -\nabla p + \mu \nabla^2 \underline{v} + \rho \underline{g} \quad , \tag{2-6}$$

and the equation of continuity for an incompressible fluid,

$$\nabla \cdot \underline{v} = 0 \quad . \tag{2-7}$$

These equations form the basis for the analysis of electrochemical systems. Some basic examples are given below, and more are developed in the following chapters.

2.2. Electrostatics

When there are no concentration gradients in the solution, equation 5 becomes

$$\underline{i} = -\kappa\nabla\Phi \quad , \tag{2-8}$$

where

$$\kappa = F^2 \sum_i z_i^2 u_i c_i \tag{2-9}$$

is the conductivity of the solution. Equation 8 is equivalent to Ohm's law. Substitution back into equation 4 and combining with equation 2 yields Laplace's equation for the potential:

$$\nabla^2\Phi = 0 \quad . \tag{2-10}$$

This is the fundamental equation of electrostatics in the absence of concentration gradients and has been analyzed for a large number of electrode geometries as reviewed by Newman[12] and others.[32,33]

Let us consider a disk electrode of radius r_o embedded in a large insulating plane. The potential far from the disk can be taken to be zero:

$$\Phi \to 0 \quad \text{as} \quad r^2 + z^2 \to \infty \quad , \tag{2-11}$$

where r and z are the radial and axial cylindrical coordinates, respectively. On the insulating plane, the current is zero, and hence from

0 0 0 0 3 9 0 7 7 3 7

equation 1, we obtain

$$\partial\Phi/\partial z = 0 \text{ at } z = 0,\ r > r_o \quad . \tag{2-12}$$

The potential is also well behaved along the axis of the disk. The solution to Laplace's equation satisfying the above conditions can be expressed conveniently in terms of the rotational elliptic coordinates,[14]

$$\Phi/V = \sum_{n=0}^{\infty} B_n P_{2n}(\eta)\ M_{2n}(\xi) \quad , \tag{2-13}$$

where P_{2n} is the Legendre polynomial of order 2n, M_{2n} is a Legendre function of order 2n, and V is a scaling factor, such as the electrode potential, introduced to render the coefficients B_n dimensionless. The rotational elliptic coordinates are related to the cylindrical coordinates by[14]

$$z = r_o \xi\eta, \quad r = r_o \sqrt{(1 + \xi^2)(1 - \eta^2)} \quad . \tag{2-14}$$

The potential is related to the current density according to equation 8 in the absence of concentration gradients:

$$\begin{aligned} i &= -\kappa \left.\frac{\partial\Phi}{\partial z}\right|_{z=0} = -\frac{\kappa}{r_o\eta} \left.\frac{\partial\Phi}{\partial\xi}\right|_{\xi=0} \\ &= -\frac{\kappa}{r_o\eta} V \sum_{n=0}^{\infty} B_n P_{2n}(\eta)\ M'_{2n}(0) \quad . \end{aligned} \tag{2-15}$$

The coefficient B_n can be calculated by applying the orthogonality property of the Legendre polynomials:

$$B_n = -\frac{r_o}{\kappa M'_{2n}(0) V} \int_0^1 i(\eta)\ P_{2n}(\eta)\ \eta d\eta \quad . \tag{2-16}$$

The current distribution on the disk is determined by mass transfer and surface conditions as well as the ohmic drop in the solution. A method of treating all these effects in a unified manner is discussed in the next chapter.

As long as the concentration is uniform throughout the system, and there are no kinetic and double-layer effects to account for, the potential in the solution adjacent to the electrode surface Φ_o is uniform and equal to the electrode potential. Equation 13 satisfies this condition for n = 0 and thus reduces to[14]

$$\Phi^p/\Phi^p_o = 1 - (2/\pi)\ \tan^{-1}\xi \quad . \tag{2-17}$$

This is the primary potential distribution for the disk electrode. The superscript p has been introduced to distinguish this solution from the general solution, equation 13.

The primary current distribution at the disk surface can now be evaluated from equation 8:

$$i_n = -\kappa \left.\frac{\partial \Phi^p}{\partial z}\right|_{z=0} = \frac{2\kappa\Phi^p_o}{\pi\sqrt{r_o^2 - r^2}} \quad . \tag{2-18}$$

The total current is, therefore,

$$I = 2\pi \int_0^{r_o} i_n r dr = 4\kappa r_o \Phi^p_o \quad , \tag{2-19}$$

and the resistance is

$$R = \Phi^p_o/I = 1/4\kappa r_o \quad . \tag{2-20}$$

0 0 0 0 0 0 0 0 0 0 0 0

Figure 1 shows the current and potential lines for the primary distribution.

Nanis and Kesselman[15] have shown how to solve Laplace's equation for the disk in cylindrical coordinates by use of Hankel transforms. It is also possible to express the relationship between the current density and the potential as an integral equation. For the disk, this is[12]

$$\Phi(r,z) = \frac{2}{\pi K} \int_0^{r_o} \frac{i_n(r') \, K(m) \, r' \, dr'}{\sqrt{z^2 + (r + r')^2}} \quad , \tag{2-21}$$

where

$$m = \frac{4rr'}{z^2 + (r + r')^2} \quad , \tag{2-22}$$

and (m) is the complete elliptic integral of the first kind,[16]

$$K(m) = \int_0^{\pi/2} \frac{d\alpha}{\sqrt{1 - m\sin^2\alpha}} \quad . \tag{2-23}$$

The analysis is similar for the spherical electrode. In spherical coordinates, the boundary conditions are

$$\left.\begin{aligned} \Phi &= 0 \quad \text{as} \quad y \to \infty \, , \\ \partial\Phi/\partial\theta &= 0 \quad \text{at} \quad \theta = 0, \, \theta = \pi/2 \, , \end{aligned}\right\} \tag{2-24}$$

and the potential distribution is given by

$$\Phi/V = \sum_{n=0}^{\infty} B_n P_{2n}(\cos\theta)(r_o/r)^{2n+1} \quad , \tag{2-25}$$

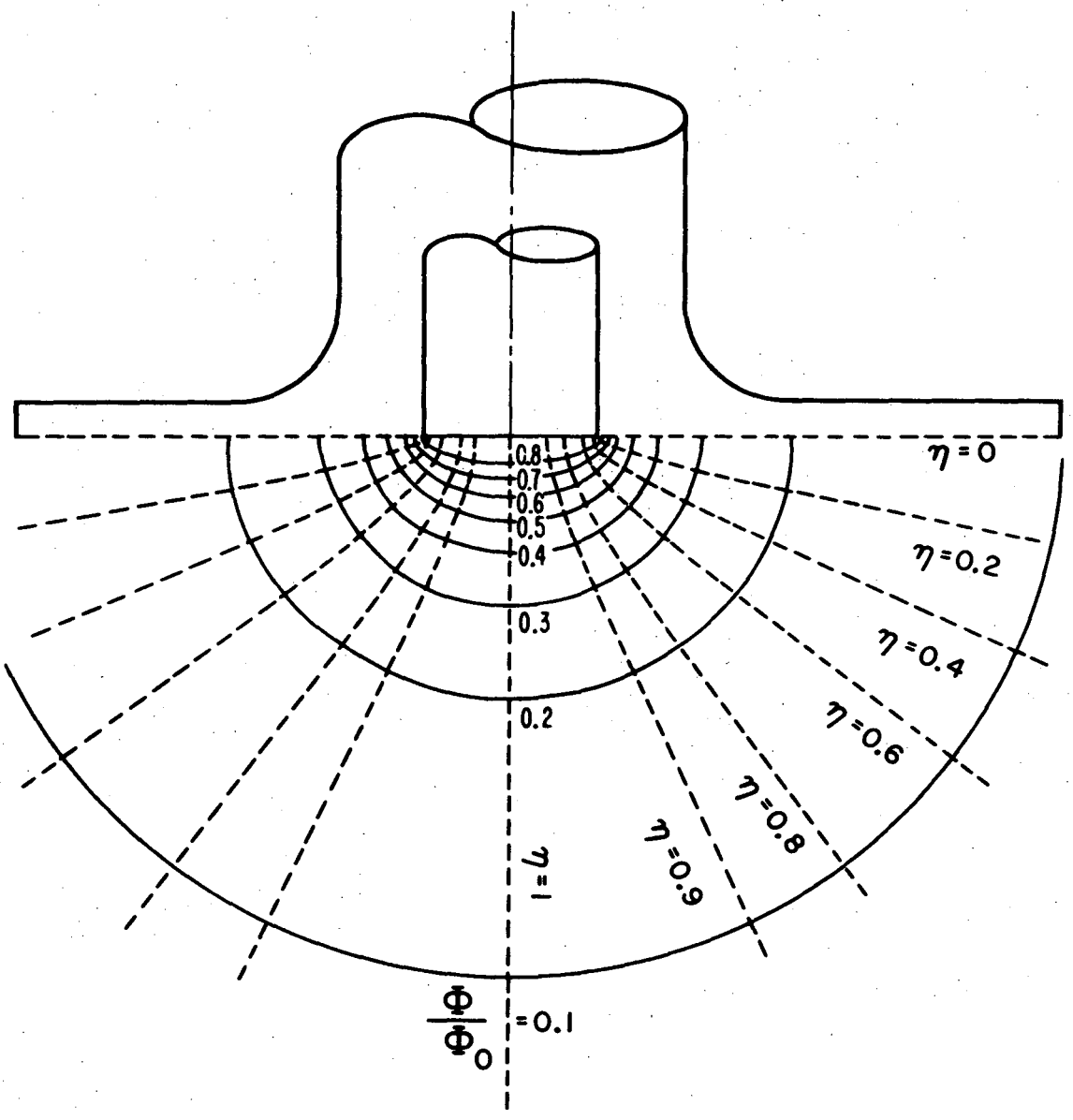

Figure 2-1. Equipotential and current flow lines corresponding to the primary distribution near a disk electrode (from reference 14).

0 0 0 0 3 9 0 7 3 9

where

$$B_n = \frac{1}{V} \frac{4m+1}{2m+1} \int_0^1 i(\cos\theta)\, P_{2n}(\cos\theta)\, d(\cos\theta) \quad . \qquad (2\text{-}26)$$

The primary distributions for the potential and the current are, respectively,

$$\Phi/\Phi_o^p = r_o/r \quad , \qquad (2\text{-}27)$$

and

$$i_n = \kappa\Phi_o^p/r_o \quad . \qquad (2\text{-}28)$$

The total current to a hemisphere is given by

$$I = 2\pi r_o \kappa \Phi_o^p \quad . \qquad (2\text{-}29)$$

The resistance therefore is

$$R = 1/2\pi r_o \kappa \quad . \qquad (2\text{-}30)$$

Results for various other boundary conditions for the sphere are given by Carslaw and Jaeger.[17] Comparison of equations 27 and 18 shows that the primary current distribution on a sphere is uniform, whereas it is highly nonuniform on a disk, becoming infinite at the edge.

2.3. Hydrodynamics

The analyses of the Navier-Stokes equation 6 and the continuity equation 7 are classical problems in fluid mechanics for the disk[18] and the sphere[19] geometries. The basic equations have to be expressed in cylindrical coordinates for the disk and in spherical coordinates for the sphere. These lengthy formulas are tabulated by Bird, Stewart,

and Lightfoot[20] and will not be repeated here. When the end effects are ignored, the boundary conditions for the disk are written as

$$\left.\begin{aligned} v_r = 0,\ v_z = 0,\ v_\theta = r\Omega \quad &\text{at } z = 0 \ , \\ v_r = 0,\ v_\theta = 0 \quad &\text{as } z \to \infty \ , \end{aligned}\right\} \tag{2-31}$$

where v_r, v_θ, and v_z are the r, θ, and z components of the velocity, respectively, and Ω is the angular rotation speed. The dynamic pressure P ($=p-\rho gz$) also has to be specified at one point. As suggested by von Kármán,[18] a separation of variables can be effected in the following manner:[12]

$$v_\theta = r\Omega G(\zeta),\ v_r = r\Omega F(\zeta),\ v_z = \sqrt{\nu\Omega}\, H(\zeta) \ , \tag{2-32}$$

where G, F, and H are the dimensionless velocity components, and

$$\zeta = z\sqrt{\Omega/\nu} \tag{2-33}$$

is the dimensionless axial distance from the disk. The dimensionless dynamic pressure is

$$P = p/\mu\Omega \ . \tag{2-34}$$

Substitution into equations 6 and 7 gives a set of coupled, nonlinear, ordinary differential equations,

$$\left.\begin{aligned} &2F + H' = 0 \ , \\ &F^2 - G^2 + HF' = F'' \ , \\ &2FG + HG' = G'' \ , \\ &HH' + P' = H'' \ , \end{aligned}\right\} \tag{2-35}$$

0 0 0 0 3 9 0 / / 4 0

with the boundary conditions,

$$\left.\begin{aligned} H = F = 0,\ G = 1 \quad &\text{at} \quad \zeta = 0 \quad , \\ F = G = 0 \quad &\text{as} \quad \zeta \to \infty \quad . \end{aligned}\right\} \tag{2-36}$$

The first three of equations 35 can be solved first for the velocity components, and the pressure can then be obtained by integrating the last equation:

$$P = P(0) + H' + \frac{1}{2} H^2 = P(0) - 2F - \frac{1}{2} H^2 \quad . \tag{2-37}$$

These equations have been solved using different numerical techniques by Cochran,[21] Rogers and Lance,[22] and Newman.[12] Newman's results are reproduced in figure 2.

In studies of mass transfer and current distribution in electrochemical systems, one is normally interested in the velocity profiles very near the surface of the electrode (see section 5). For small values of ζ, the axial component of the dimensionless velocity can be expressed as[12,21,22]

$$H = -0.51023\zeta^2 + O(\zeta^3) \quad . \tag{2-38}$$

Similar approximations can be obtained for the other velocity components by solving equation 35 for F and G:

$$\left.\begin{aligned} F &= 0.51023\zeta + O(\zeta^2) \quad , \\ G &= 1 + O(\zeta) \quad . \end{aligned}\right\} \tag{2-39}$$

For the rotating sphere, only the treatment of the boundary-layer approximations to equations 6 and 7 has been possible. Howarth[19] has expressed the velocity components as perturbation expansions in the θ - coordinate:

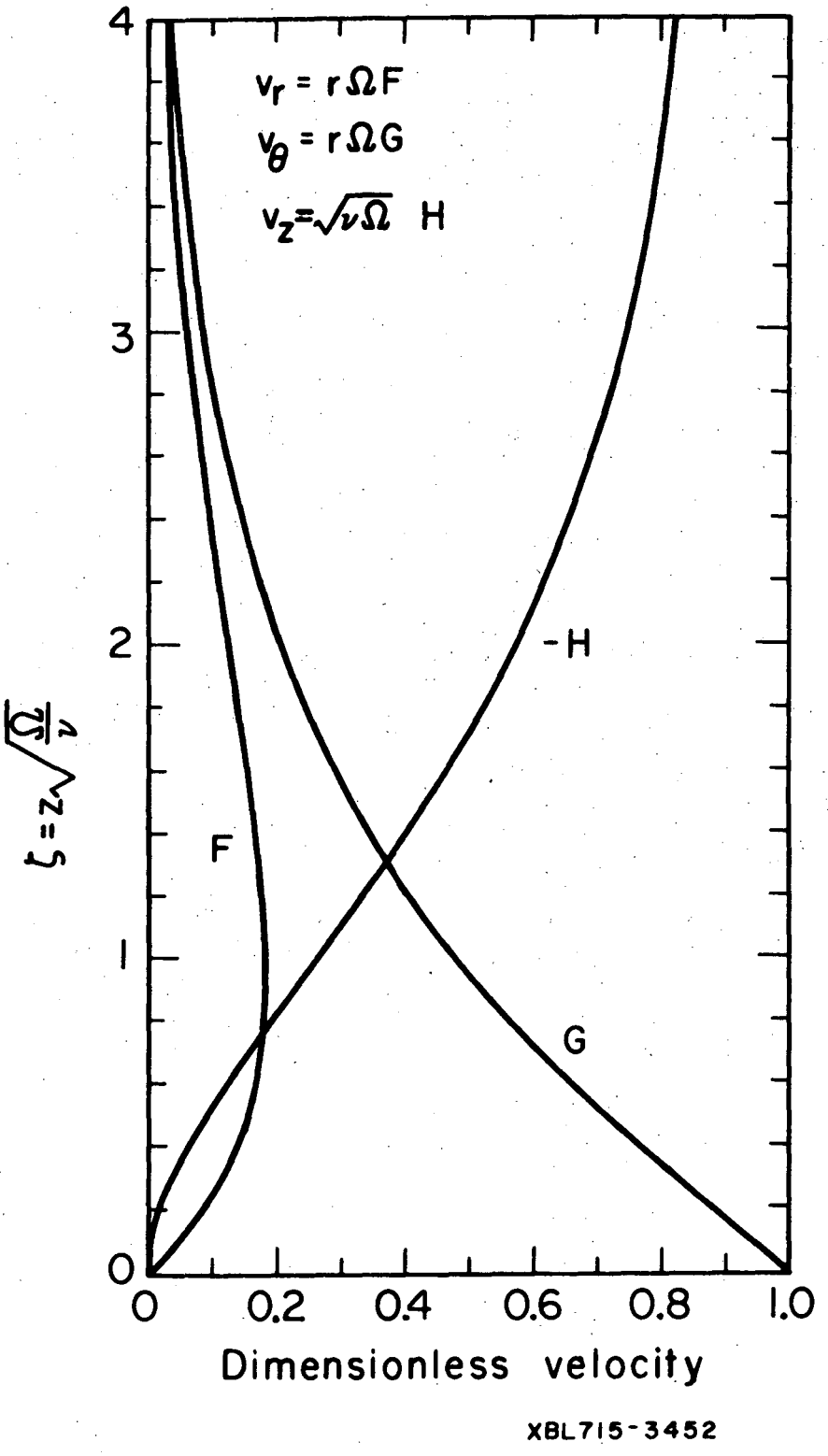

Figure 2-2. Velocity profiles for a rotating disk (from reference 12).

0 0 0 0 3 9 0 / / 4 1

$$\left.\begin{aligned} v_\theta &= r_o\Omega\,(\theta F_1 + \theta^3 F_3 + \ldots)\,, \\ v_\phi &= r_o\Omega\,(\theta G_1 + \theta^3 G_3 + \ldots)\,, \\ v_r &= \sqrt{\nu\Omega}(H_1 + \theta^2 H_2 + \ldots)\,, \end{aligned}\right\} \tag{2-40}$$

where F_n, G_n, and H_n are the functions of the stretched variable

$$Z = \sqrt{\Omega/\nu}\,(r - r_o)\quad . \tag{2-41}$$

The boundary conditions are

$$\left.\begin{aligned} &v_r = v_\theta = 0,\quad v_\phi = r_o\Omega\sin\theta \quad \text{at} \quad r = r_o\quad , \\ &v_\theta = v_\phi = 0 \quad \text{as} \quad r \to \infty\quad . \end{aligned}\right\} \tag{2-42}$$

Substitution of these equations into the boundary-layer equations for the sphere[23] and equating terms of equal order in θ give a hierarchy of coupled, nonlinear, ordinary differential equations for F_n, G_n, and H_n with the corresponding boundary conditions. Howarth[19] attempted an approximate solution by applying the von Kármán momentum integral method. Banks[23] and Manohar[24] have reported more accurate numerical calculations. Using their results, Newman[25] expressed the dimensionless shear stress $B(\theta)$ on the sphere as

$$\begin{aligned} B(\theta) &= \beta\nu^{1/2}/r_o\Omega^{3/2} \\ &= 0.51023\theta - 0.1808819\theta^3 - 0.040408\sin^3\theta\,, \end{aligned} \tag{2-43}$$

where β is the velocity derivative $\partial v_\theta/\partial r$ evaluated at the surface. Equation 43 is plotted in figure 3.

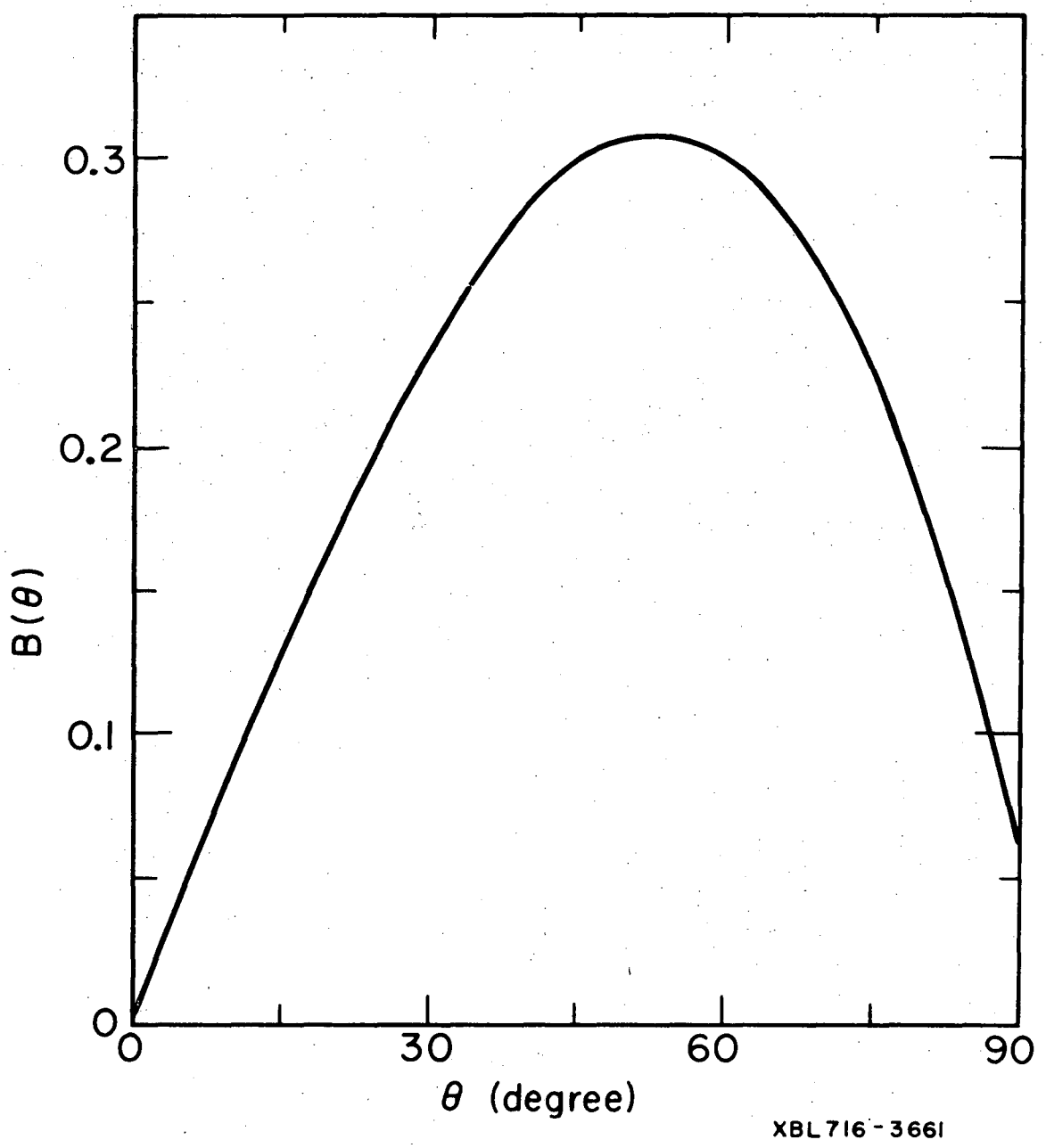

Figure 2-3. Dimensionless velocity derivative on the surface of a rotating sphere (from reference 25).

0 0 0 0 5 9 0 . 1 4 2

The boundary-layer approximation for the sphere is known to break down at a region near the equator[19] where the boundary layers originating at the poles meet and erupt in the form of a swirling radial jet.[26] Stewartson[27] has shown that the size of this region has the magnitude $0(1/Re)$, and thus it can be rendered small by increasing the Reynolds number.

2.4. Mass Transfer

Substitution of the flux equation 1 into the conservation equation 2 ($R_i = 0$) and using the equation of continuity 7 for incompressible fluids yield

$$\partial c_i/\partial t + \underline{v}\cdot\nabla c_i = z_i F\nabla\cdot(u_i c_i \nabla\Phi) + \nabla\cdot(D_i\nabla c_i) \quad . \tag{2-44}$$

If an excess amount of supporting electrolyte is used, the migration term can be neglected. Moreover, if the diffusion coefficient can be assumed to be independent of concentration, equation 44 reduces to the well-known convective diffusion equation,

$$\partial c_i/\partial t + \underline{v}\cdot\nabla c_i = D_i\nabla^2 c_i \quad , \tag{2-45}$$

which finds many applications in both electrolytic and nonelectrolytic mass transfer.

Another case, which allows a similar simplification of equation 44 is the binary system. The concentration of the electrolyte can be defined in terms of the ionic concentrations as

$$c = c_+/\nu_+ = c_-/\nu_- \quad , \tag{2-46}$$

where ν_+ and ν_- are the number of cations and anions produced by dissociation of one molecule of electrolyte. For the ionic species, equation 40 reads

$$\left.\begin{aligned} \partial c/\partial t + \underline{v}\cdot\nabla c &= z_+u_+F\nabla\cdot(c\nabla\Phi) + D_+\nabla c^2 \,, \\ \partial c/\partial t + \underline{v}\cdot\nabla c &= z_-u_-F\nabla\cdot(c\nabla\Phi) + D_-\nabla c^2 \,. \end{aligned}\right\} \tag{2-47}$$

Subtraction gives

$$(z_+u_+ - z_-u_-)\, F\nabla\cdot(c\nabla\Phi) + (D_+ - D_-)\,\nabla c^2 = 0 \,. \tag{2-48}$$

Elimination of the potential between equation 48 and either one of equations 47 leads again to the convective diffusion equation,

$$\partial c/\partial t + \underline{v}\cdot\nabla c = D\nabla c^2 \,, \tag{2-49}$$

where

$$D = \frac{z_+u_+D_- - z_-u_-D_+}{z_+u_+ - z_-u_-} \tag{2-50}$$

is the diffusion coefficient of the binary electrolyte.

For a thin diffusion layer near a disk or a spherical electrode, the steady-state form of the convective diffusion equation reduces to

$$v_x \frac{\partial c_i}{\partial x} + v_y \frac{\partial c_i}{\partial y} = D_i \frac{\partial c_i^2}{\partial y^2} \,, \tag{2-51}$$

where x is measured along the electrode from its upstream end (center of the disk and poles of the sphere), and y is measured perpendicularly from the electrode surface into the solution as indicated for a sphere in figure 4. D_i is the diffusion coefficient of the reactant, but for

0 0 0 0 6 9 0 7 7 4 3

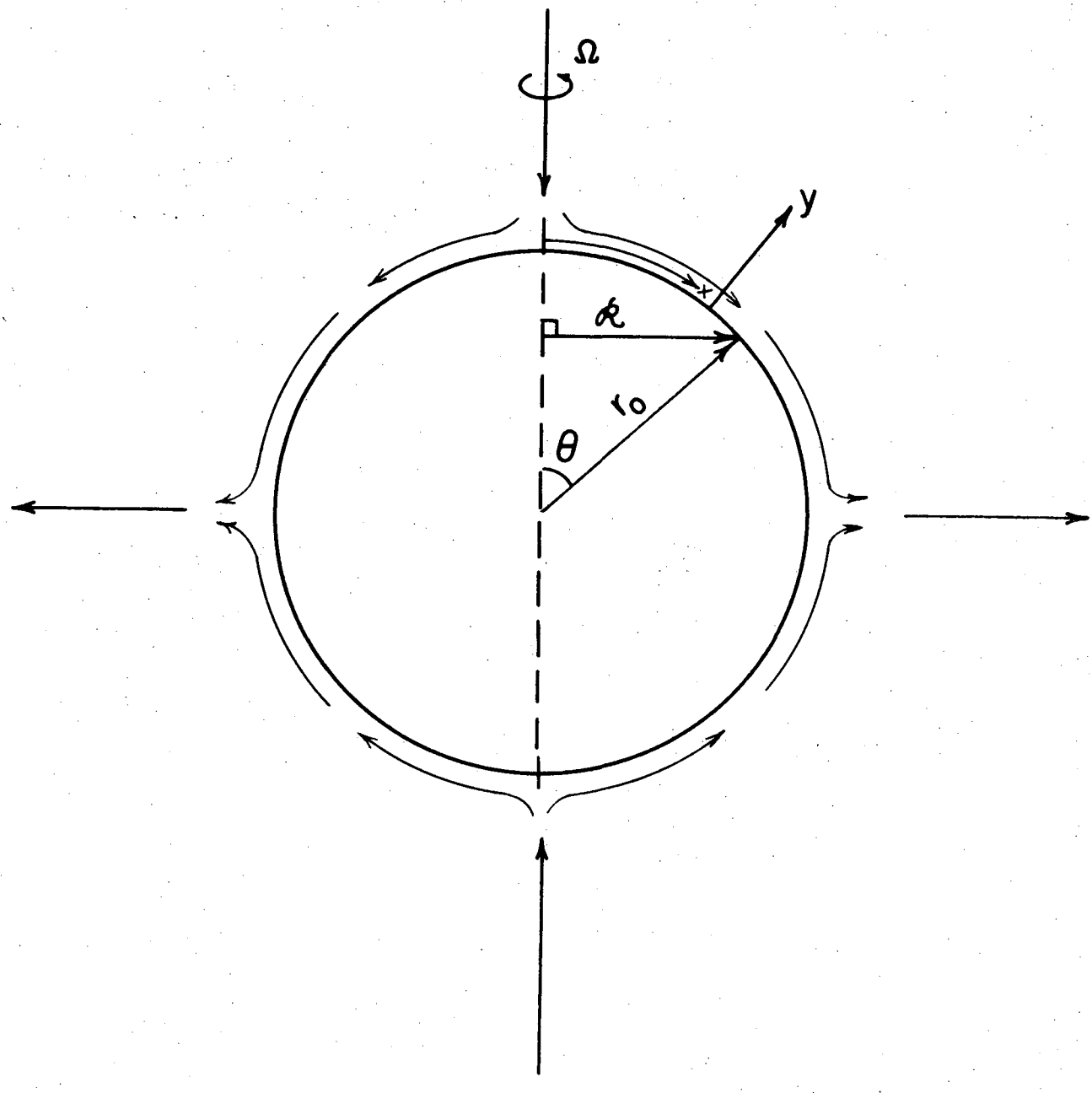

Figure 2-4. Schematic representation of some variables and parameters for the rotating sphere.

a binary electrolyte, it should be considered as the diffusion coefficient of the salt given by equation 50. Equation 51 applies to any axisymmetric diffusion layer, and a general treatment is possible.[11,12,28] For short distances from the electrode, the velocity components can be approximated by

$$v_x = y\beta(x), \quad \text{and} \quad v_y = -\frac{1}{2} y^2 \frac{1}{\mathcal{R}} \frac{d(\mathcal{R}\beta)}{dx} \quad , \tag{2-52}$$

where $\beta(x) = 0.51023\Omega\sqrt{\Omega/\nu}\, x$ for the disk as can be obtained from the results of the previous section, and for the sphere, it is given by equation 43 by setting $x = r_o\theta$. These expressions satisfy the continuity equation 7, which can be written in the form

$$\frac{\partial(\mathcal{R}v_x)}{\partial x} + \mathcal{R}\frac{\partial v_y}{\partial y} = 0 \tag{2-53}$$

for axisymmetric diffusion layers. $\mathcal{R}$ (=r for the disk and $r_o \sin\theta$ for the sphere) is the distance of the surface from the axis of symmetry.[29] The convective diffusion equation now becomes

$$y\beta \frac{\partial c_i}{\partial x} - \frac{1}{2} y^2 \frac{1}{\mathcal{R}} \frac{d\mathcal{R}\beta}{dx} \frac{\partial c_i}{\partial y} = D_i \frac{\partial^2 c_i}{\partial y^2} \quad . \tag{2-54}$$

The similarity variable,[1,30,31]

$$\xi = y\sqrt{\mathcal{R}\beta} \Big/ \left[9D_i \int_0^x \mathcal{R}\sqrt{\mathcal{R}\beta}\, dx\right]^{1/3} \quad , \tag{2-55}$$

reduces equation 54 to the form

$$\frac{d^2 c_i}{d\xi^2} + 3\xi^2 \frac{dc_i}{d\xi} = 0 \quad . \tag{2-56}$$

0 0 0 0 3 9 0 / 4 4

We want to solve this equation for the case where the concentration is zero at the surface and takes its bulk value $c_{i\infty}$ far away from the surface (the limiting current condition). Thus, the solution is

$$c_i = \frac{c_{i\infty}}{\Gamma\left(\frac{4}{3}\right)} \int_0^{\xi} e^{-x^3}\, dx \quad , \tag{2-57}$$

where the integral is a tabulated function of ξ.[16]

Application of the Faraday's law to equation 57 gives the limiting current distribution,[1]

$$i_{lim} = \frac{nFD_i c_{i\infty} \sqrt{6\beta}}{s_i \Gamma(4/3)} \Big/ \left[9D_i \int_0^x 6\sqrt{6\beta}\, dx\right] \quad , \tag{2-58}$$

where n is the number of electrons transferred by the electrode reaction (see equation 3-1), F is the Faraday's constant and s_i is the stoichiometric coefficient of species i in the electrode reaction. For the rotating disk, this reduces to the Levich equation,[1,3,9]

$$i_{lim} = 0.62048 \frac{nFD_i c_{i\infty}}{s_i r_o} Sc^{1/3} Re^{1/2} \quad , \tag{2-59}$$

and for the rotating sphere,[25] it becomes

$$i_{lim}(\theta) = 0.12443 \frac{nFD_i c_{i\infty}}{s_i r_o} \frac{\sqrt{B\sin\theta}\; Sc^{1/3} Re^{1/2}}{\left[\int_0^{\theta} \sqrt{B\sin\theta}\, \sin\theta d\theta\right]^{1/3}} \quad . \tag{2-60}$$

The average limiting current density is, therefore,

$$(i_{lim})_{ave} = 0.90159 \frac{nFD_i c_{i\infty}}{s_i r_o} Sc^{1/3} Re^{1/2} \quad . \tag{2-61}$$

Note that the limiting current distribution on a disk is uniform, whereas it is a function of θ on a sphere as shown in figure 5. The behavior of the primary and the limiting current-distributions has important consequences in determining the general mass-transfer and current-distribution characteristics of the disk and the sphere as will be shown by later examples in the thesis.

Equations 59 to 61 can be written for metal deposition from a single salt solution by replacing the ratio nD_i/s_i with $z_+D/(1 - t_+)$ (see equation 3-22), where z_+ and t_+ are the valence and transference number (defined by equation 3-15) of the reactant, and D is given by equation 50. The Schmidt number is then defined in terms of D instead of D_i.

Correction terms have been obtained for equations 59 and 60 for finite Schmidt numbers.[34-36] Sparrow and Gregg[37] give results for the disk at low Prandtl numbers for the analogous heat-transfer problem. The effects of migration and available physical properties of the solution,[38,39] and corrections due to radial diffusion[40] have also been reported for the disk electrode.

The results can be extended to accommodate arbitrary changes in the surface concentration or flux by applying the superposition integral:[12,28]

$$\left.\frac{\partial c_i}{\partial y}\right|_{y=0} = -\frac{\sqrt{R\beta}}{\Gamma\left(\frac{4}{3}\right)} \int_0^x \left.\frac{dc_{io}}{dx}\right|_{x=x_o} \frac{dx_o}{\left[9D_i \int_{x_o}^{x} R\sqrt{R\beta}\, dx\right]^{1/3}}, \quad (2\text{-}62)$$

0 0 0 0 5 9 0 7 4 5

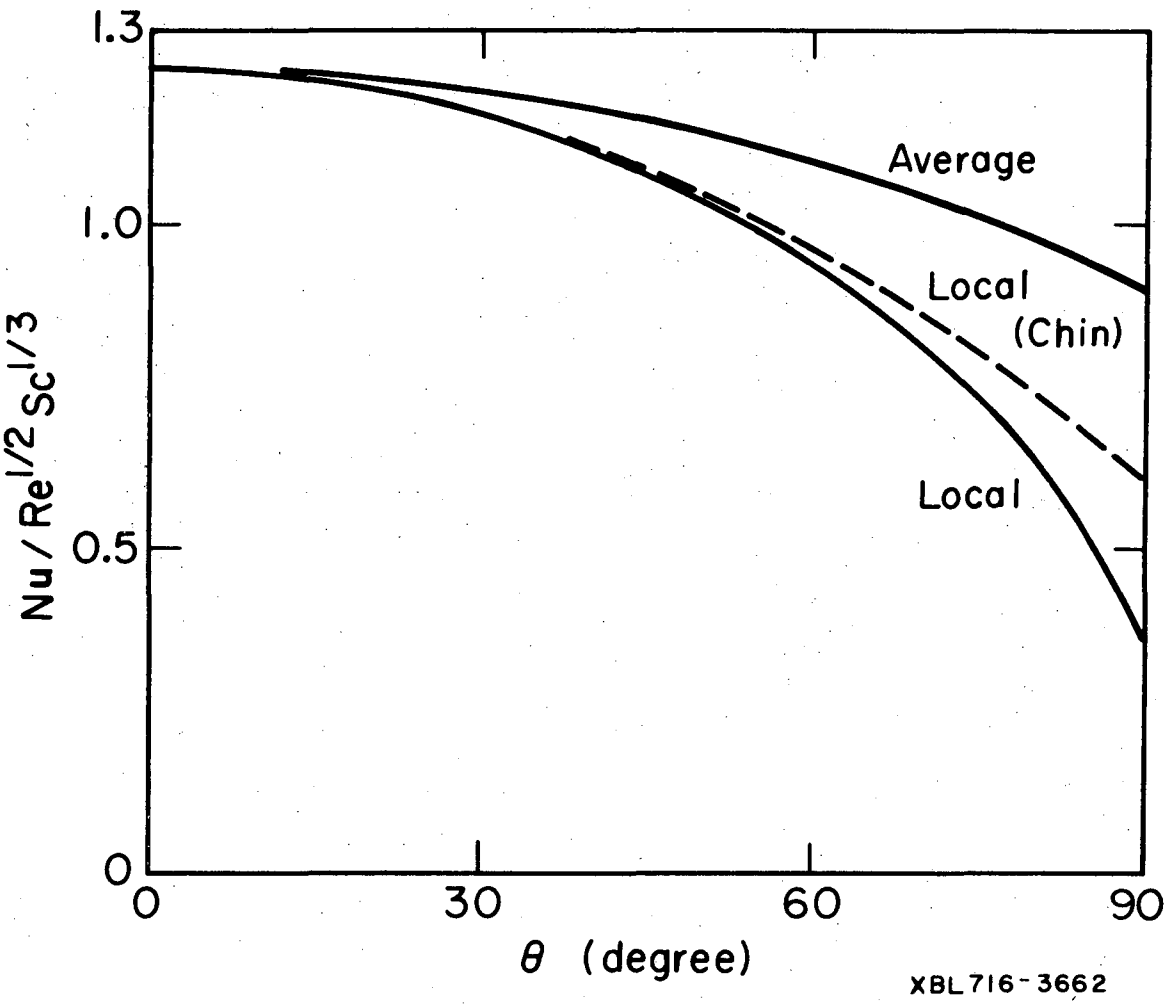

Figure 2-5. Local and average Nusselt numbers for a rotating sphere at high Schmidt numbers, as calculated by Newman[25] and compared to Chin's results.[8] The Nusselt number is related to the current density by $Nu=2r_o s_i i_n/nFD_i c_\infty$ (from reference 25).

or equivalently,

$$c_{io}(x) - c_{i\infty} = -\frac{(D_i/3)^{1/3}}{\Gamma(2/3)} \int_0^x \left.\frac{\partial c_i}{\partial y}\right|_{\substack{y=0 \\ x=x_o}} \frac{R(x_o)\, dx_o}{\left[\int_{x_o}^{x} R\sqrt{R\beta}\, dx\right]^{2/3}} \quad (2\text{-}63)$$

The transient form of the convective diffusion equation is treated for the rotating disk in chapter 6.

2.5. Basic Assumptions

Some fundamental assumptions are inherent in the forthcoming development. Many of these have already been stated in this chapter. An explitic summary[6] of these at this point may be worthwhile for later reference and to convey the overall limitations of the theory.

1. The disk electrode is embedded in an infinite insulating plane. The spherical electrode is suspended and allowed to rotate in an otherwise stagnant electrolyte. However, the analysis also applies to a hemispherical cap on an insulating plane.[8] The counter electrode is placed at infinity.

2. Dilute solution theory is applicable with constant transport and thermodynamic properties. Free convection is not taken into consideration.

3. For simplicity, the analysis is restricted to metal deposition from a single salt solution or to a single electrode reaction in the presence of excess supporting electrolyte. Migration is not accounted for explicity. Correction for migration effects can be introduced if needed by the method of successive approximations as discussed in detail elsewhere.[3,9-11] Also, there are no reactions occurring in the bulk of the electrolyte.

0 0 0 0 3 9 0 7 7 4 6

4. The fluid flow near the electrode is incompressible and laminar. Furthermore, the hydrodynamic boundary layer is thin (high Reynolds numbers), so that the boundary-layer solution of the Navier-Stokes equations is an adequate description of the hydrodynamic conditions near the surface.

5. Diffusion in the direction parallel to the electrode surface can be neglected whenever the diffusion layer is thin compared to the size of the electrode. It is further assumed that the diffusion layer is thin compared to the hydrodynamic boundary layer (high Schmidt numbers), so that the velocity components inside the diffusion layer can be approximated by their first terms in Taylor's expansions with respect to distance from the surface (equation 52).

6. Outside the diffusion layer, the concentrations are uniform, and as a consequence the potential in the bulk is governed by Laplace's equation. The gradient of the potential just outside the diffusion layer is proportional to the current density (equation 7), which in turn depends on mass transfer within the diffusion layer and the conditions at the electrode surface. As a result, the potential distribution in the bulk and the concentration distribution in the diffusion layer are coupled through the conditions prevailing at the electrode surface (see chapter 3). Mathematical treatment of the problem in the presence of this coupling may become excessively complex for nonsteady-state phenomena, and additional assumptions may be needed. These will be introduced later as they become necessary. Additional discussion relating to this assumption is given in section 3.5.

III. CONDITIONS AT THE ELECTRODE SURFACE

When current is applied to an electrochemical cell, two important processes occur at an electrode surface, namely, faradaic reaction and double-layer charging. The assessment of reaction rates and their relation to the current density lie in the field of electrode kinetics. Much work has been done in this area as reviewed by Vetter.[99] The treatment of the double-layer effects has been possible after the classical work of Grahame[41] concerning the structure of the double layer at an ideally polarizable electrode. Delahay and co-workers[42,45] discussed how one might account for the faradaic and charging effects simultaneously in working mass-transfer and current-distribution problems at nonideally polarized electrodes. More recently, Newman[1,6,11] has developed a method for analyzing electrochemical eells by considering the effects of mass transfer and potential distribution coupled with complex electrode conditions. Some of these methods are discussed here with possible simplifications for numerical analysis.

3.1. Thermodynamic Principles and Definitions

An electrode reaction of the form

$$\sum_i s_i M_i^{z_i} \rightarrow ne^- \qquad (3\text{-}1)$$

obeys the general equilibrium relationship

$$\sum_i s_i \mu_i = n\mu_{e^-} \quad , \qquad (3\text{-}2)$$

where M_i is the symbol for the chemical formula and μ_i is the electrochemical potential of species i, respectively. The stoichiometry of the chemical reaction requires

0 0 0 0 3 9 0 7 4 7

$$\sum_i s_i z_i = -n \quad . \tag{3-3}$$

For very dilute solutions, the electrochemical potential can be related to the electrostatic potential Φ by

$$\mu_i = RT \ln c_i + z_i F\Phi \quad . \tag{3-4}$$

The equilibrium states of the solution and the metal phases can thus be determined if Φ can be measured.

Newman[6] has introduced the idea of using reference electrodes to measure potentials in the solution. Consider a reference electrode, which moves in the solution with respect to a stationary reference electrode of the same kind. The manner in which the measured potential changes is expressed as

$$\nabla\mu_{e^-} = -F\nabla V_r \quad . \tag{3-5}$$

Consider also the situation, where the stationary electrode is a reference electrode of a "given kind." The potential relative to this electrode as measured by a reference electrode of a different kind and corrected for liquid-junction potentials is given by (see reference 11, section 40)

$$F(V_r - V_r') = -\mu_{e^-} - F\Phi + \text{const} \quad . \tag{3-6}$$

The constant term is characteristic of the given electrode; for a calomel electrode, for example, this is

$$\text{const} = \mu^o_{Hg} + \frac{1}{2}\mu^o_{Hg_2Cl_2} + RT \ln c_{Cl^-} \quad , \tag{3-7}$$

where μ_i^o is the electrochemical potential of a pure phase and c_{Cl^-} is the chloride concentration in the calomel-electrode compartment. The notion of measuring the potential in the solution between reference electrodes of the same kind and the definition of a potential with respect to a reference electrode of a given kind are well-defined thermodynamic constructions, which help to derive expressions for nonthermodynamic quantities such as the overpotentials in terms of measurable properties.

A few additional definitions useful for the purposes of this chapter follow from the theory of the double layer.[41] The charge density on the metal side of the double layer is given by

$$q = - F \sum_i z_i \Gamma_i \quad , \tag{3-8}$$

where Γ_i is defined as the moles of species i per unit area, which is in excess at the interface over the amount which would be present in the solution if the concentrations remained uniform. The differential capacity of the electric double layer is the derivative of the surface-charge density with respect to the potential at constant composition:

$$C = (\partial q/\partial U)_{\mu,T} \quad . \tag{3-9}$$

This is a physical property of the double layer and has to be determined experimentally.

3.2. Concentration Overpotential

Let us place two reference electrodes of the same kind as the working electrode, one (r1) just outside the electric double layer and the other (r2) outside the diffusion layer as indicated in figure 1,

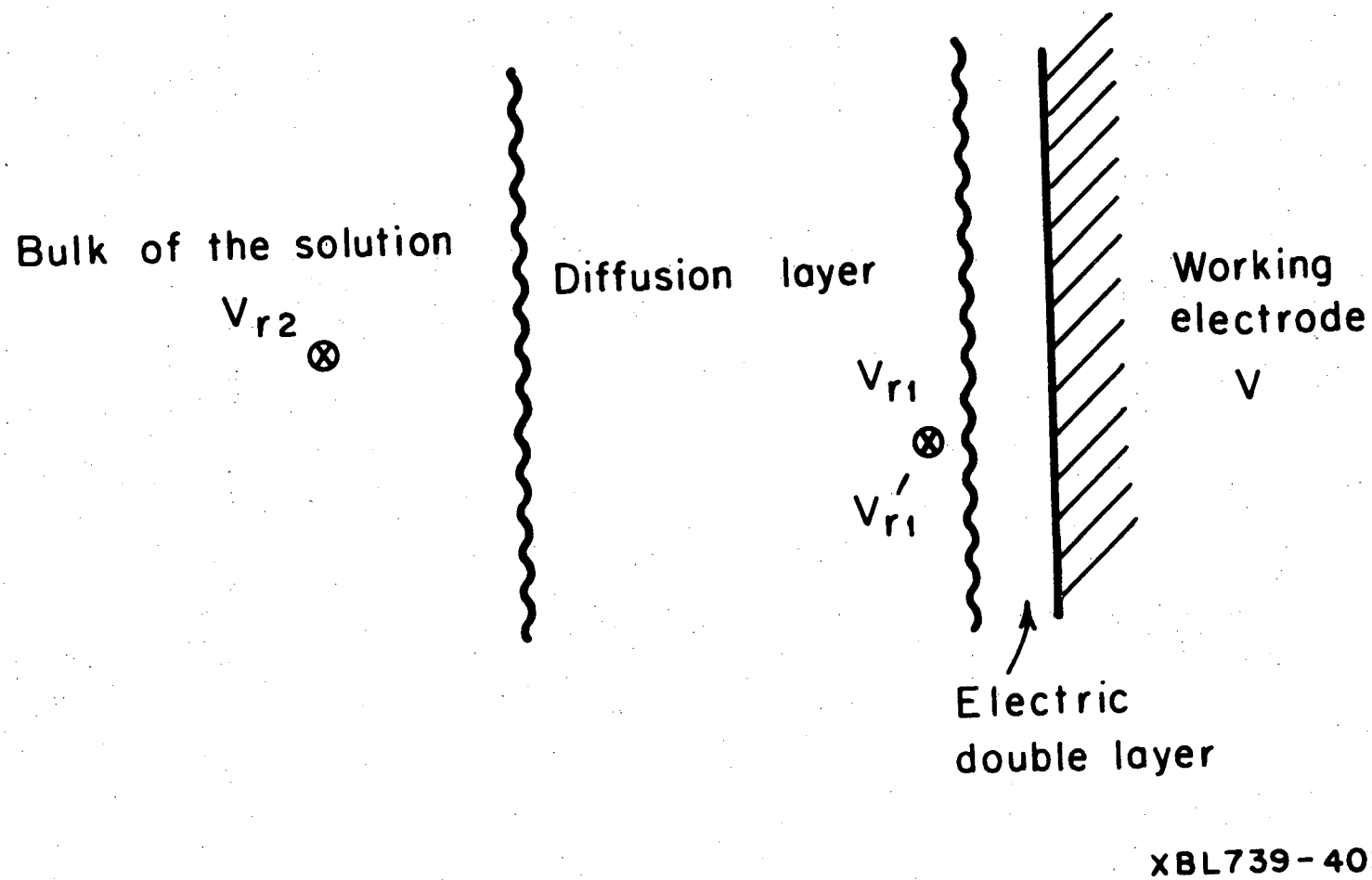

Figure 3-1. Schematic representation of the positions of reference electrodes relative to the working electrode in the thermodynamic construction. The primed quantity is the potential of an electrode of a given kind, whereas the unprimed quantities are the potentials of electrodes of the same kind.

0 0 0 3 0 9 4 8

and let $\Delta\Phi_{ohm}$ ($= \Phi_o - \Phi_\infty$) be the potential difference between these electrodes when there is the same current distribution but no concentration variations. The concentration overpotential is then defined as[6]

$$\eta_c = V_{r1} - V_{r2} - \Delta\Phi_{ohm} \quad . \tag{3-10}$$

Application of the thermodynamic principles of the previous section gives, with the aid of equations 2-3, 2-5, and 2-8,

$$\eta_c = i_n \int_0^\infty \left(\frac{1}{\kappa} - \frac{1}{\kappa_\infty}\right) dy + \frac{RT}{nF} \sum_i s_i \ln \frac{c_{i\infty}}{c_{io}} + \int_0^\infty \left[\sum_i \frac{z_i D_i}{\kappa} \frac{\partial c_i}{\partial y}\right] dy \quad , \tag{3-11}$$

where the subscripts o and ∞ refer to the electrode surface and the bulk of the solution, respectively. In the presence of excess supporting electrolyte, conductivity variations in the solution are negligible. The last term is on the order of the reactant concentration divided by the supporting electrolyte concentration and is therefore small relative to the second term. Thus, equation 11 reduces to

$$\eta_c = \frac{RT}{nF} \sum_i s_i \ln \frac{c_{i\infty}}{c_{io}} \quad . \tag{3-12}$$

Newman[6] also proposes the approximate form

$$\eta_c = \frac{(z_+ - z_-)\ RT}{z_+ z_- F} \left[\ln \frac{c_\infty}{c_o} - t_+ \left(1 - \frac{c_o}{c_\infty}\right)\right] \tag{3-13}$$

for metal deposition in a binary salt solution (see also reference 11, section 126). This expression is obtained from equation 11 by assuming

0 0 0 0 3 9 0 7 4 9

a linear concentration distribution across the diffusion layer and expressing the diffusivities by the Nernst-Einstein expression

$$D_i = RTu_i \quad . \tag{3-14}$$

Equation 8 is substituted for the conductivities, and the transference number is given by

$$t_+ = 1 - t_- = \frac{z_+ D_+}{z_+ D_+ - z_- D_-} \quad . \tag{3-15}$$

3.3. Surface Overpotential, Faradic Current, and Electrode Potential

The surface overpotential represents the departure of the working electrode from its equilibrium potential. In terms of the potential with respect to the reference electrode rl defined above, this can be written as

$$\eta_s = V - V_{rl} \quad . \tag{3-16}$$

The surface overpotential is assumed to be related to the faradaic current by the semi-empirical Butler-Volmer expression,

$$i_f = i_o(c_\infty) \left(\frac{c_o}{c_\infty}\right)^\gamma \left[\exp\left(\frac{\alpha_a F}{RT} \eta_s\right) - \exp\left(-\frac{\alpha_c F}{RT} \eta_s\right)\right] , \tag{3-17}$$

where $i_o(c_\infty)$ is the exchange-current density at the bulk composition, α_a, α_c, and γ are kinetic parameters for the electrode reaction. For small current densities $|i_f| \ll i_o$, equation 17 can be approximated with the linear expression

$$i_f = i_o(\alpha_a + \alpha_c) \frac{F}{RT} \eta_s \quad . \tag{3-18}$$

In the other extreme, where the current density is large, the overpotential is also large, so that equation 17 reduces to the Tafel expression,

$$\eta_s = - \frac{RT}{\alpha_c F} (\ln|i_f| - \ln i_o) \quad , \tag{3-19}$$

this one expressing a cathodic process. For anodic currents, α_c is replaced by $-\alpha_a$. In equations 18 and 19, $i_o = i_o(c_\infty)(c_o/c_\infty)^\gamma$, that is, the exchange-current density is concentration dependent.

In the absence of double-layer effects, the faradaic current is related to the flux by Faraday's law,

$$N_{io} = - \frac{i_f s_i}{nF} \quad . \tag{3-20}$$

For metal deposition in a binary solution, the faradaic current can be related to the concentration derivative of the salt at the electrode surface by eliminating the potential between the flux expressions (equation 2-1) for the anion and the cation:

$$\left.\frac{\partial c}{\partial y}\right|_{y=0} = - \frac{i_f(1 - t_+)}{z_+ \nu_+ FD} \quad . \tag{3-21}$$

We now wish to relate the overpotentials to the potential of the working electrode V. Equation 10 can be written as

$$\eta_c = V + V_{r1} - V - V_{r2} + \Phi_\infty - \Phi_o \quad . \tag{3-22}$$

The quantity $\Phi_\infty - V_{r2}$ in effect represents the potential difference between two reference electrodes of the same kind at the same location in the bulk and is therefore zero. Substitution of the definition for the surface overpotential gives

0 0 0 0 5 9 0 . 7 5 0

$$V = \eta + \Phi_o \quad , \tag{3-23}$$

where

$$\eta = \eta_c + \eta_s \tag{3-24}$$

is the total overpotential. The electrode potential should be regarded as determined by a reference electrode of the same kind placed at infinity with respect to the working electrode. Φ_o represents the ohmic drop calculated for the actual current distribution and extrapolated to the electrode surface. It does not contain any contributions due to concentration variations in the solution, which are compensated fully by the concentration overpotential.

3.4. Double-Layer Effects

In the presence of double-layer charging, Faraday's law has to be corrected for double-layer effects, and the surface flux is given by

$$N_{io} = - \frac{\partial \Gamma_i}{\partial t} - \frac{s_i i_f(\eta_s, c_j)}{nF} \quad . \tag{3-25}$$

Substitution into equation 2-4 gives an expression for the current density,

$$i_n = \frac{\partial q}{\partial t} + i_f(\eta_s, c_j) \quad , \tag{3-26}$$

where the surface-charge density q is defined by equation 8. The derivative can be expanded to read

$$\frac{\partial q}{\partial t} = \left[\frac{\partial q}{\partial (V - V'_{rl})}\right]_{c_{io}} \frac{\partial (V - V'_{rl})}{\partial t} + \sum_i \left(\frac{\partial q}{\partial c_{io}}\right)_{V-V'_{rl}, c_{jo,j\neq i}} \frac{\partial c_{io}}{\partial t} , \qquad (3\text{-}27)$$

where V'_{rl} is the potential of a reference electrode of a given kind placed just outside the double layer. The quantity $[\partial q/\partial (V - V'_{rl})]_{c_{io}}$ can be identified as the double-layer capacity defined by equation 9. The derivative $\partial (V - V'_{rl})/\partial t$ can be determined by writing

$$\begin{aligned} \frac{\partial (V - V'_{rl})}{\partial t} &= \frac{\partial}{\partial t} (V - V_{rl} - V'_{rl} + V_{rl}) \\ &= \frac{\partial \eta_s}{\partial t} + \frac{\partial}{\partial t} (V_{rl} - V'_{rl}) \quad . \end{aligned} \qquad (3\text{-}28)$$

Substitution of equations 6, 2, and 4 in that order gives

$$\frac{\partial (V - V'_{rl})}{\partial t} = \frac{\partial \eta_s}{\partial t} - \frac{RT}{nF} \frac{\partial}{\partial t} \sum_i s_i \ln c_{io} \quad . \qquad (3\text{-}29)$$

Comparison with equation 11 suggests

$$\begin{aligned} \frac{\partial (V - V'_{rl})}{\partial t} = \frac{\partial (\eta_s + \eta_c)}{\partial t} &- \frac{\partial}{\partial t} \int_0^\infty i_n \left(\frac{1}{\kappa} - \frac{1}{\kappa_\infty}\right) dy \\ &- F \frac{\partial}{\partial t} \int_0^\infty \left[\sum_i \frac{z_i D_i}{\kappa} \frac{\partial c_i}{\partial y}\right] dy \quad . \end{aligned} \qquad (3\text{-}30)$$

In the presence of excess supporting electrolyte, the last two terms can be dropped.

The derivatives of the type $(\partial q/\partial c_{io})_{V-V_{rl}, c_{jo,j\neq i}}$ are thermodynamic properties of the electric double layer. They either have to be

0 0 3 0 3 9 0 / / 5 1

measured experimentally[41] or estimated from the microscopic theory of the electric double layer (see reference 11, section 52). Delahay and co-workers[43-45] offer some discussion on how to evaluate these derivatives.

Simplifications of the flux equation are possible under certain conditions. If the results of this section so far are combined and simplifications introduced for the presence of an excess amount of supporting electrolyte, equation 25 reads

$$N_{io} = -D_i \left.\frac{\partial c_i}{\partial y}\right|_{y=0}$$

$$= -\frac{\partial \Gamma_i}{\partial t} - \frac{s_i}{nF}\left[i_n - C\frac{\partial \eta}{\partial t} + \sum_i \left(\frac{\partial q}{\partial c_{io}}\right)_{V-V_{rl},\ c_{jo,j\neq i}} \frac{\partial c_{io}}{\partial t}\right]. \qquad (3\text{-}31)$$

We would like to reduce this further by assuming that a single reactant is present, and the supporting electrolyte is the major contributor to the double-layer charge on the solution side. We also neglect the concentration variations of the supporting electrolyte just outside the double layer. Thus, equation 31 can be approximated as

$$D_R \left.\frac{\partial c_R}{\partial y}\right|_{y=0} = \frac{s_R}{nF}\left(i_n - C\frac{\partial \eta}{\partial t}\right), \qquad (3\text{-}32)$$

where the subscript R refers to the reactant. This is the form of the flux expression which has been criticized by Delahay.[42] The capacitive term represents here the charging current, and subtracting this from the measured current gives the faradaic current and therefore equation 20.

This constitutes an a priori separation of the faradaic and charging currents and is not permitted if the correct form of the flux expression, equation 31, is used. As Delahay shows, equation 32 is a good approximation only if the electrode reaction is highly reversible, so that the faradaic term dominates in the flux equation for the reactant.

Another type of simplification is justified if concentration variations can be ignored such as in well-stirred solutions. Equation 26 then reduces to

$$i_n = C \frac{\partial \eta}{\partial t} + i_f(\eta_s, c_{j\infty}) \quad . \tag{3-33}$$

Combining with equation 2-8 gives

$$- \kappa \left.\frac{\partial \Phi}{\partial y}\right|_{y=0} = C \frac{\partial \eta}{\partial t} + i_f(\eta_s, c_{j\infty}) \quad . \tag{3-34}$$

If faradaic reactions are not permitted (ideally polarizable electrode[41]), this further reduces to the form

$$- \kappa \left.\frac{\partial \Phi}{\partial y}\right|_{y=0} = C \frac{\partial (V - \Phi_o)}{\partial t} \quad . \tag{3-35}$$

Despite their shortcomings, the simple forms of surface conditions developed in this chapter are very useful for studying the behavior of electrochemical systems mainly because they are tractable for mathematical analysis. It is also possible, with the aid of these equations, to isolate certain aspects of the electrode phenomena for study in the absence of other complicating effects. In this way, one can obtain a better understanding of the roles played by different effects to

0 0 0 0 3 9 0 : / 5 2

determine the overall electrode behavior. Various complications can be introduced systematically as indicated. For example, equation 35 singles out the capacitive charging effect only. Equation 34 introduces the faradaic reaction term. Faraday's law is adequate in most cases to account for the surface conditions at steady state. It can also be used perhaps for nonsteady state situations in the presence of a purely reversible electrode reaction. Equation 32 adds on the effect of double-layer charging. More complex phenomena are included in equations 30 and 31.

3.5. Statement of the Mathematical Problem and the Method of Solution

We would like to investigate the current distribution and mass transfer at rotating disk and spherical electrodes with the consideration of complex electrode conditions such as a faradaic reaction and/or double-layer charging. This can be accomplished by solving the basic flux equation 2-1 to satisfy the general boundary condition 25 at the electrode surface. This is a complex problem due to the fact that the potential distribution and mass transfer are coupled and cannot be treated separately unless one or the other can be neglected. In well-stirred solutions, concentrations are uniform; hence, the problem involves the solution of Laplace's equation, as discussed in section 2.2, to satisfy the condition 34. If the effect of the electric field can be ignored, a solution of the convective diffusion equation only is necessary. Some results are given in section 2.4.

When both the electric field and mass-transfer effects are present, a straightforward method of solution is not possible. Newman[6] has made a significant contribution by developing a method for treating problems of this kind for thin diffusion layers. In the limit of high Péclet numbers, the diffusion layer is vanishingly thin. Thus, as far as the potential distribution is concerned, the concentrations are uniform in the solution, and Laplace's equation applies so as to satisfy the current distribution at the electrode surface. The diffusion layer can be treated as a separate region where the convective diffusion equation applies so as to satisfy the same current distribution at the surface as the potential and the condition of uniform concentration far from the electrode. Hence, the two solutions have to match through the boundary conditions specified at the surface. This is a singular-perturbation problem.

Nonsteady-state problems of this type are very complicated (see chapter 6) and tractable only in very few specialized cases, such as the convective Warburg problem.[46,47] However, efficient and generalized numerical methods[48] are available to treat the steady-state problem for almost any type of conditions at the electrode surface as long as the hydrodynamics are known, and Laplace's equation can be solved for an arbitrary current distribution at the surface. The numerical procedure consists of an iterative solution of equation 2-62 or 2-63 together with appropriate expressions of Faraday's law, and the surface and concentration overpotentials as derived in this chapter, and an expression for the potential in the solution, such as equation 2-13 for the disk and equation 2-25 for the sphere, evaluated at the surface.

0 3 3 0 3 9 0 , 7 5 3

Hence, a total of six equations are needed to solve for the six unknowns, c_o, $(\partial c/\partial y)_{y=0}$, i_n, η_s, η_c, and Φ_o. This method has been applied to a number of electrode geometries.[7,48-53] Some results are given for the disk in the next chapter and for the sphere in chapter 5.

IV. CURRENT DISTRIBUTION ON A ROTATING DISK BELOW THE LIMITING CURRENT

Since Levich[3] showed that the limiting current distribution is uniform on a rotating disk electrode (see equation 2-59), the disk surface has been assumed for a long time to be uniformly accessible to mass transfer also at current levels below the limiting current.[5] Newman[14] disputed this based on the reasoning that if the current distribution is intermediate between the two extreme cases of limiting current and primary current distributions, it can no longer remain uniform since the primary distribution is highly nonuniform. He went on to prove this by a detailed analysis of the current-distribution problem with the consideration of mass-transfer limitations near the disk, the influence of ohmic drop in the solution, and the effect of complex kinetics at the electrode surface.[7,50] Newman's results have been verified many times experimentally by direct measurement of the thickness of an electrodeposited metal,[54,55] measurements of the collection efficiencies on ring-disk systems,[28,55-59] application of sectioned disk electrodes,[28] and direct potential mapping by reference probes near the surface of the disk.[99,95]

Some of these results are reviewed here along with a few recent calculations. The emphasis is on the secondary distribution, which is needed in the formulation of the transient response of a disk (see chapters 7 and 8), and results for Tafel kinetics, which may be interesting to compare with the analogous results for the sphere reported in the next chapter.

4.1. Secondary Distribution for Linear Kinetics

The diffusion layer near a disk electrode can be neglected when the rate of stirring is high (high rotation speeds), so that $|i_f| << |i_{lim}|$. Under these conditions, the secondary current distribution is said to prevail at the disk surface.[7] Furthermore, for sufficiently small current densities $|i_f| << i_o$, the kinetics of the electrode reaction can be linearized, and the current density can thus be expressed by equation 3-18. In dimensionless form, this is

$$\frac{i_f r_o}{\kappa} = -\frac{1}{\eta}\left.\frac{\partial \Phi^{ss}}{\partial \xi}\right|_{\xi=0} = J(V^{ss} - \Phi_o^{ss}) \quad , \tag{4-1}$$

where η and ξ are the rotational elliptic coordinates (equation 2-14), and

$$J = i_o r_o F(\alpha_a + \alpha_c)/RT\kappa \tag{4-2}$$

is the dimensionless exchange-current density. The superscript ss denotes steady state and has been added here to distinguish the potentials for the secondary distribution from the potentials corresponding to the primary distribution (section 2.2) and the transient distribution (chapters 7 and 8).

The potential in the solution can be expressed as (see section 2.2)

$$\Phi^{ss}/\Phi_o^p = \sum_{n=0}^{\infty} B_n^{ss} P_{2n}(\eta)\, M_{2n}(\xi) \quad . \tag{4-3}$$

The choice of Φ_o^p ($= I/4r_o\kappa$) as the scaling factor is mathematically convenient since this normalizes the numerical value of B_o^{ss} to unity regardless of the electrode conditions. Combining equations 1 and 3

and employing the orthogonality properties of the Legendre polynomials give

$$V^{ss}/\Phi_o^p = 1 + 4/\pi J + 2 \sum_{n=1}^{\infty} a_{o,n} B_n^{ss} \quad , \tag{4-4}$$

and

$$\sum_{n=1}^{n_{max}} \left[a_{m,n} - 2a_{o,m}\, a_{o,n} - \delta_{m,n} \frac{M'_{2m}(0)}{(4m+1)\, J} \right] B_n^{ss} = \frac{4}{\pi J}\, a_{o,m} \tag{4-5}$$

$$(m = 1, 2, \ldots, n_{max}) \ ,$$

where

$$a_{m,n} = \int_0^1 \eta\, P_{2m}(\eta)\, P_{2n}(\eta)\, d\eta \quad , \tag{4-6}$$

$$a_{o,m} = \int_0^1 \eta\, P_{2m}(\eta)\, d\eta = - \frac{P_{2m}(0)}{2(2m-1)(m+1)} \quad , \tag{4-7}$$

$$\delta_{m,n} = \begin{cases} 0 & \text{if } m \neq n \ , \\ 1 & \text{if } m = n \ . \end{cases} \tag{4-8}$$

The series in equations 4 and 5 are truncated at n_{max} for the purposes of numerical calculation, which involves a straightforward matrix-inversion operation. The coefficients B_n^{ss} have been computed for various J values[60] by picking $n_{max} = 45$. Values for the first 10 terms in the series are listed in Table 4-1. The quantity V^{ss}/Φ_o^p, which can directly be calculated from equation 4 once B_n^{ss} are obtained from equation 5, is identified as the dimensionless, effective direct-current resistance[61] $4r_o \kappa R_{eff}$ for the disk system with the reference electrode at infinity. Some values are given in Table 4-2 for various J values.

0 0 0 0 0 0 0 0 0 0

Table 4-1. The coefficients B_n^{ss} in the series for the steady state potential.

n	J = 0	J = 0.1	J = 1	J = 10
0	1.00000	1.00000	1.00000	1.00000
1	0.31250	0.30731	0.26863	0.13306
2	-0.05273	-0.05446	-0.06568	-0.07356
3	0.01984	0.02040	0.02491	0.04037
4	-0.00993	-0.01019	-0.01232	-0.02324
5	0.00580	0.00594	0.00713	0.01423
6	-0.00373	-0.00382	-0.00455	-0.00926
7	0.00256	0.00262	0.00312	0.00636
8	-0.00185	-0.00189	-0.00224	-0.00456
9	0.00139	0.00142	0.00168	0.00339
10	-0.00107	-0.00110	-0.00130	-0.00260

Table 4-2. The effective direct-current resistance $4r_o{}^{KR}{}_{eff}$ ($= V^{ss}/\Phi_o^p$) at different values of the parameter J.

J	$4r_o{}^{KR}{}_{eff}$
0.1	13.81194
0.2	7.44458
0.5	3.62161
1	2.34368
2	1.69962
5	1.30375
10	1.16459
20	1.09002
50	1.04072
100	1.02231
200	1.01217
500	1.00543

0 0 0 0 0 9 0 / / 5 6

The current distribution is determined from equation 1. The results are shown in figure 1. The extreme case where J=∞ corresponds to a reversible faradaic reaction for which the current distribution approaches the primary distribution as a limit.

The restuls for J = 0 correspond to the other extreme case where the passage of current from the metal to the solution phase is not permitted; thus, a faradaic reaction cannot occur. This type of an electrode is said to be ideally polarizable.[41] If one tries to force a constant current I through a cell with an ideally polarizable electrode, the current will be used to charge up the double-layer capacity. The charging process will continue as long as the current is applied, and this will cause a continuous rise in the electrode potential only to be interrupted by perhaps hydrogen or oxygen evolution (see chapter 7). At the instant current is applied, the current distribution is nonuniform on the electrode since the primary distribution is nonuniform. Shortly afterwards, the current distribution is rendered uniform as the surface charge redistributes itself quickly. As a result, the potential distribution in the solution reaches a steady state even though the electrode potential keeps increasing. The boundary condition 1 can be written for this situation in the form

$$- (\partial \Phi^{ss}/\partial \xi)_{\xi=0} /\eta = I/\pi r_o \kappa \quad , \tag{4-9}$$

which allows one to express the coefficients B_n^{ss} explicitly:

$$B_n^{ss} = - 4a_{o,n}(4n + 1)/\pi M'_{2n}(0) = - \frac{(4n + 1)[P_{2n}(0)]^3}{(2n - 1)(n + 1)} \quad . \tag{4-10}$$

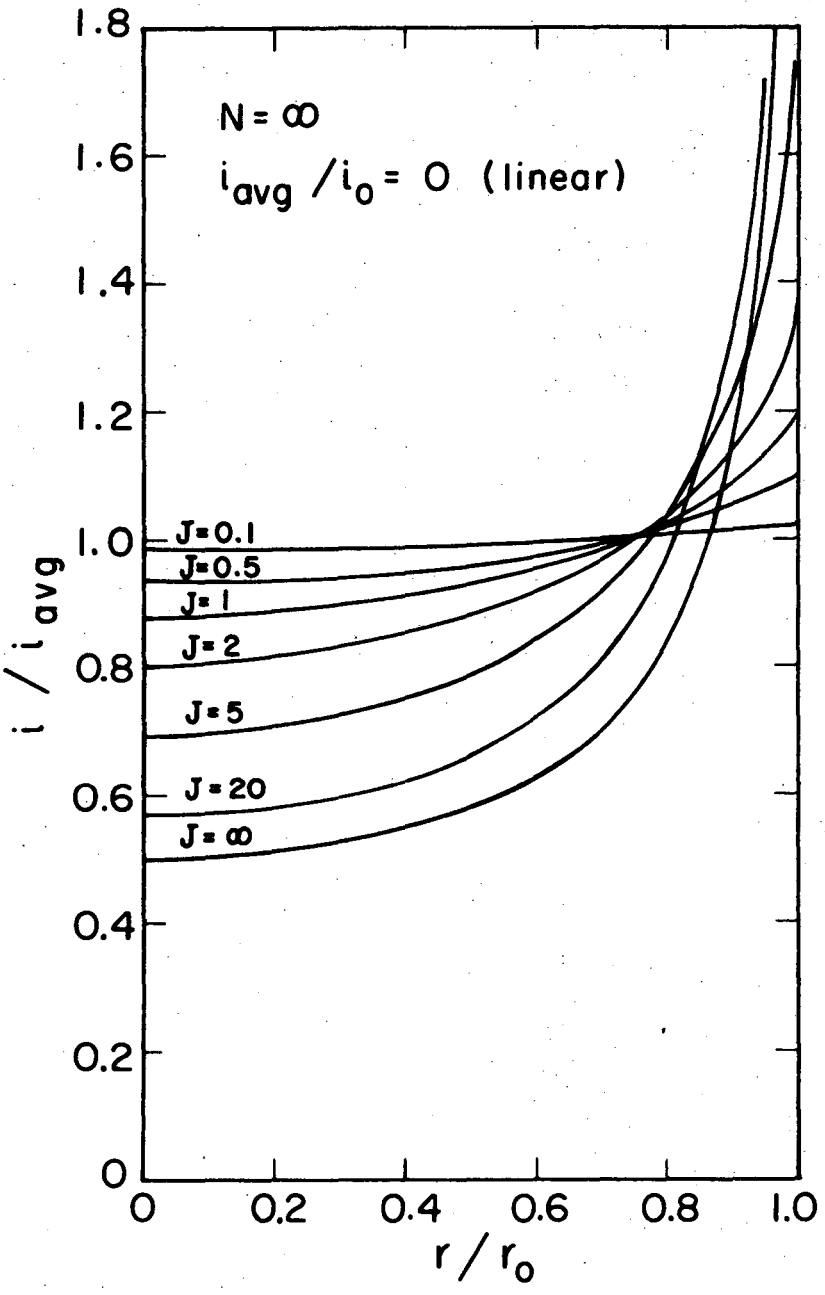

Figure 4-1. Secondary current distribution for linear polarization (from reference 7).

0 0 0 0 5 9 0 7 1 5 7

The potential distribution obtained under these circumstances is identical to the potential distribution which exists on a nonideally polarized electrode at limiting current conditions (see figure 4-6).

Newman[7] reports additional results for the secondary distribution at higher current levels, where the linear kinetic expression no longer holds.

4.2. Secondary Distribution in the Presence of a Highly Reversible Electrode Reaction

For large but finite exchange-current densities, the current distribution approximates closely the primary distribution on the disk except near the edge, where the faradaic impedance is large enough to force the current density to remain finite. Numerical results for this case are difficult to obtain by the method of the previous section because a large number of terms are required in the series. An asymptotic expression for the potential can be derived by employing the singular-perturbation technique.[62] The singular nature of this problem has been recognized earlier;[61] however, its consequences were not of immediate interest. The analysis is outlined here to render more complete the overall treatment of the secondary distribution at a disk electrode. A similar problem is encountered for the short-time response of a disk electrode and is treated in chapter 9. Still another problem of the same type at high frequencies for the alternating-current distribution on a disk electrode has been treated by Newman.[61] We follow here the same guidelines in the mathematical formulation as developed in that paper.

Since the current density is small compared to the exchange-current density, we can safely assume linear kinetics and use equation 1 to

express the conditions at the electrode surface. The potential outside the edge region is given by the primary distribution. As approximated for small ξ, this condition can be expressed by

$$\Phi^{ss}/V^{ss} = 1 - \frac{2}{\pi}\tan^{-1}\xi \approx 1 - 2\xi/\pi \quad \text{as} \quad \xi \to \infty \quad . \tag{4-11}$$

Furthermore, the condition on the insulating surface is given by

$$\partial\Phi^{ss}/\partial\eta = 0 \quad \text{at} \quad \eta = 0 \quad . \tag{4-12}$$

A set of stretched variables can be defined for the edge region as follows:

$$\bar{\Phi} = \frac{\pi}{2}\,(1 - \Phi^{ss}/V^{ss})\,\sqrt{J} \quad , \tag{4-13}$$

$$\bar{\eta} = \eta\,\sqrt{J} \quad , \quad \bar{\xi} = \xi\sqrt{J} \quad . \tag{4-14}$$

Substitution into Laplace's equation and the boundary conditions yields the system

$$\frac{\partial^2\bar{\Phi}}{\partial\bar{\eta}^2} + \frac{\partial^2\bar{\Phi}}{\partial\bar{\xi}^2} = 0 \quad , \tag{4-15}$$

$$\partial\bar{\Phi}/\partial\bar{\xi} = \bar{\eta}\bar{\Phi} \quad \text{at} \quad \bar{\xi} = 0 \quad , \tag{4-16}$$

$$\partial\bar{\Phi}/\partial\bar{\eta} = 0 \quad \text{at} \quad \bar{\eta} = 0 \quad , \tag{4-17}$$

$$\bar{\Phi} \to \bar{\xi} \ \text{as} \ \bar{\eta}^2 + \bar{\xi}^2 \to \infty \quad . \tag{4-18}$$

The solution to this system of equations was obtained numerically by finite-difference methods. The method has been described in detail by Klingert et al.[63] Doubling and overrelaxation techniques were employed to increase accuracy and speed up convergence, respectively.

These are discussed lucidly by Fleck[33] in a report where he has also developed a generalized computer program to solve Laplace's equation for arbitrary electrode geometries and boundary conditions. The overrelaxation factor used here was 1.9, the value suggested by Fleck for an L-shaped cell geometry. A listing of the computer program is given in appendix F. The results are plotted in figure 2.

The steady-state current or potential can be calculated from

$$1 - \phi_o^p/V^{ss} = 1 - I/4r_o\kappa V^{ss} = 1 - 1/4r_o\kappa R_{eff} = \int_0^1 (1 - \phi_o^{ss}/V^{ss})\, d\eta = \frac{1}{\pi J} \ln J + A/J \quad , \tag{4-19}$$

where

$$A = \frac{2}{\pi}\left\{\int_0^b \bar{\phi}_o d\bar{\eta} + \int_b^\infty (\bar{\phi}_o - 1/\bar{\eta})\, d\bar{\eta} - \ln b\right\} = 0.708 \quad . \tag{4-20}$$

These formulas are derived in appendix G. Figure 3 shows a comparison between the present results and the values for the dimensionless, effective direct-current resistance obtained in the previous section. The two results agree quite well for large values of J.

4.3. The Effect of Concentration Polarization[7]

At high current levels and moderate stirring rates, the concentration effects cannot be ignored, and therefore the diffusion layer has to be taken into consideration. This is no longer an elementary problem because the convective diffusion equation and Laplace's equation have to be solved simultaneously to satisfy the conditions at the surface

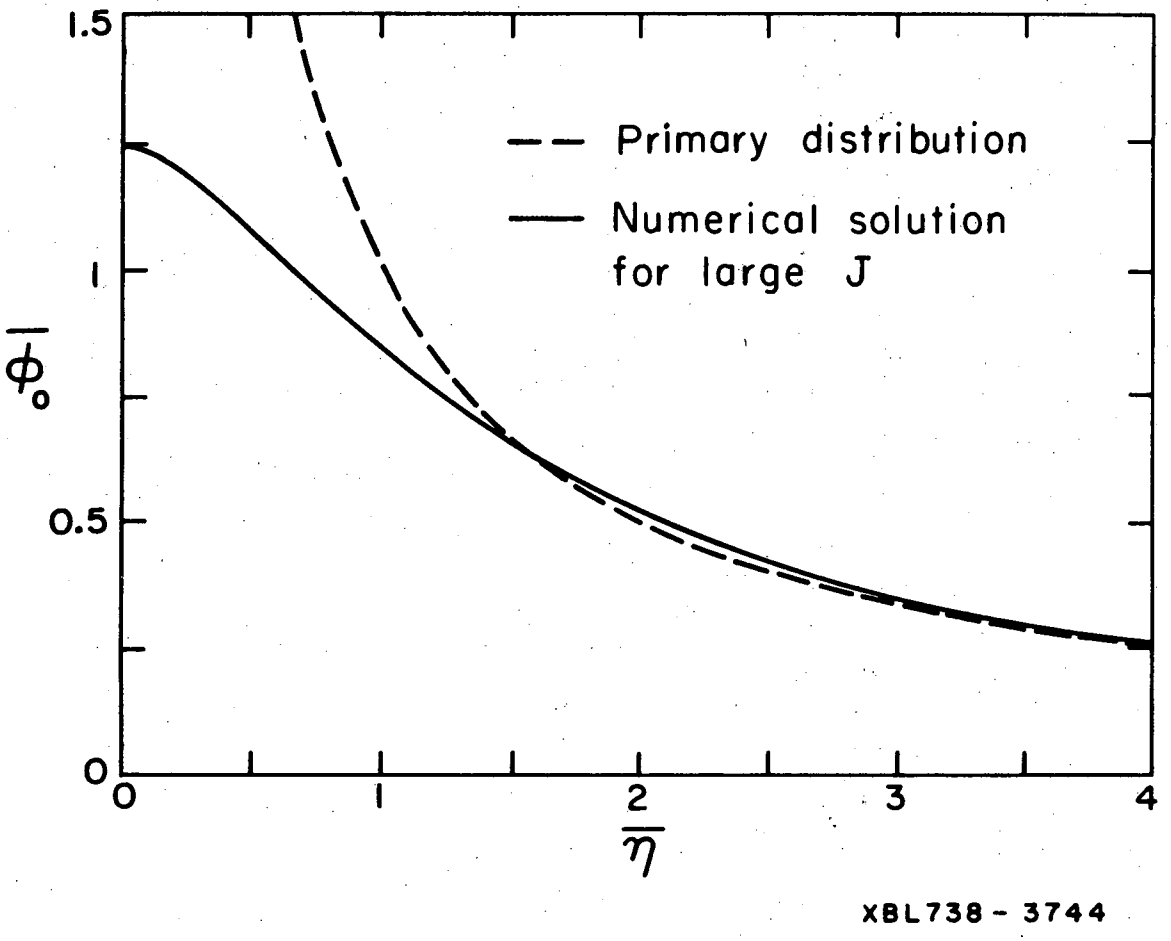

Figure 4-2. The surface potential distribution for large values of the kinetic parameter J near the edge of a disk electrode.

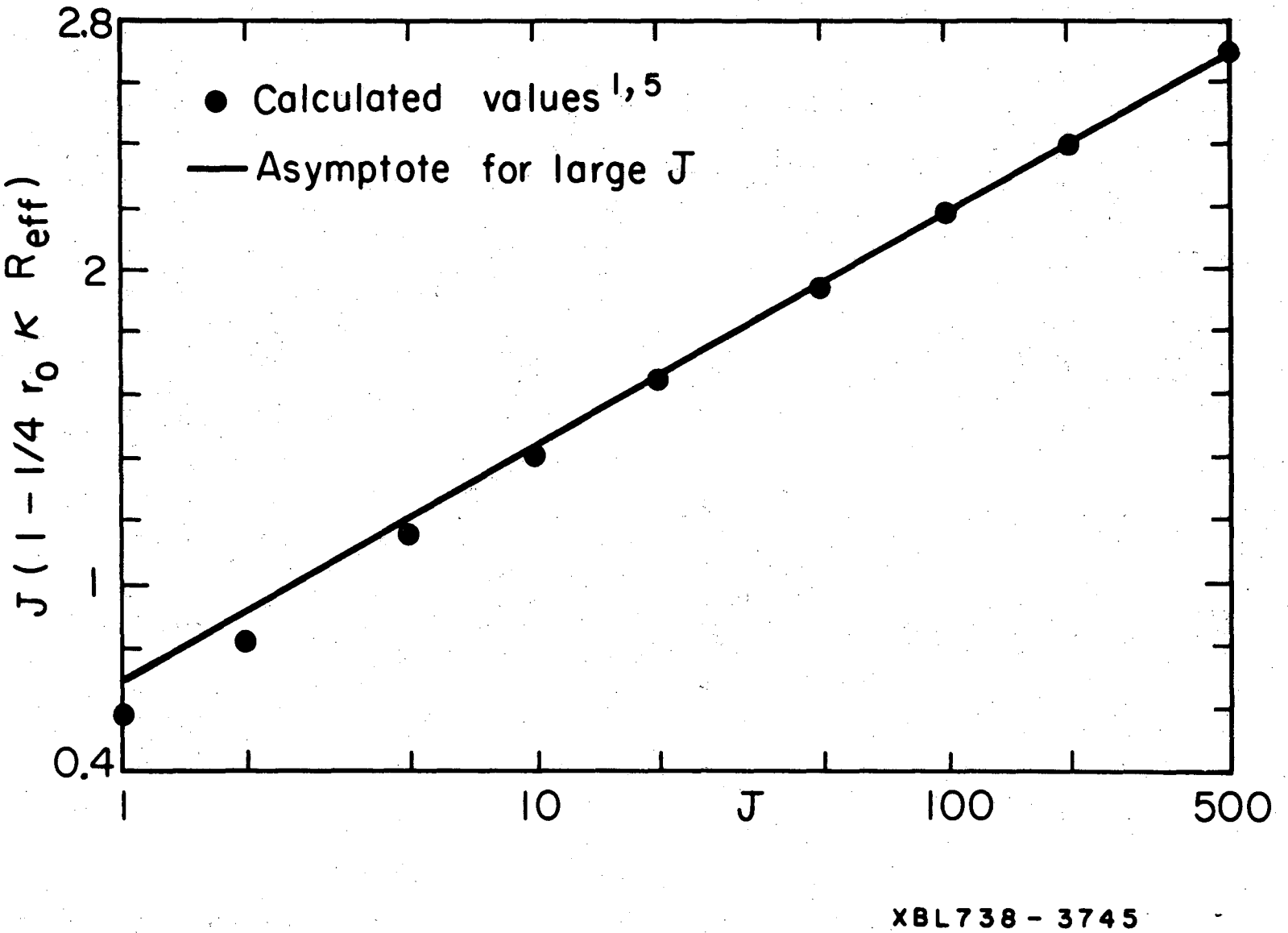

Figure 4-3. The dependence of the effective direct-current resistance on the kinetic parameter J.

6 5 / 0 6 5 0 0 0 0

as described in section 3.5. The concentration overpotential is assumed to be given by equation 3-12 in the presence of excess supporting electrolyte and equation 3-13 for a binary system. Furthermore, the effects of the other species, which may be present besides the limiting reactant in a solution with excess supporting electrolyte, are ignored as a simplifying measure. Otherwise, the convective diffusion equation has to be solved for each species, and the concentrations of these species have to be considered in calculating the overpotentials. The numerical procedure can be modified without much effort, but with increased computation time, to account for these additional complications, if necessary. The details of the mathematical analysis and the numerical method are given in appendix A.

A scaling of all parameters which appear in the problem suggests that the results can be best presented in terms of the dimensionless quantities[7] (see also appendix A),

$$J = \frac{i_o r_o ZF}{RT\kappa_\infty} \tag{4-21}$$

$$N = -\frac{NZF^2 D_R c_{R\infty}}{s_R RT\kappa_\infty (1-t_+)} \sqrt{\frac{r_o^2 \Omega}{\nu}} \left(\frac{a\nu}{3D}\right)^{1/3}, \tag{4-22}$$

in addition to the kinetic parameters α_a/Z, α_c/Z, and γ, and the transference number t_+. The parameter Z is equal to $-z_+z_-/(z_+ - z_-)$ for a single salt and $-n/s_R$ with supporting electrolyte, and a = 0.51023. In the presence of excess supporting electrolyte, D_R is the diffusion coefficient of the limiting reactant; for a solution of a single salt, D_R is the diffusion coefficient of the salt. The current level i_{ave}/i_{lim}

0 0 0 0 3 9 0 7 7 6 0

also has to be specified for a complete definition of a case problem.

The effect of varying the dimensionless exchange current density J has been demonstrated for the case of secondary distribution. Another parametric study of that type is not included in this section because the results are qualitatively similar to those of section 1; an increase in J, while the other parameters are held constant, causes the current distribution to become more nonuniform.

The parameter N can be regarded as a dimensionless limiting current; it represents the importance of mass transfer in the diffusion layer. For example, an increase in the rotation speed Ω facilitates convection, and as a result the electrode reaction can become mass-transfer limited at increasingly higher current densities. Large current densities in turn cause large ohmic drops relative to the magnitude of the concentration overpotential. As the ohmic drop becomes a major factor in determining the electrode potential, the secondary distribution is approached more closely. In addition, if the applied current is much above the exchange-current density, the kinetic effects are small, the solution is well-stirred, and the current distribution resembles the primary distribution. This state of affairs is demonstrated dramatically for the case of Tafel kinetics as depicted in figures 4 and 5. The exchange-current density contributes a constant term to the kinetic expression, equation 3-19, and hence its actual value is not important. As the figures show, the concentration and current distributions become more nonuniform with increasing values of N, but they are still limited by mass transfer at large current levels. The current density can also exceed the limiting current

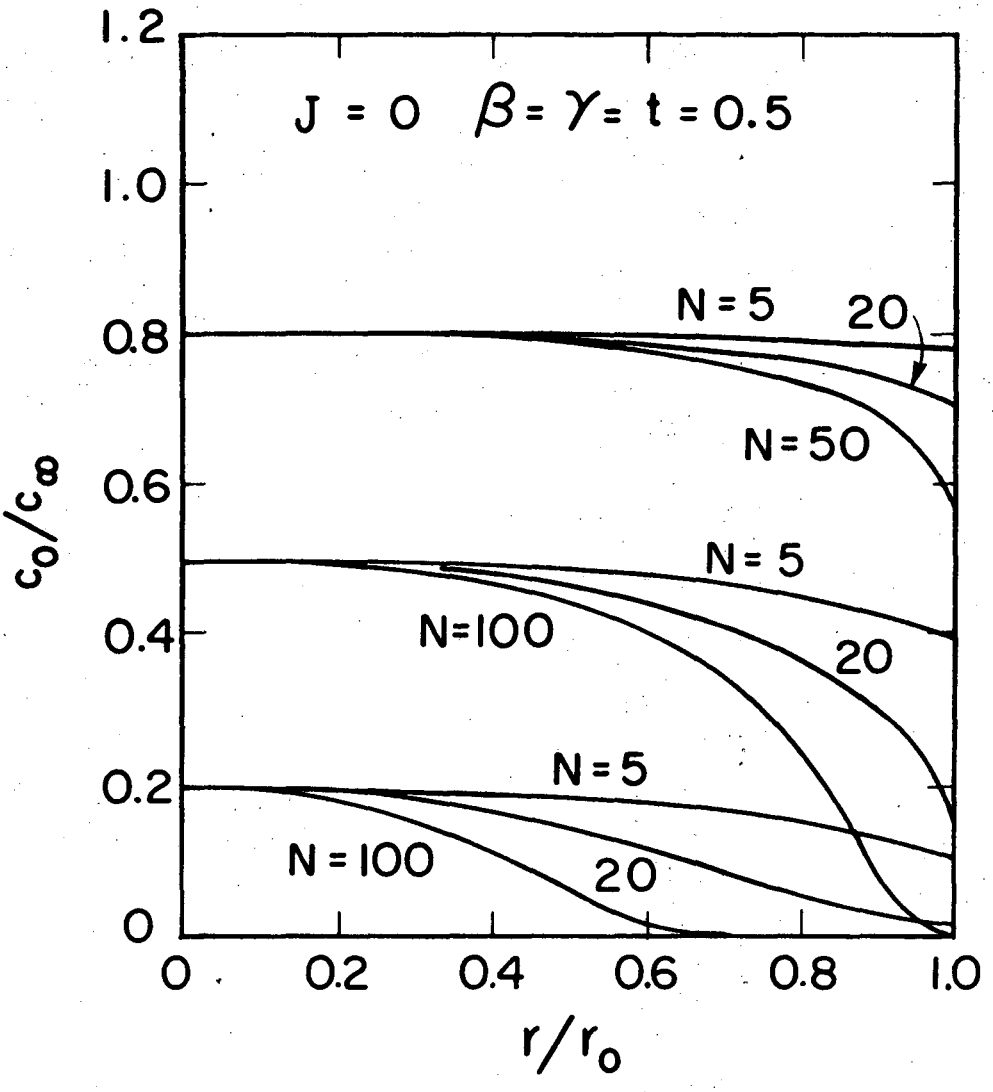

MUB-10286

Figure 4-4. Surface concentration for Tafel kinetics (from reference 7).

0 0 0 0 5 9 0 7 7 6 1

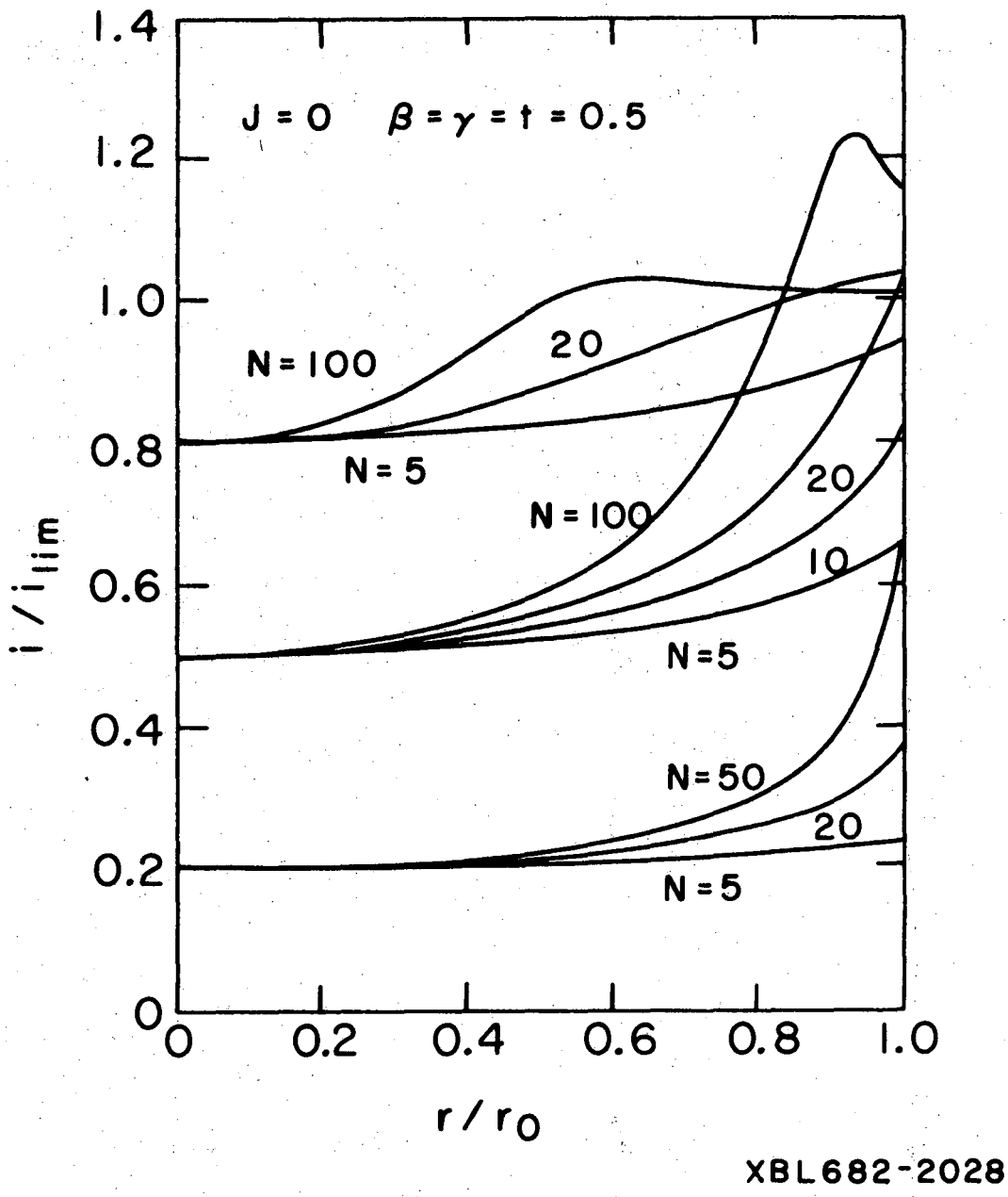

Figure 4-5. Current distribution for Tafel kinetics with an appreciable fraction of the limiting current (from reference 48).

density locally, an interesting result.

The disk electrode is commonly employed in the studies of electrode kinetics and mass transfer. The parameters such as i_o, α_a, α_c, and γ in the kinetic expression are assessed[5] from current versus voltage measurements with the incorrect presumption that the current distribution is uniform at all current levels. The calculated parameters then depend on the measured average current density or surface overpotential and cannot be generally applicable. The kinetic parameters should, at least in principle, be independent of such variables if the non-uniform current distribution is taken into consideration. Newman[7] discusses in detail how this can be accomplished using his calculated results. The ohmic drop in the solution is often determined by interrupter methods in electroanalytical applications.[81] Since the primary distribution on a disk is nonuniform, the ohmic drop between a reference probe and a given point on the disk strongly depends on the position of the probe in the solution. Tiedemann et al.[64] discuss the error which may be caused in the measurements of electrode kinetics on a disk if proper corrections are not made for the placement of the reference electrode. Miller and Bellavance[59] show how this correction can be effected properly in experimental measurements. The disk electrode, on the other hand, is well suited for mass-transfer studies which are conducted under limiting current conditions. The measurement of the limiting current for a given rotation speed along with the knowledge of the bulk concentration of the limiting reactant and viscosity of the solution makes possible the assessment of the diffusion coefficient via the Levich equation.

0 0 0 0 0 9 0 . 1 6 2

Except for the primary distribution, the potential distribution near the surface of a disk is nonuniform, and this may have important consequences in potentiostatic applications (see discussion at the end of chapter 5). The maximum potential variation between the center and the edge of the disk occurs at the limiting current[7] (figure 6) and is given by (see reference 11, section 117)

$$\Delta\Phi_o = 0.363\, r_o i_{ave}/\kappa_\infty \quad . \tag{4-23}$$

This formula may be helpful in design calculations to determine the permissible values of r_o, i_{ave}, and κ_∞ for a maximum allowable potential variation near a disk electrode.

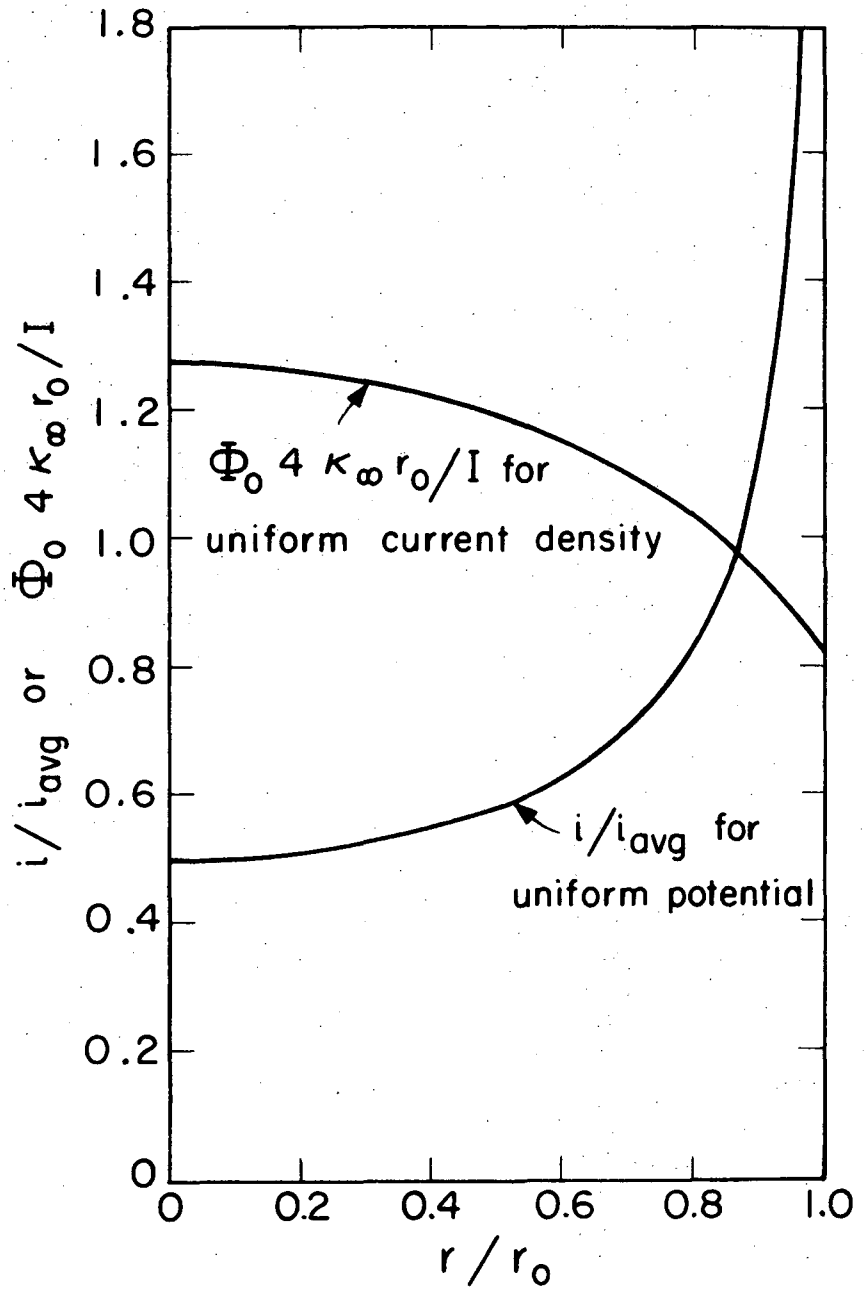

Figure 4-6. Potential distribution at the limiting current and the primary current distribution on a disk electrode (from reference 7).

0 0 0 0 3 9 0 / / 6 3

V. CURRENT DISTRIBUTION ON A ROTATING SPHERE BELOW THE LIMITING CURRENT

The sphere has been employed in the past as an important electrode geometry in electrochemical research such as the investigation of the double-layer structure on mercury drops[65] and the study of the over-potential and reaction kinetics on copper electrodes by transient methods.[66] The effects of diffusion were eigher eliminated or ignored in that work. The rotating sphere has been proposed anew as a potential tool in studies of mass transfer and reaction kinetics in electrochemical systems.[8,67] The convective diffusion equation for a thin diffusion layer at limiting current conditions has been solved recently[8,25,36] (see equation 2-60) and compared successfully with experimental data.[68]

The present interest[52] in the rotating sphere arises from the fact that the mass transfer and current distribution characteristics of the disk and the sphere turn out to be rather complementary in some respects. As reviewed in the previous chapter, the rotating disk exhibits a uniform limiting current distribution, which makes it attractive for mass transfer work. On the other hand, the spherical electrode may be more suitable for studies of electrode kinetics owing to its uniform primary distribution. The disk electrode can be polished very easily, but the surface preparation for the spherical electrode does not seem to be just as straightforward if a reasonable spherical shape is to be maintained. However, in high-rate metal deposition or dissolution studies, the disk electrode tends to rise above or recede below the insulating surface rapidly, thereby altering seriously the hydrodynamic conditions prevailing at the surface.[8] This effect is

within a much lesser degree for the sphere, which maintains its geometry to the extent permitted by the degree of uniformity of the current distribution existing at its surface. Below the limiting current, the current distribution on a rotating disk is nonuniform. It is possible in principle to attain a uniform distribution of current on a rotating sphere below the limiting current even in the presence of concentration variations at the surface as will be shown in this chapter.

The underlying theory, the basic assumptions, and the method of solution were outlined in chapters 2 and 3. Additional simplifying assumptions cited for the disk problem in section 4.3 are also retained here. A more detailed description of the mathematical analysis and the numerical method is given in appendix A.

5.1. Results for Tafel Kinetics

A problem for the sphere is completely defined, as in the case of the disk, by specifying the dimensionless parameters J, N, α_a/Z, α_c/Z, γ, t_+, and the current level $i_{ave}/(i_{lim})_{ave}$. The parameter N for the sphere is given by

$$N = - \frac{nZF^2 D_R c_{R\infty}}{s_R RT\kappa_\infty (1-t_+)} \sqrt{\frac{r_o^2 \Omega}{\nu}} \left(\frac{\nu}{9D_R}\right)^{1/3} . \qquad (5\text{-}1)$$

Since the primary distribution is uniform, the secondary current distribution, which is obtained by ignoring the concentration polarization, is also uniform regardless of the reaction kinetics. As a consequence, the results do not depend strongly upon the dimensionless exchange-current density J even when concentration polarization is present. Our numerical calculations for different J values, although not shown

0 0 0 0 3 9 0 / / 6 4

here, confirm this conclusion. Current and concentration distributions thus largely depend on N, and the specified current level with respect to the average limiting current. In view of these observations, and because mass-transfer effects are important at high current densities, we have chosen to report results for Tafel kinetics, thus, for the parameter J tending toward zero.

Figures 1 and 2 show the current and concentration distributions respectively for various current levels at N = 10. All other parameters are arbitrarily set at 0.5. The current becomes more nonuniform as the limiting current is approached whereas the concentration shows marked derivations from its average value at intermediate current levels. Figures 3 and 4 show the effect of increasing N (or increasing rotation speed) on the current and concentration distributions for a fixed concentration (c_o = 0.5 c_∞) at the pole. The current density exceeds the limiting current locally close to the equator. This can also be observed in figure 1 for large enough current levels. The same phenomenon has been reported for other geometries under similar conditions[7,48,49] (see also section 4.3). With increasing N, the concentration distribution becomes slightly more nonuniform and appears to be approaching an asymptotic profile. Meanwhile, the current distribution becomes more uniform, and the current level tends toward a limiting value different from the limiting current distribution. This represents a contrast to what has been observed for the disk[7] and plane electrodes,[48,49] where the diffusion layer is completely depleted of the reactant near the trailing edges for large enough flow rates, thereby limiting the local current density. The present results suggest

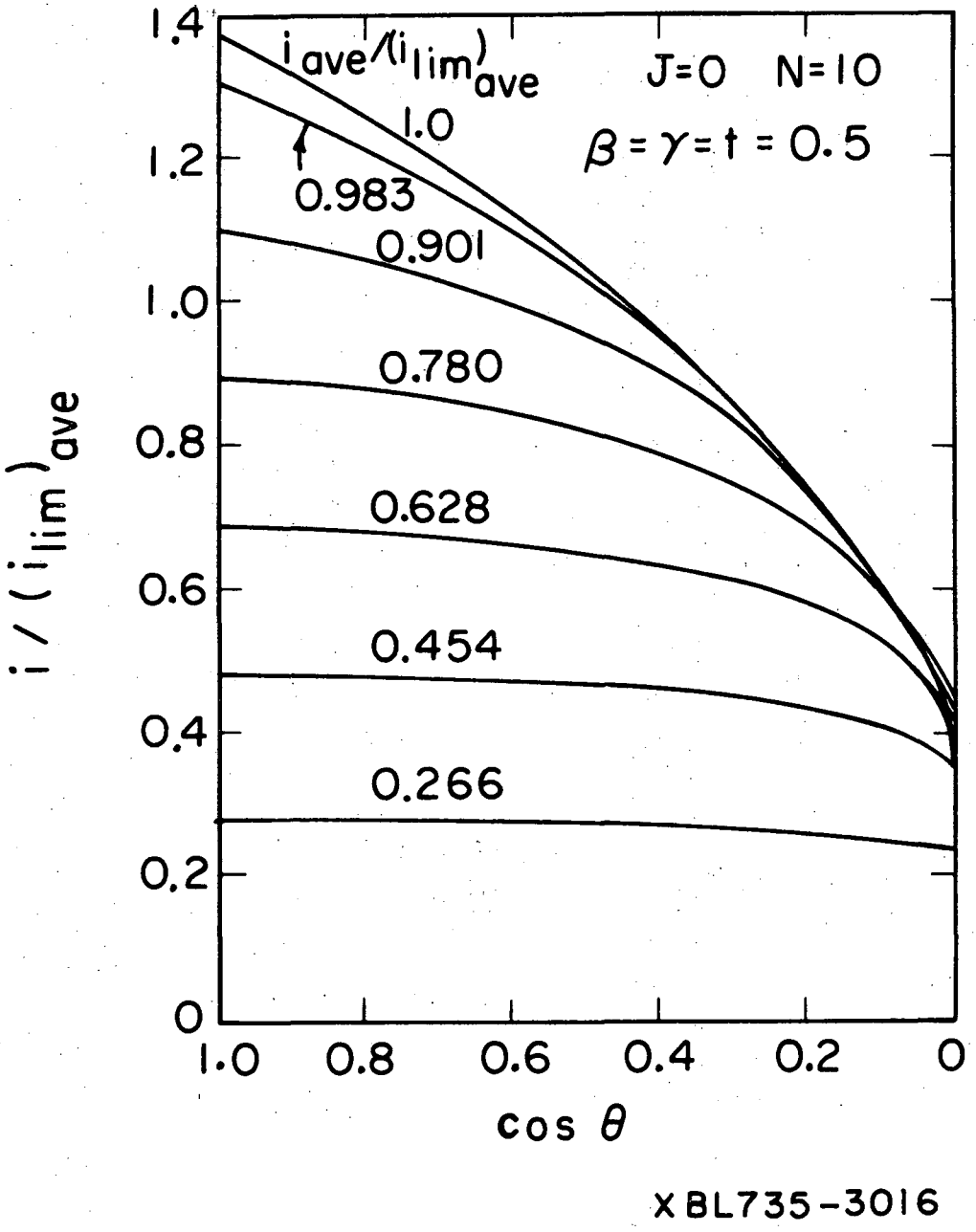

Figure 5-1. Current distribution for Tafel kinetics.

0 0 0 0 0 3 9 0 7 7 6 5

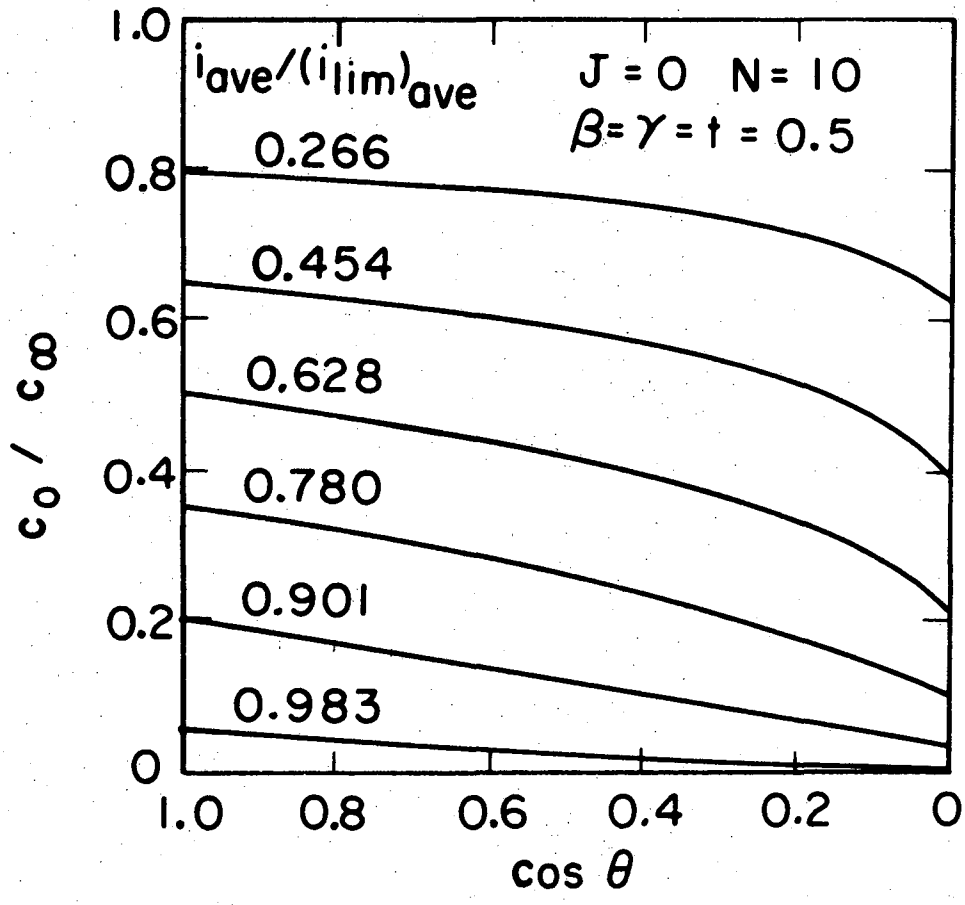

XBL735-3021

Figure 5-2. Concentration distribution for Tafel kinetics.

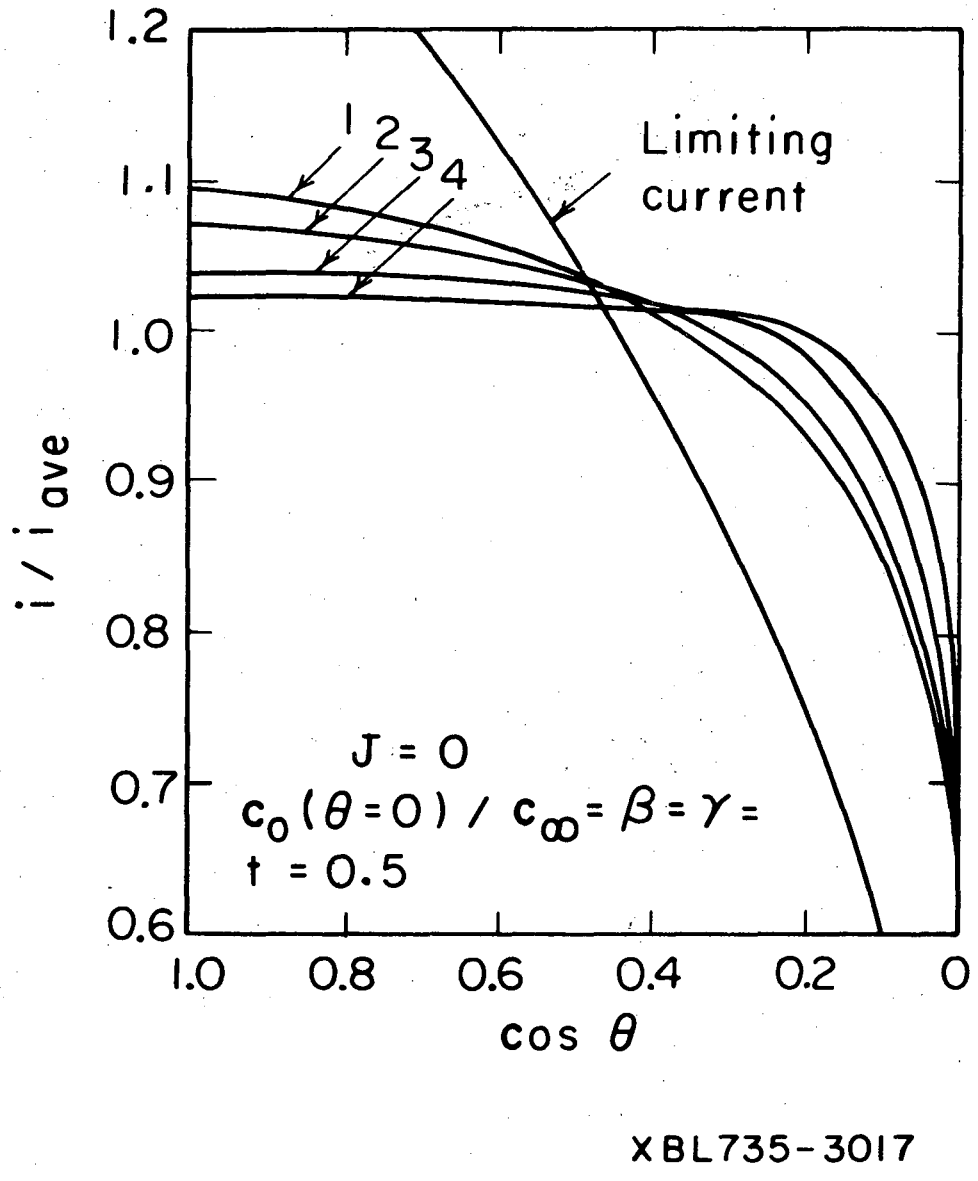

Figure 5-3. The effect of rotation speed on the current distribution for Tafel kinetics: (1) N=10, $i_{ave}/(i_{lim})_{ave}$=0.6277; (2) N-20, $i_{ave}/(i_{lim})_{ave}$=0.6432; (3) N-50, $i_{ave}/(i_{lim})_{ave}$= 0.6623; (4) N=100, $i_{ave}/(i_{lim})_{ave}$=0.6722.

0 0 0 0 3 9 0 7 7 6 6

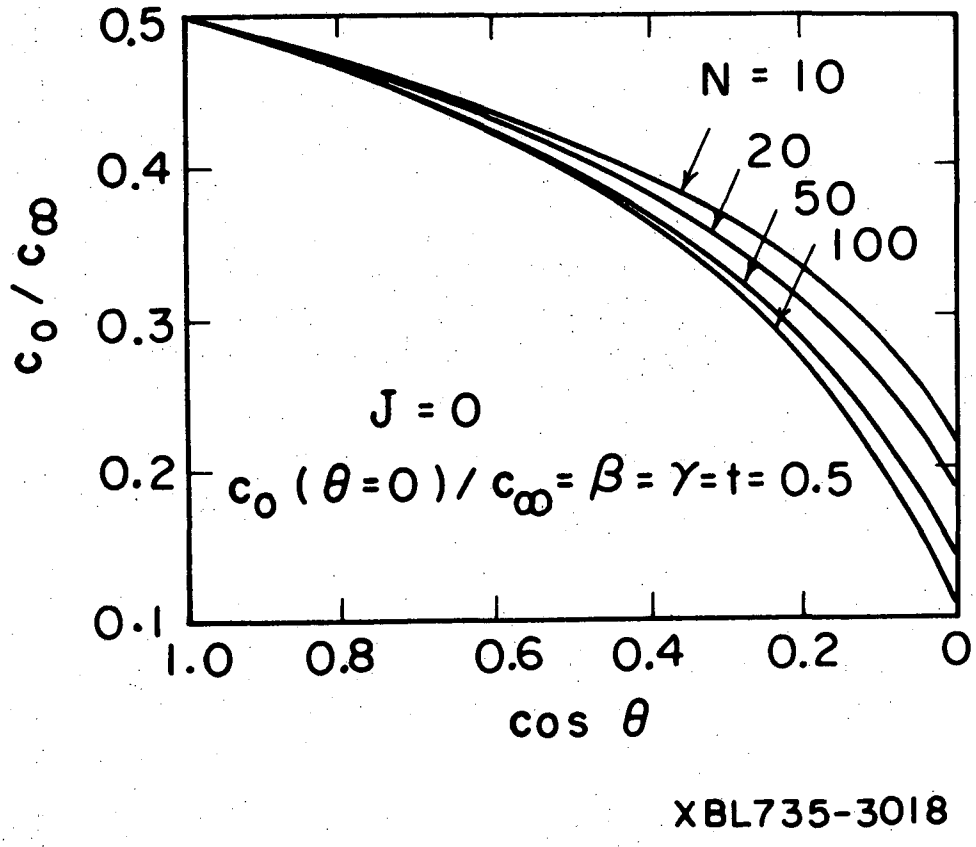

Figure 5-4. The effect of rotation speed on the concentration distribution for Tafel kinetics.

the possibility of attaining a uniform current distribution for large N on a rotating sphere in the presence of appreciable concentration polarization. Further investigation is in order below.

5.2. Conditions at High Rotation Speeds

If a constant-flux situation prevails on the surface of the sphere, the concentration derivative inside the integral in equation 2-63 is constant and related to the uniform current density by Faraday's law (equation 3-20 or 3-21). After scaling the current with respect to the average limiting current density (equation 2-61), equation 2-63 reduces to

$$1 - c_o/c_\infty = 0.230825\ F(\theta)\ i/(i_{lim})_{ave} \quad , \tag{5-2}$$

where

$$F(\theta) = \int_0^\theta \frac{\sin\theta' d\theta'}{\left[\int_{\theta'}^\theta \sin\theta\sqrt{B\sin\theta}\ d\theta\right]^{2/3}} \quad . \tag{5-3}$$

This function $F(\theta)$ is plotted in figure 5; it increases from the value 3.14768 at $\theta = 0$ (the pole) to the value 6.36850 at $\theta = \pi/2$ (the equator). Since the surface concentration is always positive or zero, equation 2 can be satisfied over the entire surface if and only if

$$i/(i_{lim})_{ave} \leqslant 0.680267 \quad . \tag{5-4}$$

It also follows from equation 2 that for currents restricted by condition 4 the concentration at the pole will be given by

$$c_o(0)/c_\infty \geqslant 0.505742 \quad . \tag{5-5}$$

0 0 0 0 3 9 0 7 1 3 7

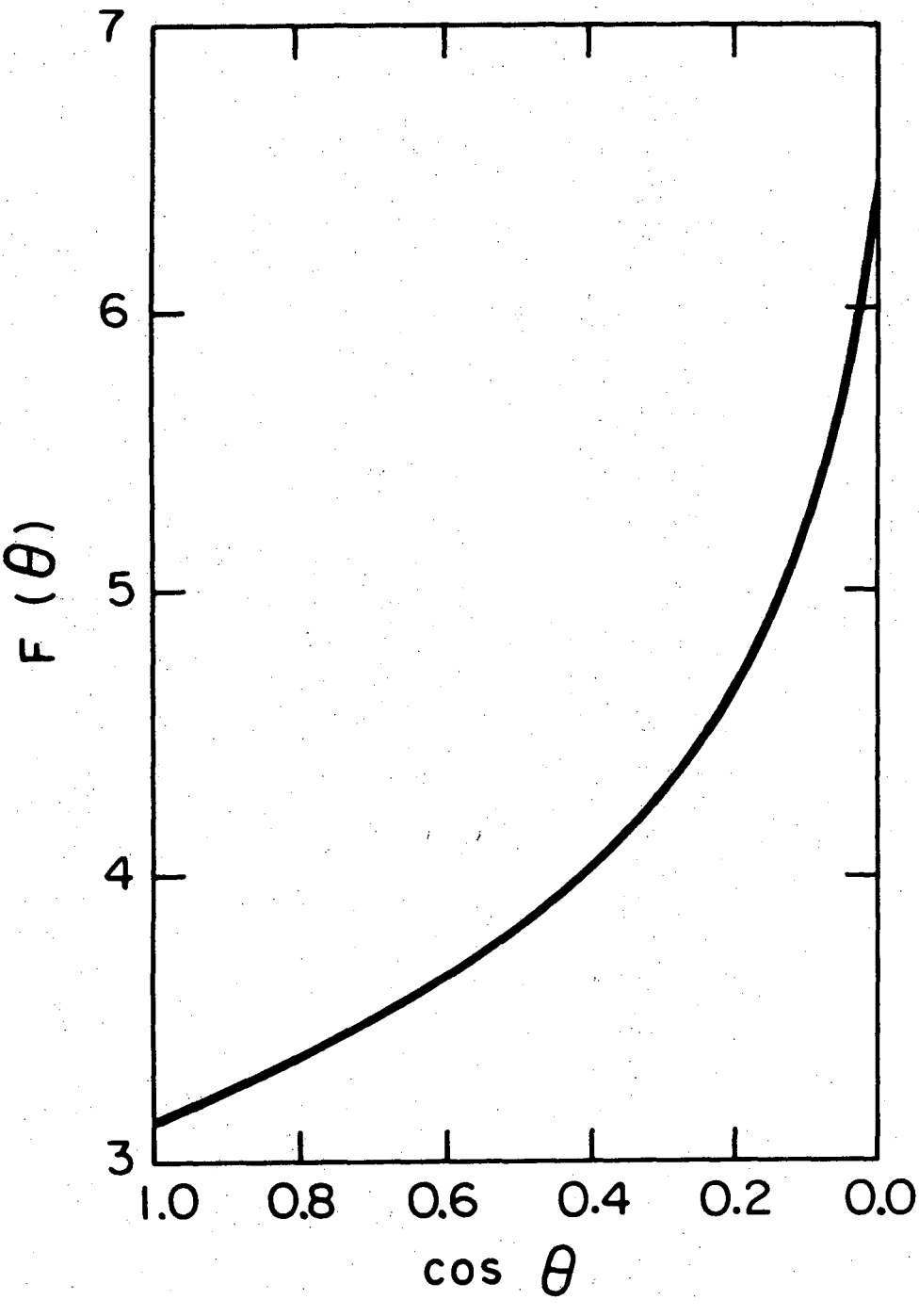

Figure 5-5. Concentration distribution for uniform flux condition at the sphere below the limiting current.

Equation 4 or 5 is the condition, therefore, for which a uniform distribution of current is possible on the sphere. The corresponding concentration distribution is given by equation 2.

If condition 4 or 5 is not met, the concentration becomes zero at a certain angle θ^*, which can be determined from equation 2 by setting $c_o = 0$. The current becomes limited for $\theta > \theta^*$ due to this zero concentration distribution and is expected to be nonuniform. Hence equation 2 is no more applicable in this region. Under these circumstances, the current density can be calculated from equation 2-62. After combining with Faraday's law and equation 2 and some rearrangement, this becomes

$$\frac{i(\theta)}{(i_{lim})_{ave}} = 0.379408\,[1 - c_o(0)/c_\infty]\,\sqrt{B\sin\theta} \times \int_{\theta}^{\theta^*} \left.\frac{dF}{d\theta}\right|_{\theta=\theta'} \frac{d\theta'}{\left[\int_{\theta'}^{\theta} \sin\theta\sqrt{B\sin\theta}\; d\theta\right]^{1/3}} \qquad (\theta>\theta^*) \quad . \tag{5-6}$$

Numerical calculations for various current levels yield the interesting results depicted in figures 6 and 7. Notice that equations 2 and 6 do not depend on any of the kinetic parameters or the exchange-current density; the current and concentration distributions are determined only by the specified current level for a galvanostatic process. The reaction parameters are necessary, however, to calculate the over-potential, or conversely, to calculate the current level if the electrode potential is fixed (potentiostatic process). These remarks are also true for the secondary distribution. In fact, the results of this section map out the transition from the secondary current

0 0 0 0 5 9 0 7 7 6 8

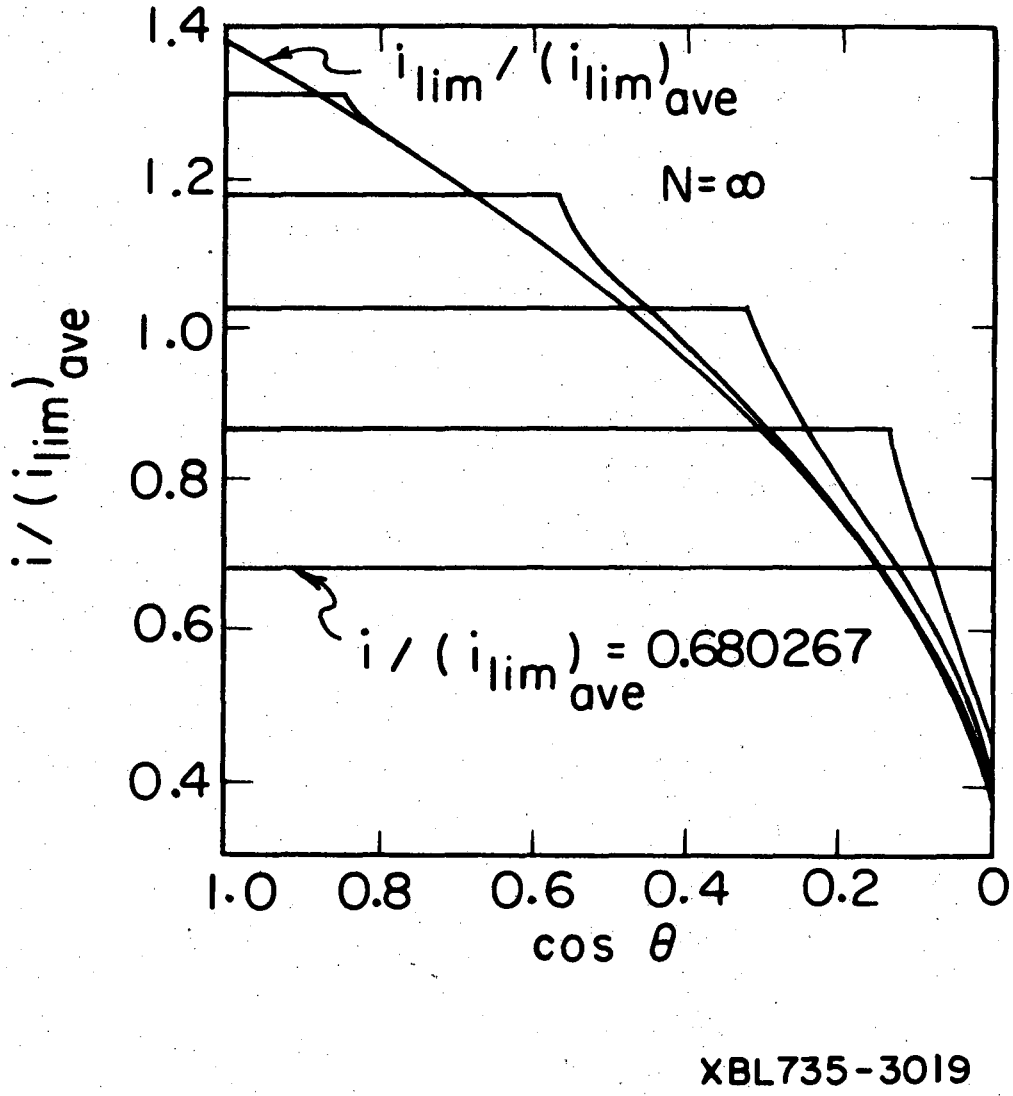

Fig. 5-6. Current distribution at high rotation speeds.

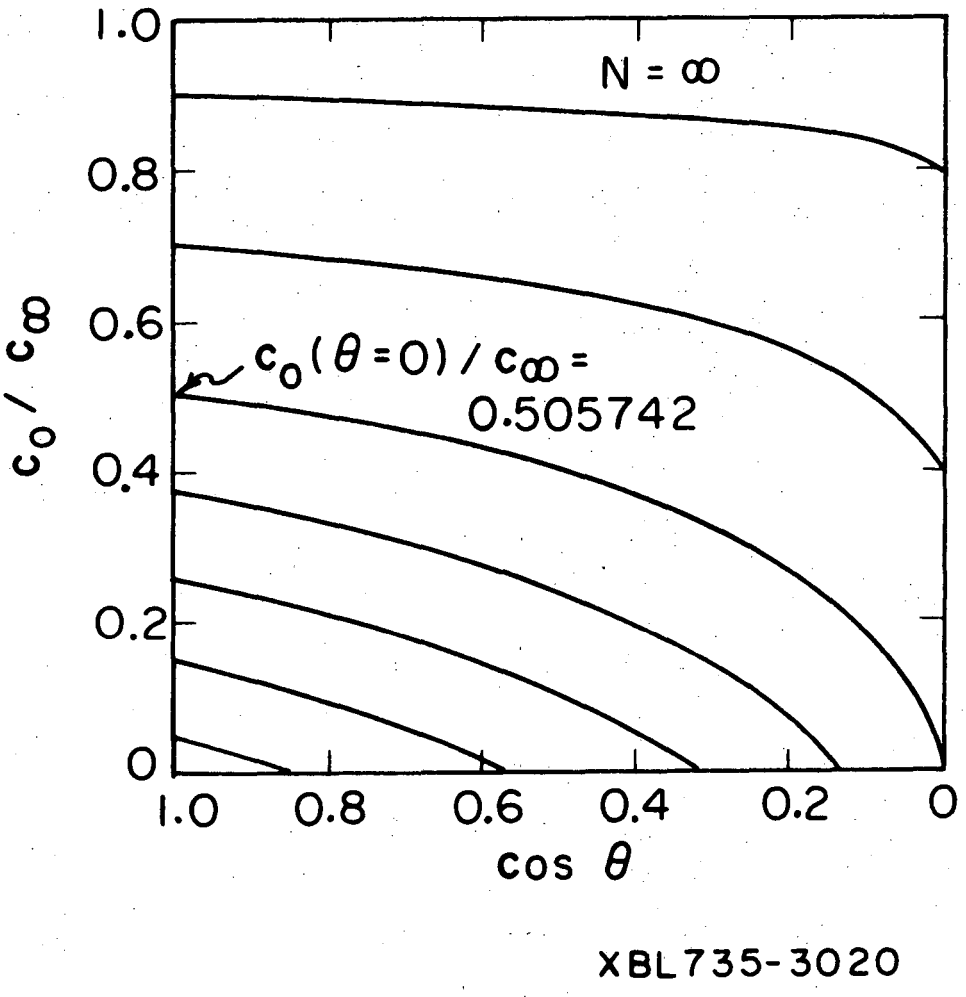

Fig. 5-7. Concentration distribution at high rotation speeds.

0 0 0 0 3 9 0 7 6 9

distribution, which is uniform, to the limiting current distribution, which is nonuniform.

At low current levels ($|i| << i_{lim}$), the secondary distribution prevails, and the surface concentration is equal to the bulk concentration. As a result, the concentration overpotential is negligible, and the electrode potential is due to the surface overpotential and the ohmic drop in the solution, the latter being given by (see equations 2-27 and 2-29)

$$\Phi = I/2\pi\kappa_{\infty}r \quad , \qquad (5\text{-}7)$$

where I is the total applied current. As the current level increases, the ohmic drop rises linearly with I according to equation 7, and the surface overpotential increases as lnI according to the Tafel expression. If there are no mass-transfer limitations, the concentration overpotential does not vary significantly. Therefore, the current distribution is controlled by the large ohmic drop, which remains uniform at the surface in the absence of mass-transfer limitations, and the current distribution is also uniform. The concentration becomes zero at the equator once a critical current level is reached as specified by equation 4. With increasing current, the depleted portion of the diffusion layer grows from near the equator toward the poles, and correspondingly the region of uniform current density shrinks in the same direction. Finally, the limiting current distribution is attained.

The present results are significant, first of all, in high-rate dissolution or deposition studies because the spherical electrode maintains its geometry, especially when the current level is kept

below $0.68(i_{lim})_{ave}$; and high rotation speeds are applied. Secondly, the placement of the reference electrode is not as crucial as for the disk because the potential distribution is uniform if constant flux prevails at the surface. If the reference electrode is close to the surface, a correction for radial position is required. This consists of a simple extrapolation to infinity since the primary distribution (equation 7) is a function of radial displacement only. Under these conditions, the assessment of the ohmic drop by the interrupter technique, which measures the value corresponding to the primary distribution,[81] is also much more straightforward in comparison to the disk electrode (see chapter 7).

Ohmic effects due to a nonuniform potential distribution near the surface of an electrode may become important in electroanalytical work. A nonuniform ohmic drop can result in a loss of control of the electrode potential in potentiostatic applications,[96,97] cause waste of current due to hydrogen evolution during the cathodic protection of metals against corrosion, or render difficult the anodic protection of metals with active-passive kinetics.[58,98] The potential variation across the surface of a sphere is at a maximum level at the limiting current (figure 8) as for the disk. The maximum potential difference between the pole and the equator is

$$\Delta\Phi_o = 0.546\ r_o i_{ave}/\kappa_\infty \quad . \tag{5-8}$$

Problems due to a nonuniform potential distribution can of course be eliminated by operating close to the conditions which effect a uniform-current and at the same time a uniform-potential distribution on the sphere as discussed in this section.

0 0 0 0 6 9 0 7 7 7 0

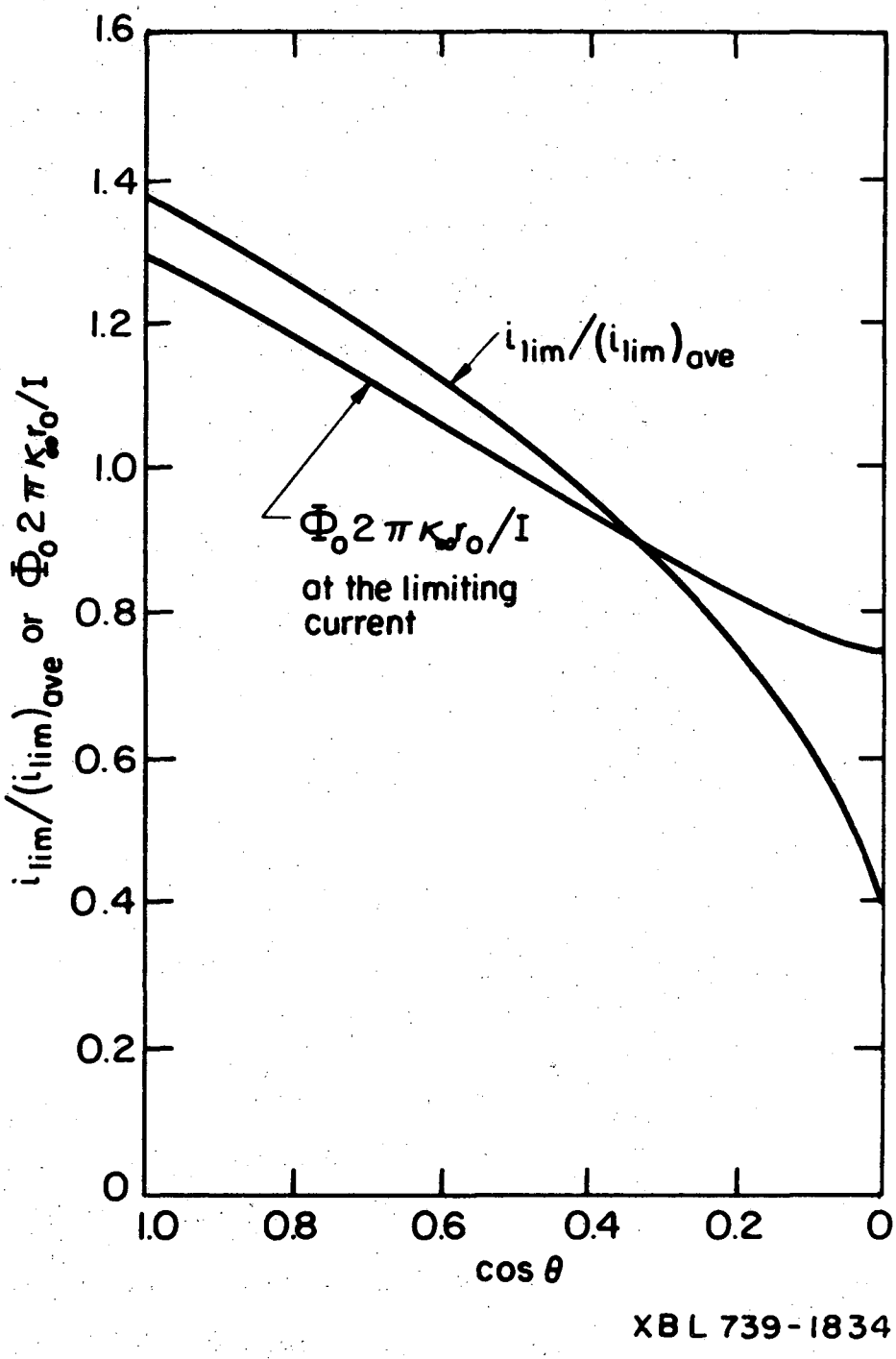

Figure 5-8. Current and potential distributions at the limiting current on a spherical electrode.

VI. TRANSIENT CONVECTIVE DIFFUSION TO A DISK ELECTRODE

Nonsteady-state methods are commonly employed in electrochemistry for the study of electrode kinetics and mass transfer in electrolytic solutions. The fundamental treatment of transient diffusion at electrode surfaces has been of interest since the classical study of the problem early in the century by Roseburgh and Lash-Miller.[70] Levich[9,71] has solved for the first time the transient diffusion equation for the disk geometry. Since convection is ignored in that treatment, the results are valid only for very short times. Subsequent analytic efforts[72,73] with the consideration of axial convection are also limited to small time intervals due to approximate methods of analysis. Fairly accurate numerical solutions are available for response to flux step[74] and concentration step[75,76] at the surface. However, analytic results are always more desirable for design calculations, determination of relaxation times, and investigation of complex boundary conditions involving electrode kinetics and capacitive effects.

Krylov and Babak[77] have recently attempted an exact solution of the axial convective-diffusion equation by a classical perturbation expansion technique. They have reported results for the concentration step and flux step conditions. Selman[76] derived independently the same solution for the concentration step. These results provide considerable improvements over the previous analytic work but are still confined to relatively short times if a reasonable number of terms are to be retained in the series expansion. We would like to contribute here to the past effort by presenting and alternative treatment for large times, so that the results can be employed interchangeably with

the short-time series of Krylov and Babak within their ranges of applicability. The method of Krylov and Babak is also reviewed.

6.1. Theoretical Formulation

We introduce the assumption here that the disk is uniformly accessible, and thus radial convection can be ignored. One should realize, however, that the latter assumption is introduced merely as a mathematical convenience. It is well accepted by now that radial convection becomes significant below the limiting current[7] (see also section 4.3). The experimental data of Nanis and Klein[78] seem to indicate that this assumption may lead to appreciable error especially during the transient build-up of overpotential after a step increase in the current. The more general case with radial convection is discussed in appendix B.

Without the radial terms, the transient equation for convective diffusion reads

$$\frac{\partial c}{\partial t} + v_y \frac{\partial c}{\partial y} = D \frac{\partial c^2}{\partial y^2} \quad , \tag{6-1}$$

where v_y is the axial velocity component for the rotating disk approximated for the diffusion layer (equation 2-52). We introduce the dimensionless variables

$$\theta = \Omega\left(\frac{D}{\nu}\right)^{1/3}\left(\frac{a}{3}\right)^{2/3} t \quad , \tag{6-2}$$

$$\zeta = y\left(\frac{a\nu}{3D}\right)^{1/3}\sqrt{\frac{\Omega}{\nu}} \quad , \tag{6-3}$$

$$\Theta = \frac{c_\infty - c}{c_\infty - c_o} \quad \text{(concentration step)} \quad , \tag{6-4}$$

or

$$\Theta = \frac{c_\infty - c}{(\partial c/\partial \zeta)_{\zeta=0}} \quad \text{(flux step)} \quad . \tag{6-5}$$

Equation 6-1 thus becomes

$$\frac{\partial \Theta}{\partial \theta} = 3\zeta^2 \frac{\partial \Theta}{\partial \zeta} + \frac{\partial^2 \Theta}{\partial \zeta^2} \quad . \tag{6-6}$$

Consider the build-up case after a step increase in the concentration or flux. The boundary conditions are

$$\left.\begin{aligned} \Theta &= 0 \quad \text{as} \quad \zeta \to \infty \\ \Theta &= 0 \quad \text{at} \quad \theta = 0 \end{aligned}\right\} , \tag{6-7}$$

$$\Theta = 1 \quad \text{at} \quad \zeta = 0, \ \theta > 0 \quad \text{(concentration step)} \quad , \tag{6-8}$$

or

$$\partial\Theta/\partial\zeta = -1 \quad \text{at} \quad \zeta = 0, \ \theta > 0 \quad \text{(flux step)} \quad . \tag{6-9}$$

Results for the decay case can be obtained simply by subtracting the results for the build-up case from the steady-state distribution (see equations 21 and 22). Therefore, a separate formulation is not necessary, contrary to the analysis given by Nanis and Klein.[78]

6.2. Short-Time Series[76,77]

The solution to equation 6 can be represented in terms of the series expansion,

$$\Theta = \sum_{n=0}^{\infty} \theta^{3n/2} \, G_n(z) \quad \text{(concentration step)} \quad , \tag{6-10}$$

or

$$\Theta = \sum_{n=0}^{\infty} \theta^{\frac{3n+1}{2}} \, F_n(z) \quad \text{(flux step)} \quad , \tag{6-11}$$

0 0 0 0 0 3 9 0 / / 7 1

where F_n and G_n are functions of the similarity variable $z = \zeta/\sqrt{2\theta}$. Substitution into the differential equation and equating the terms of equal order in θ yield

$$\left.\begin{aligned} G_o'' + zG_o' &= 0 \quad , \\ G_n'' + zG_n' - 3nG_n &= -6\sqrt{2}\, z^2 G_{n-1}' \quad (n > 0) \quad , \end{aligned}\right\} \text{(concentration step)} \tag{6-12}$$

or

$$\left.\begin{aligned} F_o'' + zF_o' - F_o &= 0 \quad , \\ F_n'' + zF_n' - (3n+1)\, F_n &= -6\sqrt{2}\, z^2 F_{n-1}' \quad (n > 0) \quad , \end{aligned}\right\} \text{(flux step)} \tag{6-13}$$

with the boundary conditions

$$\left.\begin{aligned} G_o(0) = 1, \quad G_o(\infty) &= 0 \quad , \\ G_n(0) = 0, \quad G_n(\infty) &= 0 \quad (n > 0) \quad , \end{aligned}\right\} \text{(concentration step)} \tag{6-14}$$

or

$$\left.\begin{aligned} F_o'(0) = -\sqrt{2}, \quad F_o(\infty) &= 0 \quad , \\ F_n'(0) = 0, \quad F_n(\infty) &= 0 \quad (n > 0) \quad . \end{aligned}\right\} \text{(flux step)} \tag{6-15}$$

Krylov and Babak have expressed the solutions in terms of parabolic cylinder functions.[77] The results, evaluated at the surface of the disk, are

$$-\left.\frac{\partial\theta}{\partial\zeta}\right|_{\zeta=0} = \frac{1}{\sqrt{\pi\theta}} + \frac{3}{4}\,\theta + \frac{3}{20\sqrt{\pi}}\,\theta^{5/2} + O(\theta^4) \quad \text{(concentration step)} \quad , \tag{6-16}$$

or

$$\Theta_o = 2\sqrt{\frac{\theta}{\pi}} - \frac{3}{8}\theta^2 + \frac{3}{70\sqrt{\pi}}\theta^{7/2} - O(\theta^5) \quad \text{(flux step)} \quad . \tag{6-17}$$

6.3. Long-Time Series[79]

It is possible to express Θ in terms of a steady-state and a transient part,

$$\Theta = \Theta^{ss} - \Theta^{t} \quad \text{(build-up)} \quad , \tag{6-18}$$

so that each part satisfies equation 6 separately. The boundary conditions for Θ^{ss} are

$$\left.\begin{aligned} &\Theta^{ss} = 0 \quad \text{as} \quad \zeta \to \infty \quad , \\ &\Theta^{ss} = 1 \quad \text{at} \quad \zeta = 0 \quad \text{(concentration step)} \quad , \\ \text{or} \qquad & \\ &\partial\Theta^{ss}/\partial\zeta = -1 \quad \text{at} \quad \zeta = 0 \quad \text{(flux step)} \quad . \end{aligned}\right\} \tag{6-20}$$

These yield the solutions

$$\Theta^{ss} = \frac{1}{\Gamma\left(\frac{4}{3}\right)} \int_{\zeta}^{\infty} e^{-x^3}\, dx \quad \text{(concentration step)} \quad , \tag{6-21}$$

or

$$\Theta^{ss} = \int_{\zeta}^{\infty} e^{-x^3}\, dx \quad \text{(flux step)} \quad , \tag{6-22}$$

where the integral can be found as a tabulated function of ζ.[16] The transient part of concentration satisfies the conditions

0 0 0 0 3 9 0 7 7 2

$$\left.\begin{aligned} \Theta^t &= 0 \quad \text{as} \quad \zeta \to \infty \\ \Theta^t &= \Theta^{ss} \quad \text{at} \quad \theta = 0 \end{aligned}\right\} , \tag{6-23}$$

$$\Theta^t = 0 \quad \text{at} \quad \zeta = 0, \ \theta > 0 \quad \text{(concentration step)} , \tag{6-24}$$

$$\partial\Theta^t/\partial\zeta = 0 \quad \text{at} \quad \zeta = 0, \ \theta > 0 \quad \text{(flux step)} . \tag{6-25}$$

The solution to Θ^t can be derived conveniently in terms of a boundary-value problem since equation 6 is separable, and the conditions 23 to 25 are homogeneous in the ζ-coordinate. Let us express Θ^t in the form

$$\Theta^t = \sum_{n=0}^{\infty} B_n Z_n(\zeta) \, e^{-\lambda_n \theta} , \tag{6-26}$$

where Z_n is an eigenfunction, and λ_n is the eigenvalue associated with it. Substitution into equation 6 and conditions 23 to 25 yields the Sturm-Liouville system

$$\left.\begin{aligned} &Z_n'' + 3\zeta^2 Z_n' + \lambda_n Z_n = 0 , \\ &Z_n(\infty) = 0 , \\ &Z_n(0) = 0 , \ Z_n'(0) = 1 \quad \text{(concentration step)} , \end{aligned}\right\} \tag{6-27}$$

or

$$\left.\begin{aligned} &Z_n'(0) = 0 , \ Z_n(0) = 1 \quad \text{(flux step)} . \end{aligned}\right\}$$

This system has been solved here numerically by a method commonly employed in this laboratory.[10,11,80] The coefficients B_n are given by

$$B_n = \frac{\int_0^\infty \theta^{ss} e^{\zeta^3} Z_n(\zeta)\, d\zeta}{\int_0^\infty e^{\zeta^3} Z_n^2(\zeta)\, d\zeta} , \qquad (6\text{-}29)$$

and were evaluated by numerical integration. A listing of the computer program used to calculate the eigenvalues and the coefficients is given in appendix C.

Table 1 lists the eigenvalues and the coefficients B_n after they have been extrapolated to zero mesh size. The first three eigenfunctions are plotted in figures 1 and 2 for concentration step and flux step, respectively. The results are compared with the short time series of Krylov and Babak in figures 3 and 4. The two series match quite well over a certain range of θ for each case even though only three terms of each series were used to plot these figures. The two series are also compared with the numerical solutions of Hale[74] and Selman[76] in table 2. The agreement is satisfactory within the accuracy of those solutions.

The present results enable the assessment of time constants,

$$\tau = KSc^{1/3}/\Omega , \qquad (6\text{-}30)$$

for build-up or decay of a concentration gradient after a step change in the surface concentration or flux. For a concentration step, $K = 0.45142$, and for a flux step, $K = 1.2623$. These results are accurate insofar as the radial dependence of concentration can be ignored, such as in heat-transfer studies[75] and mass transfer in nonelectrolytes. In electrolytic mass transfer, equation 30 is

0 0 3 0 3 9 0 7 7 3

Table 6-1. The first ten eigenvalues and the related coefficients B_n of the eigenfunctions.

	concentration step		flux step	
n	λ_n	B_n	λ_n	B_n
0	7.21644439	1.12818046	2.58078493	0.663516066
1	18.1596045	0.90505798	12.3099728	0.081564022
2	31.1962389	0.7907692	24.4331401	0.034457046
3	45.7926549	0.718387	38.3054830	0.01962199
4	61.6691473	0.666834	53.5740271	0.0128965
5	78.6461928	0.627481	70.0220380	0.0092267
6	96.5966836	0.596032	87.5010784	0.0069829
7	115.424957	0.570071	105.902059	0.0055048
8	135.05591	0.548117	125.140833	0.0044645
9	155.42872	0.52920	145.15016	0.0037089

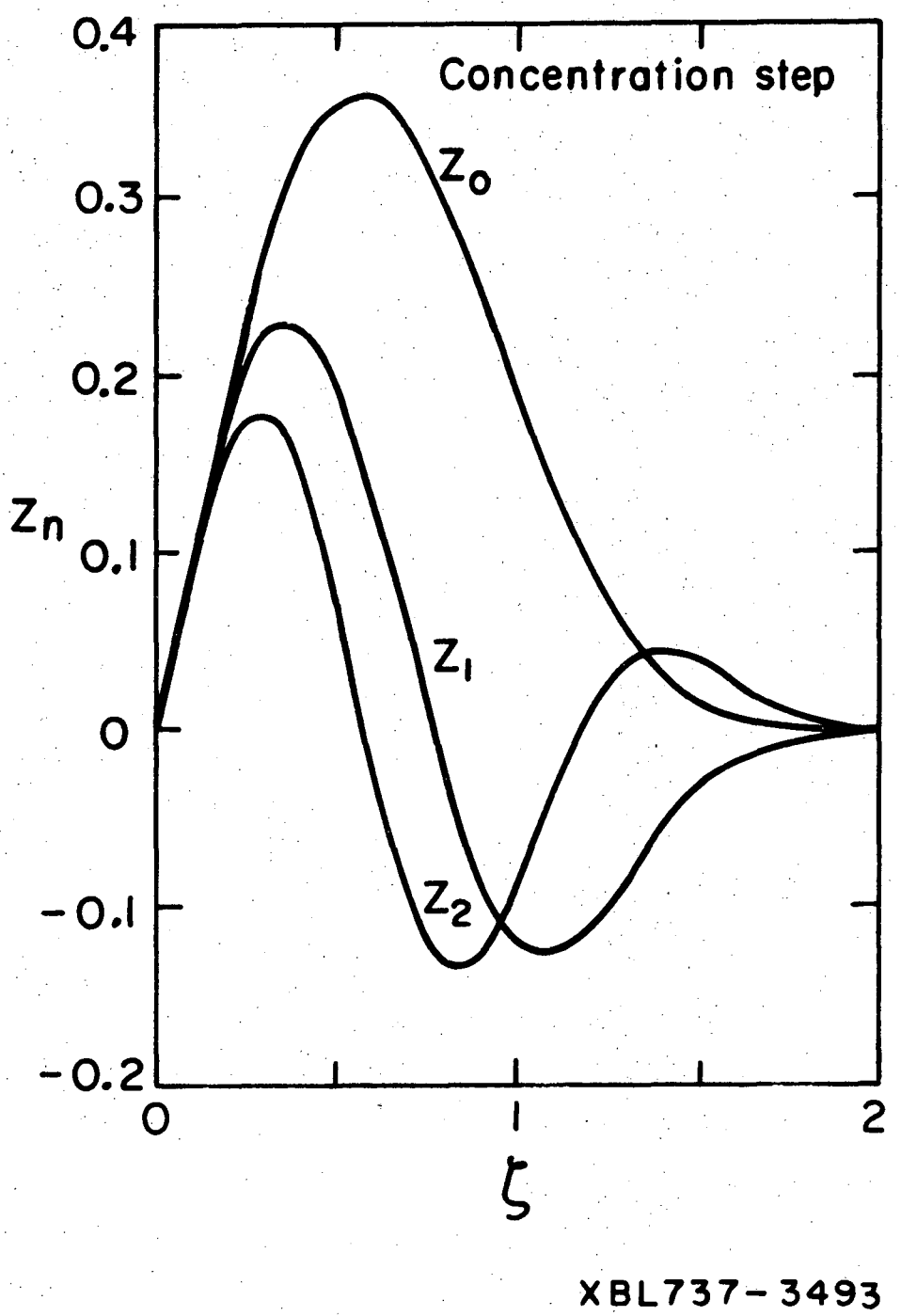

Figure 6-1. The first three eigenfunctions for the concentration-step case.

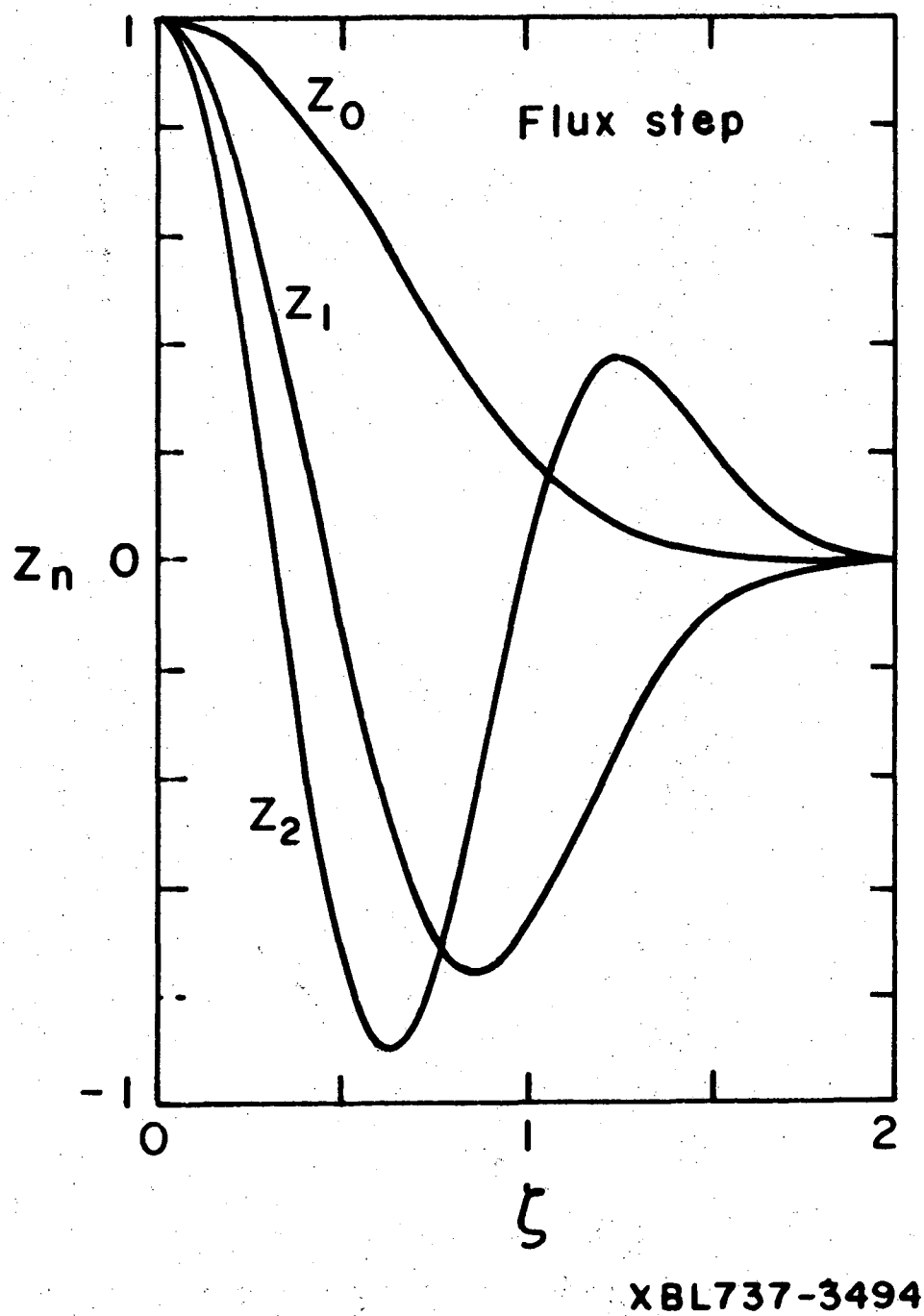

Fig. 6-2. The first three eigenfunctions for the flux-step case.

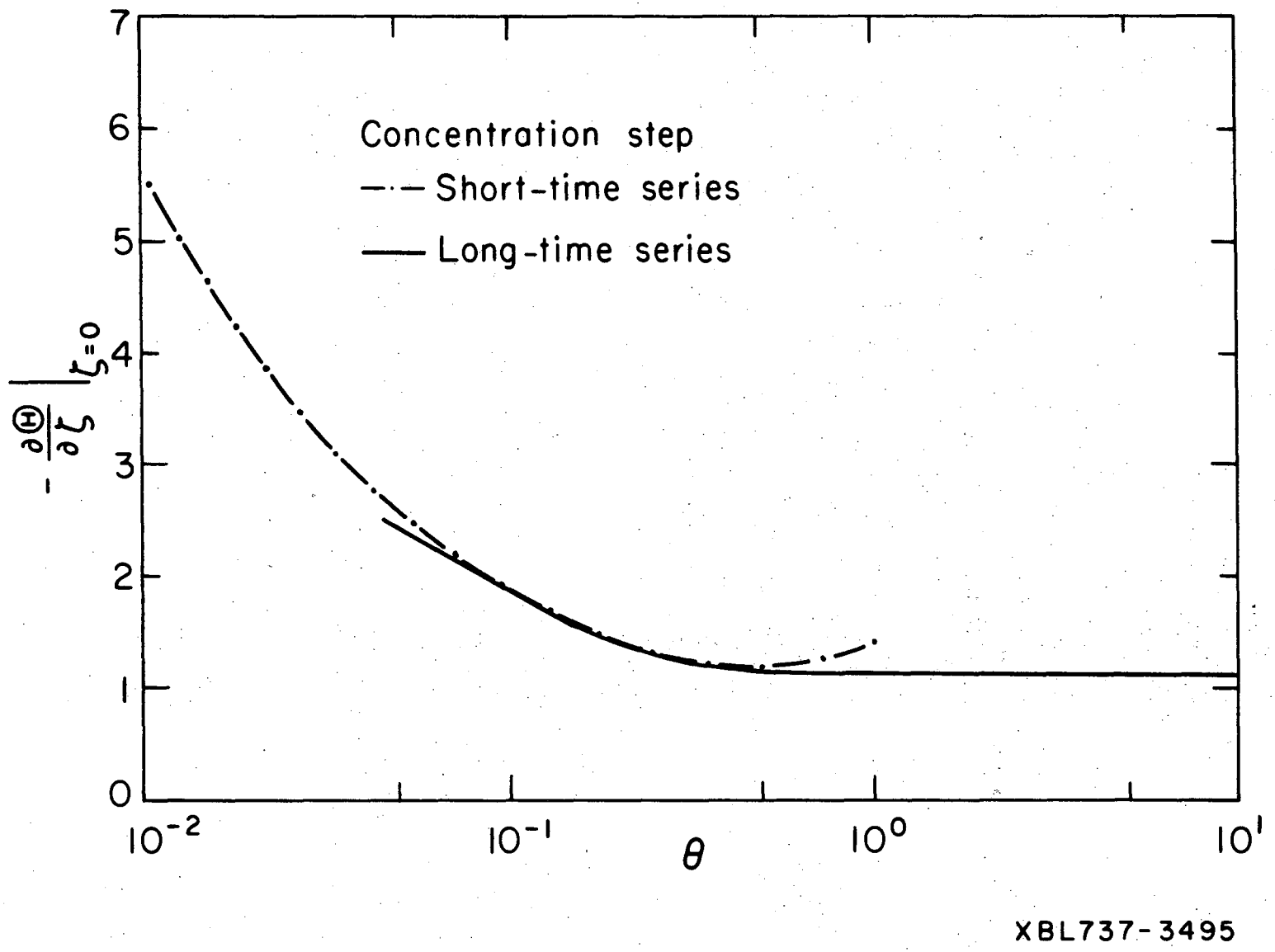

Figure 6-3. Comparison of the short-time and the long-time series for a concentration step.

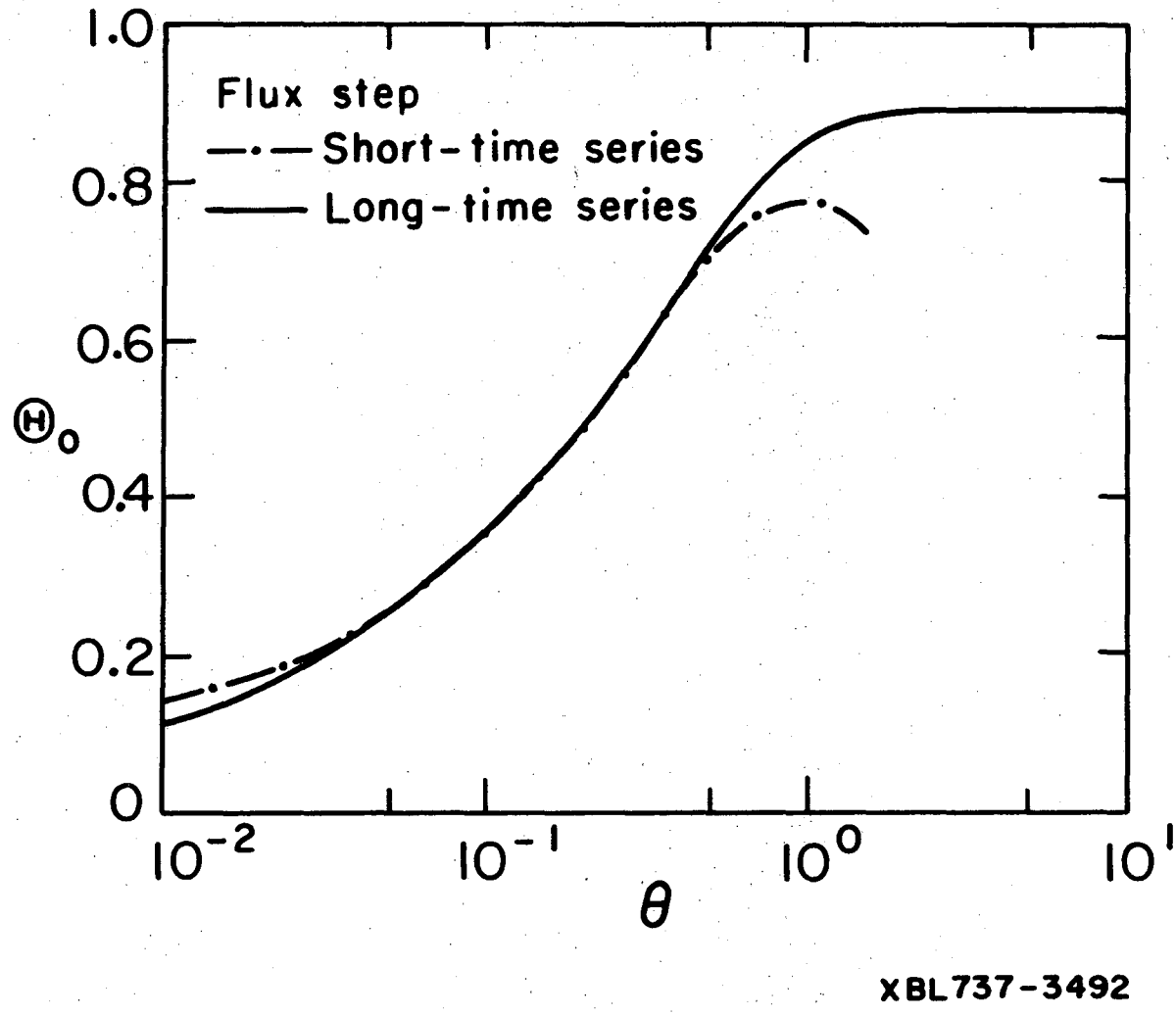

Figure 6-4. Comparison of the short-time and long-time series for a flux step.

Table 6-2. Comparison of the short-time and long-time series with the numerical solutions of Selman[76] and Hale[74] at a few selected values of θ.

Concentration Step			
θ	$-(\partial\Theta/\partial\zeta)_{\zeta=0}$		
	Short-Time Series (3 terms)	Long-Time Series (9 terms)	Numerical Solution by Selman[76]
0.0001	56.4190	8.1551	56.4190
0.01	5.6495	5.2647	5.6494
0.25	1.3265	1.3198	1.3155
1	1.3988	1.1207	1.1207
Flux Step			
θ	Θ_o		
	Short-Time Series (3 terms)	Long-Time Series (9 terms)	Numerical Solution by Hale[74]
0.0797	0.3209	0.3161	0.314
0.319	0.6759	0.6001	0.599
1.037	1.5798	0.8473	0.847
1.994	3.3551	0.8891	0.889

0 0 0 0 3 9 0 / / 7 5

sufficient for making estimates, but correction for nonuniform current distribution is probably necessary for more accurate calculations. A complete analysis of the convective diffusion equation with radial dependence appears to be very complicated and rather demanding in numerical effort. However, an asymptotic calculation for large times may be tractable to determine the necessary time constants, as discussed in appendix B.

6.4. Treatment of Complex Boundary Conditions

The above results can now be extended to treat time-dependent surface conditions. Application of the superposition integral gives

$$c - c_\infty = [c_o(0) - c_\infty]\, \Theta_c(\theta,\zeta) + \int_0^\theta \left.\frac{dc_o}{d\theta}\right|_{\theta=\theta'} \Theta_c(\theta-\theta',\zeta)\, d\theta' \quad , \tag{6-31}$$

or equivalently,

$$c - c_\infty = -\int_0^\theta \left.\frac{\partial c}{\partial \zeta}\right|_{\substack{\zeta=0 \\ \theta=\theta'}} \frac{\partial}{\partial \theta'} [\Theta_f(\theta-\theta',\zeta)]\, d\theta' \quad , \tag{6-32}$$

where the subscript o denotes conditions at the electrode surface, and Θ_c and Θ_f represent the concentration-step and the flux-step solutions, respectively. Differentiation of equation 31 yields an explicit expression for the flux at the surface,

$$\left.\frac{\partial c}{\partial \zeta}\right|_{\zeta=0} = [c_o(0) - c_\infty] \left.\frac{\partial \Theta_c}{\partial \zeta}\right|_{\zeta=0} + \int_0^\theta \left.\frac{dc_o}{d\theta}\right|_{\theta=\theta'} \left.\frac{\partial \Theta_c}{\partial \zeta}\right|_{\substack{\zeta=0 \\ \theta=\theta-\theta'}} d\theta' \quad , \tag{6-33}$$

which may prove more useful for certain calculations.

These equations are in a convenient form to calculate the potential in current-controlled applications, or vice versa, the current in potentiostatic cases. For example, if the double-layer effects can be ignored in a reversible situation, and if the time dependence of the applied current is known, the flux at the surface can be obtained from Faraday's law and substituted into equation 32 to calculate the concentration. The overpotentials, ohmic drop, and the electrode potential can then be calculated in a straightforward manner. If, on the other hand, the potential is controlled, a trial and error solution of one of the integral equations is necessary simultaneously with the expressions for the overpotentials, the potential in the solution, and the electrode potential.

Double-layer effects may become important in transient electrode processes. Delahay and co-workers[42-45] have shown how to treat the conditions at an electrode surface in the presence of mass transfer, faradaic reaction, and double-layer charging (see section 3.4). Equations 31 to 33 can be applied conveniently to treat these effects. A simple example is given below.

6.5. The Effect of Double-Layer Charging

Nanis and Klein[78] have conducted experiments to determine the transient behavior of the overpotential in the presence of a highly reversible electrode reaction. Their experimental relaxation times lag those which would be predicted by the theory formulated in the previous sections. The discrepancy is possibly due to the assumption

0 0 0 0 5 9 0 . 7 7 6

that the disk is uniformly accessible to mass transfer. When the current is initially switched on as a step, the flux is much higher at the edge than at the center of the disk, and the overpotential thus builds up at a faster rate at the edge relative to the center. This results in a rather nonuniform overpotential early in the transient process in violation of the assumption.

Another possible cause of the discrepancy is the effect of double-layer charging; some of the current may be used to charge the double layer, thereby delaying the build-up of the overpotential. This effect is investigated here for the case of a fast and highly reversible deposition of a single reactant in the presence of an excess amount of supporting electrolyte. The double-layer capacity is assumed to be independent of the potential (see chapter 7). Since the electrode reaction is fast, it is safe to assume also that $\eta_c >> \eta_s$. In the light of these assumptions, equation 3-32 should be adequate to express the conditions at the electrode surface. After substituting equation 3-12 for the concentration overpotential and putting in dimensionless form, equation 3-32 can be written as

$$\left.\frac{\partial\Theta}{\partial\zeta}\right|_{\zeta=0} = \frac{1}{\Gamma\left(\frac{4}{3}\right)} \frac{I}{I_L} + \frac{Q}{\Theta_o} \frac{d\Theta_o}{d\theta} \quad , \tag{6-34}$$

where

$$\Theta = c/c_\infty$$

$$Q = \frac{s_R^2 CRT}{c_\infty n^2 F^2 r_o} \left(\frac{a}{3}\right)^{1/3} Sc^{1/3}\, Re^{1/2} \quad , \tag{6-35}$$

and I/I_L is the current level. The importance of the double-layer charging depends on the magnitude of the parameter Q which is normally of order 10^{-3} to 10^{-2}. Even though this seems small, it is hard to predict in advance whether the double-layer effect is also small because the derivative $d\Theta_o/d\theta$ can be quite large at small times and influence the transient behavior at large times.

Equation 34 was combined with equation 33 and then solved numerically for an initial step increase in the current. The results are compared to the case where the double-layer effects are completely ignored in table 3. This latter case is identical to the flux-step solutions given in sections 2 and 3. The same results can be obtained from equations 33 and 34 by setting Q = 0 and are also included in table 3, so that errors due to the numerical method will not be attributed to double-layer effects.

The results indicate a definite delay in the relaxation of concentration with increasing Q so as to alter appreciably the characteristic time constants calculated previously in the absence of the double-layer effect. However, this delay is not at all as large as that measured by Nanis and Klein. The results of Nanis and Klein are for a redox reaction, but the consideration of the product concentration in the present calculations would probably not alter the results appreciably.[7] The present results seem to suggest that the double-layer charging does not effect significantly the transient mass-transfer phenomena at a disk in the presence of a reversible reaction. However, the validity of the assumption that the concentration of the supporting electrolyte does not change has not been tested. The

0 0 0 0 3 9 0 7 7 7

Table 6-3. The effect of double-layer charging on transient mass transfer to a disk in the presence of a highly reversible electrode reaction ($I/I_L=1$).

θ	Θ_{of}	$\Theta_o(Q=0)$	$\Theta_o(Q=0.001)$	$\Theta_o(Q=0.01)$
0	1	1	1	1
0.2	0.452	0.452	0.455	0.469
0.4	0.265	0.267	0.269	0.285
0.6	0.158	0.160	0.162	0.179
0.8	0.094	0.096	0.098	0.115
1	0.056	0.057	0.060	0.076

effect of migration has been shown to be negligible under steady-state situations;[82,83] but, it can be significant in transient phenomena since the time derivatives of concentration enter the equations for the surface flux rather than the absolute values (see equations 3-25 and 3-31). In order to incorporate into the analysis the concentration variations of the supporting electrolyte, the convective-diffusion equation has to be solved for the supporting electrolyte with the consideration of migration effects (see reference 11, section 73) for a step change in the concentration or flux and the solution generalized into a form such as equation 32 to account for arbitrary initial conditions. The system of integral equations for the supporting electrolyte and the reactant can then be solved together to satisfy a general boundary condition of the type given by equation 3-25. An analysis of this type is outside the present scope.

The numerical method of this section is discussed in appendix D. Even though the results were not conclusive, the method may be of some interest since it demonstrates an application of the equations of the previous section to a relatively complex electrode process.

0 0 0 0 3 9 0 / / 7 8

VII. THE TRANSIENT RESPONSE OF A DISK ELECTRODE UNDER GALVANOSTATIC CONTROL

In studies of electrode kinetics, the uncompensated ohmic drop in the solution has often been measured by transient methods since the development of the commutator method by Glasstone.[86] The more accurate interrupter technique has subsequently been invented[87] and perfected[88-90] as a reliable tool in the last couple of decades. The presence of a nonuniform current distribution at the electrode surface (such as in the case of a disk electrode below the limiting current), however, appears to complicate the interpretation of interrupter data, as this subject has already received ample thought and experimentation (references 15,59,64,81,89; see also the discussion on reference 15).

Newman[81] has shown that the step change in potential at interruption corresponds to the primary current distribution and discussed the time constants for decay of the double-layer capacity due to a faradaic reaction and redistribution of charge within the double layer. A more complete mathematical study will be presented here in order to determine the transient response of a disk electrode to step changes in the cell current.[60]

The problem was originally conceived for an ideally polarizable electrode with the purpose of calculating the transients one would observe during the charging and decay of the double-layer capacity. However, the effect of a faradaic reaction can be incorporated into the formulation without any added difficulty in the analysis. The more general case will therefore be analyzed with due notice of the mathematical subleties relevant to an ideally polarizable electrode.

7.1. Mathematical Model

The present analysis intends to investigate the effects of double-layer charging and a faradaic reaction on the transient behavior of the disk in the absence of concentration variations. The model therefore differs from the one described in chapter 6 because the diffusion layer is ignored, whereas the effect of the ohmic drop in the solution is considered along with the types of electrode conditions mentioned above. The results have a physical significance in situations where the current level is low and the rate of stirring is high, and hence the concentration variations in the solution can actually be neglected. It is further assumed that linear kinetic relationships govern the electrode reaction and the double-layer capacity is independent of the potential. The latter assumption is a reasonable approximation for small changes in the electrode potential, especially for cathodic polarizations with respect to the electrocapillary maximum. Some attention has been directed to the proper treatment of the capacitive effect of the diffuse double layer in transient problems in the presence of concentration and sizeable potential variations, and the reader is directed to the pertinent literature[11,41-47,91] (see also sections 3.4 and 6.5). More discussion is also in order in a later section concerning the validity of the above assumptions in practical application.

The potential in the solution satisfies Laplace's equation 2-10 and the conditions at infinity and on the insulating surface expressed by equations 2-11 and 2-12, respectively. The potential is furthermore

0 0 0 0 3 9 0 7 7 9

well behaved on the axis of the disk. The normal component of the current density at the electrode surface is given by (see equations 3-18 and 3-34)

$$i_n = C \frac{\partial \eta_s}{\partial t} + (\alpha_a + \alpha_c) \frac{i_o F}{RT} \eta_s = - \kappa \frac{\partial \Phi}{\partial z}$$

$$\text{at } z = 0, \quad r \leq r_o \quad , \tag{7-1}$$

where

$$\eta_s = V - \Phi_o \quad . \tag{7-2}$$

We would like to have our model simulate the transient response of a disk electrode for the charging or decay of the double-layer capacity immediately after the current is turned on or off respectively. The potential in solution for the charging period can then be represented as the difference of a steady state and a transient contribution,

$$\Phi = \Phi^{ss} - \Phi^t \quad , \tag{7-3}$$

such that each part satisfies Laplace's equation by itself. The electrode potential V can similarly be expressed as the difference of a steady state and a transient part. The steady state part of the potential includes the contribution of the total cell current, while the transient part contains no net current. Once the current is turned off, therefore, the steady state part vanishes, and the decay period is represented by only the transient part: $\Phi = \Phi^t$. The steady state part of the potential is treated in section 4.1.

7.2. An Eigenvalue Problem

The transient part of the potential can be expressed by a series expansion of the form

$$\frac{\Phi^t}{\Phi^p_o} = \sum_{i=1}^{\infty} C_i e^{-t/\tau_i} U_i(r,z) \quad , \tag{7-4}$$

where U_i is a characteristic dimensionless potential defined here to be independent of time, and τ_i is a time constant for decay corresponding to the potential U_i. The analysis can be pursued conveniently in terms of two additional dimensionless quantities, namely the dimensionless eigenvalue,

$$\Lambda_i = \frac{r_o C}{\kappa \tau_i} - J \quad , \tag{7-5}$$

and the dimensionless time,

$$\theta = \frac{\kappa t}{r_o C} \quad . \tag{7-6}$$

Equation 4 then transforms to the form

$$\frac{\Phi^t}{\Phi^p_o} = \sum_{i=1}^{\infty} C_i e^{-\theta(\Lambda_i+J)} U_i(\eta,\xi) \quad . \tag{7-7}$$

The transient part of the electrode potential can analogously be expressed as

$$\frac{y^t}{\Phi^p_o} = C_o e^{-\theta J} + \sum_{i=1}^{\infty} C_i e^{-\theta(\Lambda_i+J)} \upsilon_i \quad , \tag{7-8}$$

0 0 0 0 3 9 0 / / 8 0

where v_i is a constant which will henceforth be taken to be unity, thus providing a normalization for the eigenfunctions U_i.

The functions U_i satisfy Laplace's equation,

$$\nabla^2 U_i = 0 \quad , \tag{7-9}$$

and the conditions

$$\left.\begin{aligned} &\frac{\partial U_i}{\partial \eta} = 0 \quad \text{at} \quad \eta = 0 \quad , \\ &U_i = 0 \quad \text{as} \quad \xi \to \infty \quad , \\ &U_i \text{ well behaved at } \eta = 1 \quad . \end{aligned}\right\} \tag{7-10}$$

The solution can therefore be given by

$$U_i = \sum_{n=1}^{\infty} B_{n,i} \, P_{2n}(\eta) \, M_{2n}(\xi) \quad . \tag{7-11}$$

The zeroeth term is excluded from the summation since U_i includes no contribution to the net current. The boundary condition 1 now reduces to

$$\left.\frac{\partial U_i}{\partial \xi}\right|_{\xi=0} = \Lambda_i \eta (1 - U_{i,o}) \quad . \tag{7-12}$$

Combining equations 11 and 12 and invoking the orthogonality property of the Legendre polynomials yield

$$\sum_{n=1}^{n_{max}} a_{o,n} \, B_{n,i} = \frac{1}{2} \quad , \tag{7-13}$$

$$\sum_{n=1}^{n_{max}} \left[a_{m,n} + \frac{\delta_{m,n}}{\Lambda_i} \frac{M'_{2m}(0)}{4m+1} \right] B_{n,i} = a_{o,m} \quad (m = 1,2, \ldots, n_{max}) \quad . \qquad (7\text{-}14)$$

The above set of equations can be solved simultaneously for Λ_i and $B_{n,i}$. The computer program is reproduced in appendix E. Some results are given in table 1, and the first three eigenfunctions are plotted in figure 1.

Each term in equation 4, and the corresponding term in equation 8, describes a potential distribution and a state of charge in the electric double layer which can decay with a single time constant and involves no net current flow to the counter electrode at infinity. The state of charge is proportional to $V-\Phi_o$ or to $1-U_{i,o}$ for a particular eigenfunction. If this state of charge is non-uniform, it will have associated with it a flow of current through the solution in a direction which tends to make even the charge distribution across the electrode. At the same time, the double-layer charge may be decaying through the faradaic reaction (if $J > 0$).

If each eigenfunction is to represent a single time constant, the amount of current flowing through the solution (related to $\partial U_i/\partial \xi$ at $\xi = 0$) must be proportional, over the surface of the electrode, to the rate of change of the double-layer charge. Equation 12 represents this state of affairs. Only for certain characteristic decay constants Λ_i is it possible to find constant current and charge distributions which decay with a single time constant, and these eigenvalues are not known in advance. The lowest eigenvalue, either $\Lambda_o = 0$ or $\Lambda_1 = 4.12130$, is the most important because its effect can most

0 0 0 0 5 9 0 7 7 8 1

Table 7-1. The first five eigenvalues and the related coefficients $B_{n,i}$ of the eigenfunctions.

	Λ_1	Λ_2	Λ_3	Λ_4	Λ_5
	4.12130	7.34208	10.5171	13.6773	16.8308
n	i = 1	i = 2	i = 3	i = 4	i = 5
1	4.56973	3.77405	3.44403	3.25860	3.13835
2	3.58511	-3.70789	-4.65165	-4.79056	-4.75592
3	0.51738	-7.51662	-0.26793	2.76530	4.12700
4	0.10883	-2.89555	9.61986	5.38647	1.50528
5	-0.03142	-0.67828	6.80910	-8.19370	-8.96687
6	0.02274	-0.02899	2.44679	-10.7732	3.13094
7	-0.01587	-0.03991	0.44950	-5.76314	12.7102
8	0.01161	0.02427	0.11317	-1.72889	10.1185
9	-0.00879	-0.01882	-0.02225	-0.42934	4.33793
10	0.00684	0.01470	0.02444	-0.02855	1.34839

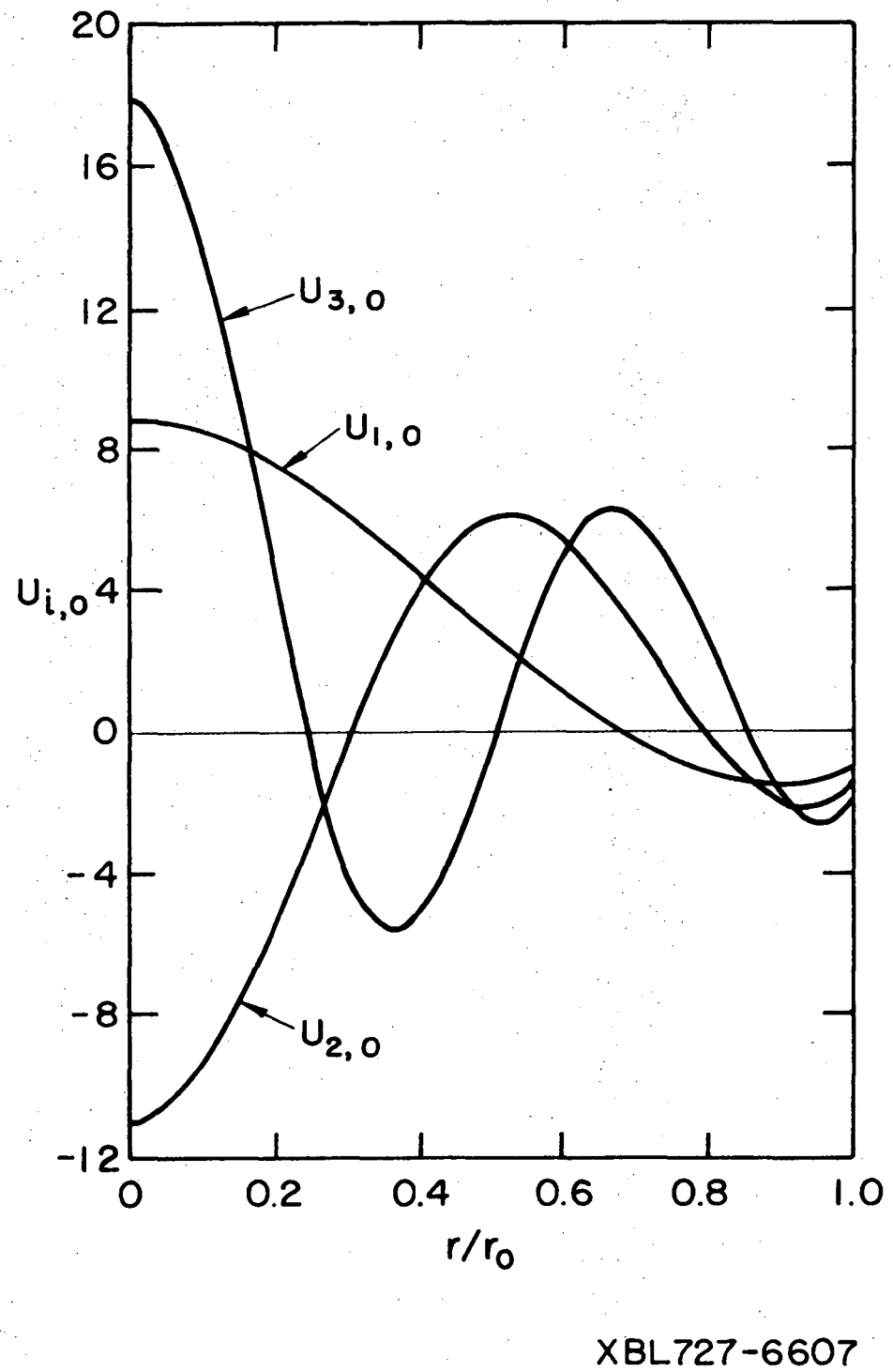

Fig. 7-1. The first three eigenfunctions for the transient solution.

0 5 0 0 3 9 0 . 7 0 2

readily be observed experimentally after the other eigenfunctions have decayed to negligible values.

It is a further consequence of boundary condition 12 (current in solution is proportional to surface charge for each eigenfunction) that the eigenfunctions U_i satisfy the unusual orthogonality relationship

$$\int_0^1 U_{i,o}(1-U_{j,o})\,\eta d\eta = \begin{cases} \frac{1}{\Lambda_i}\sum_{n=1}^{\infty}\frac{M'_{2n}(0)}{4n+1}\,B^2_{n,i} & \text{if } i = j\,, \\ 0 & \text{if } i \neq j\,. \end{cases} \tag{7-15}$$

This has much the same meaning; the potential at the surface for one eigenfunction is in a sense orthogonal to the current density for another eigenfunction.

One can study the eigenfunctions in figure 1 to visualize how the current flows through the solution. The potential is nonuniform for a given eigenfunction because the state of charge is nonuniform. The current density in the solution is proportional to $1-U_{i,o}$ and flows from a region of high charge to a region of low charge. The higher order eigtnfunctions have more minima and maxima in the curves. The current need therefore flow a shorter distance in order to even up the charge, and the time constants are correspondingly shorter.

7.3. Transient Potential Distribution

In order to be able to calculate the values of C_i and thereby complete the analysis, we need to specify suitable initial conditions for the problem. Let us assume that the current is switched on as a step at $\theta = 0+$ and kept constant until $\theta = \theta_{ch}$, at which instant it

is turned off. The time scale for the decay period can be defined as

$$\theta' = \theta - \theta_{ch} \quad . \tag{7-16}$$

Therefore, for the charging period,

$$V = \Phi_o = \Phi_o^p \quad \text{at} \quad \theta = 0+ \, , \; \xi = 0 \quad , \tag{7-17}$$

and for the decay period,

$$\left.\begin{aligned} V &= V(\theta_{ch}) - \Phi_o^p \\ \Phi_o &= \Phi_o(\theta_{ch}) - \Phi_o^p \end{aligned}\right\} \quad \text{at} \quad \theta' = 0+, \; \xi = 0 \quad . \tag{7-18}$$

Application of the initial condition (17) for the charging period to equation 3 gives

$$\frac{\Phi_o^{ss}}{\Phi_o^p} - 1 = \sum_{i=1}^{\infty} C_i U_{i,o} \quad . \tag{7-19}$$

Multiplication by $(1-U_{j,o})\eta$ and integration with respect to η yields

$$C_j = \frac{\displaystyle\int_0^1 \frac{\Phi_o^{ss}}{\Phi_o^p} (1-U_{j,o}) \, \eta d\eta \quad \sum_{n=1}^{\infty} \frac{M'_{2n}(0)}{4n+1} B_n^{ss} B_{n,j}}{\displaystyle\int_0^1 U_{j,o}(1-U_{j,o}) \, \eta d\eta \quad \sum_{i=1}^{\infty} \frac{M'_{2n}(0)}{4n+1} B_{n,j}^2} \quad . \tag{7-20}$$

Application of the corresponding initial condition for the electrode potential gives

$$C_o = \frac{V^{ss}}{\Phi_o^p} - 1 - \sum_{i=1}^{\infty} C_i = \frac{4}{\pi J} \quad . \tag{7-21}$$

0 0 0 0 3 9 0 , 7 8 3

For the decay period where $\Phi = \Phi^t$ (the negative of the transient part for charging), the same results, summarized by equations 19 through 21, also apply as long as θ_{ch} is large enough so that the steady state has been reached right before interruption. If this is not the case, the equations for decay become

$$\frac{\Phi}{\Phi_o^p} = \sum_{i=1}^{\infty} C_i \left[1 - e^{-\theta_{ch}(\Lambda_i+J)}\right] e^{-\theta'(\Lambda_i+J)} U_i \qquad (7\text{-}22)$$

for the potential in the solution, and

$$\frac{V}{\Phi_o^p} = C_o\left(1-e^{-\theta_{ch}J}\right) e^{-\theta' J} + \sum_{i=1}^{\infty} C_i \left[1-e^{-\theta_{ch}(\Lambda_i+J)}\right] e^{-\theta'(\Lambda_i+J)} \qquad (7\text{-}23)$$

for the electrode potential. The coefficients C_i are the same as for the charging period, given by equations 20 and 21.

For an ideally polarizable electrode (J=0), the same relationships hold to express the potential in the solution, both for charging and for decay. The electrode potential, however, increases indefinitely once the current is turned on and decays to a nonzero value after the interruption of current. This is because of the fact that the net double-layer charge has no means for decay in the absence of an electrode reaction; it can only redistribute by flow of current through the solution in order to attain a final uniform state. Hence, for the charging period we have

$$\frac{V}{\Phi_o^p} = \frac{4}{\pi}\theta + D - \sum_{i=1}^{\infty} C_i e^{-\Lambda_i \theta} \quad . \qquad (7\text{-}24)$$

The constant term can be obtained by intergrating condition 1 over the electrode surface for the total period of charging to obtain the net charge added to the double layer:

$$2\pi C \int_0^{r_o} \int_0^{t_{ch}} \frac{(V-\Phi_o)}{\partial t} \, dtrdr = 2\pi \int_0^{r_o} \int_0^{t_{ch}} i_n \, dtrdr = It_{ch} \quad . \tag{7-25}$$

Substitution of equations 3 and 24 into the left side and integration lead to the result

$$D = 2 \sum_{n=0}^{\infty} B_n^{ss} a_{o,n} = 1.08076 = 32/3\pi^2 \quad . \tag{7-26}$$

Finally, the electrode potential for the decay period is

$$\frac{V}{\Phi_o^p} = \frac{4}{\pi} \theta_{ch} + \sum_{i=1}^{\infty} C_i e^{-\Lambda_i \theta'} \left(1-e^{-\Lambda_i \theta_{ch}}\right) \quad . \tag{7-27}$$

The analysis at this point can readily be extended to account for arbitrary changes in the cell current by a straightforward application of the superposition integral. If the time dependent cell current is given by $I(\theta)$, the electrode potential can be expressed as

$$4r_o \kappa V = I(\theta) + C_o J e^{-\theta J} \int_0^{\theta} I(\theta) \, e^{\theta J} d\theta + \sum_{i=1}^{\infty} C_i (\Lambda_i + J) \, e^{-\theta(\Lambda_i + J)} \int_0^{\theta} I(\theta) \, e^{\theta(\Lambda_i + J)} \, d\theta \tag{7-28}$$

0 0 0 0 3 9 0 7 0 4

in the presence of an electrode reaction, and

$$4r_o \kappa V = I(\theta) + \frac{4}{\pi}\int_0^{\theta} I(\theta)\, d\theta + \sum_{i=1}^{\infty} C_i \Lambda_i e^{-\Lambda_i \theta} \int_0^{\theta} I(\theta)\, e^{\Lambda_i \theta}\, d\theta \qquad (7\text{-}29)$$

for an ideally polarizable electrode. One application of these equations would be for an alternating current situation, where the frequency dispersion of the measured impedance is of interest. This discussion is postponed to the next chapter where an analogous equation for the potentiostatic case is developed.

7.4. Results and Discussion

Figure 2 depicts a typical potential trace for double layer charging and decay in the presence of a faradaic reaction, and figure 3 shows potential decay curves after the interruption of current for various values of the kinetic parameter J. For both representations, the current is interrupted after the double layer is charged to steady state conditions. For large decay periods, the slope of each curve approaches the corresponding J value on a semi-logarithmic scale as can be inferred from equation 23. Curves similar to figure 2 could be constructed for different J values by making use of the information contained in figure 3 and by remembering that the ohmic drop is given by the primary distribution Φ_o^p and the charging and decay portions of each curve are symmetric.

The fact that the instantaneous potential step immediately preceding both the charging and decay portions of figure 2 corresponds to the primary current distribution[81] is implicit in the present analysis by virtue of the particular initial conditions (equations 17

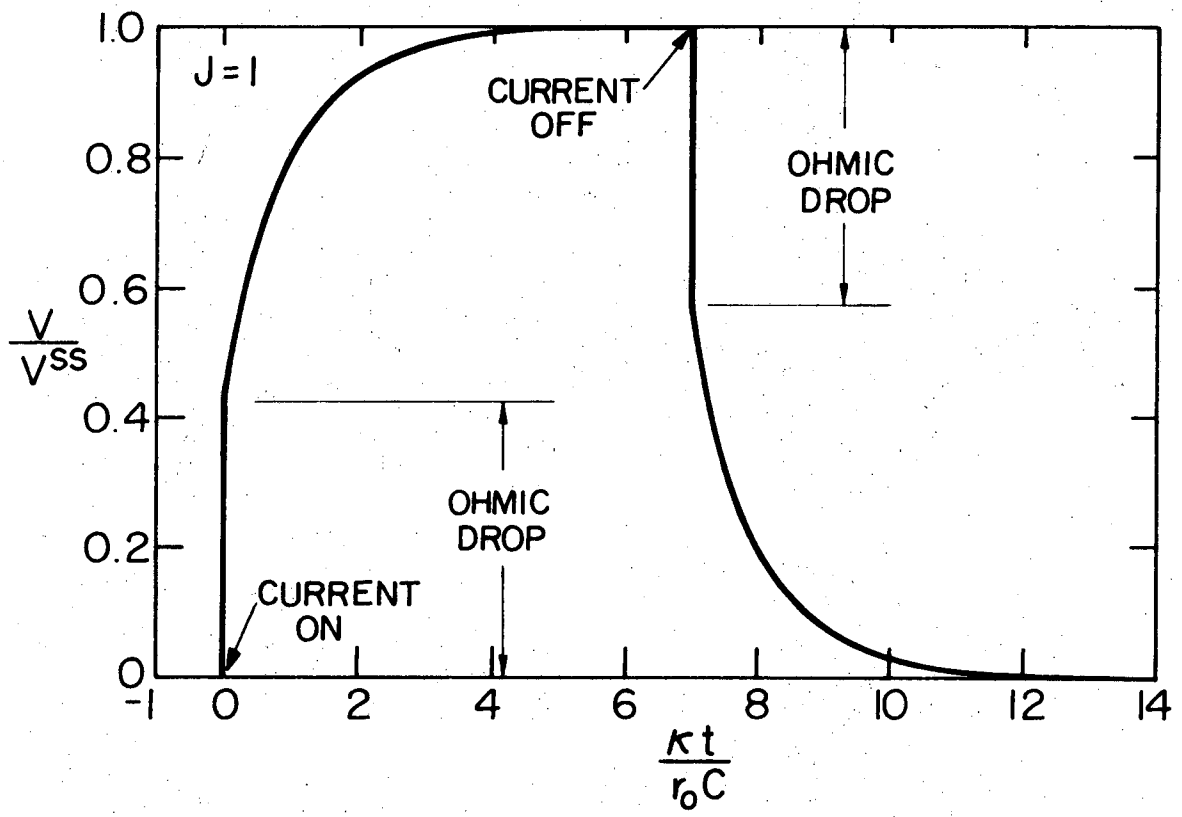

Figure 7-2. Double layer charging and decay in the presence of a faradaic reaction.

0 0 0 0 0 5 9 0 7 7 8 5

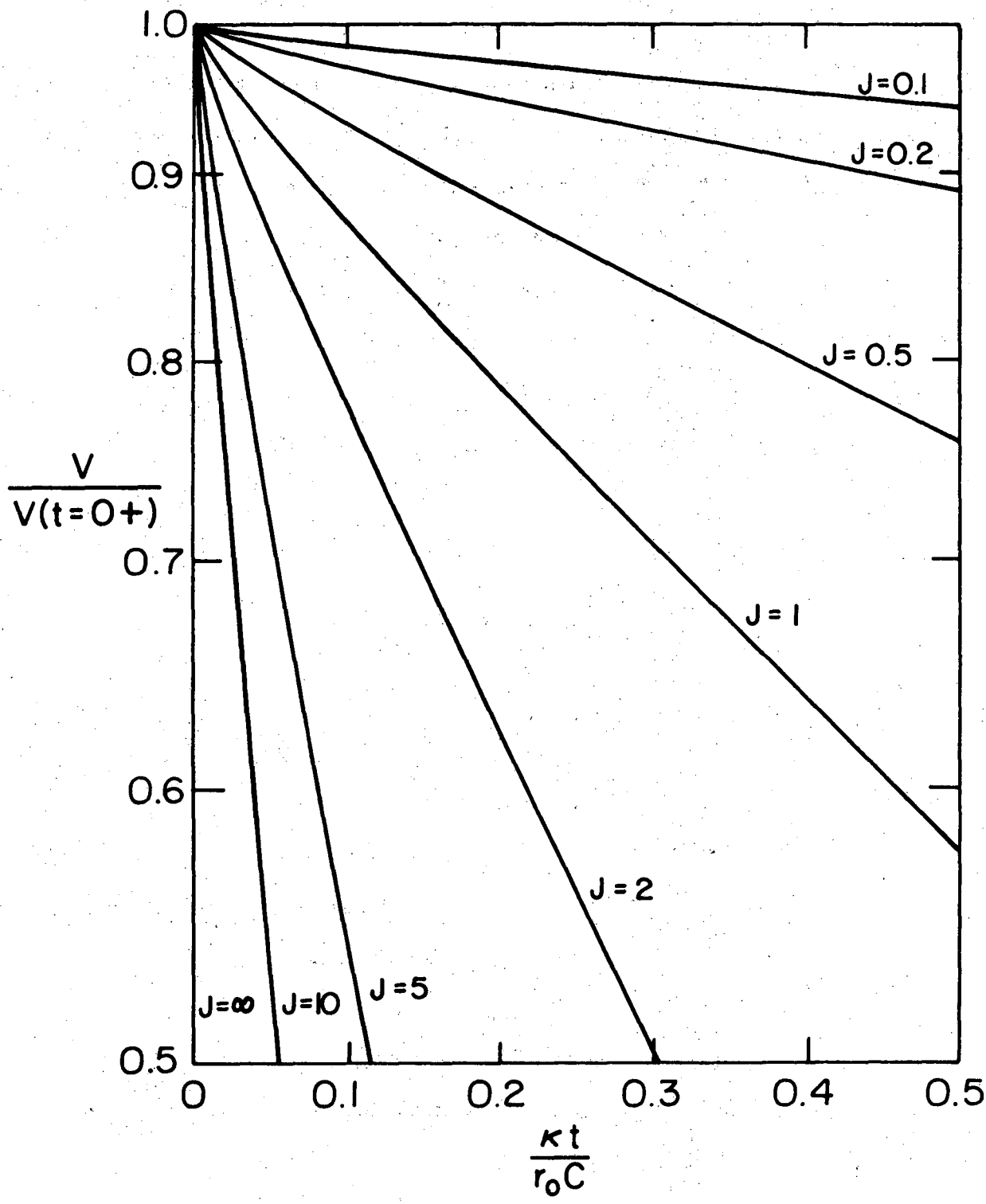

XBL 727-6606

Figure 7-3. Decay of the electrode potential for various values of the kinetics parameter J. A steady condition was attained before interruption of the current.

and 18) employed. Nanis and Kesselman[15] have expressed the contrary view in this regard. We would like to stress that the same criterion would hold for the ohmic drop even if the diffusion layer were taken into consideration. An experimental verification along these lines has been provided by Miller and Bellavance.[59]

The transient response of an ideally polarizable electrode to step changes in the current is depicted in figure 4. The step portions again correspond to the primary distribution. The differences in comparison to figure 2 are obvious. The potential-time relationship becomes linear for sufficiently large charging periods as the surface current density attains a uniform distribution. After the interruption of current, the electrode potential decays to a nonzero value, given by $4\theta_{ch}/\pi$. Decay curves for various charging periods are sketched in figure 5 to show the effect of short charging times on the potential decay. The same effect is also discernable when J is greater than zero, but the dependence on the charging period was not of prime interest in constructing figure 3 and was suppressed by allowing a steady state to develop before current interruption.

An important result of the present analysis is the assessment of an accurate time constant for the decay of the double-layer capacity in the absence of concentration gradients at the electrode surface. From equation 5, we obtain

$$\tau_i = \frac{1}{\Lambda_i + J} \frac{r_o C}{\kappa} \quad . \tag{7-30}$$

0 0 0 0 3 9 0 7 7 3 6

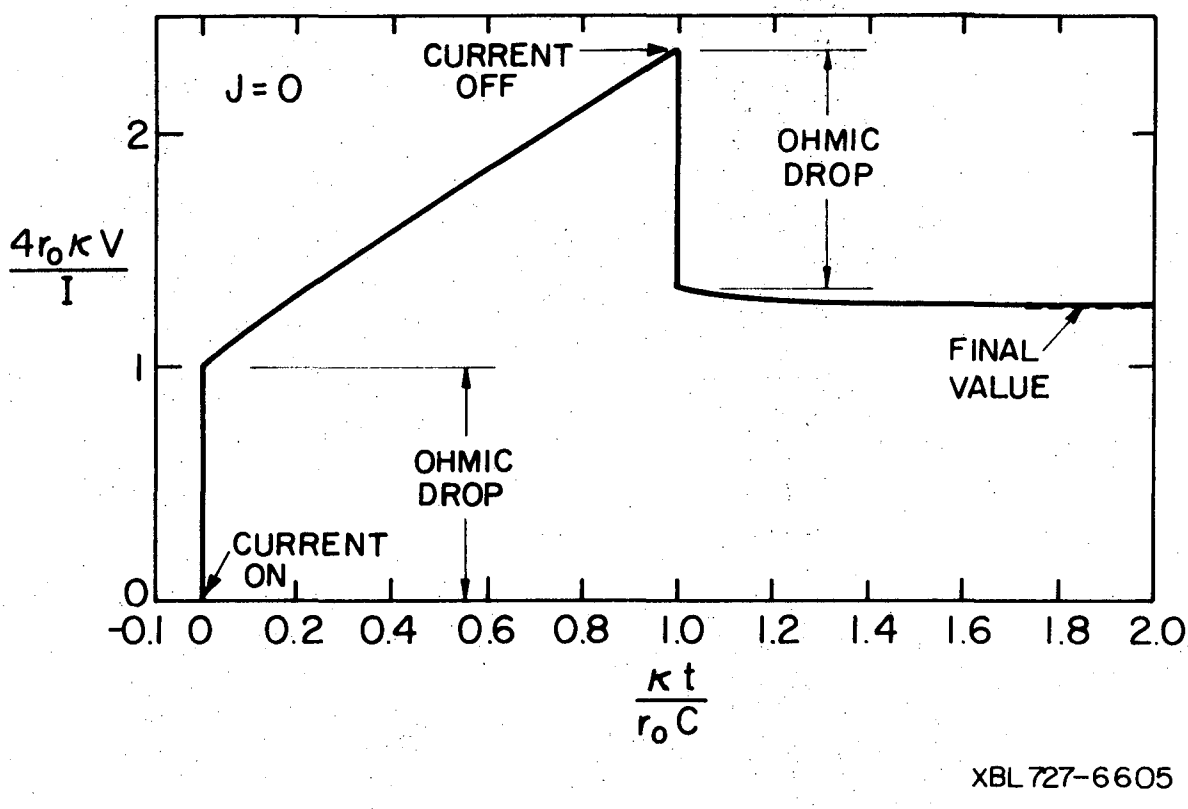

Figure 7-4. Double layer charging and decay in the absence of a faradaic reaction.

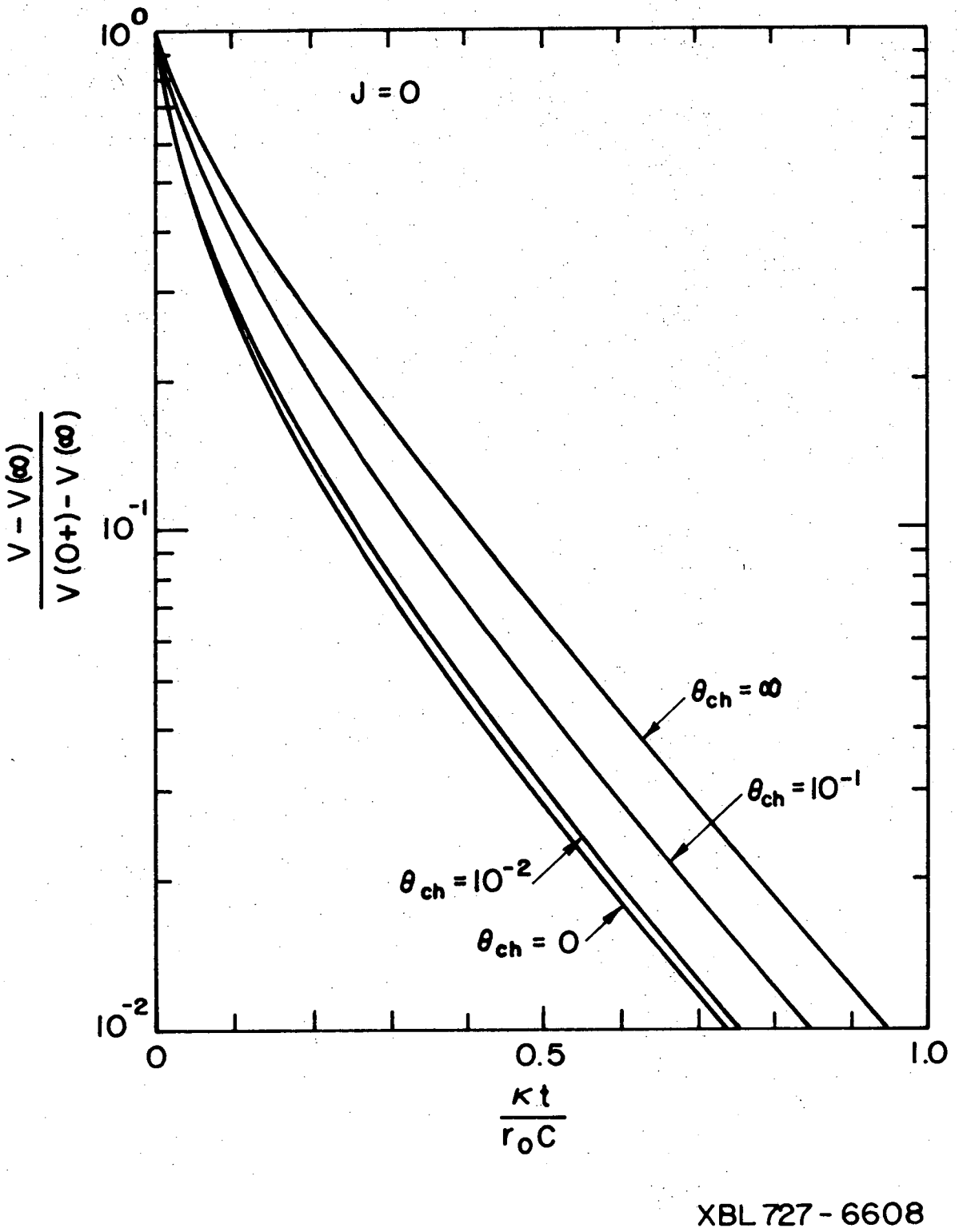

Figure 7-5. Decay of the electrode potential for various charging periods in the absence of a reaction. The slope here is related at long times to the first eigenvalue Λ_1.

0 0 0 0 5 9 0 7 7 8 7

When an electrochemical reaction is possible, the dominant time constant at long times is

$$\tau = \frac{r_o C}{\kappa J} \tag{7-31}$$

as identified by Newman.[81] When an electrochemical reaction is not possible (the ideally polarizable electrode), this time constant becomes infinite, and the potential decays to a nonzero constant. The dominant time constant then is

$$\tau = \frac{r_o C}{\Lambda_1 \kappa} = \frac{1}{4.12} \frac{r_o C}{\kappa} \quad , \tag{7-32}$$

also suggested in the same context[81] but without the determination of the numerical factor. The present analysis amplifies the roles and interrelationship of these two quantities and the processes they describe.

A direct experimental test of these time constants may be performed with the utility of an original reference electrode system designed by Miller and Bellavance.[59] This consists of two probes positioned coaxially with the disk in the solution, so that the potential drop between two distinct locations in the solution could be measured. If linear electrode kinetics and finite exchange current densities are ensured, and concentration gradients near the surface of the disk are avoided, the time constant so measured should correspond to equation 30 for $i = 1$.

7.5. Validity and Significance of Theoretical Results in Practical Application

The reference electrode was assumed to be positioned at infinity relative to the working electrode in obtaining all our results. In practical situations, the reference electrode has to be placed at a finite distance from the disk, and if this is not accounted for in the evaluation of experimental data, serious errors may result.[64] The necessary correction is rather simple to accomplish; since one can assume without significant error that the primary distribution prevails in the bulk of the solution, the reading on the reference electrode can be extrapolated to infinite distance from the disk.[59]

A possible application of the present results might be in the study of the double-layer structure at solid surfaces. Difficulties are encountered in the measurement of differential capacities at solid electrodes due to the frequency dispersion effect,[61] except when it is feasible to construct and employ spherical electrodes.[65,66] Such difficulties may be overcome by attempting to measure relaxation times in interrupter experiments; in the absence of mass transfer, these relaxation times are related to the differential capacity of the disk electrode as shown in previous sections.

In practice, one first investigates the structure of the double layer in the presence of supporting electrolyte alone. If currents due to gas evolution and reduction of impurities are avoided, the working electrode is an ideally polarizable electrode. In this way, one finds out about the relationship between the electrode potential and the surface charge density.[41] One may then add a small amount of reactant

0 0 0 0 3 9 0 7 8 8

and assume that the same charge-potential dependence prevails. Investigations along these lines appear to be successful in depicting qualitatively the influence of the double-layer structure on faradaic reactions, as reviewed by Parsons.[92]

Let us consider an ideally polarizable disk system where $r_o = 0.635$ cm, $C = 30\ \mu f/cm^2$, $\kappa = 0.036\ ohm^{-1}\text{-}cm^{-1}$, and the ohmic drop is 11 ohms. The current is interrupted after charging the electrode for 1 msec at $I = 5$ mA. The characteristic time constant for decay can be calculated from equation 32 as $\tau = 128\ \mu sec$. We can further compute

$$\Phi_o^p = 55 \text{ mV} \quad ,$$

$$\Delta V \equiv V(\theta' = 0+) - V(\theta' = \infty) = 0.08076\ \Phi_o^p = 4.44 \text{ mV} \quad .$$

If the reference electrode is placed along the axis of the disk, we have

$$\begin{aligned} \Delta\Phi_o(r = 0) &\equiv \Phi_o(r = 0,\ \theta' = 0+) - \Phi_o(r = 0,\ \theta' = \infty) \\ &= \Phi_o(r = 0,\ \theta' = 0+) = \Phi_o^{ss}(r = 0) - \Phi_o^p \\ &= \Phi_o^p \left(\sum_{n=0}^{\infty} B_n^{ss} - 1 \right) = \Phi_o^p \left(\frac{4}{\pi} - 1 \right) \\ &= 15 \text{ mV} \quad , \end{aligned}$$

$$\Delta(V - \Phi_o) = \Delta V - \Delta\Phi_o(r = 0) = -10.6 \text{ mV} \quad ,$$

$$V - \Phi_o(\theta' = \infty) = V(\theta' = \infty) = \frac{It_{ch}}{\pi r_o^2 C} = 132 \text{ mV} \quad .$$

It is interesting to note that $\Delta\Phi_o(r = 0)$ is larger than ΔV and can be detected with relative ease with a double-probe reference electrode.[59]

The negative value of $\Delta(V - \Phi_o)$ indicates that this quantity (which we would have called the electrode overpotential if a faradaic reaction were present) actually increases at the center of the disk as the charge redistributes itself in the double layer to effect a final uniform and nonzero charge distribution. The change in $V - \Phi_o$ during the transient process is also moderately small compared to its absolute value, so that the double-layer capacity C can be assumed to be independent of the potential in this range without much error.

In reality, it is impossible to have a perfect ideally polarizable electrode. One can approximate it by maintaining its potential by an external source.[41] If the current is interrupted, the potential of a real electrode will decay more or less slowly to its open-circuit potential due to the reduction of impurities present in the solution.[41] Thus if an electrode reaction is possible either owing to the presence of impurities or a reactant in the solution, the characteristic times for decay are

$$\tau_e = \frac{r_o C}{\kappa J} \tag{7-33}$$

for the electrode potential, and

$$\tau_s = \frac{1}{4.12+J} \frac{r_o C}{\kappa} \tag{7-34}$$

for the potential in the solution. Even if Tafel kinetics might govern the electrode reaction soon after interruption, linear kinetics will take over at large times as the overpotential decays, and the above time constants will become prevalent. Thus, if J is small, let us say 0.005, then the electrode potential will decay with a time

0 3 0 0 3 9 0 / / 8 9

constant τ_e = 106 msec whereas the potential in the solution will decay much more rapidly, with the time constant τ_s = 0.13 msec.

If, however, J is of order unity or larger, this effect is rather appreciable and has to be accounted for. One possibility is to measure τ_s and τ_e simultaneously by a disk electrode-double probe reference electrode set-up appropriately hooked up to a dual-beam oscilloscope. By subtracting the reciprocals of the two time constants, we obtain

$$\frac{1}{\tau_s} - \frac{1}{\tau_e} = \frac{4.12\kappa}{r_o C} \quad , \tag{7-35}$$

which is independent of the exchange current density.

If the electrode reaction is mass-transfer controlled, the characteristic times depend on additional parameters such as the diffusion coefficient of active species and the diffusion-layer thickness. For the situation where one is concerned about the reduction of impurities at the disk after the interruption of current, a reasonable estimate of the faradaic current can be obtained from

$$i_f = \frac{nFD_i}{s_i} \frac{c_{i\infty} - c_{io}}{\delta} \quad , \tag{7-36}$$

where δ is the Nernst diffusion layer thickness. Assuming a highly reversible reaction controlled by diffusion and the capacitive effect of the double layer, the capacitive current is

$$i_c = C \frac{\partial \eta_c}{\partial t} \quad , \tag{7-37}$$

where η_c is the concentration overpotential given by equation 3-12. Since the net current is zero,

$$i = i_f + i_c = 0 \quad . \tag{7-38}$$

When we combine these four equations and integrate, we obtain a characteristic time constant for this case (compare to equation 6-35):

$$\tau_D = \frac{s_i^2 CRT\delta}{n^2 F^2 D_i c_{i\infty}} \quad . \tag{7-39}$$

τ_D thus depends inversely on the concentration of impurities, which has to be kept as small as possible. Consider the reduction of a bivalent ion ($n/s_i = 2$) with $D = 10^{-5}$ cm^2/sec, $\delta = 10^{-3}$ cm, and $c_\infty = 10^{-9}$ mole/cm^3. Then, $\tau_D = 0.2$ msec.

In case the capacitive effect can be ignored, and a purely mass-transfer-controlled electrode process in considered, the appropriate time constant is proportional to δ^2/D, or more exactly,

$$\tau_D = \frac{3.26\ Sc^{1/3}}{\Lambda_D \Omega} \quad , \tag{7-40}$$

where Ω is the angular frequency of rotation of the disk and Λ_D is a constant characteristic of the diffusion process. Determination of this constant requires a detailed analysis of the transient mass transfer problem at a disk electrode as discussed in chapter 6 and appendix B. With the simplifying assumption of a radially independent concentration distribution, we obtained $\Lambda_D = 2.581$ for a step change of flux (see chapter 6). Using this value for Λ_D, Sc = 1000, and

0 0 0 0 3 9 0 / / 9 0

Ω = 250 radians/sec, we obtain τ_D = 51 msec. Nanis and Klein report experimental relaxation times (defined as the time required for the overpotential to decay to 99 percent of its initial value) of 50 to 0.5 seconds for rotational Reynolds numbers between 130 and 8500, respectively, in 0.005 M ferrocyanide-ferricyanide redox system in 2M KOH solution.

The above discussion suggests that the effects of the double layer and mass transfer can be controlled according to the needs of the experimenter by proper design of the electrochemical system and the experimental method. It is possible to reduce mass transfer effects by choosing a system where the relaxation times due to mass transfer are of a much larger scale than the relaxation times associated with the diffuse double layer. The magnitude of the effect is also important as well as its duration. Note that while the time constant in equation 40 becomes smaller as Ω increases, the amplitude of the corresponding concentration disturbance would decrease. In other words, the other extreme where the concentration effects would become negligible is the well-stirred solution case, one of our assumptions in treating the theoretical problem.

7.6. Experimental Measurement

We have performed some experiments in an attempt to test our theoretical results. These experiments were rather crude, preliminary runs executed with limited equipment in a limited amount of time, and thus the results are not in any way conclusive. Some of our experience, which is still at a somewhat primitive stage, is summarized below.

The electrolytic cell (see figure 6) consisted of a large, 7-gallon capacity pyrex tank equipped with a mechanical stirrer, a tube with a fritted glass end for bubbling nitrogen into the solution, and a counter electrode of platinum foil (0.00025 in. thick, ~1000 cm^2 in area) pasted on the container wall. The cell was filled with 0.01 molar KCl solution. The solutions were prepared by weighing dried KCl crystals (Baker Reagent) into a known volume of distilled water (conductivity - 10^{-7} to 10^{-6} ohm^{-1}-cm^{-1}). No temperature control was used; owing to the large volume of the electrolyte, temperatures remained remarkably stable (within 0.02°C during experimental runs. The conductivity of the solution was assessed by interpolation from published data[102] at the measured concentration and temperature.

A few types of reference electrodes were tried such as platinum or copper wires extended to position in the solution in sealed glass jackets and calomel electrodes (commercial types purchased from Corning Glass Works) connected to Luggin capillaries. Platinum and copper wires provide to the oscilloscope strong signals, which can be detected easily by standard preamplifier units employed with oscilloscopes. The calomel electrode should be a better choice for this experiment since it is reversible to the chloride ion. On the other hand, the resistance of the calomel electrode along with the resistance of the Luggin capillary is probably comparable to the input resistance of the oscilloscope preamplifier; hence, a more sophisticated amplification may be necessary to register a strong enough signal and minimize the noise. However, not much attention was paid to the proper measurement nor the magnitude of the potential,

0 0 0 0 5 9 0 , 7 9 1

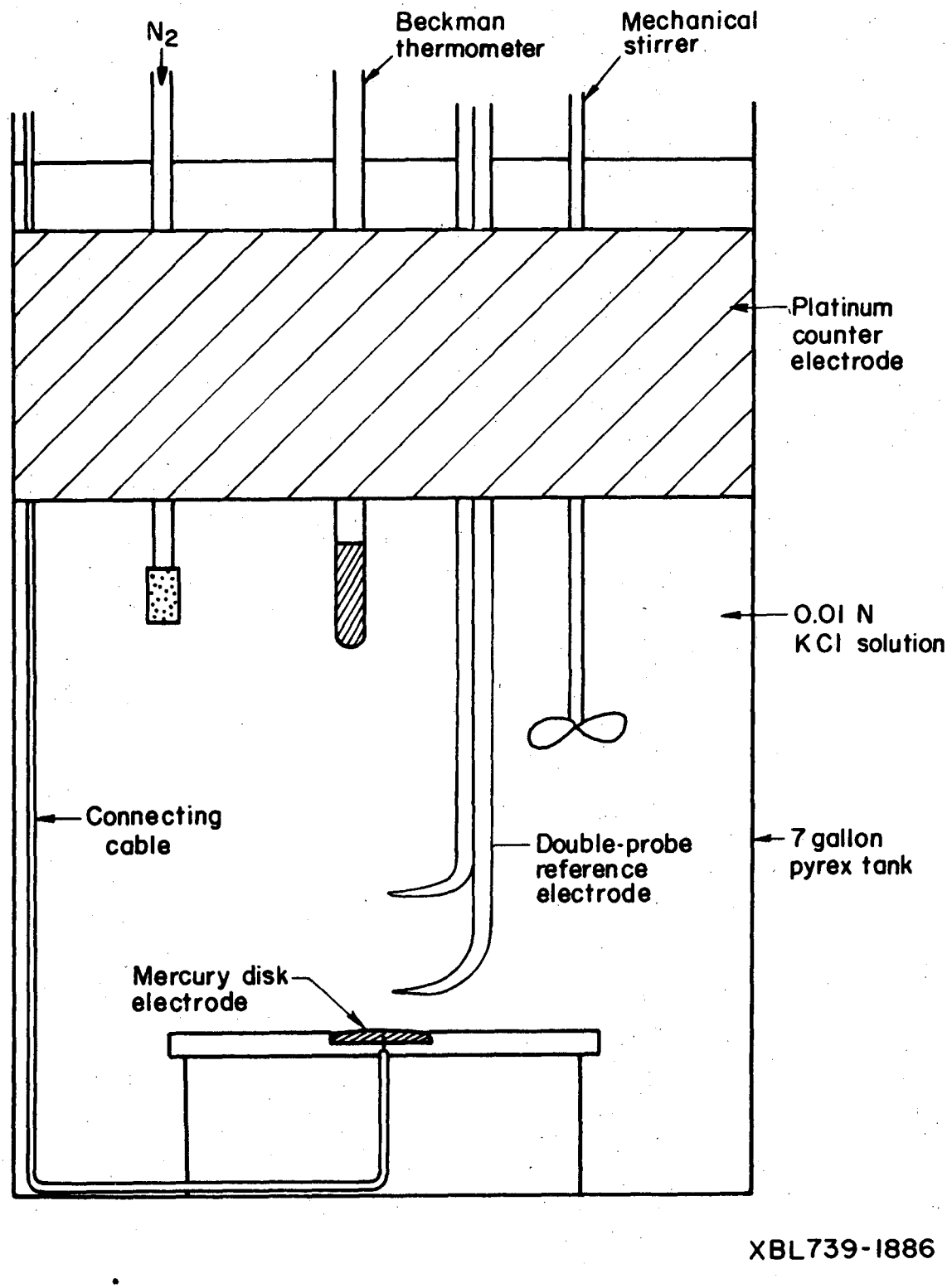

Figure 7-6. Electrolytic cell.

other than making sure that the hydrogen overpotential was not exceeded, because the main purpose of the present effort was to measure the time constants of the transient potentials in the solution and at the disk rather than the potentials thermselves.

The disk electrodes used were made of copper (CDA Copper No. 110) and mercury (Ballard's, triple distilled) with lucite insulating planes. The copper electrode (r_o = 2.54 cm) was polished with successively finer grades of sandpaper and finished with 1 micron diamond paste. The mercury electrode (r_o = 2.17 cm) was prepared by machining a circular compartment in lucite with slanted walls (see figure 7) in order to offset the contact angle and attain a reasonably flat mercury surface. Mercury was chosen as an electrode metal because accurate and reliable data are available for its double-layer capacity.[41,103]

Figure 8 shows the electronic circuitry. The current source was obtained from Electronic Instruments, Inc. (Model C612). Transient potential signals were observed on a Tektronix, Type-555 Dual Beam Oscilloscope with Type-D Plug-in Units. A high-gain operational amplifier (Type-0 Plug-in Unit) was used occasionally to improve weak signals from the calomel electrodes. The test pulser (USAEC No. 91315) and the interrupter (IMRD No. 02191) were built in the Lawrence Berkeley Laboratory. The pulser generated regular and delayed signals to trigger the interrupter and the oscilloscope, respectively. The pulser-interrupter system could be operated continuously to generate pulses at a certain frequency or manually to provide a single pulse whenever necessary. The performance of the interrupter circuit is demonstrated by figures 9 and 10. Duration of the pulse is about 2 msec,

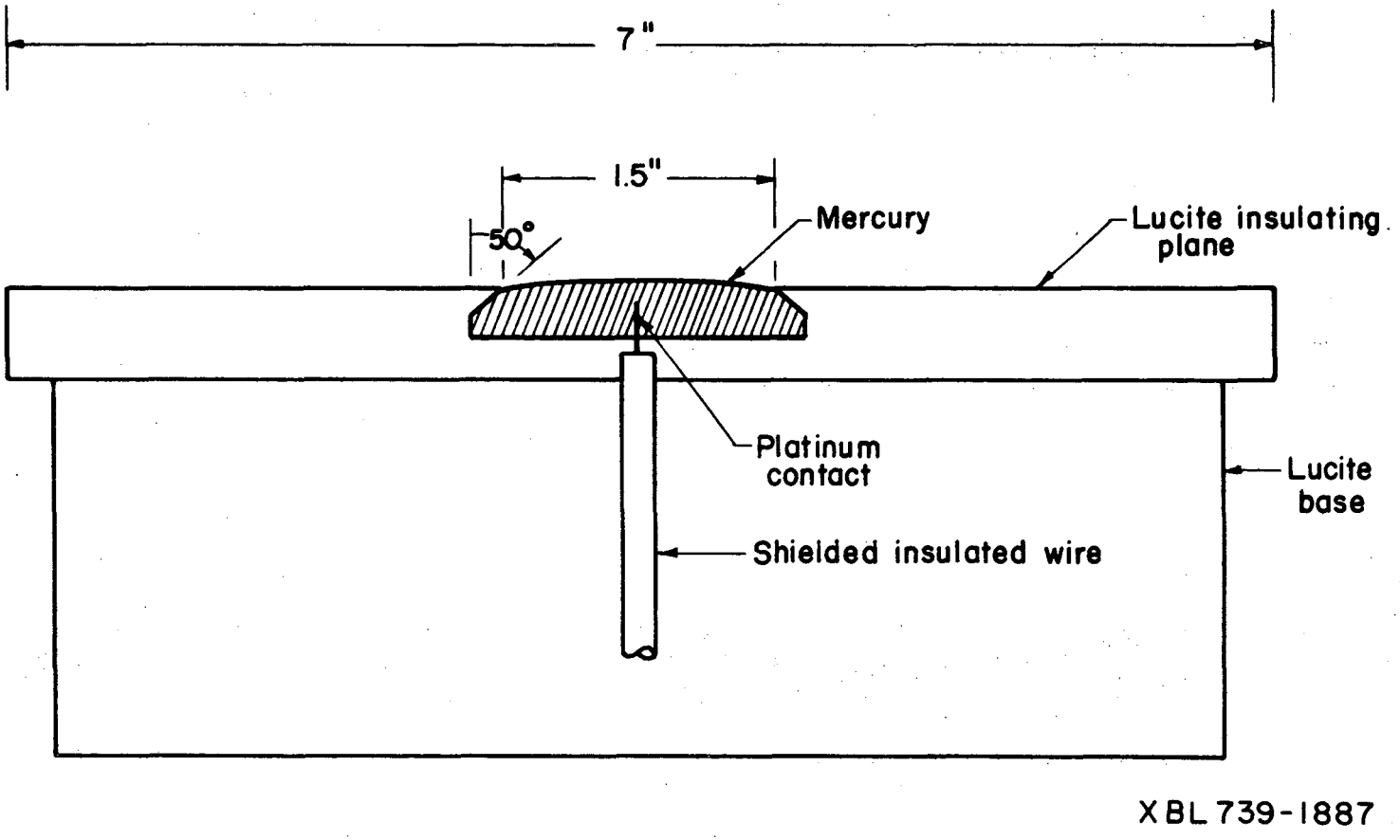

Figure 7-7. Mercury-disk electrode (approximate dimensions).

0 0 0 5 6 9 0 1 6 2

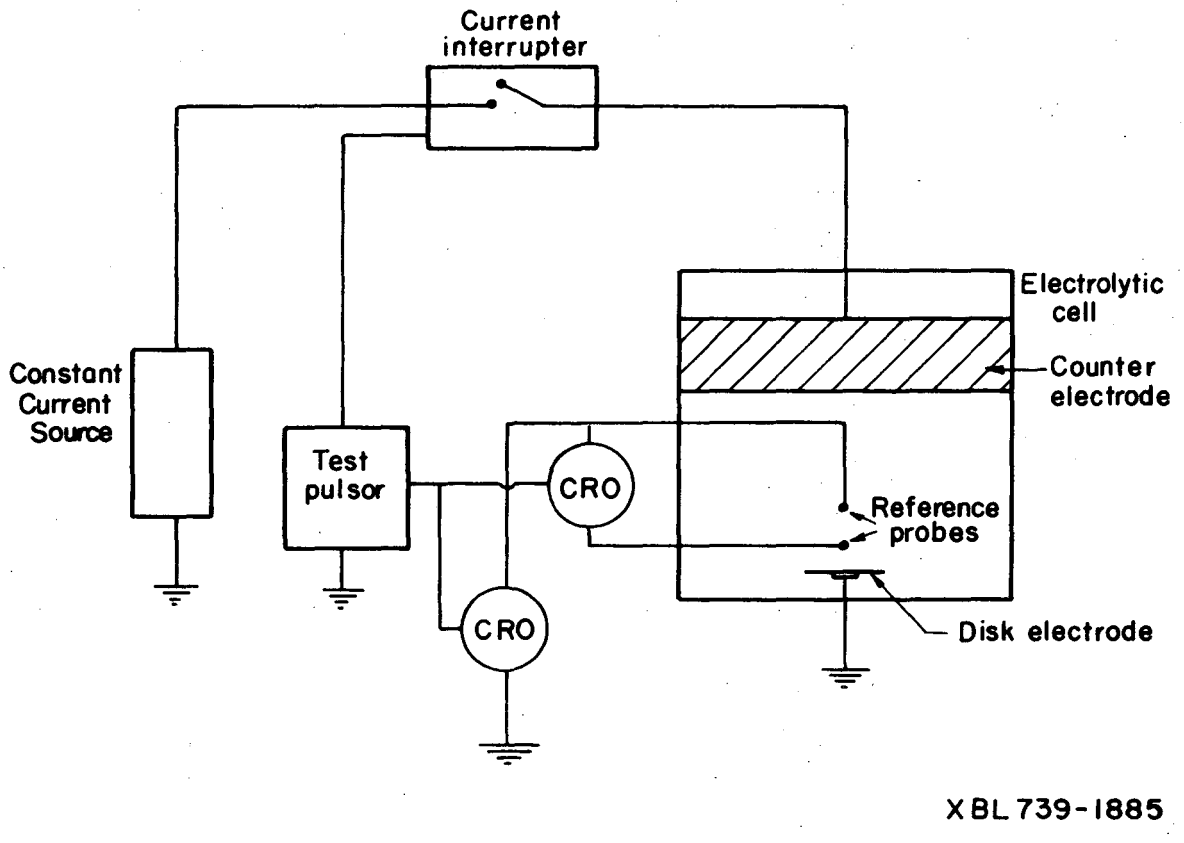

Figure 7-8. Electronic circuit.

0 0 0 0 3 9 0 7 9 3

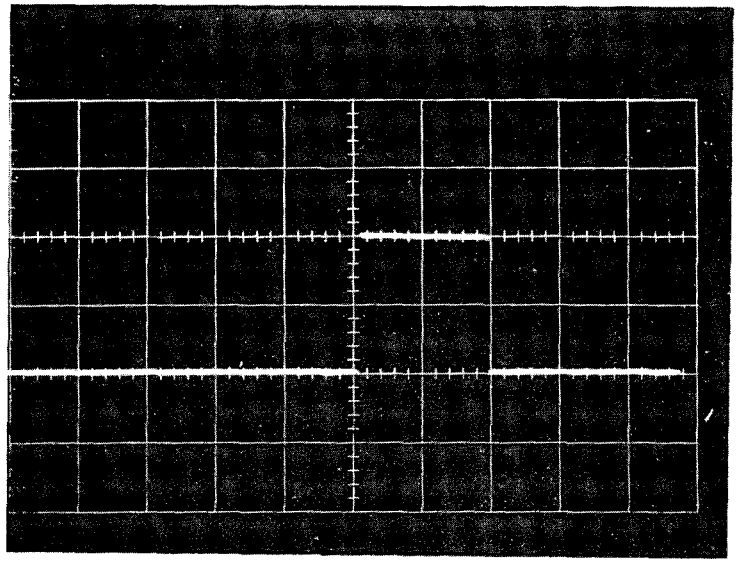

Figure 7-9. Interrupter signal with a 100 Ω resistor in place of the electrolytic cell (I=10 mA; 0.5 V/division, vertical; 1 msec/division, horizontal).

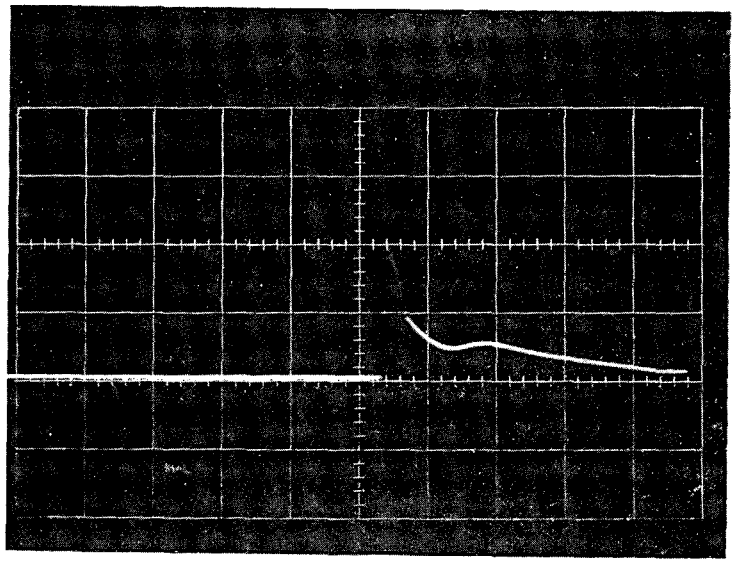

XBB 739-5609

Figure 7-10. Interrupter signal with a 100 Ω resistor in place of the electrolytic cell: expanded time scale (I=10 mA; 10 V/division, vertical; 20 μsec/division, horizontal).

the shortest that could be obtained with the given equipment. The step increase in the signal in figure 9 corresponds to the instant when the current is switched on. If this portion of the trace is expanded horizontally (time axis), a sharp spike becomes visible (figure 10). This is due to a discharge of electrons as the circuit is being closed. The spike reaches a height of about 40 volts when a current of 10 mA is passed across a 100 Ω resistor. The step decrease in the signal when the current is interrupted appears to be clean of sparks.

The oscilloscope traces were normally photographed on Polaroid transparencies using a Tektronix Type C-12 camera. These were then analyzed with the aid of a Jarrell-Ash Recording Microphotometer. This instrument measures the intensity of a very narrow light beam transmitted through a transparent photograph. It is also equipped with a traveling stage, which moves in the longitudinal and transverse directions, and vernier scales in each direction for measuring the position of the stage. The transparencies were placed on the stage and traced to measure the coordinates of the potential decay curves. Readings were taken at intensity maxima along the curves at regular intervals of the time coordinate. These points were plotted on a semi-logarithmic graph paper as suggested by figure 3 or 5 and time constants calculated from slopes of the linear portions of the curves.

Figures 11 to 14 show typical oscilloscope traces observed during a regular experiment; these were obtained with a mercury-disk electrode. Figure 11 and 12 depict the potential of the disk as measured with respect to the upper and lower reference probes, respectively. The

0 0 0 0 3 9 0 7 7 9 4

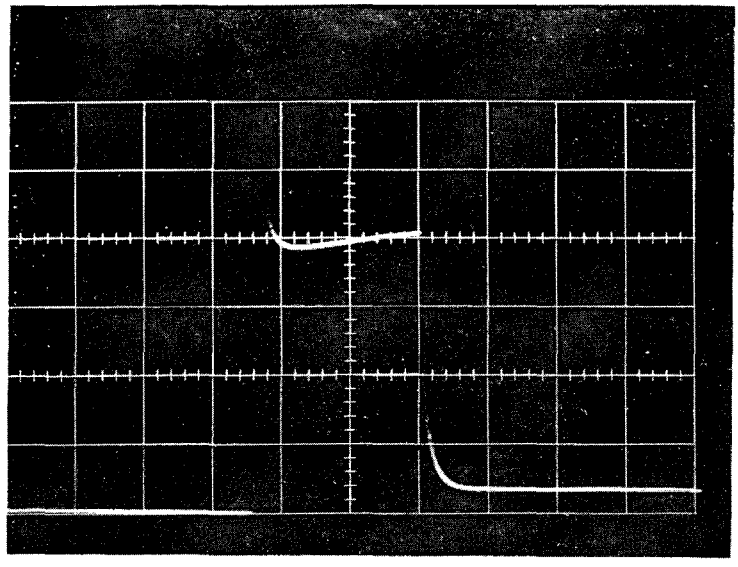

Figure 7-11. The transient response of the mercury disk with respect to the upper probe for charging and decay (I=10 mA; 1 msec/division, horizontal).

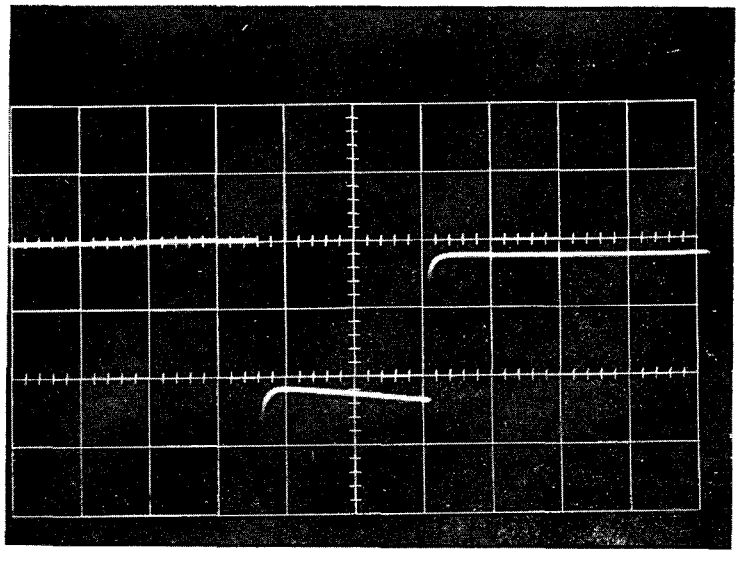

XBB 739-5611

Figure 7-12. The transient response of the mercury disk with respect to the lower probe for charging and decay (I=10 mA; 1 msec/division, horizontal).

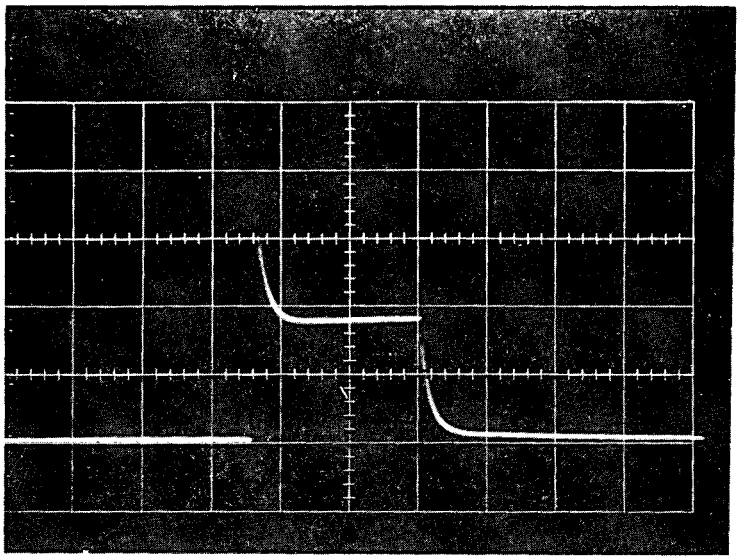

Figure 7-13. The double-probe response to charging and decay of the double-layer capacity (I=10 mA; 1 msec/ division, horizontal).

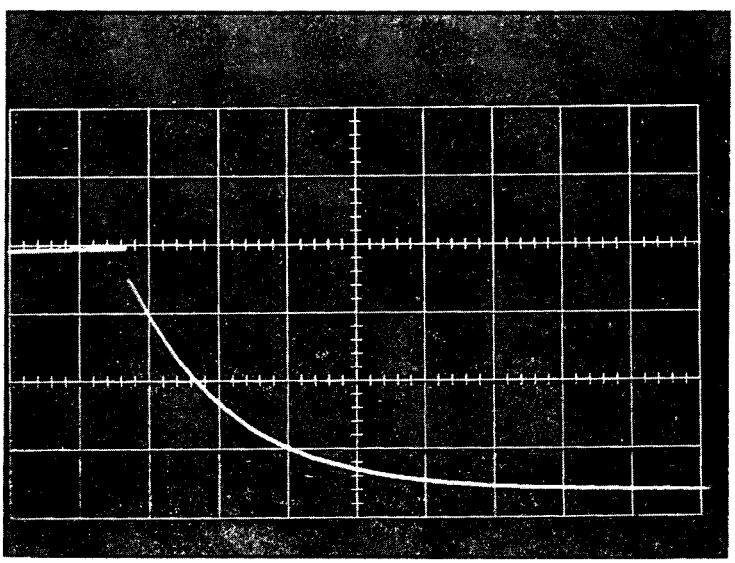

XBB 739-5610

Figure 7-14. The double-probe response to decay of the double-layer capacity: expanded scale (I=10 mA; 0.1 msec/ division, horizontal).

0 0 0 0 3 9 0 7 9 5

signal of the lower probe has been multiplied by -1. The sum of these two signals is shown in figure 13 and represents the double-probe potential. Figure 14 shows the decay part of the same signal on a expanded scale and is more suitable for final analysis to calculate the desired time constants. The overshoot of voltage when the current is turned on is due to the sparking effect discussed above.

The time constants obtained from both the single-probe and double-probe traces generally turned out to be much smaller than those calculated from equations 33 and 34 assuming a small J value relative to Λ_1. For example, with the mercury-disk electrode, double-probe traces gave a time constant of about 250 μsec whereas the value calculated from equation 34 for C = 20 $\mu f/cm^2$ and small J is about 7.5 msec. The time constant from the single-probe measurement was very close to the double-probe result; but, it was generally larger than the double-probe measurement, the difference ranging from as low as a few microseconds up to about 50 microseconds. These time constants yielded double-layer capacities between 5 to 50$\mu f/cm^2$, which are within the correct order of magnitude for a mercury surface.[103] The time constants measured with the copper disk were even worse in reproducibility; the values fluctuated in the range 10^{-1} to 10 msec. Nonetheless, the calculated capacities varied between 10 to $10^2 \mu f/cm^2$, again within the correct order of magnitude.[66]

It appears from these results that impurities are present in the solution, and these react with the disk electrode either with a high exchange-current density or by a mass-transfer-controlled process. For the former case, the time constants for decay of the potential in

the solution and the disk electrode are given by equations 33 and 34. These equations yield time constants, which become smaller and at the same time closer in value to one another, with larger values of the parameter J. If the rate of discharge of impurities at the electrode surface is limited by mass transfer, equation 39 gives a better extimate of the time constant. The value calculated in the numerical example following that equation is in fact fairly close to the present experimental results for mercury.

The mercury-disk electrode is superior to the copper disk in obtaining more reproducible results because the mercury surface can be regenerated by cathodic polarization, whereas the copper surface is altered irreversibly during an experimental run. The situation can be improved for the mercury electrode by operating at cathodic potentials at all times. This can be accomplished by interrupting the current from a higher cathodic level to a lower one instead of altogether breaking the circuit. If the current is interrupted by breaking a closed circuit, as was the case in the present experiment, the electrode potential decays to its open-circuit potential with respect to the reference electrode being used. This potential is usually low enough to cause considerable adsorption of impruities on the mercury surface, thereby altering its differential capacity significantly.

It also seems quite possible that vigorous bubbling of nitrogen through the solution was not adequate in deaerating the large volume of electrolyte used. Presence of oxygen in the solution could have complicated the electrokinetic behavior of the disk electrode appreciably. Further purification of the water from ionic and organic impurities by

0 0 0 0 3 9 0 7 7 9 6

repeated distillation may also be necessary. Ionic impurities can be removed by reducing them on an auxiliary electrode which can later be removed from the solution. Other electrochemical purification techniques are reviewed by Parsons.[92]

The bulky design of the present electrolytic cell was decided upon in order to amplify the effect of double-layer charging, so that this effect could be observed with relative ease. Smaller designs may however prove to be more feasible for improving the purification and deaeration of the electrolytic solution.

VIII. THE TRANSIENT RESPONSE OF A DISK ELECTRODE UNDER POTENTIOSTATIC CONTROL

In the previous chapter, we developed a model for treating the transient response of a disk electrode in the absence of concentration gradients near the surface. We will report here a mathematical analysis developed for the same model but with the electrode potential put under control instead of the current.[93] The results could be relevant to some electroanalytical applications of the disk electrode; for instance, interrupter methods under potentiostatic control are already in common use.[89,90]

The problem was formulated with certain assumptions in chapter 7 and will not be repeated here. The only difference in the present formulation lies in the fact that the electrode potential is set at zero time as a step to a given value V and maintained at that value thereafter. Our purpose here is therefore to simulate the transient decay of the cell current from an initial value I_o corresponding to the primary distribution to a final steady-state value I_∞.

8.1. Analysis

The potential in the solution can be expressed in terms of a steady state and a transient contribution as given by equation 7-3. A detailed analysis of the steady-state problem is given in section 4.1. The treatment given in that section for the ideally polarizable electrode, however, does not apply for the present situation; Φ^{ss} vanishes in the absence of an electrode reaction since no net current is associated with the working electrode at steady state when the potential is fixed.

0 0 0 0 5 9 0 1 1 9 7

In terms of the rotational elliptic coordinates η and ξ, the transient part of the potential can be expressed as

$$\frac{\Phi^t}{V} = \sum_{i=0}^{\infty} C_i e^{-\theta(\lambda_i+J)} T_i(\eta,\xi) \quad , \tag{8-1}$$

where T_i is a dimensionless potential independent of time, λ_i is an eigenvalue characteristic of the potential T_i, and θ and J are the dimensionless time and exchange current density, respectively. Since Φ^t satisfies Laplace's equation, the functions T_i also satisfy

$$\nabla^2 T_i = 0 \quad . \tag{8-2}$$

The boundary conditions associated with T_i are

$$\left.\begin{aligned} &\frac{\partial T_i}{\partial \eta} = 0 \quad \text{at} \quad \eta = 0 \text{ (on the insulating portion of the disk)} \quad , \\ &T_i = 0 \quad \text{as} \quad \xi \to \infty \text{ (far from the disk)} \quad , \\ &T_i \text{ well behaved at } \eta = 1 \text{ (on the axis of the disk)} \quad , \end{aligned}\right\} \tag{8-3}$$

and

$$\frac{\partial T_i}{\partial \xi} + \lambda_i \eta T_i = 0 \quad \text{at} \quad \xi = 0 \text{ (on the disk electrode)} \quad , \tag{8-4}$$

which is obtained by a direct substitution of equation 1 into the boundary condition on the disk electrode.

Equations 2 to 4 constitute an eigenvalue problem, which can be solved in a straightforward fashion (see section 7.2). The solution to equation 2 satisfying the conditions 3 is

$$T_i = \sum_{n=0}^{\infty} B_{i,n} P_{2n}(\eta)\, M_{2n}(\xi) \quad . \tag{8-5}$$

Substitution into equation 4 for each i and inversion of the resulting set of linear equations with the normalization condition $B_{i,o} = 1$ yield the numerical values of the eigenvalues λ_i and the coefficients $B_{i,n}$ (see table 1 and appendix E). The first four eigenfunctions are plotted with respect to the radial position on the surface of the disk in figure 1.

The functional behavior of $T_{i,o}$ has much the same significance as the corresponding eigenfunctions $U_{i,o}$ of the galvanostatic problem in depicting the nonuniform state of charge and the pattern of local current flow on the surface of the disk during the transient process. One may note, in fact, that $T_{i,o}$ in figure 1 are quite similar to the corresponding curves for $U_{i,o}$ given in figure 7-1 for $i > 0$. The eigenvalues λ_i also become more similar in numerical value to Λ_i of the galvanostatic series with increasing i.

An important departure from the galvanostatic case is clearly that Φ^t does include a net current in the present situation. This additional contribution is contained, for example, in the first eigenfunction T_o, which unlike U_o is nonzero. The fact that $T_{o,o}$ exhibits no extremum points nor any zeroes suggests that it persists the longest during the decay process and is therefore associated with the largest time constant.

The eigenfunctions $T_{i,o}$ satisfy the orthogonality relationship

$$\int_0^1 \eta T_{i,o} T_{j,o} \, d\eta = \begin{cases} 0 & \text{if } i \neq j \ , \\ -\frac{1}{\lambda_i} \sum_{n=0}^{\infty} \frac{M'_{2n}(0)}{4n+1} B_{n,i}^2 & \text{if } i = j \ . \end{cases} \tag{8-6}$$

Table 8-1. The first six eigenvalues and the related coefficients $B_{n,i}$ of the eigenfunctions.

	λ_0	λ_1	λ_2	λ_3	λ_4	λ_5
	1.15777	4.31680	7.46018	10.6023	13.7441	16.8858
n	i=0	i=1	i=2	i=3	i=4	i=5
0	1.00000	1.00000	1.00000	1.00000	1.00000	1.00000
1	0.39451	-3.30704	-3.20144	-3.08673	-3.00260	-2.94030
2	-0.01974	-3.09447	2.69232	3.87544	4.20749	4.29990
3	0.01259	-0.52802	6.45944	0.65745	-2.15584	-3.53764
4	-0.00657	-0.10223	2.64610	-8.32547	-5.09803	-1.69133
5	0.00393	0.02410	0.63787	-6.16121	7.06426	8.21141
6	-0.00256	-0.01843	0.03554	-2.27051	9.75697	-2.49615
7	0.00178	0.01289	0.03502	-0.43176	5.33233	-11.5222
8	-0.00129	-0.00946	-0.02056	-0.10618	1.62964	-9.36731
9	0.00097	0.00718	0.01605	0.01863	0.40730	-4.07287
10	-0.00075	-0.00559	-0.01255	-0.02158	0.02998	-1.27763

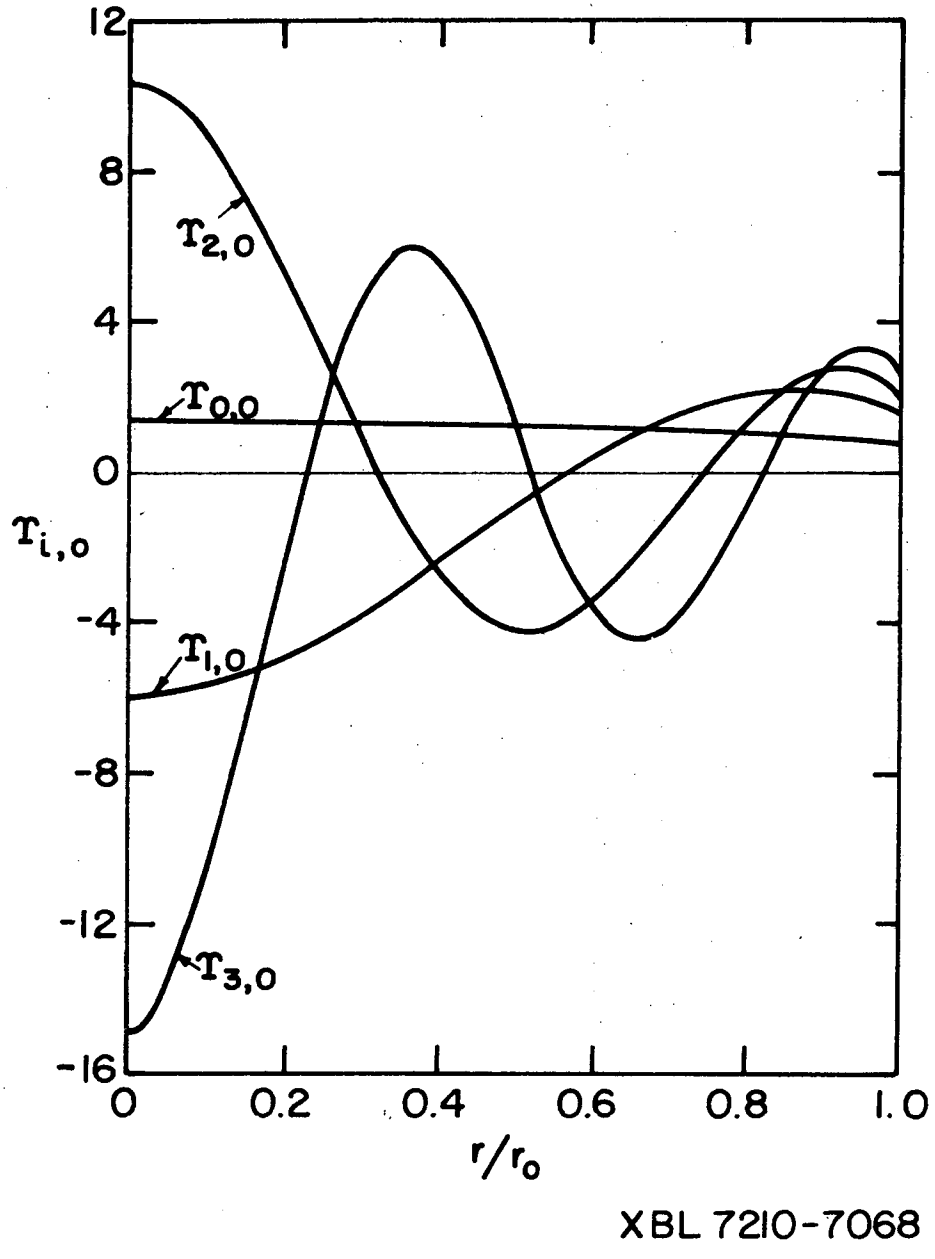

Figure 8-1. Behavior of the first four eigenfunctions on the surface of the disk electrode (potentiostatic case).

0 0 0 0 0 5 9 0 7 7 9 9

From the initial condition

$$\Phi = V \quad \text{at} \quad \theta = 0+ \ , \ \xi = 0 \ , \tag{8-7}$$

the coefficients C_i can now be calculated from the equation

$$C_i = \frac{2\lambda_i}{\pi(\lambda_i+J) \sum_{n=0}^{\infty} \frac{M'_{2n}(0)}{4n+1} B^2_{n,i}} \ . \tag{8-8}$$

The current is given by

$$I = -2\pi r_o \kappa \int_0^1 \left.\frac{\partial \Phi}{\partial \xi}\right|_{\xi=0} d\eta$$

$$= I_o \left[\frac{I_\infty}{I_o} - \sum_{i=0}^{\infty} C_i e^{-\theta(\lambda_i+J)} \right] \ . \tag{8-9}$$

The ratio I_∞/I_o is a known quantity once the value of J is specified and can be obtained directly from the steady-state analysis. Some calculated values are given in table 4-2 (reciprocal of $4r_o \kappa R_{eff}$). Figure 2 shows current versus time traces for various J values. Each curve is characterized by a time constant for decay given by

$$\tau = \frac{1}{1.16+J} \ \frac{r_o C}{\kappa} \ . \tag{8-10}$$

The analysis can be generalized by superposition to incorporate an arbitrary time dependence of the applied potential $V(\theta)$. The current is then given by

$$\frac{I}{4r_o \kappa} = V(\theta) + \sum_{i=0}^{\infty} C_i(\lambda_i+J) \ e^{-\theta(\lambda_i+J)} \int_0^{\theta} e^{\theta(\lambda_i+J)} \ V(\theta) \ d\theta \ . \tag{8-11}$$

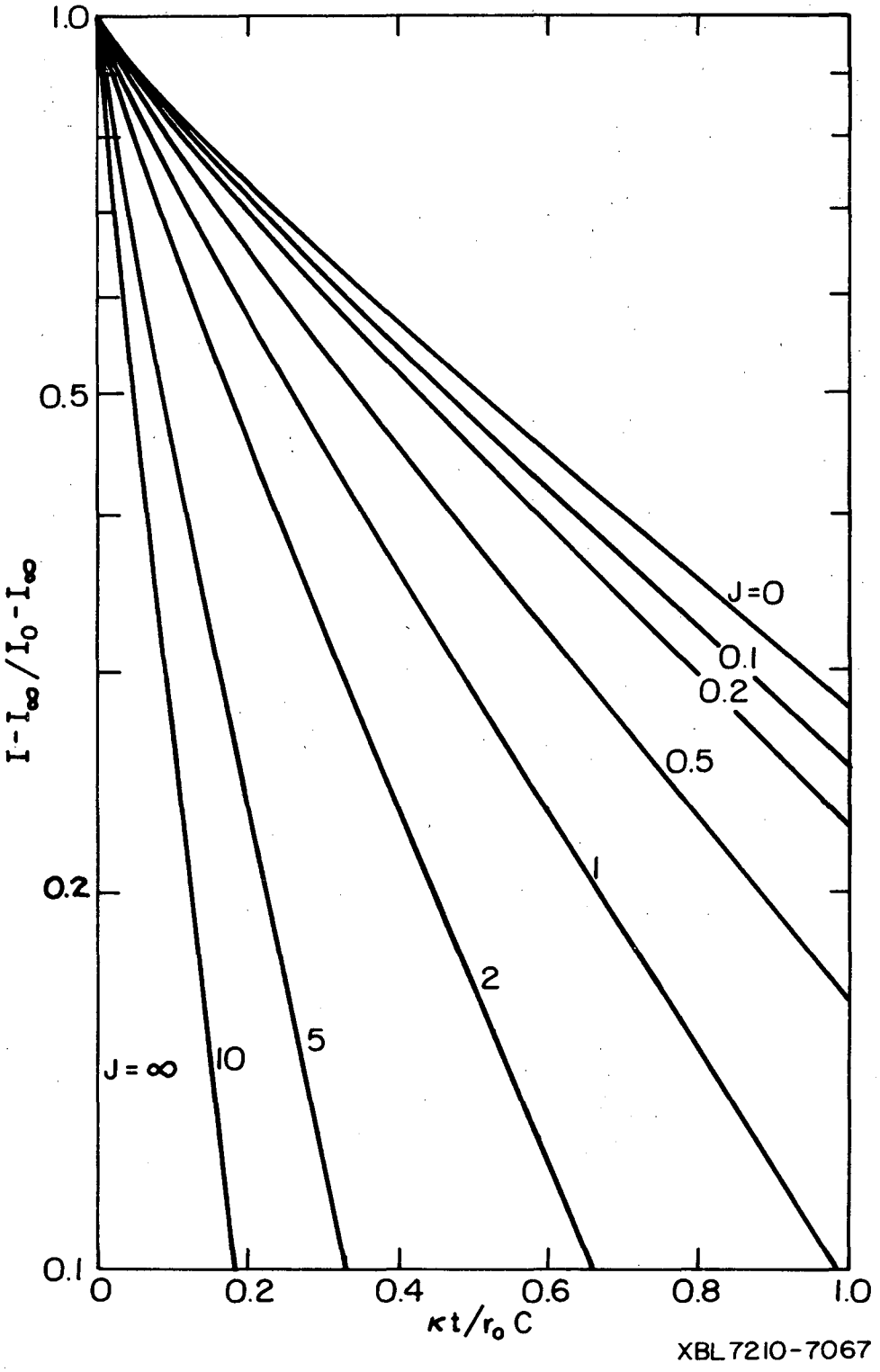

Figure 8-2. Current traces at various J values for decay (or charging) of the double-layer capacity. The slope of each curve at large times is related to λ_1+J.

0 0 0 0 3 9 0 7 3 0 0

8.2. Frequency Dispersion in Capacity Measurements

The alternating-current impedance of an electrode is often interpreted in terms of an equivalent circuit consisting of a capacitor and a resistor in series (figure 3). With this kind of a representation, the measured values of the effective resistance and capacity for a smooth electrode may become frequency dependent in situations where faradaic reactions are important[61] or for certain electrode geometries, such as the disk, which exhibit different current distributions with different frequencies.[61,94] As discussed by Bauer et al.,[94] electrode geometries such as concentric spheres, concentric cylinders, and infinite parallel planes should be free of the frequency-dispersion effect since they have a uniform current distribution independent of the frequency. We can also add to this cathegory the spherical electrode and its hemispherical-cap variety[8] discussed in chapter 5. As reviewed by Bauer et al., Grahame observed the frequency dispersion effect in his experiments with a growing mercury drop at the tip of a capillary. However, the cause must have been the shielding effect of the blunt capillary tip[61] which distorts the spherical equipotential surfaces, so that the current distribution becomes nonuniform.

Newman[61] has given a rigorous analysis of the frequency-dispersion effect in capacity measurements at a disk electrode. According to this treatment, the electrode potential and the potential in the solution can be expressed as

$$V = V_o e^{j\omega t} \quad , \tag{8-12}$$

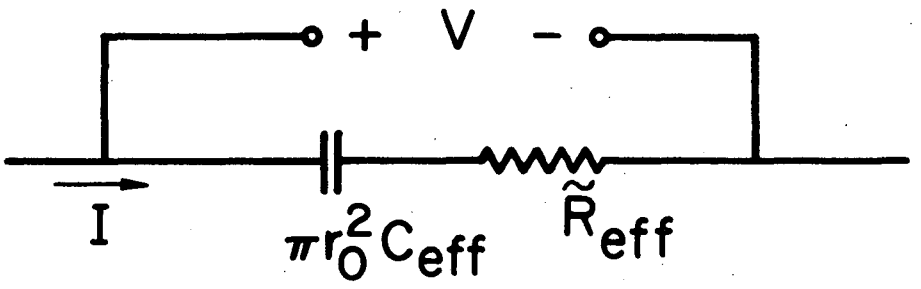

XBL694-2406

Figure 8-3. Equivalent circuit for impedance measurements at an electrode (from reference 61).

and

$$\Phi = V_o e^{j\omega t}\, \tilde{U}(r,z) \quad , \tag{8-13}$$

respectively, where V_o is the amplitude and ω the frequency of the applied potential, and $\tilde{U}$ is a complex potential determined by the solution of Laplace's equation:

$$\tilde{U} = \sum_{n=0}^{\infty} \tilde{B}_n P_{2n}(\eta)\, M_{2n}(\xi) \quad . \tag{8-14}$$

The complex coefficients $\tilde{B}_n$ are determined from condition 7-1, which gives

$$\sum_{n=0}^{\infty} \left[a_{m,n} - \frac{\delta_{m,n}}{j\Omega + J} \frac{M'_{2m}(0)}{4m+1} \right] \tilde{B}_n = a_{o,m} \tag{8-15}$$

$$(M = 0,1,2, \ldots) \quad ,$$

where $\Omega = \omega C r_o / \kappa$ is the dimensionless frequency. $\tilde{B}_n$ are obtained numerically from equation 15 by carrying a finite number of terms in the series.

The impedance is given by[61]

$$Z = V/I = 1/4 r_o \kappa \tilde{B}_o \quad . \tag{8-16}$$

In terms of the resistance and capacity of the equivalent circuit, this is

$$Z = \tilde{R}_{eff} + 1/j\omega C_{eff} \pi r_o^2 \quad . \tag{8-17}$$

Therefore, we obtain

$$4 r_o \kappa \tilde{R}_{eff} = B_{or}/(B_{or}^2 + B_{io}^2) \quad , \tag{8-18}$$

and

$$C/C_{eff} = (\pi/4)\ \Omega B_{oi}/(B_{or}^2 + B_{oi}^2) \quad , \tag{8-19}$$

where B_{or} and B_{oi} are the real and imaginary parts of $\tilde{B}_o$, respectively. The tilde over R_{eff} serves to distinguish between the effective direct current resistance defined in section 4.1 and the present alternating-current resistance.

An indirect method of calculating $\tilde{R}_{eff}$ and C_{eff} is to use equation 7-28 by setting $I(\theta) = I_o e^{j\omega t}$ or equation 8-11 by substituting $V(\theta)=V_o e^{j\omega t}$. The results obtained by this method should be identical with Newman's results and provide a good way of checking the validity of the theory and results presented in chapter 7 and the previous section of this chapter. Hence, B_{or} and B_{oi} can also be expressed in terms of the coefficients C_i and λ_i as follows:

$$B_{or} = 1 + \frac{1}{4r_o \kappa R_{eff}} \sum_{i=1}^{\infty} \frac{C_i(\lambda_i + J)^2}{(\lambda_i + J)^2 + \Omega^2} \quad , \tag{8-20}$$

$$B_{oi} = -\frac{\Omega}{4r_o \kappa R_{eff}} \sum_{i=1}^{\infty} \frac{C_i(\lambda_i + J)}{(\lambda_i + J)^2 + \Omega^2} \quad . \tag{8-21}$$

In terms of the results of chapter 7, one can also derive the expressions

$$4r_o \kappa \tilde{R}_{eff} = 1 + \sum_{i=0}^{\infty} \frac{C_i(\Lambda_i + J)^2}{(\Lambda_i + J)^2 + \Omega^2} \quad , \tag{8-22}$$

and

$$C/C_{eff} = (\pi/4)\ \Omega^2 \sum_{i=0}^{\infty} \frac{C_i(\Lambda_i + J)}{(\Lambda_i + J)^2 + \Omega^2} \quad . \tag{8-23}$$

0 3 3 0 3 9 0 7 3 0 2

The results are compared in table 2 for various values of Ω and J. The first 20 terms were used in both the galvanostatic and potentiostatic series. The results obtained from the former compare quite well with the more accurate calculations of Newman at low frequencies, whereas the agreement is very poor at high frequencies. Better agreement is obtained at high frequencies by the potentiostatic series; however, the accuracy is not as good as would be expected at low frequencies. This is probably due to the fact that the error introduced by truncating the series in equations 20 and 21 is amplified when these equations are substituted into equations 18 and 19 to calculate the effective resistance and capacity. The truncation error is introduced only once when the galvanostatic series are used for the same calculation via equations 22 and 23. This reasoning leads us to speculate that the potentiostatic series are probably more accurate than the galvanostatic series over a moderate time range. The present results indicate, however, that numerical difficulties are inevitable for very short times (or high frequencies) because a large number of terms are required in both the galvanostatic and potentiostatic series to attain a reasonably accuracy. A separate treatment of the potential at short times overcomes these difficulties as discussed in the next chapter.

Table 8-2. The effect of frequency and exchange-current density on the effective resistance and capacity of the equivalent circuit as calculated from the galvanostatic and potentiostatic series and compared to Newman's results.

		Galvanostatic Series		Potentiostatic Series		Newman's Results[61]	
	Ω	$4r_o\kappa R_{eff}$	C/C_{eff}	$4r_o\kappa R_{eff}$	C/C_{eff}	$4r_o\kappa R_{eff}$	C/C_{eff}
J=0.1	0.1	7.441	0.50009	7.358	0.464	7.44572	0.50009
	1.0	1.198	0.9987	1.204	0.987	1.20335	0.99906
	10.0	1.052	1.53	1.029	1.218	1.03478	1.23430
	100.0	1.021	15.7	1.001	1.563	1.00462	1.73404
J=1	0.1	2.326	0.00997	2.304	0.0097	2.33106	0.00997
	1.0	1.702	0.508	0.693	0.498	1.70571	0.50658
	10.0	1.062	1.44	1.041	1.192	1.04657	1.20762
	100.0	1.022	15.0	1.002	1.561	1.00480	1.73084

0 0 0 0 3 9 0 7 0 3

IX. THE SHORT-TIME RESPONSE OF A DISK ELECTRODE

Series expressions were obtained in chapters 7 and 8 for the potential and the current under galvanostatic and potentiostatic control, respectively. Those results are readily applicable to describe the long-time response of the disk and determine the relaxation time of the overpotential after a step change in the applied current or the current decay after a step change in the potential. However, a large number of terms need to be included in the series to express the short-time behavior accurately. This can be accomplished more efficiently by deriving an asymptotic solution to the problem valid at small times. A similar problem is encountered in connection with the steady-state distribution for large values of the exchange-current density. This situation resembles closely the present problem from a mathematical standpoint and has been treated in section 4.2.

9.1. Mathematical Model

Shortly after the cell current is turned on, the current distribution on the surface is given by the primary distribution everywhere except at a small region near the edge of the disk. Since the primary current density is infinite at the edge, the double-layer capacity is charged more rapidly in this region than at other parts of the disk, so that the current density is reduced to a finite value. On the insulating plane of the disk, the current density vanishes, as expressed in equation 2-12. Furthermore, at the surface, the passage of current is primarily due to the charging of the electric double layer; hence, equation 3-35 applies. Charge transfer may also occur by means of a

faradaic reaction. This effect is small at short times as long as the exchange current density is not too large (see section 4.2), and it is neglected here. Diffusion is also neglected.

Let us now introduce the stretched variables appropriate to the edge region:

$$\bar{\phi} = \frac{\pi}{2\sqrt{\theta}} \left(\frac{V - \Phi}{\Phi_o^p} \right) , \tag{9-1}$$

$$\bar{\eta} = \eta/\sqrt{\theta} , \quad \bar{\xi} = \xi/\sqrt{\theta} , \tag{9-2}$$

where η and ξ are the rotational elliptic coordinates, and θ is the dimensionless time defined by equation 7-6. Φ_o^p is the uniform potential in the solution just outside the double layer corresponding to the primary distribution (see sections 2.2 and 4.1). If the electrode potential is kept at a constant value V, then $\Phi_o^p = V$. If, however, the electrode is under galvanostatic control, $\Phi_o^p = I/4r_o\kappa$. With this difference in mind, the present analysis applies to both galvanostatic and potentiostatic cases unless stated otherwise. Equation 1 represents a separation of variables, such that $\bar{\phi}$ is a function of $\bar{\eta}$ and $\bar{\xi}$ only.

Substitution of the stretched variables into Laplace's equation and the boundary conditions and subsequent simplification as θ is made to approach 0 yields a set of equations, which are identical to equations 4-15 through 4-18, except for the condition at the surface which reads for the present case

$$\frac{\partial \bar{\phi}}{\partial \bar{\xi}} = \frac{1}{2} \bar{\eta} \bar{\phi} - \frac{\bar{\eta}^2}{2} \frac{\partial \phi}{\partial \bar{\eta}} \quad \text{at} \quad \bar{\xi} = 0 . \tag{9-3}$$

0 0 0 0 6 9 0 , 0 0 4

These results indicate that the inner region is of order $r_o\theta$ in the original, cylindrical coordinate system. Moreover, the dimensionless potential is of order $\sqrt{\theta}$, and the dimensionless current density, given by

$$ir_o/\kappa\Phi_o^p = -(V - \Phi_o)/2\Phi_o^p\theta \quad , \tag{9-4}$$

is of order $1/\sqrt{\theta}$.

9.2. Numerical Method and Results

One possible way of solving the system of equations 4-15, 4-17, 4-18, and 9-3 is by finite difference methods[33,63] as in the case of the steady-state problem for large exchange-current densities. This scheme did not prove to be straightforward in converging to a stable solution due to the complex nature of the present surface condition, equation 3. The problem for the potential at the surface can also be expressed (see appendix H) in terms of the integral equation,

$$\bar{\phi}_o(\bar{\eta}) = \frac{1}{\pi}\int_0^\infty \ln\left|\bar{\eta}_*^2 - \bar{\eta}^2\right|\left[\frac{\bar{\eta}_*}{2}\bar{\phi}_o(\bar{\eta}_*) - \frac{\bar{\eta}_*^2}{2}\left.\frac{\partial\bar{\phi}}{\partial\bar{\eta}}\right|_{\substack{\bar{\xi}=0\\ \bar{\eta}=\bar{\eta}_*}} - 1\right] d\bar{\eta}_* \quad . \tag{9-5}$$

In order to bring the problem into a finite domain, this integral equation can be written in the form

$$\begin{aligned}\bar{\phi}_o = \frac{1}{\pi}\int_0^{\eta_s} \ln\left|\bar{\eta}_*^2 - \bar{\eta}^2\right|\left(\frac{\bar{\eta}_*}{2}\bar{\phi}_o - \frac{\bar{\eta}_*^2}{2}\frac{\partial\bar{\phi}_o}{\partial\bar{\eta}_*} - 1\right) d\bar{\eta}_* \\ + \frac{1}{2\pi}\int_0^{1/\eta_s^4} \ln\left|\frac{1}{\sqrt{x_*}} - \frac{1}{\sqrt{x}}\right| \frac{1}{x_*^{3/4}}\frac{\partial\bar{\phi}_o'}{\partial x_*}\, dx_* \quad ,\end{aligned} \tag{9-6}$$

where

$$\bar{\phi}_o' = (\bar{\phi}_o - 1/\bar{\eta}_*)/\bar{\eta}_* \ , \qquad x = 1/\bar{\eta}^4 \ , \qquad (9\text{-}7)$$

and η_s is a convenient breaking point. Equation 6 can now be integrated for the entire range of $\bar{\eta}$, whereas equation 5 has to be truncated at some point with the possibility of neglecting an important contribution to the integral. Numerical solution of this integral equation (see appendix H) turned out to be more efficient than the finite difference technique in obtaining results for the present problem.

The results are shown in figure 1. The shape of the curves is also characteristic of the current distribution near the edge since the dimensionless potential $\bar{\phi}_o$ is proportional to the current density as indicated by equation 4. The current distribution approaches the primary distribution toward the center of the disk. However, it remains finite and much more uniform than the primary distribution in the edge region; the finite capacity of the electric double layer does not allow it to become infinite.

The electrode potential for the galvanostatic case or the applied current for the potentiostatic case is given by

$$\left.\begin{array}{rl} \text{(galvanostatic)} & V/\Phi_o^p - 1 \\ \text{(potentiostatic)} & 1-I/4r_o\kappa\Phi_o^p \end{array}\right\} = \int_0^1 \left(\frac{V-\Phi_o}{\Phi_o^p}\right) d\eta \ . \qquad (9\text{-}8)$$

0 0 0 0 3 9 0 7 3 0 5

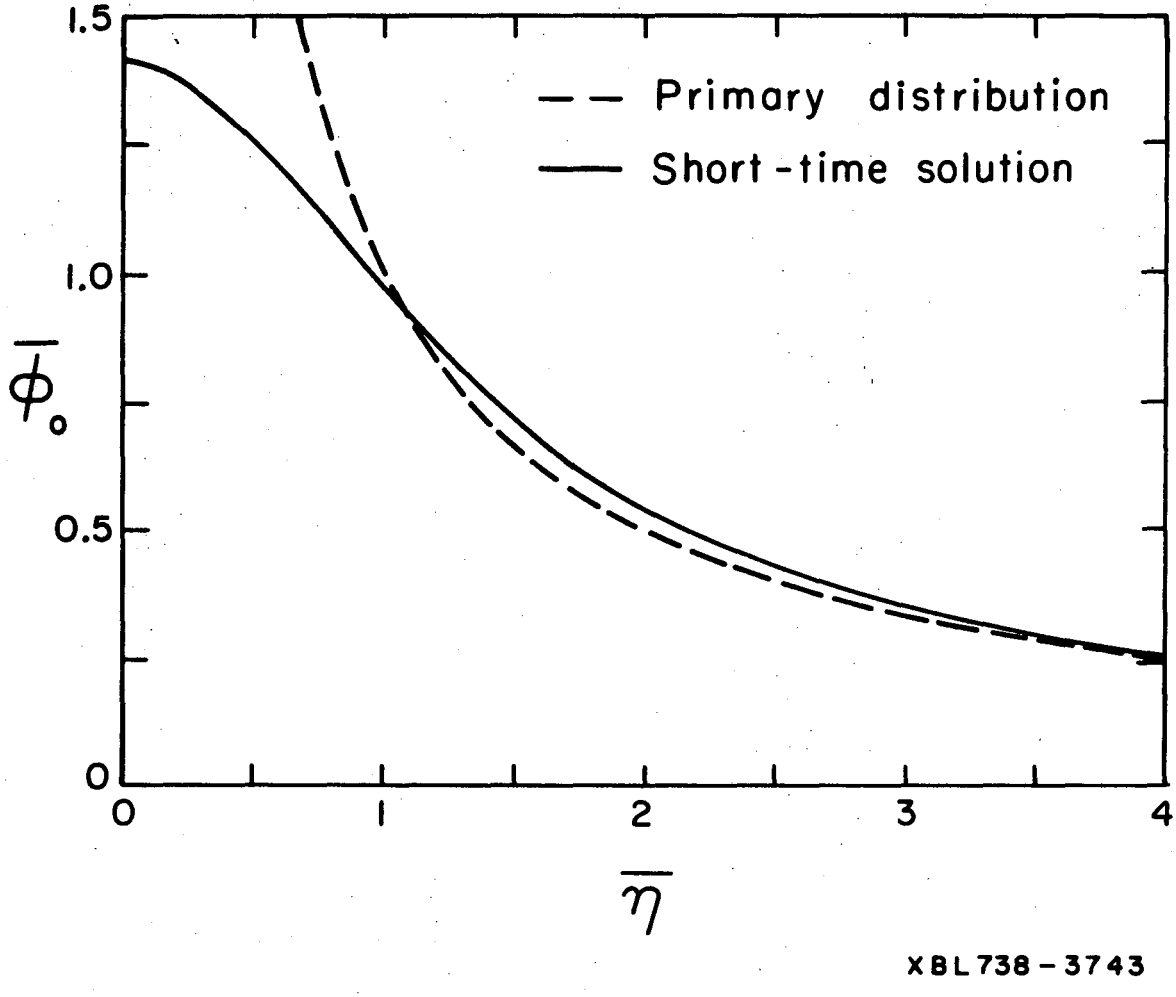

Figure 9-1. The surface potential distribution at short times near the edge of a disk electrode.

Substitution of the stretched variables and integration yields (see appendix G)

$$\int_0^1 \left(\frac{V-\Phi_o}{\Phi_o^p}\right) d\eta = -\frac{1}{\pi}\theta\ln\theta + A\theta \quad , \tag{9-9}$$

where A is given by equation 4-20. The numerical solution obtained from equation 6 was integrated according to equation 4-20 for the whole range of $\bar{\eta}$, and the value of A was found to be 0.841. Equation 8 is plotted in figure 2 using this value and compared to the results of chapters 7 and 8. The long-time series approach the present short-time series as an asymptote for small values of θ. The potentiostatic series appears to be more accurate than the galvanostatic series for the same number of terms. The same conclusion was reached in section 8.2 after comparing the results obtained from those series with the more accurate calculations of Newman[61] concerning the frequency dispersion of the alternating-current impedance of a disk electrode.

The present work demonstrates once more the efficiency and convenience of the singular-perturbation method in obtaining asymptotic solutions to problems which would otherwise be laborious to solve numerically. In electroanalytical applications, one usually focuses attention to the conditions at the electrode surface, and the conditions in the bulk can be accounted for adequately by using the expression for the primary distribution. Therefore, expressing the surface potential in terms of an integral equation provides additional economy in the numerical work since the bulk of the solution does not enter the calculations explicitly.

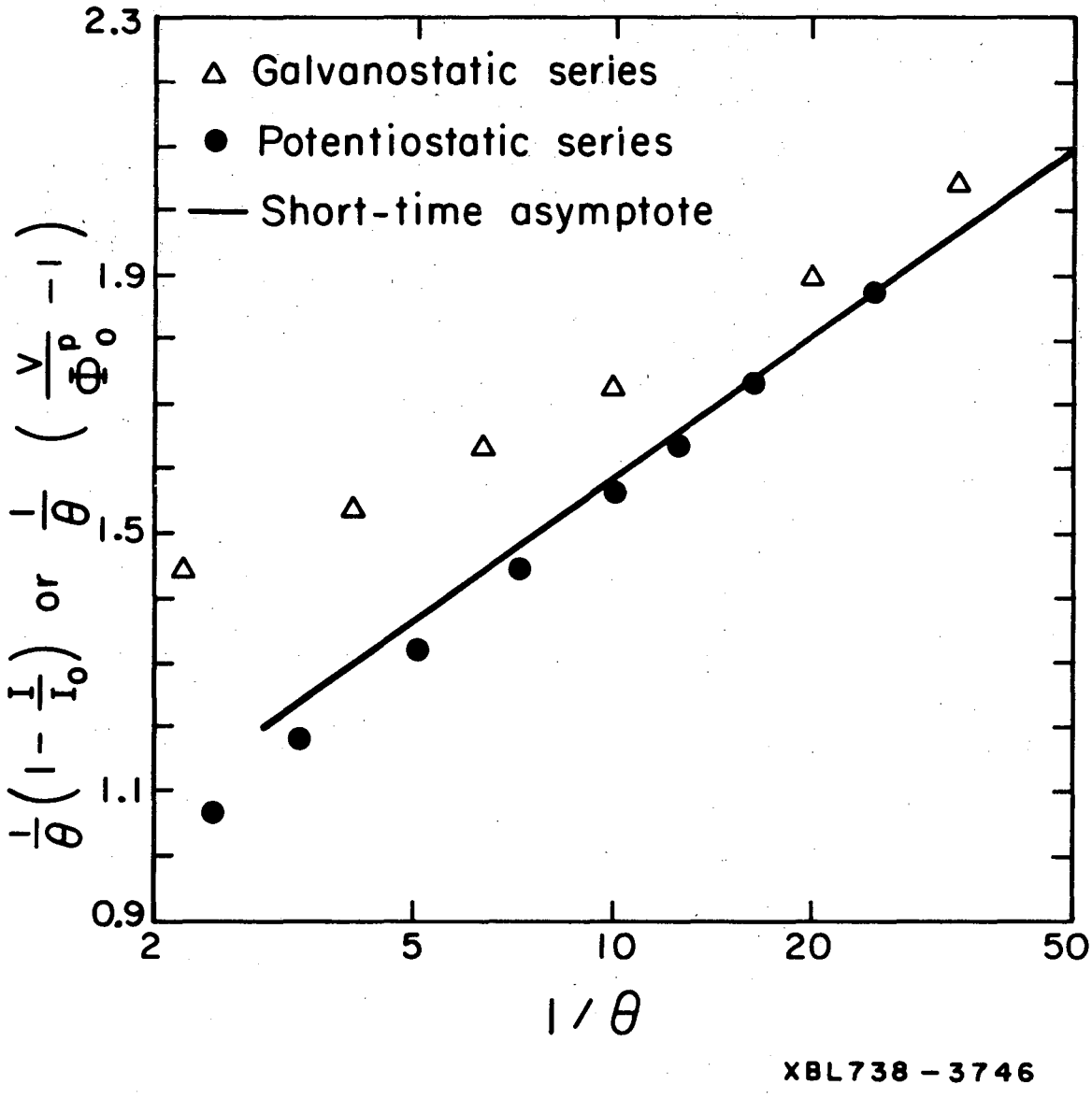

Figure 9-2. Comparison of the short-time solution and the long-time series[1,2] for the transient response of a disk electrode.

The results reported above are universally applicable since no parameters appear in the problem, and numerical calculations need not be repeated. Furthermore, the results are, in a sense, independent of the disk geometry because the formulation is confined to a small region near the edge. Hence, they can also be made to apply under similar conditions to any electrode geometry embedded in an insulating plane.

0 0 0 0 3 9 0 / 8 0 7

X. CONCLUSIONS AND RECOMMENDATIONS

Generalized schemes for treating current-distribution and mass-transfer problems in electrochemical systems have been reviewed. Mathematical relationships are set forth for expressing convective transport in the electrolyte and faradaic and nonfaradaic processes at the electrode surface. A method for obtaining solutions to these equations, simultaneously with the solution of Laplace's equation for the potential in the electrolyte, is discussed to determine the steady-state and transient behavior of electrochemical systems. Specific applications are presented for the rotating-disk and -spherical electrodes.

The steady-state current and concentration distributions below the limiting current have been calculated for a rotating spherical electrode. Mass transfer is assumed to be restricted to a thin diffusion layer near the electrode surface so that the current distribution can be obtained by solution of Laplace's equation in the bulk and the convective diffusion equation in the diffusion layer. The two solutions are matched according to the conditions at the electrode surface including complex electrode kinetics. Analogous solutions for the disk electrode are reviewed and compared with the results for the sphere.

Numerical results for the sphere indicate that the current distribution becomes more nonuniform with increasing mass-transfer limitations, and that the exchange-current density is not an important parameter in contrast to the results for the disk. Furthermore, the current distribution is shown to reach a uniform distribution below a certain current level, suggesting the possibility of operating at

uniform flux below the limiting current even if the concentration distribution may be nonuniform. The disk electrode exhibits a uniform flux and concentration at the limiting current, and this property makes the disk a convenient tool for mass-transfer studies. The spherical electrode, on the other hand, may be more suitable for kinetic studies since it can have uniform current and potential distributions near the surface below the limiting current at high rotation speeds.

The spherical electrode also exhibits a uniform secondary-current distribution. Since its primary distribution is uniform as well, the transient response of a sphere to changes in the applied current or potential in the absence of mass transfer constitutes an elementary problem. The transient behavior of a rotating sphere in the presence of convective diffusion, however, appears to be difficult to treat analytically due to the complex dependence of its shear stress distribution on position at the surface. The problem may be worth investigation, but there seems to be no immediate interest in it at present.

The treatment of transient diffusion to a rotating disk has drawn significant attention in the past. Analytic solutions are obtained at large times for the transient convective diffusion equation for the disk in the absence of radial concentration gradients considering a step change in the concentration and a step change in the flux at the surface. These solutions are shown to match available results for short times with the suggestion that the series for short times and long times can be employed interchangeably for nonsteady-state

0 0 0 0 3 9 0 7 8 0 8

calculations. The results are extended to investigate the effect of double-layer charging on transient mass transfer in the presence of a highly reversible electrode reaction. The effect is shown to be small under the present assumptions. A method is proposed to calculate the transient behavior of a disk in the presence of radial convection as well as faradaic and nonfaradaic effects at the electrode surface. The formulation can be extended, if needed, to apply at moderate times by adding more terms to the regular perturbation expansions. The numerical method, even though straightforward, seems to require lengthy computations.

The transient behavior of a disk electrode due to double-layer charging and a faradaic reaction has been worked out theoretically in the absence of mass-transfer effects. Both galvanostatic and potentiostatic cases have been considered. For either case, the analysis leads to a boundary-value problem, which yields analytic solutions in terms of a new set of eigenfunctions. These equations are extended to account for arbitrary variations in the applied current or potential by employing the superposition integral. The results demonstrate the effect of a faradaic reaction and a nonuniform current distribution on the double-layer charging and decay at a disk electrode. The overall treatment of the problem allows the determination of accurate time constants characteristic of decay due to a faradaic reaction and due to redistribution of charge in the double layer in the presence of a nonuniform current distribution.

The theoretical results seem to promise practical uses in the measurement of double-layer capacities at solid surfaces and estimation of exchange-current densities. Design criteria are discussed for possible applications. A preliminary experiment is conducted, and double-layer capacities are obtained for copper and mercury electrodes within the correct order of magnitude. Improvements for the experimental design are suggested to increase accuracy and reproducibility. The use of smaller cell and electrode dimensions and employment of more sophisticated purification procedures to reduce the content of impurities in the solution to a minimal level would probably be necessary.

Series solutions for the secondary distribution and transient response of a disk electrode prove to become inadequate for large exchange-current densities and at short times, respectively. A singular-preturbation analysis is given to obtain asymptotic solutions for such cases. The results show that the potential distribution for each case resembles the primary distribution closely except in a small region near the edge where the current distribution remains finite and much more uniform than the primary distribution.

0 0 0 0 5 9 0 7 3 0 9

ACKNOWLEDGEMENTS

I would like to express my gratitude to Professor John Newman, my research director, for his continuous interest and support throughout this work. He originally suggested the transient-response problem and offered generous guidance as the thesis branched out into its present form.

I am grateful to Professors Goren and Berger for reviewing the manuscript.

My thanks are due to Jean Wolslegel for her fast and efficient typing of this manuscript out of the first handwritten draft.

I am indebted much to my wife, Anne Grete, without whose presence this thesis would not have been possible.

This work was supported by the United States Atomic Energy Commission.

APPENDIX A. Evaluation of the Integral Equation for Concentration in an Axisymmetric Diffusion Layer

Equation 2-62 can be combined with Faraday's law to obtain an explicit expression for the current density:

$$i_n = -\frac{nFD_R\sqrt{\mathcal{R}\beta}}{\Gamma\left(\frac{4}{3}\right) s_R(1-t_+)} \int_0^x \left.\frac{dc_{Ro}}{dx}\right|_{x=x_o} \frac{dx_o}{\left[9D_R \int_{x_o}^x \mathcal{R}\sqrt{\mathcal{R}\beta}\, dx\right]^{1/3}} , \tag{A-1}$$

where the symbols have their meanings as defined in sections 2.4 and 4.3. In dimensionless form, this can be written as

$$\frac{RT\kappa_\infty i_n}{r_o ZF} = \phi(\zeta) \int_0^\zeta \left.\frac{d\theta_o}{d\zeta}\right|_{\zeta=\zeta'} \frac{d\zeta'}{(\zeta - \zeta')^{1/3}} , \tag{A-2}$$

where

$$\theta_o = c_{Ro}/c_{R\infty} , \tag{A-3}$$

$$\left.\begin{aligned} \zeta &= (r/r_o)^3 \quad \text{(disk)} , \\ \zeta &= \int_0^\theta \sin\theta\sqrt{B(\theta)\,\sin\theta}\, d\theta \quad \text{(sphere)} , \end{aligned}\right\} \tag{A-4}$$

$$\left.\begin{aligned} \phi(\zeta) &= N\zeta^{1/3}/\Gamma\left(\tfrac{4}{3}\right) \quad \text{(disk)} , \\ \phi(\zeta) &= N\sqrt{B(\theta)\,\sin\theta}/\Gamma\left(\tfrac{4}{3}\right) \quad \text{(sphere)} , \end{aligned}\right\} \tag{A-5}$$

and N is given by equation 4-22 for the disk and equation 5-1 for the sphere.

0 0 0 0 3 9 3 / 3 1 0

We define the dimensionless overpotentials

$$E_s = ZF\eta_s/RT, \quad E_c = ZF\eta_c/RT \quad , \tag{A-6}$$

$$ZF\eta/RT = E = E_s + E_c \quad , \tag{A-7}$$

so that equations 3-13 and 3-17 can be expressed as

$$\frac{RT\kappa_\infty i_n}{r_o ZF} = J\Theta_o^\gamma \left[e^{\alpha E_s} - e^{-\beta E_s} \right] \quad , \tag{A-8}$$

$$E_c = \ln \Theta_o + t_+(1 - \Theta_o) \quad , \tag{A-9}$$

respectively, where J is given by equation 4-21, and

$$\alpha = \alpha_a/Z, \quad \beta = \alpha_c/Z \quad . \tag{A-10}$$

By combining equations 6 to 10, equation 2 can be expressed in the form

$$R(\Theta_o) = \phi(\zeta) \int_0^\zeta \left. \frac{d\Theta_o}{d\zeta} \right|_{\zeta=\zeta'} \frac{d\zeta'}{(\zeta - \zeta')^{1/3}} \quad , \tag{A-11}$$

where

$$R(\Theta_o) = \Theta_o^{\gamma-\alpha} e^{\alpha E} e^{\alpha t_+(\Theta_o - 1)} - \Theta_o^{\gamma+\alpha} e^{-\alpha E} e^{\alpha t_+(1-\Theta_o)} \quad . \tag{A-12}$$

Equation 11 is now in a suitable form for numerical analysis. The method used was devised by Acrivos and Chambré[69] for solving integral equations of this type. The manner by which equation 11 is broken into a finite-difference form and integrated is explained clearly by those authors and will not be repeated here. One should note, however, that the right-hand side of equation 11 has a nonzero limit

as $\zeta \to 0$, and this has to be taken into account in the finite-difference formulation. At $x = 0$, equation 1 reduces to

$$\frac{RT\kappa_\infty i_n(0)}{r_o ZF} = \delta \frac{N}{\Gamma\left(\frac{4}{3}\right)} [1 - \theta_o(0)] \quad , \tag{A-13}$$

where $\delta = 1$ for a disk, and $\delta = 1.15247$ for a sphere.

The following numerical procedure was employed:

1. The current density or the concentration was specified at the center of the disk or pole of the sphere. As an initial guess, this was assumed to apply to the whole electrode. Equivalently, one has the option to specify the electrode potential V or the current level $i_{ave}/(i_{lim})_{ave}$. However, this choice requires an additional iteration loop in the numerical procedure.[49]

2. The overpotentials were determined from equations 8, 9, and 7.

3. Equation 11 was solved to obtain a new concentration distribution at the surface. The current was calculated from equation 12.

4. The coefficients B_n were calculated from equation 2-16 for the disk and 2-26 for the sphere by setting $V = RT/ZF$. The Gaussian numerical integration technique was employed. The potential distribution at the surface Φ_o was then computed.

5. The electrode potential was determined according to equation 3-23 by using the values of η and Φ_o at r or θ equal to zero. A new overpotential distribution was then calculated from the same equation.

6. The steps 3 through 5 above were repeated until no significant changes occurred in the calculated quantities.

0 0 0 0 3 9 0 7 3 1 1

A listing of the computer program for the sphere is given below. The first input card in the main program reads the number of mesh points LMAX needed to divide the ζ domain into LMAX-1 equally spaced increments as required by the Acrivos and Chambré method. NMAX is the number of terms carried in the series for Φ_o. IH is the total number of Gaussian abscissae and weight factors used in step 4 above. The next two cards read the Gaussian abscissae X(I) and the corresponding weight factors W(I). The final input card reads the parameters for the problem. The key to notation is as follows:

C(1): $\Theta_o(0)$

AN: N

TPLUS: t_+

ALPHA: α

BETA: β

GAMMA: γ

EXCH: 1/J

DAMP: A damping factor for speeding up the iteration procedure. A value of 1 corresponds to no damping and 0 to 100% damping.

A blank input card terminates the program. The output prints Θ_o, i/i_{ave}, and E as a function of $\cos\theta$ along with the coefficients B_n. The current level $i_{ave}/(i_{lim})_{ave}$ (= AVG in program notation) is also printed. SUBROUTINE THETA solves equation 11 by the method of Acrivos

and Chambré. FUNCTION P(N,X) computes the Legendre polynomials of order N and argument X. SUBROUTINE ZETA has been written to transform between equally-spaced ζ and θ coordinates and to calculate $\phi(\zeta)$. FUNCTION GRAND(T) calculates the dimensionless shear stress $B(\theta)$ on the rotating sphere.

```
      PROGRAM CURD(INPUT,OUTPUT)
C     CURRENT DISTRIBUTION ON A ROTATING SPHERE WITH AN INTEGRAL
C     EQUATION FOR THE DIFFUSION LAYER
      DIMENSION        B(21),C(201),CUR(201),E(201),PP(21,201),R(201),AA
     1(200),BB(200),X(40),W(40),CUG(40),PG(21,40),ZG(40),ZIG(201)
      COMMON     LMAX,ZMAX,ZIG,IM,X,ZG,R
      COMMON E,CUR,C      ,TPLUS,AN,EXCH,ALPHA,BETA,GAMMA,TAF,AA,BB,C1,C2
     1,EX
  101 FORMAT (6H ERROR,I4)
  102 FORMAT (3H N=,F10.4,10H ,  TPLUS=,F8.4,6H ,  V=,F10.5,8H ,  AVG=,
     1F10.6/41H0      R           C           CUR        ETA/(4F11.5))
  103 FORMAT (3I4)
  104 FORMAT (9E8.4)
  105 FORMAT (7H1ALPHA=,F8.4,9H ,  BETA=,F8.4,10H ,  GAMMA=,F8.4,9H ,  E
     1XCH=,F8.4)
  107 FORMAT (2H0B,F9.5,5F11.5/(6F11.5))
  108 FORMAT (6E12.9)
      READ 103, LMAX,NMAX,IH
      EX= 2.0/3.0
      DO 29 L=1,LMAX
      A= L
      AA(L)= 2.0*A**EX - (A+1.0)**EX - (A-1.0)**EX
   29 BB(L)= A**EX - (A-1.0)**EX
      IM=2*IH
      IHP1= IH + 1
      READ 108, (X(I),I=IHP1,IM)
      READ 108, (W(I),I=IHP1,IM)
      DO 33 I=1,IM
      IF (I-IH)  31,31,32
   31 IR=IM-I+1
      X(I)= 0.5 - 0.5*X(IR)
      W(I)= W(IR)
      GO TO 33
   32 X(I)= 0.5 + 0.5*X(I)
   33 CONTINUE
      CALL ZETA
      DO 34 N=1,NMAX $ DO 34 I=1,IM
   34 PG(N,I)= P(2*N-2,X(I))
      DO 1 L=1,LMAX
      DO 1 N=1,NMAX
    1 PP(N,L)= P(2*N-2, R(L))
      DZ=ZMAX/FLOAT(LMAX-1)
      EX= 1.0/3.0
      C2= 1.11984652
    3 READ 104, C(1),AN,TPLUS,ALPHA,BETA,GAMMA,EXCH,DAMP
      C1= C2*(1.0-C(1))
      IF (C(1))  4,4,5
    4 STOP
    5 JCOUNT= 0
      TAF= 1.0
      IF (EXCH-400)  7,7,6
    6 TAF= 0.0
      EXCH= 1.0
    7 ETAC=ALOG(C(1)) + TPLUS*(1.0-C(1))
      CUR(1)= - (1.0-C(1))*AN*EXCH*1.11984652/C(1)**GAMMA*1.15247
      ETAS= -ALOG(TAF-CUR(1))/BETA
      IF (CUR(1))  8,10,8
    8 DO 9 J=1,100
      F= TAF*EXP(ALPHA*ETAS)-EXP(-BETA*ETAS)
      FP= TAF*ALPHA*EXP(ALPHA*ETAS)+BETA*EXP(-BETA*ETAS)
      IF (ABS(CUR(1)-F) - 0.0000001*ABS(CUR(1)))  10,10,9
    9 ETAS= ETAS + (CUR(1)-F)/FP
   10 CUR(1)=    1.11984652*AN*(1.0-C(1))*1.15247
```

```
      DO 11 L=1,LMAX
      C(L)= C(1)
   11 E(L)= ETAC + ETAS
      B(1)= 0.0
      PRINT 105, ALPHA,BETA,GAMMA,EXCH
   12 BOLD= B(1)
      JCOUNT= JCOUNT + 1
      CALL THETA
      DO 16 I=1,IM
      LI= ZG(I)  /DZ + 1
   16 CUG(I)= CUR(LI)+(CUR(LI+1)-CUR(LI))*(X(I)**2-R(LI)**2)/(R(LI+1)**2
     1-R(LI)**2)
      V= E(1)
      DO 15 N=1,NMAX
      B(N)= 0.0
      DO 14 I=1,IM
   14 B(N)= B(N) + CUG(I)      *PG(N,I)*W(I)
      B(N)=-0.5*B(N)*(4*N-3)/(2*N-1)
   15 V= V + B(N)*PP(N,1)
      DO 18 L=2,LMAX
      PHI= V
      DO 17 N=1,NMAX
   17 PHI= PHI - B(N)*PP(N,L)
   18 E(L)= E(L) + DAMP*(PHI-E(L))
      JERR= 1
      IF (JCOUNT-100)  19,19,20
   19 IF (ABS(B(1)-BOLD) - 0.000001*ABS(B(1)))  21,21,12
   20 PRINT 101, JERR
   21 AVG=              -B(1)/AN/1.11984652/1.5/ZMAX**(2./3.)
      DO 22 L=1,LMAX
   22 CUR(L)=  -CUR(L)/B(1)
      RAT1= CUR(1)*AVG
      RAT2= (V-E(1))/B(1)
      PRINT 102, AN,TPLUS,V,AVG,(R(J),C(J),CUR(J),E(J),J=1,LMAX)
      PRINT 107, (B(I),I=1,NMAX),TAF,RAT2,RAT1
      PRINT 103, JCOUNT
      GO TO 3
      END
```

0 0 0 0 5 9 0 7 3 1 3


```
      SUBROUTINE THETA
C     SUBPROGRAM FOR CALCULATING CONCENTRATION
      DIMENSION E(201),CUR(201),A(200),B(200),TH(201),ZIG(201)
      DIMENSION X(40),ZG(40),R(201)
      COMMON    NZT1,ZMAX,ZIG,IM,X,ZG,R
      COMMON E,CUR,TH     ,T,PN,EXCH,AL,BE,GAM,TAF,A,B,C1,C2,EX
  101 FORMAT (17HONOT CONVERGED AT,I4)
      NZT= NZT1-1
      DEVM = 0.0001
      DZ = 1.0/NZT $ DZ=DZ*ZMAX
      S= TH(1)
      DO 60  NZ = 2,NZT1
      Z = (NZ - 1)*DZ
      SUM = 0.0
      IF (NZ .LE. 2) GO TO 42
C     CALC. SUM(TH(J)*A(K))
      DO 40 J=3,NZ
      K = NZ - J + 1
   40 SUM = SUM + TH(J-1)*A(K)
   42 ETA= E(NZ)
      NJ = NZ - 1
      DO 56 N=1,20
      X1 = TAF*S**(GAM - AL)*EXP(AL*ETA)*EXP(AL*T*(S - 1.0))
      DX1 = X1*((GAM - AL)/S + AL*T)
      X2 = S**(GAM + BE)*EXP(-BE*ETA)*EXP(BE*T*(1.0 - S))
      DX2 = X2*((GAM + BE)/S - BE*T)
      C3 = 1.50*C2*ZIG(NZ)/DZ**(1./3.)
      X3= C3*(TH( 1)*B(NJ) + SUM - S)+C1*ZIG(NZ)/Z**(1./3.)
      DTH= S - ((X1-X2)/PN +      X3 *EXCH)/((DX1-DX2)/PN - C3*EXCH)
      CUR(NZ)= PN*     X3
      IF (ABS(S-DTH) - DEVM*ABS(DTH))  60,60,56
   56 S = DTH
      PRINT 101, NZ
   60 TH(NZ) = DTH
      RETURN
      END
```

```
      FORTRAN II FUNCTION P(N,X)
C     CALCULATION OF LEGENDRE POLYNOMIALS
      P1= 1.0
      P2= X
      IF (N-1)  1,2,3
    1 P= P1
      RETURN
    2 P= P2
      RETURN
    3 NM1= N - 1
      DO 4 NU=1,NM1
      P=(X*FLOATF(2*NU+1)*P2-FLOATF(NU)*P1)/FLOATF(NU+1)
      P1= P2
    4 P2= P
      RETURN
      END
```

```
      SUBROUTINE ZETA
      DIMENSION X(40),ZG(40),ZIG(201),XZ(201),XX(40)
      COMMON     LMAX,ZMAX,ZIG,IM,X,ZG,XZ
      N=101 $ ZMAX=0.417077493
      DZ=ZMAX/FLOAT(LMAX-1) $ Z=DZ $ XZ(1)=1.0 $ J=2
      GRAND3=GRAND(0.0) $ SUM=0.0 $ XOLD=0.0 $ IMP1=IM+1
      T3OLD=0.0 $ SUMOLD=0.0
      DO 3 M=1,IMP1 $ IF(M.NE.IMP1) DT=(X(M)-XOLD)/(N-1)
      IF(M.EQ.IMP1) DT=(1.-XOLD)/(N-1) $ DO 2 I=3,N,2
      T2=XOLD+DT*(I-2) $ T3=T2+DT $ GRAND1=GRAND3
      GRAND2=GRAND(T2) $ GRAND3=GRAND(T3)
      SUM=SUM+(GRAND1+4.0*GRAND2+GRAND3)*DT/3.0
      IF(SUM.LE.Z) GO TO 15
   12 K=LMAX-J+1
      XZ(K)=T3OLD+(T3-T3OLD)*(Z-SUMOLD)/(SUM-SUMOLD)
      J=J+1 $ Z=Z+DZ $ IF(J.NE.LMAX) GO TO 13 $ XZ(J)=0.0 $ GO TO 15
   13 IF(SUM.GT.Z) GO TO 12
   15 SUMOLD=SUM
    2 T3OLD=T3 $ IF(M.EQ.IMP1) GO TO 3
      XOLD=X(M) $ ZG(M)=SUM
    3 CONTINUE $ DO 4 M=1,IM $ MM=IM-M+1 $ XX(MM)=X(M)
    4 ZG(M)=SUM-ZG(MM) $ DO 5 M=1,LMAX
    5 ZIG(M)=GRAND(XZ(M )) $ DO 6 M=1,IM
    6 X(M)=XX(M)
      RETURN $ END
```

```
      FUNCTION GRAND(T)
      X=T
      AC=ACOS(X) $ X=1.0-X*X $ IF(X.GT.0.) GO TO 1
      GRAND=0.0 $ RETURN
    1 RX=SQRT(X)
      B=0.51023*AC-0.1808819*AC**3-0.040408*X*RX
      GRAND=SQRT(B*RX)$ RETURN $ END
```

APPENDIX B. A Method for Calculating the Time Constant for the Transient Response of a Disk Electrode in the Presence of Mass Transfer, Nonuniform Electric Field, and Double-Layer Charging.

For a thin diffusion layer on the surface of a disk, the transient convective diffusion equation is

$$\frac{\partial c_R}{\partial t} + v_r \frac{\partial c_R}{\partial r} + v_y \frac{\partial c_R}{\partial y} = D_R \frac{\partial^2 c_R}{\partial y^2} \quad , \tag{B-1}$$

where the concentration and the diffusion coefficient are those of the limiting reactant; the concentration variations of the other species are not considered. The velocity components are expressed by equation 2-52. Equation 1 can be transformed into the dimensionless form

$$\frac{\partial \Theta}{\partial \theta} + 3\zeta\left(r \frac{\partial \Theta}{\partial r} - \zeta \frac{\partial \Theta}{\partial \zeta}\right) = \frac{\partial^2 \Theta}{\partial \zeta^2} \quad , \tag{B-2}$$

where

$$\Theta = c_R / c_{R\infty} \quad , \tag{B-3}$$

$$\zeta = y \left(\frac{a\nu}{3D}\right)^3 \sqrt{\frac{\Omega}{\nu}} \quad , \tag{B-4}$$

$$\theta = \Omega\left(\frac{D}{\nu}\right)^{1/3} \left(\frac{a}{3}\right)^{2/3} t \quad . \tag{B-5}$$

The boundary conditions are

$$\Theta = 1 \quad \text{as} \quad \zeta \to \infty \quad , \tag{B-6}$$

$$\partial\Theta/\partial r = 0 \quad \text{at} \quad r = 0 \quad . \tag{B-7}$$

Another condition has to be specified at the surface. The initial condition will be left as arbitrary. Since the present analysis seeks the purpose of obtaining a characteristic time constant for large times, an initial condition does not have to be specified.

For large θ, the solution to the convective-diffusion equation satisfying the conditions 6 and 7 can be expressed as

$$\Theta = 1 + ke^{-\Lambda_D \theta} \sum_{m=0}^{\infty} A_m (r/r_o)^{2m} Z_m(\zeta) \quad , \tag{B-8}$$

where k is a dimensionless constant, Λ_D is an eigenvalue, Z_m are functions yet to be determined, and A_m are coefficients in the series for Z_m. Substitution back into equation 1 gives

$$Z_m'' + 3\zeta^2 Z_m' + (\Lambda_D - 6m\zeta) Z_m = 0 \tag{B-9}$$

$$(m = 0,1,2, \ldots)$$

with the boundary condition,

$$Z_m = 0 \quad \text{as} \quad \zeta \to \infty \quad , \tag{B-10}$$

and a normalizing condition,

$$Z_m = 1 \quad \text{at} \quad \zeta = 0 \quad . \tag{B-11}$$

Let us assume that an excess amount of supporting electrolyte is present, and the electrode reaction is reversible and fast. The third necessary condition to solve the diffusion-layer equations can be expressed as (see equation 3-32)

$$D_R \left.\frac{\partial c_R}{\partial y}\right|_{y=0} = \frac{s_R}{nF} \left(i_n - C \frac{\partial \eta_c}{\partial t} \right) \quad . \tag{B-12}$$

0 0 0 0 5 9 0 / 3 1 5

The concentration overpotential is given by equation 3-12 which can be linearized at large times and combined with equation 8 to read

$$\eta_c = - \frac{s_R RT}{nF} \; ke^{-\Lambda_D \theta} \sum_{m=0}^{\infty} A_m (r/r_o)^{2m} \quad . \tag{B-13}$$

At large times, the potential distribution in the solution can be expressed by (see equations 2-13 and 7-7)

$$\Phi = - \frac{s_R RT}{nF} \; ke^{-\Lambda_D \theta} \sum_{n=0}^{\infty} B_n P_{2n}(\eta) \; M_{2n}(\xi) \quad . \tag{B-14}$$

Application of Ohm's law (equation 2-8) gives the current density,

$$i_n = -\kappa_\infty \left.\frac{\partial \Phi}{\partial y}\right|_{y=0} = - \frac{\kappa_\infty}{r_o \eta} \left.\frac{\partial \Phi}{\partial \xi}\right|_{\xi=0} \quad . \tag{B-15}$$

Substitution of equations 8, 13, 15 and 14 into equation 12 yields after some arrangement

$$\frac{1}{\eta} \sum_{n=0}^{\infty} B_n P_{2n}(\eta) \; M'_{2n}(0) = \sum_{m=0}^{\infty} A_m (1-\eta^2)^m \; [NZ'_m(0) + P\Lambda_D)] \quad , \tag{B-16}$$

where N is given by equation 4-22, and

$$P = \frac{r_o C\Omega}{\kappa_\infty} \left(\frac{D}{\nu}\right)^{1/3} \left(\frac{a}{3}\right)^{2/3} \tag{B-17}$$

is the dimensionless capacity. Application of orthogonality property of the Legendre polynomials gives

$$B_n = \frac{4n+1}{M'_{2n}(0)} \sum_{m=0}^{\infty} A_m [NZ'_m(0) + P\Lambda_D] \; L_{m,n} \quad , \tag{B-18}$$

where

$$L_{m,n} = \int_0^1 \eta\,(1 - \eta^2)^m\, P_{2n}(\eta)\, d\eta \quad . \qquad \text{(B-19)}$$

But, since Φ contains no net current, $B_o = 0$ (see section 7.3), and for n = 0, equation 18 reduces to

$$\sum_{m=0}^{\infty} A_m [N Z_m'(0) + P\Lambda_D]/(m + 1) = 0 \quad . \qquad \text{(B-20)}$$

The electrode potential can be expressed as

$$V = \eta_c + \Phi_o = - \frac{s_R RT}{nF}\, ke^{-\Lambda_D \theta} \quad . \qquad \text{(B-21)}$$

Substitution of equations 13 and 14 and again due to the orthogonality property of $P_{2n}(\eta)$, we obtain the result

$$B_n = (4n + 1)\,(1 - \sum_{m=0}^{\infty} A_m L_{m,n}) \qquad (n>0) \quad . \qquad \text{(B-23)}$$

Combining this with equation 18 yields

$$\sum_{m=0}^{\infty} A_m L_{m,n} \left[\frac{N Z_m'(0) + P\Lambda_D}{M_{2n}'(0)} + 1 \right] = 1 \qquad (n>0) \quad , \qquad \text{(B-24)}$$

$$\sum_{m=0}^{\infty} \frac{Am}{m + 1} = 1 \qquad (n=0) \quad . \qquad \text{(B-25)}$$

From here on, the problem involves a numerical solution of equations 9 to 11, 20, 24, and 25 once the parameters N and P are specified. Equation 9 has to be solved numerically n_{max} times considering that the series in n and m are both truncated at n_{max}, or a power series solution

0 0 0 0 3 9 0 . 0 1 6

has to be worked out. Moreover, the numerical solution can only be obtained by an iterative procedure, which may be somewhat demanding in the computation time. Because of this, and since there seems to be no immediate interest in the numerical results, a numerical analysis has not been pursued. The numerical work, however, should be straightforward. One possible method of solution is to guess Λ_D, and calculate $Z_m'(0)$ by solving the set of equations 9 to 11. Then, equations 20 and 24 can be solved for the coefficients A_m. This procedure can be repeated until the coefficients satisfy equation 25. After Λ_D is calculated, the desired time constant can be obtained from equation 7-40. Another method, which would simplify the iteration procedure significantly, is to specify Λ_D and N (or P) and back calculate N (or P). In this way, one needs to solve the set of differential equations B-9 only once; the desired parameter N (or P) and the coefficients A_m can then be obtained iteratively from equations 20, 24, and 25. It is possible to perform a parametric study by this method and map out Λ_D as a function of N and P. Afterwards, the results can be interpolated easily to calculate Λ_D for specified values of P and N.

APPENDIX C. Computation of the Transient Convective Diffusion to a Disk Electrode in the Absence of Radial Convection

The numerical problem involves the solution of the system of equations 6-27. We added to this system another equation

$$d\lambda_n/d\zeta = 0 \quad , \tag{C-1}$$

and obtained solutions to this nonlinear, coupled set of differential equations by employing the numerical method developed by Newman[10,11,80] for equations of this type. The coefficients B_n were computed by numerical integration using Simpson's rule. Calculation of Φ^{ss} also involves numerical integration; Simpson's rule was used for $\zeta \leq 1.375$, and Gauss-Laguerre integration proved to be more accurate for larger values of ζ.

The error due to the finite-difference approximation of the differential equations is $O(h^2)$,[80] where h is the mesh size. The numerical results were thus corrected to zero mesh size by extrapolating linearly with respect to h^2. Another source of error is due to the fact that the ζ axis is unbounded at one end and has to be truncated for numerical calculation. The maximum value set for ζ was increased for several successive calculations until the results did not change significantly.

The key to notation on the input cards for the computer program is as follows:

0 0 0 0 3 9 0 / 0 1 7

Z(I),W(I): abscissae and weight factors for 8-point Gauss-Laguerre integration

NJ: number of mesh points. A value of zero terminates the execution of the program

H: mesh size

MODE: chooses between the boundary conditions for a concentration step (MODE=1) or a flux step (MODE=2). A blank card terminates operation with a specified set of NJ and H; the next card should be blank to terminate execution or define new values for NJ and H.

NAMBDA: subscript for the eigenvalue of interest and the corresponding coefficient B_n in the series such as 0,1,2,3,...

AMBDA: first guess for an eigenvalue. A value of zero terminates calculation in a specified MODE; the next card should be blank or set a new MODE.

A set of input cards have to be read in twice with different values of NJ and H for each time in order to obtain results which are automatically extrapolated to zero mesh size by the computer.

```
      PROGRAM TRNDIF(INPUT,OUTPUT)
C
C     TRANSIENT DIFFUSION TO A DISK-- RESPONSE TO A STEP CHANGE IN
C     CONCENTRATION OR FLUX
C
      DIMENSION A(2,2),B(2,2),C(2, 802),D(2,5),G(2),X(2,2),Y(2,2),
     1SS( 802),AA(2,10),BB(2,10),Z(8),W(8)
      COMMON A,B,C,D,G,X,Y,NJ,N,H,MODE,AMBDA
C
C     STEADY STATE DISTRIBUTION
C
      C1=1.11984652 $ NZ=8$ READ 109,(Z(I),W(I),I=1,NZ)
 1001 PRINT 102 $ ICHECK=0 $ HH=0.0
      DO 1100 I=1,2 $ DO 1100 J=1,10 $ AA(I,J)=0.0
 1100 BB(I,J)=0.0
    1 READ 101,NJ,H     $ IF(NJ.EQ.0) STOP
      ICHECK=ICHECK+1 $ HH0=HH $ NM1=NJ-1
      PRINT 103,NJ $ ZMAX=H*(NJ-2) $ H=H/2.0
      N=2*NJ-3 $ SSUM =0.0 $ GRAND3=1.0
      J=1 $ DO 2 I=3,N,2 $ J=J+1 $ T2=H*(I-2)
      IF(T2.GT.1.375) GO TO 61 $ T3=T2+H $ GRAND1=GRAND3
      GRAND2=EXP(-T2**3) $ GRAND3=EXP(-T3**3)
      SS(J)=SSUM    +(GRAND1+4.0*GRAND2+GRAND3)*H/3.0 $ SSUM=SS(J)
    2 SS(J)=1.0-C1*SS(J)
   61 H=2.0*H $ HH=H*H
      DO 63 I=J,NM1 $ T3=H*(I-1) $ SS(I)=0.0 $ DO 62 L=1,NZ
   62 SS(I)=SS(I)+W(L)*1.0/(1.0+Z(L)/T3**3)**(2.0/3.0)
   63 SS(I)=C1/3.0*EXP(-T3**3)/T3/T3*SS(I)
C
C     TRANSIENT DISTRIBUTION
C
    3 READ 101,MODE $ IF(MODE) 35,35,4
   35 GO TO (1,26),ICHECK
    4 GO TO (41,42),MODE
   41 PRINT 104 $ GO TO 43
   42 PRINT 105
   43 READ 101,NAMBDA,AMBDA $ IF(AMBDA) 3,3,45
   45 CALL GUESS $ JCOUNT=0 $ N=2
    5 COLD=C(2,1)
      JCOUNT=JCOUNT+1 $ J=0 $ DO 6 I=1,N $ DO 6 K=1,N $ Y(I,K)=0.0
    6 X(I,K)=0.0
    7 J=J+1 $ DO 8 I=1,N $ G(I)=0.0 $ DO 8 K=1,N
      A(I,K)=0.0 $ B(I,K)=0.0
    8 D(I,K)=0.0 $ IF(J-1) 9,9,13
    9 GO TO (10,11),MODE
   10 X(1,1)=1.0 $ B(1,1)=-1.0 $ G(1)=2.0*H
      B(2,2)=-1.0 $ D(2,2)=1.0 $ GO TO 12
   11 B(1,1)=-1.0 $ X(1,1)=1.0
      D(2,1)=H $ G(2)=H $ B(2,2)=-1.0 $ D(2,2)=1.0
      CALL BAND(J) $ GO TO 7
   13 IF(J-NJ) 14,15,15
   14 ZETA=H*(J-2) $ A(1,1)=1.0/H/H-1.5*ZETA*ZETA/H $ A(2,2)=-1.0
      B(1,1)=C(2,J)-2.0/H/H $ B(1,2)=C(1,J) $ B(2,2)=1.0
      D(1,1)=1.0/H/H+1.5*ZETA*ZETA/H $ G(1)=C(1,J)*C(2,J)
      IF(J.GT.3) GO TO 12 $ A(2,2)=0.0 $ IF(J.EQ.2) GO TO 51
      B(2,2)=0.0 $ A(2,1)=1.0 $ IF(MODE.EQ.2) G(2)=1.0 $ GO TO 12
   51 D(2,2)=-1.0
   12 CALL BAND(J) $ GO TO 7
   15 B(1,1)=1.0 $ B(2,2)=1.0 $ A(2,2)=-1.0
      CALL BAND(J)
      IF(ABS(C(2,1)-COLD)-0.000001*ABS(C(2,1))) 18,18,16
   16 IF(JCOUNT-20) 5,5,17
   17 PRINT 106
```

```
C
C     CALCULATION OF COEFFICIENTS IN SERIES
C
   18 SUM1=0.0 $ SUM2=0.0 $ GO TO (19,20),MODE
   19 GRAND3=0.0 $ GRAND6=0.0 $ GO TO 21
   20 GRAND3=1.0 $ GRAND6=1.0
   21 DO 23 I=3,NM1,2 $ T2=H*(I-2) $ T3=T2+H $ GRAND1=GRAND3
      GRAND2=EXP(T2**3)*C(1,I  ) $ GRAND3=EXP(T3**3)*C(1,I+1)
      GRAND4=GRAND6 $ GRAND5=GRAND2*C(1,I  ) $ GRAND6=GRAND3*C(1,I+1)
      GRAND2=GRAND2*SS(I-1) $ GRAND3=GRAND3*SS(I)
      SUM1=SUM1+(GRAND1+4.0*GRAND2+GRAND3)*H/3.0
   23 SUM2=SUM2+(GRAND4+4.0*GRAND5+GRAND6)*H/3.0 $ SUM=SUM1/SUM2
      AK=(C(1,NJ-2)-C(1,NJ))/2.0/H*EXP(T2**3)
      IF(MODE.EQ.2) SUM=SUM/C1
      PRINT 107,NAMBDA,C(2,1),SUM,AK
C
C     LINEAR EXTRAPOLATION TO INFINITE NUMBER OF MESH POINTS
C
      GO TO (24,25),ICHECK
   24 AA(MODE,NAMBDA+1)=C(2,1) $ BB(MODE,NAMBDA+1)=SUM  $ GO TO 43
   25 IF(AA(MODE,NAMBDA+1).EQ.0.0) GOTO 43
      AA(MODE,NAMBDA+1)=(AA(MODE,NAMBDA+1)*HH-C(2,1)*HH0)/(HH-HH0)
      BB(MODE,NAMBDA+1)=(BB(MODE,NAMBDA+1)*HH-SUM *HH0)/(HH-HH0)
      GO TO 43
C
C     OUTPUT
C
   26 PRINT 108,ZMAX $ DO 27 I=1,10
   27 IF(AA(1,I).GT.0.0) GO TO 28 $ GO TO 30
   28 PRINT 104 $ DO 29 I=1,10 $ J=I-1
   29 IF(AA(1,I).GT.0.0) PRINT 107,J,AA(1,I),BB(1,I)
   30 DO 31 I=1,10
   31 IF(AA(2,I).GT.0.0) GO TO 32 $ GO TO 1001
   32 PRINT 105 $ DO 33 I=1,10 $ J=I-1
   33 IF(AA(2,I).GT.0.0) PRINT 107,J,AA(2,I),BB(2,I) $ GO TO 1001
  101 FORMAT(I4,E8.4)
  102 FORMAT(1H1)
  103 FORMAT(///6X,*JMAX=*,I4)
  104 FORMAT(/6X,*CONCENTRATION STEP*/(9X,*N*,7X,*LAMBDA*,6X,*COEFF*))
  105 FORMAT(/6X,*FLUX STEP*/(9X,*N*,7X,*LAMBDA*,6X,*COEFF*))
  106 FORMAT(6X,*NEXT RUN DID NOT CONVERGE*)
  107 FORMAT(I10,5E15.8)
  108 FORMAT(1H1,///6X,*JMAX=INFINITY      ZMAX=*,F8.5)
  109 FORMAT(4E18.12)
      END
```

```
      SUBROUTINE GUESS
C
C     FIRST GUESS FOR THE TRANSIENT DISTRIBUTION
C
      DIMENSION A(2,2),B(2,2),C(2, 802),D(2,5),G(2),X(2,2),Y(2,2)
      COMMON A,B,C,D,G,X,Y,NJ, N,H,MODE,AMBDA
      J=0 $ N=1
      DO 10 I=1,N $ DO 10 K=1,N $ Y(I,K)=0.0
   10 X(I,K)=0.0
   11 J=J+1 $ DO 12 I=1,N $ G(I)=0.0 $ DO 12 K=1,N
      A(I,K)=0.0 $ B(I,K)=0.0
   12 D(I,K)=0.0 $ IF(J-1) 13,13,17
   13 GO TO (14,15),MODE
   14 B(1,1)=-1.0 $ X(1,1)=1.0 $ G(1)=2.0*H $ GO TO 16
   15 B(1,1)=-1.0 $ X(1,1)=1.0 $ D(1,1)=2.0*H $ G(1)=2.0*H
   16 CALL BAND(J) $ GO TO 11
   17 IF(J-NJ) 18,19,19
   18 ZETA=H*(J-1) $ A(1,1)=1.0/H/H-1.5*ZETA*ZETA/H
      B(1,1)=AMBDA-2.0/H/H $ D(1,1)=1.0/H/H+1.5*ZETA*ZETA/H
      CALL BAND(J) $ GO TO 11
   19 B(1,1)=1.0 $ CALL BAND(J) $ DO 20 I=1,NJ
   20 C(2,I)=AMBDA $ RETURN $END
```

```
      SUBROUTINE BAND(J)
C
C     SOLUTION OF COUPLED ORDINARY DIFFERENTIAL EQUATIONS
C
      DIMENSION A(2,2),B(2,2),C(2, 802),D(2,5),G(2),X(2,2),Y(2,2),
     1E(2,3,802)
      COMMON A,B,C,D,G,X,Y,NJ,N
  101 FORMAT (21H        DETERM=0 AT J=,I4)
      IF (J-2) 1,6,8
    1 NP1=N+1
      DO 2 I=1,N
      D(I,2*N+1)=G(I)
      DO 2 L=1,N
      LPN=L+N
    2 D(I,LPN)=X(I,L)
      CALL MATINV(N,2*N+1,DETERM)
      IF (DETERM) 4,3,4
    3 PRINT 101,J
    4 DO 5 K=1,N
      E(K,NP1,1)=D(K,2*N+1)
      DO 5 L=1,N
      E(K,L,1)=-D(K,L)
      LPN=L+N
    5 X(K,L)=-D(K,LPN)
      RETURN
    6 DO 7 I=1,N
      DO 7 K=1,N
      DO 7 L=1,N
    7 D(I,K)=D(I,K)+A(I,L)*X(L,K)
    8 IF(J-NJ) 11,9,9
    9 DO 10 I=1,N
      DO 10 L=1,N
      G(I)=G(I)-Y(I,L)*E(L,NP1,J-2)
      DO 10 M=1,N
```

0 0 3 0 3 9 0 , 8 1 9


```
   10 A(I,L)=A(I,L)+Y(I,M)*E(M,L,J-2)
   11 DO 12 I=1,N
      D(I,NP1)=-G(I)
      DO 12 L=1,N
      D(I,NP1)=D(I,NP1)+A(I,L)*E(L,NP1,J-1)
      DO 12 K=1,N
   12 B(I,K)=B(I,K)+A(I,L)*E(L,K,J-1)
      CALL MATINV(N,NP1,DETERM)
      IF (DETERM) 14,13,14
   13 PRINT 101,J
   14 DO 15 K=1,N
      DO 15 M=1,NP1
   15 E(K,M,J)=-D(K,M)
      IF(J-NJ) 20,16,16
   16 DO 17 K=1,N
   17 C(K,J)=E(K,NP1,J)
      DO 18 JJ=2,NJ
      M=NJ-JJ+1
      DO 18 K=1,N
      C(K,M)=E(K,NP1,M)
      DO 18 L=1,N
   18 C(K,M)=C(K,M)+E(K,L,M)*C(L,M+1)
      DO 19 L=1,N
      DO 19 K=1,N
   19 C(K,1)=C(K,1)+X(K,L)*C(L,3)
   20 RETURN
      END
```

```
      SUBROUTINE MATINV(N,M,DETERM)
C
C     MATRIX INVERSION
C
      DIMENSION A(2,2),B(2,2),C(2, 802),D(2,5),ID(2)
      COMMON A,B,C,D
      DETERM=1.0
      DO 1 I=1,N
    1 ID(I)=0.
      DO 18 NN=1,N
      BMAX=0.
      DO 6 I=1,N
      IF (ID(I)) 2,2,6
    2 DO 5 J=1,N
      IF (ID(J)) 3,3,5
    3 IF(ABS (B(I,J))-BMAX) 5,5,4
    4 BMAX=ABS (B(I,J))
      IROW=I
      JCOL=J
    5 CONTINUE
    6 CONTINUE
      IF (BMAX) 7,7,8
    7 DETERM=0.
      RETURN
    8 ID(JCOL)=1
      IF(JCOL-IROW) 9,12,9
    9 DO 10 J=1,N
      SAVE=B(IROW,J)
      B(IROW,J)=B(JCOL,J)
   10 B(JCOL,J)=SAVE
      DO 11 K=1,M
      SAVE=D(IROW,K)
      D(IROW,K)=D(JCOL,K)
   11 D(JCOL,K)=SAVE
   12 F=1./B(JCOL,JCOL)
      DO 13 J=1,N
   13 B(JCOL,J)=B(JCOL,J)*F
      DO 14 K=1,M
   14 D(JCOL,K)=D(JCOL,K)*F
      DO 18 I=1,N
      IF(I-JCOL) 15,18,15
   15 F=B(I,JCOL)
      DO 16 J=1,N
   16 B(I,J)=B(I,J)-F*B(JCOL,J)
      DO 17 K=1,M
   17 D(I,K)=D(I,K)-F*D(JCOL,K)
   18 CONTINUE
      RETURN
      END
```

0 0 0 0 3 9 0 , 3 2 0

APPENDIX D. Numerical Solution of the Integral Equation for the Transient Concentration on a Rotating Disk in the Presence of Double-Layer Charging

We wish to solve the integral equation

$$\frac{I/I_L}{\Gamma(4/3)} + \frac{Q}{\Theta_o}\,\frac{d\Theta_o}{d\theta} = \int_0^{\theta} \left.\frac{d\Theta_o}{d\theta}\right|_{\theta=\theta'} \left.\frac{\partial\Theta_c}{\partial\zeta}\right|_{\substack{\zeta=0 \\ \theta=\theta-\theta'}} d\theta' \quad . \tag{D-1}$$

The θ axis can be broken into $n_{max} - 1$ intervals of size $\Delta\theta$ and equation 1 thus written in the finite-difference form as follows:

$$\frac{I/I_L}{\Gamma(4/3)} + \frac{Q}{\Delta\theta}\,\frac{\Theta_{o,k} - \Theta_{o,k-1}}{\Theta_{o,k}} \tag{D-2}$$

$$= \frac{1}{\Delta\theta} \sum_{j=2}^{k} (\Theta_{o,j} - \Theta_{o,j-1}) \int_{(j-2)\Delta\theta}^{(j-1)\Delta\theta} H(\theta - \theta')\, d\theta' = f(\theta) \ ,$$

where

$$H(\theta - \theta') = \left.\frac{\partial\Theta_c}{\partial\zeta}\right|_{\substack{\zeta=0 \\ \theta=\theta-\theta'}} \quad . \tag{D-3}$$

Forward differences have been used for the time derivatives, hence the error associated with the finite difference approximation is $O(\Delta\theta)$. The error can however be reduced to $O[(\Delta\theta)^2]$ by averaging the coefficient of the derivative between the mesh points k and k-1. Let us also define

$$G(\theta) = \int_0^{\theta} H(x)\, dx \quad , \tag{D-4}$$

where $x = \theta - \theta'$. For small θ, H(x) is given by equation 6-16,

$$H(x) = -1/\sqrt{\pi x} - 3x/4 \quad ; \tag{D-5}$$

therefore, equation 4 becomes

$$G(\theta) = -2\sqrt{\theta/\pi} - 3\theta^2/8 \quad . \tag{D-6}$$

For large θ, equation 4 can be broken up as follows:

$$G(\theta) = \int_0^{\theta} [H(x) - H(\infty)]\, dx - \int_0^{\theta} [H(x) - H(\infty)]\, dx + \theta H(\infty) \quad . \tag{D-7}$$

This can be evaluated by substituting the results of the long-time solution (section 6.3) to obtain

$$G(\theta) = \int_0^{\infty} [H(x) - H(\infty)]\, dx + \sum_{n=0}^{\infty} B_n e^{-\lambda_n \theta}/\lambda_n - \theta/\Gamma(4/3) \quad , \tag{D-8}$$

where

$$\int_0^{\infty} [H(x) - H(\infty)]\, dx = \text{const.} \tag{D-9}$$

The constant term can be calculated by picking a convenient time θ^* for switching from the short-time to long-time series. Equations 6 and 8 can be equated at θ^* and solved for the constant term:

$$\text{const.} = -2\sqrt{\theta^*/\pi} + \theta^*/\Gamma(4/3) - 3\theta^{*2}/8 - \sum_{n=0}^{\infty} B_n e^{-\lambda_n \theta^*}/\lambda_n \tag{D-10}$$

$$= -0.336 \quad .$$

0 0 0 0 3 9 0 7 0 2 1

This method provides a smooth transition from one series to the other. Equation 2 can now be written in the form

$$f(\theta) = \frac{1}{\Delta\theta}\sum_{j=2}^{k}(\Theta_{o,j} - \Theta_{o,j-1})\int_{(k-j)\ \Delta\theta}^{(k-j+1)\ \Delta\theta} H(x)\ dx \qquad (D\text{-}11)$$

$$= \frac{1}{\Delta\theta}\sum_{j=2}^{k}(\Theta_{o,j} - \Theta_{o,j-1})\{G[(k-j+1)\ \Delta\theta] - G[(k-j)\ \Delta\theta]\},$$

which becomes, after some rearrangement,

$$\frac{I/I_L}{\Gamma(4/3)} + \frac{Q}{\Delta\theta}\ \frac{\Theta_{o,k} - \Theta_{o,k-1}}{\Theta_{o,k}} = A\Theta_{o,k} - b_{k-1} + \sum_{j=2}^{k=1} d_{k-j}\Theta_{o,j} \quad , \qquad (D\text{-}12)$$

where

$$A = G(\Delta\theta)/\Delta\theta \quad , \qquad (D\text{-}13)$$

$$b_\ell = \{G(\ell\Delta\theta) - G[(\ell-1)\ \Delta\theta]\}/\Delta\theta \ , \qquad (D\text{-}14)$$

$$d_\ell = \{G[(\ell+1]\ \Delta\theta] - 2G(\ell\Delta\theta) + G[(\ell-1)\ \Delta\theta]\}/\ \Delta\theta \ . \qquad (D\text{-}15)$$

The algebraic solution to equation 12 can be expressed as

$$\Theta_{o,k} = \Delta_{k-1}/2 + \frac{1}{2}\left(\Delta_{k-1}^2 - \frac{4Q}{A\Delta\theta}\ \Theta_{o,k-1}\right)^{1/2} \quad , \qquad (D\text{-}16)$$

where

$$\Delta_\ell = \frac{1}{A}\left[\frac{I/I_L}{\Gamma(4/3)} + Q/\Delta\theta + b_\ell - \sum_{j=2}^{\ell} d_{\ell-j+1}\Theta_{o,j}\right] . \qquad (D\text{-}17)$$

Equation 16 can now be used to calculate Θ_o at the mesh points $k = 2, 3, 4, \ldots$, each time using the values of Θ_o at smaller values of k, which have already been calculated. The value of $\Theta_{o,1}$ of course corresponds to the initial condition and has been set equal to unity here.

A listing of the computer program follows. The key to the input notation is

LMAX: number of terms used in the long-time series

NMAX: number of mesh points

TMAX: the upper limit desired for θ

TS: θ^*

WL(L),AA(L): eigenvalues and coefficients in the long-time series for concentration step

WR(L),BB(L): eigenvalues and coefficients in the long-time series for flux step

CUR: I/I_L

QO: Q

DT: $\Delta\theta$

Setting CUR=0 terminates the execution. The initial value of $\Delta\theta$ should be a small number, such as 10^{-4}, because $(\partial\theta_c/\partial\zeta)_{\zeta=0}$ goes to infinity as $1/\sqrt{\theta}$, and hence the contribution to the integral may be significant at small times. The program first computes the surface concentration in the interval θ = 0.0001 to θ = 0.001 (smaller θ can be used if desired). The mesh size is then increased by a factor of 10, and the calculation is repeated for the interval 0.001 to 0.01 using the results of the previous cycle as the first (NMAX-1)/10 points. A similar method was employed by Hsueh[84] to calculate the transient response of a stagnant diffusion cell.[85]

```
      PROGRAM CAPEFF(INPUT,OUTPUT)
C
C     TRANSIENT DIFFUSION TO A DISK IN PRESENCE OF THE CAPACITIVE EFFECT
C
      DIMENSION C(101),CC(101),B(101),D(101),G(101),WL(10),AA(10),WR(10)
     1,BB(10)
      PI=3.141592654 $ C1=0.8929795116 $ C(1)=1.0
      READ 101,LMAX,NMAX,TMAX,TS
      READ 102,(WL(L),L=1,LMAX) $ READ 102,(AA(L),L=1,LMAX)
      READ 102,(WR(L),L=1,LMAX) $ READ 102,(BB(L),L=1,LMAX)
    1 READ 103,CUR,Q0,DT $ IF(CUR.LE.0.0) STOP $ JBEGIN=2 $ Q=C1*Q0
      AK=TS/C1-2.0*SQRT(TS/PI)-3.0/8.0*TS*TS $ DO 2 L=1,LMAX
    2 AK=AK-AA(L)/WL(L)*EXP(-WL(L)*TS)
    3 PRINT 104,CUR,Q0,DT $ DO 6 I=1,NMAX $ T=(I-1)*DT
      IF(T.GT.TS) GO TO 4 $ X=2.0*SQRT(T/PI) $ Y=3.0/8.0*T*T
      G(I)=-X-Y $ CC(I)=X-Y $ GO TO 6
    4 G(I)=AK-T/C1 $ CC(I)=C1 $ DO 5 L=1,LMAX
      G(I)=G(I)+AA(L)/WL(L)*EXP(-WL(L)*T)
    5 CC(I)=CC(I)-BB(L)*EXP(-WR(L)*T)
    6 CC(I)=1.0-CC(I)/C1*CUR $ A=G(2)/DT*C1 $ NM1=NMAX-1 $ DO 7 I=1,NM1
      B(I)=(G(I+1)-G(I))*C1/DT $ IF(I.EQ.NM1) GO TO 7
      D(I)=(G(I+2)-2.0*G(I+1)+G(I))*C1/DT
    7 CONTINUE $ DO 10 J=JBEGIN,NMAX $ JM1=J-1
      DEL=CUR+Q/DT+B(JM1)
      IF(J.EQ.2) GO TO 9 $ DO 8 I=2,JM1
    8 DEL=DEL-C(I)*D(J-I)
    9 DEL=DEL/A
   10 C(J)=0.5*(DEL+SQRT(DEL*DEL-4.0*Q*C(JM1)/A/DT))
      DO 11 I=1,NMAX,2 $ T=(I-1)*DT $ IF(T.GT.TMAX) GO TO 1
   11 PRINT 105,T,C(I),CC(I) $ DO 12 K=1,11 $ J=K*10-9
      CC(K)=CC(J)
   12 C(K)=C(J) $ JBEGIN=12 $ DT=10.0*DT $ GO TO 3
  101 FORMAT(2I4,2E8.4)
  102 FORMAT(6E12.8)
  103 FORMAT(9E8.4)
  104 FORMAT(1H1,6X,*I/ILIM=*,F5.3,6X,*Q=*,F7.5, 6X,*DT=*,E7.1//(12X,*T*
     1,14X,*C*,14X,*CC*))
  105 FORMAT(3F15.5)
      END
```

APPENDIX E. Calculation of the Transient Response of a Disk in the Absence of Mass Transfer

The transient response of a disk electrode can be calculated once the eigenvalues and the corresponding coefficients in the series, discussed in chapters 7 and 8, are determined. We wish to solve the nonlinear set of equations

$$\sum_{n=1}^{n_{max}} a_{o,n} B_{n,i} = 1/2 \quad , \tag{7-13}$$

$$\sum_{n=1}^{n_{max}} \left[a_{m,n} + \frac{\delta_{m,n}}{\Lambda_i} \frac{M'_{2m}(0)}{4m+1} \right] B_{n,i} = a_{o,m} \tag{7-14}$$

$$(m=1,2,\ldots,n_{max})$$

for the galvanostatic problem and the analogous set

$$\sum_{n=1}^{n_{max}} a_{o,n} B_{n,i} = 2/\pi\lambda_i - 1/2 \quad , \tag{E-1}$$

$$\sum_{n=1}^{n_{max}} \left[a_{m,n} + \frac{\delta_{m,n}}{\lambda_i} \frac{M'_{2m}(0)}{4m+1} \right] B_{n,i} = - a_{o,m} \tag{E-2}$$

$$(m=1,2,\ldots, n_{max})$$

for the potentiostatic problem. The fact that $B_{o,i} = 0$ is implicit in equations 7-13 and 7-14, and that $B_{o,i}$ is normalized to unity, in equations E-1 and E-2, respectively. The following iterative scheme is used, utilizing the Newton-Raphson convergence method, to obtain numerical solutions:

1. An initial guess is made for Λ_i or λ_i as close to the actual value as possible. A bad guess may converge to a different eigenvalue than the one desired, or convergence may not be attained at all. However, the spacing between the eigenvalues appears to be approaching π with increasing order; if the value of an eigenvalue is known, a good guess for the next one can be obtained by adding or subtracting π. The same arguments also apply to λ_i.

2. Equation 7-14 or E-2 is solved by matrix inversion. We next solve the expression

$$\sum_{n=1}^{n_{max}} \left[a_{m,n} + \frac{\delta_{m,n}}{\Lambda_i} \frac{M'_{2m}(0)}{4m+1} \right] \frac{dB_{n,i}}{d\Lambda_i} = \frac{M'_{2m}(0)}{4m+1} \frac{B_m}{\Lambda_i^2} \qquad \text{(E-3)}$$

for the derivatives $dB_{n,i}/d\Lambda_i$. A similar equation can be written for the potentiostatic case by differentiating equation 2 with respect to λ_i.

3. A correction term for the eigenvalue is calculated by expanding equation 7-13 or E-1 in the following manner:

$$\sum_{n=1}^{n_{max}} a_{o,n} \left(B_{n,i} + \frac{dB_{n,i}}{d\Lambda_i} \Delta\Lambda_i \right) = \frac{1}{2} \quad , \qquad \text{(E-4)}$$

or

$$\sum_{n=1}^{n_{max}} a_{o,n} \left(B_{n,i} + \frac{dB_{n,i}}{d\lambda_i} \Delta\lambda_i \right) = \frac{2}{\pi\lambda_i} \left(1 - \Delta\lambda_i/\lambda_i \right) - 1/2 \; . \qquad \text{(E-5)}$$

Solving for $\Delta\Lambda_i$ or $\Delta\lambda_i$ gives

$$\Delta\Lambda_i = \frac{1/2 - \sum_{n=1}^{n_{max}} a_{o,n} B_{n,i}}{\sum_{n=1}^{n_{max}} a_{o,n} dB_{n,i}/d\Lambda_i} \quad , \tag{E-6}$$

or

$$\Delta\lambda_i = \frac{2/\pi\lambda_i - 1/2 - \sum_{n=1}^{n_{max}} a_{o,n} B_{n,i}}{2/\pi\lambda_i^2 + \sum_{n=1}^{n_{max}} a_{o,n} dB_{n,i}/d\lambda_i} \quad . \tag{E-7}$$

The new value of the eigenvalue is thus

$$\Lambda_{i,new} = \Lambda_{i,old} + \Delta\Lambda_i \quad , \tag{E-8}$$

or

$$\lambda_{i,new} = \lambda_{i,old} + \Delta\lambda_i \quad . \tag{E-9}$$

4. The numerical steps 3 and 4 are repeated until no significant change occurs in Λ_i or λ_i. Convergence, of course, is very rapid because the problem has been linearized around trial values which become very close to the true solution.

A listing of the computer program is reproduced below for performing these calculations for any number of eigenvalues desired. Results for the eigenvalues and the coefficients $B_{n,i}$ or $B_{n,i}$ are punched on cards as output for separate computations of the eigenfunctions, the coefficients C_i and C_i, the electrode potential for the galvanostatic problem, the current for the poltentiostatic problem, and other desired calculations

according to the formulae developed in chapters 7 and 8. The integral $a_{o,m}$ is calculated according to equation 4-7, and $a_{m,n}$ (equation 4-6) is obtained by Gaussian integration.

Important symbols in the program have meanings as follows:

NMAX: n_{max}

IH: number of points used in Gaussian integration

IMAX: number of eigenfunctions required

X(I),W(I): Gaussian abscissae and corresponding weight factors

MODE: specifies the mode of operation for the galvanostatic problem (MODE=1) or the potentiostatic problem (MODE=2). A value of 0 terminates execution.

The program calls the subprograms FUNCTION P(N,X) (appendix A) and SUBROUTINE MATINV (appendix C).

```
      PROGRAM SECLIN(INPUT,OUTPUT,PUNCH)
C
C     PROGRAM FOR SECONDARY CURRENT DISTRIBUTION ON A DISK ELECTRODE
C     WITH LINEAR KINETICS
      DIMENSION X(96),W(96),R(45,96),PM(45),B(45,45),Q(45,45),D(45,1),
     1Q0(45),BT(45,20),AMBDA(20)
      COMMON B,D
C
C     COMPUTATION AND INTEGRATION OF LEGENDRE POLYNOMIALS
  103 FORMAT(5I4)
  106 FORMAT(1H1)
  108 FORMAT(2X,F19.16,2X,F19.16)
  132 FORMAT(4E18.6)
      READ 103,NMAX,IH,IMAX $ IHP1=IH+1 $ IM=2*IH
      READ 108, (X(I),W(I),I=IHP1,IM)
      DO 3 I=1,IM $ IF(I.LT.IHP1) GO TO 1 $ X(I)=0.5+0.5*X(I) $ GO TO 2
    1 IR=IM-I+1 $ X(I)=0.5-0.5*X(IR) $ W(I)=W(IR)
    2 XX=SQRT(1.0-X(I)**2) $                    DO 3 NN=1,NMAX $ N=NN-1
    3 R(NN,I)=P(2*N,XX) $ DO 4 NN=1,NMAX $ N=NN-1
      DO 4 L=1,NMAX $ Q(NN,L)=0.$ DO 4 I=1,IM
    4 Q(NN,L)=Q(NN,L)+R(L,I)*X(I)*R(NN,I)*W(I)
      DO 5 M=1,NMAX $ DO 5 N=1,NMAX
    5 Q(M,N)=Q(M,N)/2. $  PI=3.141592654 $ Q0(1)=0.5 $ Q0(2)=0.125
      PM(1)=-2./PI $ PM(2)=4.*PM(1) $ NXM1=NMAX-1 $ DO 10 N=2,NXM1
      Q0(N+1)=-Q0(N)/FLOAT(N+1)*(FLOAT(N)-1.5)
   10 PM(N+1)=PM(N)*(FLOAT(2*N)/ FLOAT(2*N-1))**2
C
C     TRANSIENT DISTRIBUTION
   12 READ 103,MODE $ IF(MODE.EQ.0) STOP
      PRINT 106 $ I=0 $ AMBDA(1)=4.1213
      IF(MODE.EQ.2) AMBDA(1)=1.1578 $ DLAMDA=3.19
   15 I=I+1 $ IF(I.GT.IMAX) GO TO 28 $ IF(I.EQ.1) GO TO 20
      IF(I.LT.3) GO TO 16 $ DLAMDA=AMBDA(I-1)-AMBDA(I-2)
   16 AMBDA(I)=AMBDA(I-1)+DLAMDA
   20 DO 22 M=1,NXM1 $ D(M,1)=Q0(M+1)
      IF(MODE.EQ.2) D(M,1)=-D(M,1) $ DO 21 N=1,NXM1
   21 B(M,N)=Q(N+1,M+1)
   22 B(M,M)=B(M,M)+PM(M+1)/FLOAT(4*M+1)/AMBDA(I) $ F=0.5
      IF(MODE.EQ.2) F=2./PI/AMBDA(I)-F
      CALL MATINV(NXM1,1,DETERM) $ DO 24 M=1,NXM1 $ BT(M,I)=D(M,1)
      F=F-Q0(M+1)*BT(M,I)
      D(M,1)=D(M,1)*PM(M+1)/FLOAT(4*M+1)/AMBDA(I)**2  $ DO 23 N=1,NXM1
   23 B(M,N)=Q(N+1,M+1)
   24 B(M,M)=B(M,M)+PM(M+1)/FLOAT(4*M+1)/AMBDA(I)
      CALL MATINV(NXM1,1,DETERM) $   DAMBDA=0.0
      IF(MODE.EQ.2)DAMBDA=2./PI/AMBDA(I)**2 $ DO 25 N=1,NXM1
   25 DAMBDA=DAMBDA+Q0(N+1)*D(N,1) $ DAMBDA=F/DAMBDA
      AMBDA(I)=AMBDA(I)+DAMBDA
   26 IF(ABS(DAMBDA).GT.1.E-6*ABS(AMBDA(I))) GO TO 20 $ GO TO 15
   28 PRINT 132,(AMBDA(I),I=1,IMAX)
      PRINT 132,((BT(N,I),I=1,IMAX),N=1,NXM1)
      PUNCH 132,(AMBDA(I),I=1,IMAX)
      PUNCH 132,((BT(N,I),I=1,IMAX),N=1,NXM1)
      GO TO 12 $ END
```

0 0 0 0 3 9 0 , 3 2 4

APPENDIX F. Numerical Solution of Laplace's Equation for the Edge Region of a Disk Electrode for Large Exchange-Current Densities

We reproduce below a listing of the computer program, which was adapted from a program written by Newman[61] and used in this work to solve the system of equations 4-15 to 4-18 by finite difference methods with successive overrelaxation.[33,63] The solution is first obtained for a coarse mesh size H, which is then reduced to finer mesh sizes by successive doubling.[33] The number of mesh points is kept constant, thereby shrinking the $\bar{\eta}$ and $\bar{\xi}$ axes at each doubling, so that a higher accuracy can be attained for the potential closer to the edge.

The program has to be rerun for each doubling; consequtive runs may also be necessary to reach a desired level of accuracy. A disk file (TAPE 5) is therefore needed to store the calculated values of $\bar{\phi}$ each time execution is terminated, to be read again as the initial values for the next run. TERR is the desired error limit and MM the maximum number of iterations allowed for each run.

At the end of a run, $\bar{\phi}_o$ values are printed along with the total number of iterations (JCOUNT) for that run and the number of mesh points (KERR) where the desired accuracy has not been reached. Execution stops when the desired accuracy is attained (KERR=0). Numerical integration is also performed to calculate the value of A (SADD in program notation) according to equation 4-20.

```
      PROGRAM EDGE(INPUT,OUTPUT,TAPE 5)
      DIMENSION TR( 81, 81),X(101),Y(101)
      COMMON TR,X,Y
  101 FORMAT (E8.4,I4)
  102 FORMAT (1H0,2I6,F10.5)
  103 FORMAT (1H1,E10.2, F10.6/(F10.3, F20.7))
  104 FORMAT (E24.8)
  105 FORMAT (F10.3,2E24.8)
      REWIND 5
C
C     DIVIDE H BY 1/2 AT EACH DOUBLING
      N= 81 $ H=0.20  $ READ 101, TERR,MM $ DO 1 J=1,N $ X(J)=H*(J-1)
      Y(J)=X(J) $ DO 1 I=1,N
    1 TR(I,J)=Y(J) +1.0/H/FLOAT(N-1) $ OMEG=1.9 $ NN=N-1
C
C     REMOVE NEXT CARD FOR FIRST RUN
      READ (5) ((TR(I,J),I=1,N),J=1,N) $ REWIND 5
C
C     REPUNCH NEXT CARD WITH LAST VALUE OF SADD WHEN DOUBLING
      SAD=0.0
C
C     REMOVE NEXT SEVEN CARDS EXCEPT WHEN DOUBLING
      DO 15 IN=1,41 $ I=42-IN $ IS=2*I -1 $ TR(IS,81)=TR(I,41)
      DO 13 JN=1,40 $ J=41-JN $ JS=2*J-1 $ TR(IS,JS)=TR(I,J)
   13 TR(IS,JS+1)=0.5*(TR(IS,JS)+TR(IS,JS+2))
      IF(IN.EQ.1) GO TO 15
      DO 14 J=1,81 $ TR(IS+1,J)=0.5*(TR(IS,J)+TR(IS+2,J))
   14 CONTINUE
   15 CONTINUE
      DO 9 M=1,MM $ JCOUNT=M $ KERR=0 $ DO 8 J=1,NN$ DO 8 I=1,NN
      IF (I.EQ.1) GO TO 2 $ IF (I.EQ.N) GO TO 3
      AR=TR(I-1,J)+TR(I+1,J) $ GO TO 4
    2 AR=2.0*TR(2,J) $ GO TO 4
    3 AR=2.0*TR(N-1,J)
    4 IF (J.EQ.N) GO TO 5 $ IF (J.EQ.1) GO TO 6
      TNUR=AR+TR(I,J+1)+TR(I,J-1)-4.0*TR(I,J) $ GO TO 7
    5 TNUR=AR+2.0*TR(I,J-1)+2.0*H-4.0*TR(I,J) $ GO TO 7
    6 AR=AR+2.0*TR(I,2)
      TNUR=4.0*(AR/(4.0+2.0*H*X(I))-TR(I,J))
    7 TNUR=OMEG*TNUR/4.0
      IF(ABS(TNUR).GT.TERR*ABS(TR(I,J)))KERR=KERR+1
    8 TR(I,J)=TR(I,J)+TNUR
    9 IF(KERR.EQ.0) GO TO 10
   10 SUM=-0.5*TR(1,1) $ DO 11 I=2,N,2
   11 SUM=SUM+TR(I-1,1)+2.0*TR(I,1)
      SUM=H/1.5*(SUM+0.5*TR(81,1))-1.0*ALOG(X(N))
      SUM=SUM*2.0/3.141592654    + SAD
      SADD=-0.5*(TR(41,1)-1.0/X(41)) $ DO 16 I=42,N,2
   16 SADD=SADD+TR(I-1,1)-1.0/X(I-1)+2.0*TR(I,1)-2.0/X(I)
      SADD=H/1.5*(SADD+0.5*TR(81,1)-0.5/X(81))
      SADD=SADD*2.0/3.141592654 + SAD $ PRINT 104, SADD
      DO 17 I=41,N $ DIFF=TR(I,1)-1.0/X(I)
   17 PRINT 105, X(I),DIFF
      PRINT 103, TERR,SUM,(X(I),TR(I,1),  I=1,N)
      WRITE(5) ((TR(I,J),I=1,N),J=1,N) $ REWIND 5
      PRINT 102, JCOUNT,KERR,OMEG $ STOP $ END
```

0 0 0 0 5 9 0 7 3 2 5

APPENDIX G. Integration of the Potential at the Surface at Short Times or High Exchange-Current Densities

The calculation of the current or the potential at short times (chapter 9) or the effective cell resistance in the presence of high exchange-current densities (section 4.2) requires evaluation of the integral,

$$\int_0^1 \left(\frac{V-\Phi_o}{\Phi_o^p}\right) d\eta \quad ,$$

where Φ_o^p is to be replaced by the electrode potential V in problems involving high exchange-current densities or a potentiostatic process. Since the solutions obtained for Φ_o in these cases are singular-perturbation expansions valid at two separate regions near the disk electrode, the integration is not straightforward.[61]

The potential distribution in the edge region is obtained by solving Laplace's equation for the boundary conditions prescribed for each problem as discussed in detail in section 4.2, appendix F, chapter 9, and appendix H. The potential in the outer region is given by equation 4-11 or H-3. The first approximation for the integrand in the outer region is obtained by substituting the outer solution into the boundary condition at the surface (equation 3-35):

$$(V - \Phi_o)/\Phi_o^p = 2Y/\pi\eta \quad , \qquad \text{(G-1)}$$

where Y is the stretching variable which is equal to θ or $1/J$ depending on the type of problem at hand.

Let us define,

$$S(\eta) = \int_0^{\eta} \left(\frac{V-\Phi_o}{\Phi_o^p} \right) d\eta \quad . \tag{G-2}$$

For the outer region, this becomes

$$\begin{aligned} \tilde{S}(\eta) &= S(1) - \int_{\eta}^{1} \left(\frac{V-\Phi_o}{\Phi_o^p} \right) d\eta \\ &= S(1) + (2\theta/\pi) \ln \eta \quad . \end{aligned} \tag{G-3}$$

For the inner region, equation 2 can be expanded in the following manner:

$$\begin{aligned} \bar{S}(\bar{\eta}) = \sqrt{Y} \int_0^{\bar{\eta}} \left(\frac{V-\Phi_o}{\Phi_o^p} \right) d\bar{\eta} &= \sqrt{Y} \left\{ \int_0^{b} \left(\frac{V-\Phi_o}{\Phi_o^p} \right) d\bar{\eta} + \int_b^{\bar{\eta}} \left(\frac{V-\Phi_o}{\Phi_o^p} - \frac{2Y}{\pi\eta} \right) d\bar{\eta} \right. \\ &\left. + \frac{2Y}{\pi} \int_b^{\bar{\eta}} \frac{1}{\eta} \, d\bar{\eta} \right\} = (2/\pi)\, Y \ln\eta - (Y/\pi) \ln Y \end{aligned} \tag{G-4}$$

$$+ (2Y/\pi) \left\{ \int_0^{b} \bar{\phi}_o d\bar{\eta} + \int_b^{\bar{\eta}} (\bar{\phi}_o - 1/\bar{\eta})\, d\bar{\eta} - \ln b \right\} \quad .$$

The matching condition,

$$\lim_{\eta \to 0} \tilde{S}(\eta) = \lim_{\bar{\eta} \to \infty} \bar{S}(\bar{\eta}) \quad , \tag{G-5}$$

gives the result

$$S(1) = - (1/\pi)\, Y \ln Y + AY \quad , \tag{G-6}$$

0 0 0 0 3 9 0 . 0 2 6

where

$$A = \frac{2}{\pi} \left\{ \int_0^b \bar{\phi}_o d\bar{\eta} + \int_b^\infty (\bar{\phi}_o - 1/\bar{\eta})\, d\bar{\eta} - \ln b \right\} . \qquad \text{(G-7)}$$

The integral has been broken up this way because the first integral in equation 7 is unbounded as $b \to \infty$ and the second integral as $b \to 0$. The value of b should be picked so that $\bar{\phi}_o$ deviates appreciably from the primary distribution $1/\bar{\eta}$ in the range $0 \leq \bar{\eta} \leq b$. The second integral then corrects for the small difference between $\bar{\phi}_o$ and $1/\bar{\eta}$ at larger values of $\bar{\eta}$.

APPENDIX H. Integral Representation for the Potential at Short Times

H.1. Mathematical Formulation

The integral equation for the potential in the solution near a disk electrode is given by equation 2-21. After substituting equation 3-35 for the current density and converting into rotational elliptic coordinates, equation 2-21 can be expressed as

$$\frac{\Phi_o}{\Phi_o^p} = \frac{2}{\pi} \int_0^1 \frac{K(m)}{1 + \sqrt{1 - \eta_*^2}} \frac{\partial}{\partial \theta} \left(\frac{V - \Phi_o}{\Phi_o^p} \right) \eta_* d\eta_* \quad , \tag{H-1}$$

where the assumption $\eta \ll 1$ has been introduced for the edge region. The assumption cannot be applied to the dummy variable η_* because the integration has to be carried over the entire surface of the disk.

Define,

$$F(\eta,\eta') = \frac{2}{\pi} \int_0^{\eta'} \frac{K(m)}{1 + \sqrt{1 - \eta_*^2}} \frac{\partial}{\partial \theta} \left(\frac{V - \Phi_o}{\Phi_o^p} \right) \eta_* d\eta_* \quad . \tag{H-2}$$

The potential distribution in the outer region is approximated by (see equation 4-11)

$$\Phi / \Phi_o^p = 1 - 2\xi/\pi \quad . \tag{H-3}$$

Substitution into equation 3-35 and integration gives

$$\frac{V - \Phi_o}{\Phi_o^p} = \frac{2}{\pi} \frac{\theta}{\eta} \quad . \tag{H-4}$$

Hence, for the outer region, equation 2 can be written as

$$\tilde{F}(\eta,\eta') = F(\eta,1) - \frac{4}{\pi^2}\left[\int_0^1 \frac{K(m)}{1+\sqrt{1-\eta_*^2}}\,d\eta_* - \int_0^{\eta'} \frac{K(m)}{1+\sqrt{1-\eta_*^2}}\,d\eta_*\right] . \tag{H-5}$$

The first integral in the brackets corresponds to the primary distribution. Proof:

Let us write equation 2-21 for the primary distribution by replacing Φ with Φ^p and i with the primary current density (see equation 2-18):

$$\Phi_o^p = I/4\kappa r_o = \frac{2}{\pi\kappa}\int_0^{r_o} \frac{I}{\pi r_o^2}\,\frac{0.5}{\sqrt{1-(r_*/r_o)^2}}\,\frac{K(m)\,r_*dr_*}{r+r_*} \tag{H-6}$$

$$= \frac{4\Phi_o^p}{\pi^2}\int_0^1 \frac{K(m)}{\sqrt{1-\eta^2}+\sqrt{1-\eta_*^2}}\,d\eta_* .$$

Thus, independent of the value of η, we have

$$\frac{4}{\pi^2}\int_0^1 \frac{K(m)}{\sqrt{1-\eta^2}+\sqrt{1-\eta_*^2}}\,d\eta_* = 1 . \tag{H-7}$$

For small values of η', the second integral in equation 5 can be approximated by

$$\int_0^{\eta'} \frac{K(m)}{1+\sqrt{1-\eta_*^2}}\, d\eta_* \approx \int_0^{\eta'} \ln\frac{4}{\eta}\, d\eta = \eta'\left(\ln\frac{4}{\eta'}+1\right). \quad \text{(H-8)}$$

Equation 5 for the outer region therefore reduces to

$$\tilde{F}(\eta,\eta') = F(\eta,1) - 1 + \frac{4\eta'}{\pi^2}\left(\ln\frac{4}{\eta'}+1\right). \quad \text{(H-9)}$$

In the inner region, equation 2 can be expressed in the form

$$\bar{F}(\eta,\bar{\eta}') = \frac{\sqrt{\theta}}{\pi^2}\int_0^{\bar{\eta}'} K(m)\left[\bar{\phi}_o(\bar{\eta}_*) - \bar{\eta}_*\left.\frac{\partial\bar{\phi}_o}{\partial\bar{\eta}}\right|_{\bar{\eta}=\bar{\eta}_*}\right]\bar{\eta}_*\, d\bar{\eta}_* \quad . \quad \text{(H-10)}$$

Both η and η_* are small in the inner region. Therefore,

$$\lim_{\eta,\eta_*\to 0} K(m) = \lim_{\eta,\eta_*\to 0} \frac{1}{2}\ln\frac{16}{1-m} = \ln\frac{16/\theta}{|\bar{\eta}^2-\bar{\eta}_*^2|} \quad . \quad \text{(H-11)}$$

Equation 10 can now be broken up into several parts:

$$\bar{F}(\bar{\eta},\bar{\eta}') = \frac{2\sqrt{\theta}}{\pi^2}\left\{\int_0^{\infty}\ln(16/\theta)\, G(\bar{\eta}_*)\, d\bar{\eta}_* - \int_0^{\infty}\ln\left|\bar{\eta}_*^2-\bar{\eta}^2\right| G(\bar{\eta}_*)\, d\bar{\eta}_*\right.$$
$$\left. - \int_{\bar{\eta}'}^{\infty}\ln\frac{16/\theta}{|\bar{\eta}_*^2-\bar{\eta}^2|}\, G(\bar{\eta}_*)\, d\bar{\eta}_* + \int_0^{\bar{\eta}'}\ln\frac{16/\theta}{|\bar{\eta}_*^2-\bar{\eta}^2|}\, d\bar{\eta}_*\right\}, \quad \text{(H-12)}$$

0 0 0 0 3 9 0 / 3 2 8

where

$$G(\eta_*) = \frac{\bar{\eta}_*}{2}\,\bar{\phi}_o(\bar{\eta}_*) - \frac{\bar{\eta}_*^2}{2}\left.\frac{\partial\bar{\phi}_o}{\partial\bar{\eta}}\right|_{\bar{\eta}=\bar{\eta}_*} - 1 \quad . \tag{H-13}$$

In the original unstretched coordinate system, the first integral can be expressed as

$$\ln(16/\theta)\int_0^\infty G(\bar{\eta}_*)\,d\bar{\eta}_* = -\frac{\ln(16/\theta)}{\sqrt{\theta}}\int_0^1\left(\frac{\pi}{2\Phi_o^p}\left.\frac{\partial\Phi}{\partial\xi}\right|_{\xi=0} + 1\right)d\eta \tag{H-14}$$

$$= \frac{\ln(16/\theta)}{\sqrt{\theta}}\left(\frac{1}{4\kappa r_o\Phi_o^p}\int_0^{r_o} 2\pi i r dr - 1\right) = \frac{\ln(16/\theta)}{\sqrt{\theta}}\left(\frac{I}{4\kappa r_o\Phi_o^p} - 1\right) \quad .$$

Under galvanostatic control, $I = 4\kappa r_o\Phi_o^p$, and the integral is identically zero. For potentiostatic control, the current is given by equation 9-9, and the integral is therefore of order $\sqrt{\theta}$ and still small compared to the second integral, which is of order unity. For large $\bar{\eta}'$, the last integral in equation 12 can be approximated by

$$\int_0^{\bar{\eta}'} \ln\frac{16/\theta}{|\bar{\eta}_*^2 - \bar{\eta}^2|}\,d\bar{\eta}_* \approx \bar{\eta}'\ln\frac{16}{\theta} - \bar{\eta}'\ln\bar{\eta}'^2 + 2\bar{\eta}' \quad . \tag{H-15}$$

Equation 12 for the inner region thus becomes at large $\bar{\eta}'$

$$\bar{F}(\bar{\eta},\bar{\eta}') = -\frac{2\sqrt{\theta}}{\pi^2}\left\{\int_0^\infty \ln\left|\bar{\eta}_*^2 - \bar{\eta}^2\right| G(\bar{\eta}_*)\,d\bar{\eta}_* + \int_{\bar{\eta}'}^\infty \ln\frac{16/\theta}{|\bar{\eta}_*^2-\bar{\eta}^2|}\,G(\bar{\eta}_*)\,d\bar{\eta}_* - \bar{\eta}'\ln\frac{16}{\theta} + \bar{\eta}'\ln\bar{\eta}'^2 - 2\bar{\eta}'\right\} . \tag{H-16}$$

Finally, the matching condition,

$$\lim_{\eta' \to 0} \tilde{F}(\eta,\eta') = \lim_{\bar{\eta}' \to \infty} \bar{F}(\bar{\eta}_*,\bar{\eta}') \qquad \text{(H-17)}$$

has to be satisfied. Substitution of equations 16 and 9 gives, after cancelling the matching terms,

$$\bar{\phi}_o(\bar{\eta}) = \frac{1}{\pi} \int_0^\infty \ln|\bar{\eta}_*^2 - \bar{\eta}^2| \; G(\bar{\eta}_*) \; d\bar{\eta}_* \quad , \qquad \text{(H-18)}$$

which is identical to equation 9-5.

H.2. Numerical Analysis

The evaluation of equation 18 for numerical solution may become quite complicated algebraically; however, we will outline here the present method for the interested reader and try to keep the analysis as rigorous as possible. The bars over the stretched variables and the subscript o, which implies that a quantity is evaluated at the electrode surface, will henceforth be eliminated for simplicity in notation.

Equation 18 can be broken up as follows:

$$a(\eta) + b(\eta) + d(x) = \pi(\eta_s \phi'' + 1/\eta_s) \text{ for } \eta \leq \eta_s \quad , \qquad \text{(H-19a)}$$

$$= \pi(\eta\phi' + 1/\eta) \text{ for } \eta > \eta_s \quad , \qquad \text{(H-19b)}$$

where

$$a(\eta) = \eta_s \int_0^{\eta_s} \left|\eta_*^2 - \eta^2\right| \left(\frac{\eta_*}{2}\phi'' - \frac{\eta_*^2}{2}\frac{\partial \phi''}{\partial \eta_*}\right) d\eta_* \quad , \qquad \text{(H-20)}$$

0 0 0 0 3 9 0 , 0 2 9

$$b(\eta) = \int_0^{\eta_s} \ln\left|\eta_*^2 - \eta^2\right| \left(\frac{\eta_*}{2\eta_s} - 1\right) d\eta_* \quad , \tag{H-21}$$

$$d(x) = \frac{1}{2}\int_0^{1/\eta_s^4} \ln\left|\frac{1}{\sqrt{x_*}} - \frac{1}{\sqrt{x}}\right| \frac{1}{x_*^{3/4}} \frac{\partial \phi'}{\partial x_*} dx_* \quad , \tag{H-22}$$

$$\phi' = (\phi - 1/\eta)/\eta \quad , \tag{H-23}$$

$$\phi'' = (\phi - 1/\eta_s)/\eta_s \quad , \tag{H-24}$$

$$x = 1/\eta^4 \quad . \tag{H-25}$$

This way, equation 18 can be integrated inside a finite domain. The variable ϕ'' is defined for convenience in the numerical solution of the integral equation because at the breaking point η_s, $\phi' = \phi''$.

Let j_{max} denote the mesh point at $\eta = \eta_s$ and jj_{max} at $\eta = \infty$ or $x = 0$. We divide the η axis into $j_{max} - 1$ equally-spaced increments of $\Delta\eta$ and the x axis into $jj_{max} - j_{max}$ equally-spaced increments of Δx, namely,

$$\Delta\eta = \frac{\eta_s}{j_{max} - 1} \quad , \tag{H-26}$$

$$\Delta x = \frac{1}{\eta_s^4 (jj_{max} - j_{max})} \quad . \tag{H-27}$$

In finite difference form, the first integral in equation 19 can be written as

$$a(\eta) = \eta_s \sum_{j=2}^{j_{max}} \int_{(j-2)\Delta\eta}^{(j-1)\Delta\eta} \ln\left|\eta_*^2 - \eta^2\right| \left[\frac{\eta_*}{2} \frac{\phi''_{*,j} - \phi''_{*,j-1}}{2} - \frac{\eta_*^2}{2} \frac{\phi''_{*,j} - \phi''_{*,j-1}}{\Delta_\eta}\right] d\eta_* \quad . \tag{H-28}$$

We define the functions,

$$f(\eta_*,\eta) = \eta_s \int_0^{\eta_*} \ln\left|\eta_*^2 - \eta^2\right| \left(\frac{\eta_*}{4} + \frac{\eta_*^2}{2\Delta\eta}\right) d\eta_* \quad , \qquad \text{(H-29)}$$

$$h(\eta_*,\eta) = \eta_s \int_0^{\eta_*} \ln\left|\eta_*^2 - \eta^2\right| \left(\frac{\eta_*}{4} - \frac{\eta_*^2}{2\Delta\eta}\right) d\eta_* \quad , \qquad \text{(H-30)}$$

which can be integrated analytically to give

$$\begin{aligned} f(\eta_*,\eta)/\eta_s = {} & \left\{\frac{1}{8}\left(\eta_*^2 - \eta^2\right) - \frac{\eta_*^3}{6\Delta\eta}\right\} \ln\left|\eta_*^2 - \eta^2\right| + \frac{\eta^2}{8} \ln \eta^2 \\ & + \frac{\eta^3}{6\Delta\eta} \ln\left|\frac{\eta_* - \eta}{\eta_* + \eta}\right| - \frac{\eta_*^2}{8} + \frac{\eta_*^3}{9\Delta\eta} + \frac{\eta_*\eta^2}{3\Delta\eta} \quad , \end{aligned} \qquad \text{(H-31)}$$

$$\begin{aligned} h(\eta_*,\eta)/\eta_s = {} & \left\{\frac{1}{8}\left(\eta_*^2 - \eta^2\right) + \frac{\eta_*^3}{6\Delta\eta}\right\} \ln\left|\eta_*^2 - \eta^2\right| + \frac{\eta^2}{8} \ln \eta^2 \\ & + \frac{\eta^3}{6\Delta\eta} \ln\left|\frac{\eta_* - \eta}{\eta_* + \eta}\right| - \frac{\eta_*^2}{8} - \frac{\eta_*^3}{9\Delta\eta} - \frac{\eta_*\eta^2}{3\Delta\eta} \quad , \end{aligned} \qquad \text{(H-32)}$$

Note the limiting cases,

$$\begin{aligned} \lim_{\eta_* \to \eta} f(\eta_*,\eta) = - \lim_{\eta_* \to \eta} h(\eta_*,\eta) = {} & \frac{\eta_s \eta^3}{3\Delta\eta} \left(\ln 2\eta - \frac{4}{3}\right) \\ & + \frac{\eta^2}{8} \left(\ln\eta^2 - 1\right) \quad . \end{aligned} \qquad \text{(H-33)}$$

In terms of these functions f and h, equation 28 becomes, after some rearrangement,

$$\begin{aligned} a(\eta) = {} & \phi_{*,1}[f(\Delta\eta,\eta) - f(0,\eta)] + \sum_{j=2}^{j_{max}-1} \{h[(j-1)\Delta\eta,\eta] - h[(j-2)\Delta\eta,\eta] \\ & + f(j\Delta\eta,\eta) - f[(j-1)\Delta\eta,\eta]\} + \phi_{*,j_{max}}[h(\eta_s,\eta) - h(\eta_s-\Delta\eta,\eta)] \quad . \end{aligned} \qquad \text{(H-34)}$$

The second integral in equation 19 can also be evaluated analytically:

$$b(\eta) = -\frac{1}{4\eta_s}\left(3\eta_s^2 + \eta^2\right)\ln\left|\eta_s^2 - \eta^2\right| + \frac{\eta^2}{4\eta_s}\ln\eta^2 + \eta\ln\left|\frac{\eta_s - \eta}{\eta_s + \eta}\right| + \frac{7}{4}\eta_s \quad , \tag{H-35}$$

and

$$\lim_{\eta\to\eta_s} b(\eta) = -2\eta_s \ln\eta_s + \frac{\eta_s}{4}\left(\ln\eta_s^2 + 7\right) \quad . \tag{H-36}$$

The third integral can be written in finite difference form as follows:

$$d(x) = \frac{1}{2}\sum_{j=j_{max}+1}^{jj_{max}} \int_{(jj_{max}-j)\Delta x}^{(jj_{max}-j+1)\Delta x} \ln\left|\frac{1}{\sqrt{x_*}} - \frac{1}{\sqrt{x}}\right| \frac{1}{x_*^{3/4}} \times \frac{\phi'_{*,j} - \phi'_{*,j-1}}{\Delta x}\, dx_* \quad . \tag{H-37}$$

This can be transformed into the form,

$$\begin{aligned} d(x) = {} & \phi'_{*,j_{max}}\left\{e[(jj_{max} - j_{max} - 1)\,\Delta x, x] - e\left(1/\eta_s^4, x\right)\right\} \\ & + \sum_{j=j_{max}+1}^{jj_{max}-1} \phi'_{*,j}\left\{e[(jj_{max} - j + 1)\,\Delta x, x] - 2e[(jj_{max} - j)\,\Delta x, x]\right. \\ & \left. + e[(jj_{max} - j - 1)\,\Delta x, x]\right\} + \phi'_{*,jj_{max}}\, e(\Delta x, x) \quad , \end{aligned} \tag{H-38}$$

where

$$e(x_*,x) \equiv \frac{1}{2\Delta x} \int_0^{x_*} \ln\left|\frac{1}{\sqrt{x_*}} - \frac{1}{\sqrt{x}}\right| \frac{1}{x_*^{3/4}}\, dx_* \qquad \text{(H-39)}$$

$$= \frac{2}{\Delta x}\left\{x_*^{1/4} \ln\left|\frac{1}{\sqrt{x_*}} - \frac{1}{\sqrt{x}}\right| - x^{1/4} \ln\left|\frac{x_*^{1/4} - x^{1/4}}{x_*^{1/4} + x^{1/4}}\right|\right\} .$$

Note also that as $x \to 0$,

$$e(x_*,x) = \frac{2}{\Delta x}\left(x_*^{1/4} \ln \frac{1}{\sqrt{x_*}} + 2x_*^{1/4}\right) , \qquad \text{(H-40)}$$

and as $x_* \to x$,

$$e(x,x) = \frac{2}{\Delta x} x^{1/4} \ln \frac{4}{\sqrt{x}} . \qquad \text{(H-41)}$$

Equation 19 can now be represented by the generalized expression,

$$\sum_{j=1}^{jj_{max}-1} [B_{j,k} + \delta_{j,k}A_k] X_j = D_k \qquad \text{(H-42)}$$

$$(k=1,2,\ldots, jj_{max}-1) ,$$

where $X_j = \phi''_{*,j}$ for $j \leq j_{max}$, $X_j = \phi'_{*,j}$ for $j \geq j_{max}$, $\delta_{j,k}$ is the Kronecker delta, and the coefficients $B_{j,k}$, A_k, and D_k are given as follows:

$$B_{1,k} = f(\Delta\eta,\eta_k) - f(0,\eta_k) , \qquad \text{(H-43)}$$

$$B_{j,k}\Big|_{1<j<j_{max}} = h[(j-1)\,\Delta\eta,\eta_k] - h[(j-2)\,\Delta\eta,\eta_k] + f(j\Delta\eta,\eta_k) - f[(j-1)\,\Delta\eta,\eta_k] \quad , \tag{H-44}$$

$$B_{j_{max},k} = h(\eta_s,\eta_k) + e[(jj_{max}-j_{max}-1)\,\Delta x,x_k] - e\left(1/\eta_s^4,x_k\right) - h(\eta_s-\Delta\eta,\eta_k) \quad , \tag{H-45}$$

$$B_{j,k}\Big|_{j_{max}<j<jj_{max}} = e[(jj_{max}-j+1)\,\Delta x,x_k] - 2e[(jj_{max}-j)\,\Delta x,x_k] + e[(jj_{max}-j-1)\,\Delta x,x_k] \quad , \tag{H-46}$$

$$A_k\Big|_{k\leq j_{max}} = -\pi\eta_s \quad , \tag{H-47}$$

$$A_k\Big|_{j_{max}<k<jj_{max}} = -\pi\eta_k \quad , \tag{H-48}$$

$$D_k\Big|_{k\leq j_{max}} = -b(\eta_k) + \pi/\eta_s \quad , \tag{H-49}$$

$$D_k\Big|_{j_{max}<k<jj_{max}} = -b(\eta_k) + \pi/\eta_k \quad . \tag{H-50}$$

Equation 42 represents a set of linear equations which can be solved by standard methods for the unknowns X_j. The equation including the unknown $X_{jj_{max}}$ has been dropped from this set because its coefficient is infinite (the function e is undefined at x = 0). However, we know in advance that $X_{jj_{max}}$ should become zero as $x \to 0$.

H.3. Computer Program

PROGRAM SHORT calculates the potential $\bar{\Phi}_o$ at small times on the surface of a disk electrode, and integrates it according to equation 4-20. It calls SUBROUTINE MATINV (see appendix C) to solve equation 42. One input card is required in order to specify j_{max}, jj_{max}, η_s, and b (see equation 4-20).

```
      PROGRAM SHORT(INPUT,OUTPUT)
C     TRANSIENT RESPONSE OF A DISK AT SHORT TIMES
      DIMENSION B(101,101),D(101,1),E(20,101),F(101,101),G(101),
     1H(101,101)
      COMMON B,D
      HP=3.141592654 $ BB=1.39      $ READ 101,JMAX,JJMAX,ES
      SES=ES*ES $ JJM1=JJMAX-1 $ JM1=JMAX-1
      JP1=JMAX+1 $ JJMJ=JJMAX-JMAX $ DE= ES/JM1 $ DZ=1.0/JJMJ/ES**4
      DO 18 K=1,JJM1 $ IF(K-JMAX) 1,1,2
    1 ETAS=(K-1)*DE $ SETAS=ETAS*ETAS $ IF(K.EQ.1) GO TO 3
      ZS=1.0/SETAS/SETAS $ RZS=SETAS $ RRZS=1.0/ETAS
      IF(K.NE.JMAX) GO TO 3
      G(K)=-2.0*ES*ALOG(2.0*ES)+ES/4.0*(2.0*ALOG(ES)+7.0) $ GO TO 4
    2 ZS=(JJMAX-K)*DZ $ RZS=1.0/SQRT(ZS) $ RRZS=ZS**0.25
      ETAS=SQRT(RZS) $ SETAS=RZS
    3 XL1=ALOG(ABS(SES-SETAS)) $ XL2=ALOG(ABS(( ES-ETAS)/( ES+ETAS)))
      G(K)=-0.25/ES*(3.0*SES+SETAS)*XL1+ETAS*XL2+1.75*ES
      IF(K.NE.1) G(K)=G(K)+0.25*SETAS*ALOG(SETAS)/ES
    4 DO 7 J=1,JMAX
      ETA=(J-1)*DE $ SETA=ETA*ETA $ IF(J.NE.K) GO TO 5
      IF(K.NE.1) GO TO 41 $ H(J,K)=0.0 $ F(J,K)=0.0 $ GO TO 7
   41 F(J,K)=ETAS*SETAS/3.0/DE*(ALOG(2.0*ETAS)-4.0/3.0)*ES
      H(J,K)=-F(J,K) $ GO TO 7
    5 XL1=ALOG(ABS(SETA-SETAS)) $ XL2=ALOG(ABS((ETA-ETAS)/(ETA+ETAS)))
    6 HH=(SETA-SETAS)/8.0*(XL1-1.0)
      F(J,K)=((SETA*ETA*XL1-SETAS*ETAS*XL2)/2.0-SETA*ETA/3.0-ETA*SETAS)/
     13.0/DE $ H(J,K)=(HH-F(J,K))*ES $ F(J,K)=(HH+F(J,K))*ES
    7 CONTINUE          $ DO 13 J=JMAX,JJMAX $ Z=(JJMAX-J)*DZ
      IF(J.NE.JJMAX) GO TO 8 $ E(1,K)=0.0 $ GO TO 13
    8 RZ=1.0/SQRT(Z) $ RRZ=Z**0.25 $ IF(J.NE.K) GO TO 10
      E(JJMAX-J+1,K)=-2.0/DZ*RRZS*ALOG(4.0*RZS) $ GO TO 13
   10 IF(K.NE.1) GO TO 11
      E(JJMAX-J+1,K)=-2.0/DZ*RRZ*(ALOG(RZ)+2.0) $ GO TO 13
   11 XL1=ALOG(ABS(RZ-RZS)) $ XL2=ALOG(ABS((RRZ-RRZS)/(RRZ+RRZS)))
      E(JJMAX-J+1,K)=-2.0/DZ*(RRZ*XL1-RRZS*XL2)
   13 CONTINUE $ B(K,1)=F(2,K)-F(1,K) $ DO 14 J=2,JM1
   14 B(K,J)=H(J,K)-H(J-1 ,K)+F(J+1,K)-F(J,K)
      B(K,JMAX)=H(JMAX,K)-H(JMAX-1,K)+E(JJMJ,K)-E(JJMJ+1,K)
      DO 15 J=JP1,JJM1
   15 B(K,J)= E(JJMAX-J+2,K)-2.0*E(JJMAX-J+1,K)+E(JJMAX-J,K)
      B(K,JJMAX)= E(2,K) $ B(JJMAX,K)=0.0 $ IF(K-JMAX) 16,16,17
   16 B(K,K)=B(K,K)-HP*ES $ D(K,1)=-G(K)+HP/ES $ GO TO 18
   17 B(K,K)=B(K,K)-HP*ETAS $ D(K,1)=-G(K)+HP/ETAS
   18 CONTINUE $ D(JJMAX,1)=0.0 $ CALL MATINV(JJM1,1,DETERM)
      PRINT 102 $ DO 19 J=1,JMAX $ E(1,J)=(J-1)*DE
   19 B(J,1)=ES*D(J,1)+1.0/ES $ DO 20 J=JMAX,JJM1
      F(1,J)=(JJMAX-J)*DZ $ E(1,J)=1.0/F(1,J)**0.25
   20 B(J,1)=E(1,J)*D(J,1)+1.0/E(1,J)
      PRINT 103,(E(1,J),B(J,1),J=1,JJM1) $ SUM=0.0
      DO 21 I=3,JMAX,2 $ SUM=SUM+D(I-2,1)+4.0*D(I-1,1)+D(I,1)
   21 IF(E(1,I).GE. BB) GO TO 22
   22 PRINT 104,E(1,I) $ SUMM=(1.0/ES+SUM*DE/3.0*ES-ALOG(E(1,I)))*2.0/HP
      J=I+2 $ SUM=0.0 $ DO 23 I=J,JMAX,2
   23 SUM=SUM+B(I-2,1)-1.0/E(1,I-2)+4.0*(B(I-1,1)-1.0/E(1,I-1))+B(I,1)-1
     1.0/E(1,I) $ SUM=SUMM+SUM*DE/3.0*2.0/HP $ PRINT 105,SUM,SUMM
      PRINT 102 $ DO 24 I=JMAX,JJM1
      G(I)=D(I,1)/F(1,I) $ F(1,I)=SQRT(F(1,I))
   24 PRINT 106,F(1,I),G(I) $ SUM=0.0 $ DO 25 I=JP1,JJM1
   25 SUM=SUM+(G(I)+G(I-1))*(F(1,I-1)-F(1,I))/2.0/HP
      PRINT 106,SUM $ STOP
  101 FORMAT(2I4,E8.4)
  102 FORMAT(1H1,5X,*ETA*,15X,*PHI*)
  103 FORMAT(F10.3,F20.7)
```

```
104 FORMAT(//6X,*B=*,F8.3)
105 FORMAT(6X,*A=*,E13.6,6X,E13.6)
106 FORMAT(2E15.6)
    END
```

0 0 0 0 5 9 0 , 6 3 3

NOMENCLATURE

The numbers in parentheses refer to equation numbers.

a	0.51023
$a_{o,n}$	see equation 4-7
$a_{m,n}$	see equation 4-6
A	constant defined in equation 4-20
A_m	coefficient in series for concentration (B-8)
b	constant defined in equation G-7
$B(\theta)$	dimensionless velocity derivative on the surface of a rotating sphere (2-43)
B_n	coefficient in series for potential (2-13)
B_n	coefficient in series for concentration (6-29)
$B_{n,i}$	coefficient in series for U_i
$\tilde{B}_n$	coefficient in series for $\tilde{U}$
$B_{n,i}$	coefficient in series for T_i
c	concentration of salt, mole/cm^3
c_i	concentration of species i, mole/cm^3
C	double-layer capacity, f/cm^2
C_{eff}	apparent double-layer capacity in the equivalent circuit (figure 8-3), f/cm^2
C_i	coefficient in the galvanostatic series for Φ^t (7-4)
C_i	coefficient in the potentiostatic series for Φ^t (8-1)
D	$32/3\pi^2$ (7-26)
D	diffusion coefficient of salt, cm^2/sec (2-50)
D_i	diffusion coefficient of species i, cm^2/sec

e^-	symbol for the electron
E	dimensionless overpotential (A-7)
E_s	dimensionless surface overpotential (A-6)
E_c	dimensionless concentration overpotential (A-6)
F	Faraday's constant, 96,487 C/equiv
$F(\eta,\eta')$	function defined by equation H-2
$F(\theta)$	dimensionless concentration on a sphere at high rotation speeds (5-3)
F,G,H	dimensionless velocity components for the rotating disk (2-32)
$F_n(Z),G_n(Z),$ $H_n(Z)$	functions in series for the velocity components of the rotating sphere (2-40)
$F_n(z),G_n(z)$	functions in short-time series for concentration (6-10,11)
$\underline{g}$	gravitational acceleration, cm/sec^2
$G(\eta_*)$	function defined by equation H-13
$\underline{i}$	current density, A/cm^2
i_c	capacitive current density, A/cm^2
i_f	faradaic current density, A/cm^2
i_n	normal component of the current density, A/cm^2
i_o	exchange-current density, A/cm^2
I	total current, A
I_o	initial current, A
I_∞	final current, A
I_L	limiting current, A

J	dimensionless exchange-current density (4-21)
J	dimensionless exchange-current density for linear kinetics (4-2)
k	undetermined constant in appendix B
K	$(1/\lambda_o)(3/a)^{2/3}$, constant defined in equation 6-30
$K(m)$	complete elliptic integral of the first kind
$L_{m,n}$	see equation B-19
m	see equation 2-22
M_i	symbol for the chemical formula of species i
M_{2n}	Legendre function of order 2n (see reference 7)
n	number of electrons transferred by the electrode reaction (3-1)
N	dimensionless limiting current density (4-22, 5-1)
$\underline{N}_i$	flux of species i, mole/cm^2-sec
p	pressure, dyne/cm^2
P	dimensionless dynamic pressure (2-34)
P	dimensionless capacity (B-17)
P_{2n}	Legendre polynomial of order 2n
P	dynamic pressure, dyne/cm^2
q	charge density on the metal side of the double layer, C/cm^2
Q	dimensionless capacity (6-35)
r	radial distance, cm
r_o	radius of disk or sphere, cm

R	universal gas constant, 8.3143 J/mole-deg
R	resistance, ohm
R_i	homogeneous rate of production of species i, mole/cm^3-sec
R_{eff}	apparent direct-current resistance of equivalent circuit (figure 8-3), ohm
$\tilde{R}_{eff}$	apparent alternating-current resistance of equivalent circuit (figure 8-3), ohm
$\mathcal{R}$	normal distance of surface from axis of cymmetry, cm
Re	$r_o^2\Omega/\nu$, rotational Reynolds number
s_i	stoichiometric coefficient of species i in electrode reaction
$S(\eta)$	function defined by equation G-2
Sc	Schmidt number
t	time, sec
t_{ch}	total period of charging, sec
T	absolute temperature, °K
u_i	mobility of species i, cm^2-mole/J-sec
U_i	eigenfunction in the galvanostatic series for Φ^t
$\tilde{U}$	complex, dimensionless potential in the solution (8-13)
$\underline{v}$	velocity, cm/sec
V	electrode potential relative to infinity, V
V_o	amplitude of applied alternating potential, V
V_r	potential with respect to a reference electrode of the same kind, V
V_r'	potential with respect to a reference electrode of a given kind, V

0 0 0 0 5 9 0 7 3 3 5

V	scaling factor for the potential, V
x	distance along electrode from its upstream end, cm
x	variable defined in equation 9-7
y	normal distance from the electrode surface, cm
Y	stretching variable (G-1)
z	axial distance, cm
z	$\zeta/\sqrt{2\theta}$, similarity variable in short-time series for concentration
z_i	charge number of species i
Z	stretched radial coordinate (2-41)
Z	$-z_+z_-/(z_+-z_-)$ for a single salt, $-n/s_R$ with supporting electrolyte
Z	impedance, ohm
Z_n	eigenfunction in series for concentration (6-26)
Z_m	eigenfunction in series for concentration (B-8)

Greek symbols:

α_a,α_c	transfer coefficients
α,β	α_a/Z, α_c/Z, transfer coefficients
β	velocity derivative at the electrode surface, sec^{-1}
δ	Nernst diffusion-layer thickness, cm
δ	constant defined in equation A-13
$\delta_{m,n}$	Kronecker delta
η	rotational elliptic coordinate (2-14)
η	total overpotential, V
η_c	concentration overpotential, V

η_s	surface overpotential, V
$\bar{\eta}$	parabolic coordinate (4-14 or 9-2)
γ	exponent in composition dependence of exchange-current density
Γ_i	surface concentration of species i, mole/cm^2
κ	conductivity, ohm^{-1}-cm^{-1}
λ_i	eigenvalue characteristic of T_i
λ_n	eigenvalue characteristic of Z_n
Λ_i	eigenvalue characteristic of U_i
Λ_D	eigenvalue characteristic of diffusion
μ	viscosity, g/cm-sec
μ_i	electrochemical potential of species i, J/mole
ν	kinematic viscosity, cm^2/sec
ν_i	number of species i formed due to dissociation of one mole of electrolyte
ω	frequency of applied potential, radian/sec
Ω	$\omega Cr_o/\kappa$, dimensionless frequency
Ω	angular rotation speed, radian/sec
ϕ	polar angle in spherical coordinates
$\phi(\zeta)$	function defined by equation A-5
$\bar{\Phi}$	stretched dimensionless potential in the solution (4-13 or 9-1)
Φ	potential in the solution, V
$\Delta\Phi_{ohm}$	ohmic drop in the solution, V
ξ	rotational elliptic coordinate (2-14)
ξ	similarity variable for Lighthill transformation (2-55)

0 0 0 0 3 9 0 / 3 3 5

ξ	parabolic coordinate (4-14 or 9-12)
ρ	density, g/cm^3
τ	time constant for decay
θ	angle from pole of sphere
θ	dimensionless time (6-2)
θ	dimensionless time for charging (7-6)
θ'	dimensionless time for decay (7-16)
θ_{ch}	dimensionless total period of charging
Θ	dimensionless concentration
Θ_c	dimensionless concentration for concentration step (6-14)
Θ_f	dimensionless concentration for flux step (6-15)
υ_i	constant in series for V^t (normalized to unity)
T_i	eigenfunction in the potentiostatic series for Φ^t
ζ	dimensionless axial coordinate (2-33)
ζ	dimensionless axial coordinate (6-3)

subscripts:

ave	average
lim	limiting current
R	reactant
o	at the electrode surface
∞	far from the surface
+	anion
-	cation

superscripts:

o	pure state
p	corresponds to primary distribution
ss	steady-state part
t	transient part

0 0 0 0 3 9 0 / 3 3 7

REFERENCES

1. John Newman, "Engineering Design of Electrochemical Systems," Industrial and Engineering Chemistry, 60(4), 12-27 (April, 1968).

2. N. Ibl, "Probleme des Stofftransportes in der angewandten Electrochemie," Chemie-Ingenieur-Technik, 35, 353-361 (1963).

3. B. Levich, "The Theory of Concentration Polarization," Acta Physicochimica U.R.S.S., 17, 257-307 (1942).

4. M. Eisenberg, C. W. Tobias, and C. R. Wilke, "Ionic Mass Transfer and Concentration Polarization at Rotating Electrodes," Journal of the Electrochemical Society, 101, 306-319 (1954).

5. A. C. Riddiford, "The Rotating Disk System," Advances in Electrochemistry and Electrochemical Engineering, 4, 47-116 (1966).

6. John Newman, "The Effect of Migration in Laminar Diffusion Layers," International Journal of Heat and Mass Transfer, 10, 983-997 (1967).

7. John Newman, "Current Distribution on a Rotating Disk below the Limiting Current," Journal of the Electrochemical Society, 113, 1235-1241 (1966).

8. Der-Tau Chin, "Convective Diffusion on a Rotating Sphere Electrode," ibid., 118, 1434-1438 (1971).

9. Veniamin G. Levich, Physicochemical Hydrodynamics (Englewood Cliffs: Prentice-Hall, Inc., 1962).

10. John Newman, "Transport Processes in Electrolytic Solutions," Advances in Electrochemistry and Electrochemical Engineering, 5, 87-135 (1967).

11. John S. Newman, Electrochemical Systems (Englewood Cliffs: Prentice-Hall, Inc., 1973).

12. John Newman, "The Fundamental Principles of Current Distribution and Mass Transport in Electrochemical Cells," Electroanalytical Chemistry, 6, 187-352 (1973).

13. John Newman, Douglas Bennion, and Charles W. Tobias, "Mass Transfer in Concentrated Binary Electrolytes," Berichte der Bunsengesellschaft für physicalische Chemie, 69, 608-612 (1965). For corrections see ibid. 70, 493 (1966).

14. John Newman, "Resistance for Flow of Current to a Disk, "Journal of the Electrochemical Society, 113, 501-502 (1966).

15. Leonard Nanis and Wallace Kesselman, "Engineering Applications of Current and Potential Distributions in Disk Electrode Systems," ibid, 118, 452-461 (1971).

16. Milton Abramowitz and Irene A. Stegun, eds., Handbook of Mathematical Functions (Washington: National Bureau of Standards, 1964).

17. H. S. Carslaw and J. C. Jaeger, Conduction of Heat in Solids (Oxford: Clarendon Press, 1959).

18. Th. v. Kármán, "Über laminare und turbulente Reibung," Zeitschrift für angewandte Mathematik und Mechanik, 1, 233-252 (1921).

19. L. Howarth, "Note on the Boundary Layer on a Rotating Sphere," Philosophical Magazine (7th Ser.), 42, 1308-1315 (1951).

20. R. Byron Bird, Warren E. Stewart, and Edwin N. Lightfoot, Transport Phenomena (New York: John Wiley & Sons, Inc., 1960).

0 0 0 0 3 9 0 0 3 3 8

21. W. G. Cochran, "The flow due to a rotating disc," Proceedings of the Cambridge Philosophical Society, 30, 365-375 (1934).

22. M. H. Rogers and G. N. Lance, "The rotationally symmetric flow of a viscous fluid in the presence of an infinite rotating disk," Journal of Fluid Mechanics, 7, 617-631 (1960).

23. W. H. H. Banks, "The Boundary Layer on a Rotating Sphere," The Quarterly Journal of Mechanics and Applied Mathematics, 18, 443-454 (1965).

24. R. Manohar, "The Boundary Layer on a Rotating Sphere," Zeitschrift für angewandte Matematik und Physik, 18, 320-330 (1967).

25. John Newman, "Mass Transfer to a Rotating Sphere at High Schmidt Numbers," Journal of the Electrochemical Society, 119, 69-71 (1972).

26. F. P. Bowden and R. G. Lord, "The aerodynamic resistance to a sphere rotating at high speed," Proceedings of the Royal Society (London), A271, 143-153 (1963).

27. K. Stewartson, "On rotating laminar boundary layers," in Boundary Layer Research, IUTAM Symposium, 59-71 (1957).

28. William H. Smyrl and John Newman, "Ring-Disk and Sectioned Disk Electrodes," Journal of the Electrochemical Society, 119, 212-219 (1972).

29. Hermann Schlichting, Boundary-Layer Theory (New York: McGraw-Hill Book Company, 1968), p. 223.

30. M. J. Lighthill, "Contributions to the theory of heat transfer through a laminar boundary layer," Proceedings of the Royal Society (London), A202, 359-373 (1950).

31. Andreas Acrivos, "Solution of the Laminar Boundary Layer Energy Equation at High Prandtl Numbers," The Physics of Fluids, 3, 657-658 (1960).

32. Kaoru Kojima, "Engineering Analysis of Electrolytic Cells: Electric Resistance between Electrodes," Research Reports of the Faculty of Engineering, Niigata University, no. 13 (1964).

33. R. N. Fleck, D. N. Hanson, and C. W. Tobias, "Numerical Evaluation of Current Distribution in Electrochemical Systems" (UCRL-11612), September, 1964.

34. John Newman, "Schmidt Number Correction for the Rotating Disk," Journal of Physical Chemistry, 70, 1327-1328 (1966).

35. D. P. Gregory and A. C. Riddiford, "Transport to the Surface of a Rotating Disc," Journal of the Chemical Society, 3756-3764 (1956).

36. Der-Tau Chin, "Rotating Spherical Electrode: A Perturbation Theory for Schmidt Number Corrections," Journal of the Electrochemical Society, 119, 1049-1052 (1972).

37. E. M. Sparrow and J. L. Gregg, "Heat Transfer from a Rotating Disk to Fluids of Any Prandtl Number," Journal of Heat Transfer, 81C, 249-251 (1959).

38. J. Newman and L. Hsueh, "The Effect of Variable Transport Properties on Mass Transfer to a Rotating Disk," Electrochimica Acta, 12, 417-427 (1967).

39. L. Hsueh and J. Newman, "Mass Transfer and Polarization at a Rotating Disk Electrode," ibid., 12, 429-438 (1967).

0 0 0 3 3 9 0 7 3 3 9

40. William H. Smyrl and John Newman, "Limiting Current on a Rotating Disk with Radial Diffusion," Journal of the Electrochemical Society, 118, 1079-1081 (1971).

41. David C. Grahame, "The Electrical Double Layer and the Theory of Electrocapillarity," Chemical Reviews, 41, 441-501 (1947).

42. Paul Delahay, "Electrode Processes without a Priori Separation of Double-Layer Charging," Journal of Physical Chemistry, 70, 2373-2379 (1966).

43. Paul Delahay and Gilles G. Susbielles, "Double-Layer Impedance of Electrodes with Charge-Transfer Reaction," ibid., 70, 3150-3157 (1966).

44. P. Delahay, K. Holub, G. Susbielles, and G. Tessari, "Double-Layer Perturbation without Equilibrium between Concentrations and Potential," ibid., 71, 779-780 (1967).

45. Karel Holub, Gino Tessari, and Paul Delahay, "Electrode Impedance without a Priori Separation of Double-Layer Charging and Faradaic Process," ibid., 71, 2612-2618 (1967).

46. Peter Appel, Dissertation, University of California, Berkeley, in progress.

47. Eugene Levart and Daniel Schuhmann, "Migration-Diffusion Coupling and the Concept of Electrochemical Impedance," Journal of Electroanalytical Chemistry and Interfacial Electrochemistry, 24, 41-52 (1970).

48. W. R. Parrish and John Newman, "Current Distribution on a Plane Electrode below the Limiting Current," Journal of the Electrochemical Society, 116, 169-172 (1969).

49. W. R. Parrish and John Newman, "Current Distributions on Plane Parallel Electrodes in Channel Flow," ibid., 117, 43-48 (1970).

50. John Newman, "The Diffusion Layer on a Rotating Disk Electrode," ibid., 114, 239 (1967).

51. Richard Alkire and Ali Asghar Mirarefi, "The Current Distribution within Tubular Electrodes under Laminar Flow," submitted to Journal of the Electrochemical Society.

52. Kemal Nişancioğlu and John Newman, "Current Distribution on a Rotating Sphere below the Limiting Current" (LBL-1837), ibid., to be published.

53. Robert V. Homsy and John Newman, "Current Distribution on a Plane below a Rotating Disk" (LBL-1887), submitted to Journal of the Electrochemical Society.

54. Vinay Marathe and John Newman, "Current Distribution on a Rotating Disk Electrode," ibid., 116, 1704-1707 (1969).

55. Stanley Bruckenstein and Barry Miller, "An Experimental Study of Nonuniform Current Distribution at Rotating Disk Electrodes," ibid., 117, 1044-1048 (1970).

56. W. J. Albery and J. Ulstrup, "The Current Distribution on a Rotating Disk Electrode," Electrochimica Acta, 13, 281-284 (1968).

57. W. J. Albery and M. L. Hitchman, "Current Distribution on a Rotating Disc Electrode," Transactions on the Faraday Society, 67, 2408-2413 (1971).

58. William H. Smyrl and John Newman, "Detection of Nonuniform Current Distribution on a Disk Electrode," Journal of the Electrochemical Society, 119, 208-212 (1972).

0 0 0 0 0 9 0 , 0 4 0

59. Barry Miller and Maria I. Bellavance, "Measurement of Current and Potential Distribution at Rotating-Disk Electrodes," ibid., 120, 42-53 (1973).

60. Kemal Nişancioğlu and John Newman, "The Transient Response of a Disk Electrode" (LBL-1109), ibid., to be published.

61. John Newman, "Frequency Dispersion in Capacity Measurements at a Disk Electrode," ibid., 117, 198-203 (1970).

62. Kemal Nişancioğlu and John Newman, "The Short-Time Response of a Disk Electrode" (LBL-1896), submitted to Journal of the Electrochemical Society.

63. J. A. Klingert, S. Lynn, and C. W. Tobias, "Evaluation of Current Distribution in Electrode Systems by High-Speed Digital Computers," Electrochimica Acta, 9, 297-311 (1964).

64. William H. Tiedemann, John Newman, and Douglas N. Bennion, "The Error in Measurements of Electrode Kinetics Caused by Nonuniform Ohmic Potential Drop to a Disk Electrode," Journal of the Electrochemical Society, 120, 256-258 (1973).

65. David C. Grahame, "Properties of the Electrical Double-Layer at a Mercury Surface. I. Methods of Measurement and Interpretation of Results," Journal of the American Chemical Society, 63, 1207-1215 (1941).

66. E. Mattson and J. O'M. Bockris, "Galvanostatic Studies of the Kinetics of Deposition and Dissolution in Copper + Copper Sulphate System," Transactions of the Faraday Society, 55, 1586-1601 (1959).

67. Der-Tau Chin, "A Rotating Ring-Hemispherical Electrode in Electroanalytical Applications," Journal of the Electrochemical Society, 120, 631-635 (1973).

68. Der-Tau Chin, "An Experimental Study of Mass Transfer on a Rotating Spherical Electrode," ibid., 118, 1764-1769 (1971).

69. Andreas Acrivos and Paul L. Chambré, "Laminar Boundary Layer Flows with Surface Reactions," Industrial and Engineering Chemistry, 49, 1025-1029 (1957).

70. T. R. Roseburgh and W. Lash-Miller, "Mathematical Theory of the Changes of Concentration at the Electrode, Brought about by Diffusion and by Chemical Reaction," Journal of Physical Chemistry, 14, 816-884 (1910).

71. B. Levich, "Theory of Concentration Polarization. III," Acta Physicochimica U.R.S.S., 19(2-3), 133-138 (1944).

72. Yu. G. Siver, "Unsteady Electrode Processes in Stirred Media. II. Voltammetry at Constant Current Density," Russian Journal of Physical Chemistry, 34, 273-276 (1960) (Zhurnal Fizicheskoi Khimii, 34, 577-584 (1960)).

73. V. Yu. Filinovskii and V. A. Kiryanov, "Contribution to the Theory of Nonstationary Convective Diffusion near a Rotating Disc Electrode," Doklady Physical Chemistry, 156, 650-652 (1964) (Doklady Akademii Nauk SSSR, 156, 1412-1415 (1964)).

74. J. M. Hale, "Transients in Convective Systems. I. Theory of Galvanostatic and Galvanostatic with Current Reversal Transients at a Rotating Disk Electrode," Journal of Electroanalytical Chemistry, 6, 187-197 (1963).

75. Donald R. Olander, "Unsteady-State Heat and Mass Transfer in the Rotating-Disk-Revolving-Fluid System," International Journal of Heat and Mass Transfer, 5, 826-836 (1962).

76. Jan Robert Selman, Measurement and Interpretation of Limiting Currents, Ph. D. Thesis (UCRL-20557), University of California, Berkeley, June, 1971.

77. V. S. Krylov and V. N. Babak, "Nonsteady-State Diffusion to the Surface of a Rotating Disc," Soviet Electrochemistry, 7, 626-632 (1971) (Élektrokhimiya, 7, 649-654 (1971)).

78. Leonard Nanis and Irving Klein, "Transient Mass Transfer at the Rotating Disk Electrode," Journal of the Electrochemical Society, 119, 1683-1687 (1972).

79. Kemal Nişancioğlu and John Newman, "Transient Convective Diffusion to a Disk Electrode" (LBL-1881), submitted to Journal of Electroanalytical Chemistry and Interfacial Electrochemistry.

80. John Newman, "Numerical Solution of Coupled, Ordinary Differential Equations," Industrial and Engineering Chemistry Fundamentals, 7, 514-517 (1968).

81. John Newman, "Ohmic Potential Measured by Interrupter Techniques," Journal of the Electrochemical Society, 117, 507-508 (1970).

82. John Newman, "Effect of Ionic Migration on Limiting Currents," Industrial and Engineering Chemistry Fundamentals, 5, 525-529 (1966).

83. Stanley L. Gordon, John S. Newman, and Charles W. Tobias, "The Role of Ionic Migration in Electrolytic Mass Transport; Diffusivities of $[Fe(CN)_6]^{3-}$ and $[Fe(CN)_6]^{4-}$ in KOH and NaOH solutions, "Berichte der Bunsengesellschaft für physicalische Chemie, 70, 414-420 (1966).

84. Limin Hsueh, Diffusion and Migration in Electrochemical Systems, Ph. D. Thesis (UCRL-18597), University of California, Berkeley, December, 1968.

85. Limin Hsueh and John Newman, "The Approach to Limiting Current in a Stagnant Diffusion Cell," Journal of the Electrochemical Society, 117, 1242-1245 (1970).

86. Samuel Glasstone, "Intermittent Current Electrolysis. Part II. Overvoltage Study of the Lead Electrode," Journal of the Chemical Society (London), 123, 2926-2934 (1923).

87. A. Hickling, "Studies in Electrode Polarisation. Part I. The Accurate Measurement of the Potential of a Polarized Electrode," Transactions of the Faraday Society, 33, 1540-1546 (1937).

88. Sigmund Schuldinger and Roger E. White, "Studies of Time-Potential Changes on an Electrode Surface during Current Interruption. I. Zinc-Steel Couple in Synthetic Sea Water," Journal of the Electrochemical Society, 97, 433-447 (1950).

89. J. D. E. McIntyre and W. F. Peck, Jr., "An Interrupter Technique for Measuring the Uncompensated Resistance of Electrode Reactions under Potentiostatic Control." ibid., 117, 747-751 (1970).

90. Richard Bezman, "Sampled-Data Approach to the Reduction of Uncompensated Resistance Effects in Potentiostatic Experiments," Analytical Chemistry, 44, 1781-1785 (1972).

91. A. M. Johnson and John Newman, "Desalting by Means of Porous Carbon Electrodes," Journal of the Electrochemical Society, 118, 510-517 (1971).

0 0 0 0 3 9 0 . 3 4 1

92. Roger Parsons, "The Structure of the Electrical Double Layer and Its Influence on the Rates of Electrode Reactions," Advances in Electrochemistry and Electrochemical Engineering, 1, 1-64 (1961).

93. Kemal Nişancioğlu and John Newman, "The Transient Response of a Disk Electrode with Controlled Potential" (LBL-1173), Journal of the Electrochemical Society, to be published

94. Henry H. Bauer, Michael S. Spritzer, and Philip J. Elving, "Double-Layer Capacity at a Pyrolytic Graphite Disk Electrode," Journal of Electroanalytical Chemistry and Interfacial Electrochemistry, 17, 299-307 (1968).

95. D. H. Angell, T. Dickinson and R. Greef, "The Potential Distribution near a Rotating-Disk Electrode," Electrochimica Acta, 13, 120-123 (1968).

96. J. E. Harrar and Irving Shain, "Electrode Potential Gradients and Cell Design in Controlled Potential Electrolysis Experiments," Analytical Chemistry, 38, 1148-1158 (1966).

97. John Newman and J. E. Harrar, "Potential Distribution in Axisymmetric Mercury-Pool Electrolysis Cells at the Limiting Current," Journal of the Electrochemical Society, 120, 1041-1044 (1973).

98. Nader Vahdat and John Newman, "Corrosion of an Iron Rotating Disk" (LBL-896), ibid., to be published.

99. Klaus J. Vetter. Elektrochemische Kinetik (Berlin: Springer-Verlag, 1961). English translation: Electrochemical Kinetics. Theoretical and Experimental Aspects (New York: Academic Press, 1967).

100. J. O'M. Bockris, "Electrode Kinetics," Modern Aspects of Electrochemistry, 1, 180-276 (1954).

101. Roger Parsons, "Faradaic and Nonfaradaic Processes," Advances in Electrochemistry and Electrochemical Engineering, 7, 177-219 (1970).

102. Thomas W. Chapman and John Newman, A Compilation of Selected Thermodynamic and Transport Properties of Binary Electrolytes in Aqueous Solution (UCRL-17767), Lawrence Berkeley Laboratory, University of California, Berkeley, May, 1968.

103. A. Frumkin, "The Study of the Double Layer at the Metal-Solution Interface by Electrokinetic and Electrochemical Methods," Transactions of the Faraday Society, 36, 117-127 (1940).

LEGAL NOTICE

This report was prepared as an account of work sponsored by the United States Government. Neither the United States nor the United States Atomic Energy Commission, nor any of their employees, nor any of their contractors, subcontractors, or their employees, makes any warranty, express or implied, or assumes any legal liability or responsibility for the accuracy, completeness or usefulness of any information, apparatus, product or process disclosed, or represents that its use would not infringe privately owned rights.

TECHNICAL INFORMATION DIVISION
LAWRENCE BERKELEY LABORATORY
UNIVERSITY OF CALIFORNIA
BERKELEY, CALIFORNIA 94720